Terbium doped glasses: their optical properties and potential applications

A. Hoaksey

TERBIUM DOPED GLASSES :

their optical properties and potential applications

by

A Hoaksey, BSc

(Grey)

A thesis presented in candidature for the degree of Doctor of Philosophy in the University of Durham

December 1975

To my parents

ACKNOWLEDGEMENTS

The first two years of my study for this thesis were spent in the Department of Physics. I would like to thank my supervisor during this period, Dr K N R Taylor,* for his guidance and continued assistance throughout this work. My third year of study was spent in the Department of Applied Physics and Electronics. I would therefore also like to express to Dr J Woods, my final year supervisor, thanks for his help and direction.

I am indebted to the SCR for a CAPS award, which was in conjunction with the International Research and Development Co Ltd. I gratefully acknowledge the co-operation of the staff of the latter. In addition, my appreciation must go to the entire staffs of the Department of Physics and Applied Physics and Electronics, and especially to their heads, Professor G D Rochester and Professor D A Wright respectively. Finally I wish to thank all others who have given support, in particular Mrs B Billinghurst for typing this thesis.

* Now Professor Taylor, University of New South Wales, Australia.

ABSTRACT

The optical properties of inorganic glasses doped with terbium have been investigated with particular emphasis on silicate glass systems. The effect of increasing terbium concentration on the refractive index of silicate glasses has been investigated and the optical absorption from 0.2 to 40 microns has also been studied. The energy levels of the trivalent terbium ions involved in the various optical processes have been identified by reference to theoretical predictions and spectra in other media.

Glasses doped with terbium show intense series of blue and green luminescence emissions when excited by ultra-violet or X-ray radiation. Emissions from the $^5D_3$ level of the Tb^{3+} ions produce the blue luminescence while the green emission results from transitions from the $^5D_4$ level.

At terbium concentrations above 0.3 mole % the blue emissions are quenched by multipolar transitions from the $^5D_3$ level to the $^5D_4$ level. The green emissions are quenched at concentrations above 6 mole % by an exchange-dipole mechanism.

The effect of temperature on the emission characteristics has been determined. Intense luminescence persists to temperatures above 500°C in silicate glasses. The reduction in temperature does not greatly change the emission intensity. Inhomogeneous broadening, due to the random nature of the glass matrix, persists even at liquid helium temperatures.

Decay rates have been measured at various temperatures with both ultra-violet and X-ray excitation. The effect of other rare earths on the photoluminescence has also been investigated, and a model for the lanthanide ion site is proposed.

The thermoluminescence characteristics of terbium doped silicate glasses have also been measured. Increased terbium concentration reduces the glow peak intensity. A model of the mechanism producing thermoluminescence is proposed.

Differences between binary (sodium silicate) and ternary (lithium aluminosilicate) glasses, observed in both photo- and thermoluminescence, are discussed.

Other optical properties, such as the Faraday effect and cathodoluminescence, are reviewed in a survey of the literature.

CONTENTS

LIST OF FIGURES

page

CHAPTER 5

page

page

page

CHAPTER 7

LIST OF TABLES

CHAPTER I

INTRODUCTION

1.1 Introductory

The inclusion of rare earth oxides as dopants into glass and crystal environments has led to many applications of these materials both as absorbers (1.1) and as practical phosphors (1.2). Europium in various oxide crystals finds use as the red phosphor in colour television, while terbium phosphors have been developed for cathode ray tubes.

The practicality of a phosphor depends upon both its ease of manufacture and the cost of basic materials. Where optically homogeneous materials are required, for instance where the luminescence is to be viewed through the phosphor, the advantages of a glass over crystals is obvious in that lengthy crystal growth processes are not required for amorphous solids. In terms of cost, the rare earths (especially terbium, here investigated) are expensive, so that an attempt has been made to minimise expense by enhancing the luminescence by energy transfer from other (usually cheaper) rare earths to terbium.

Terbium phosphors are characterised by a greenish luminescence which becomes rapidly more intense with increasing dopant concentration above about $\frac{1}{2}$ mole % (1.3). This is in contrast with the emission characteristics, above such concentrations, of other rare earths which give visible luminescence (Ce, Sm, Eu, Dy and Tm).

This work has been concentrated on the luminescence properties of Tb^{3+} ions in binary ($Na_2O:SiO_2$) and ternary ($Li_2O:Al_2O_3:SiO_2$) component silicate glass systems. The luminescence was excited by both

ultra-violet and X-ray radiation, and the effect of temperature on the phosphor has also been investigated. The practicability of rare earth doped glass dosimeters has also been considered, together with a discussion of the feasibility of terbium glass lasers. An attempt has been made to suggest a model for the ligands of Tb^{3+} ions in a glassy environment. The literature has also been reviewed with regard to other optical properties of terbium glasses, such as Faraday rotation and electroluminescence.

1.2 The Nature of the Glassy State

Many attempts to define a glass have been made in the last forty years (1.4, 1.5, 1.6) with varying degrees of success (1.7). However, a rigorous definition is still forthcoming, and this should take into account the relationship of glasses with other amorphous solids (1.8). The definition of Mackenzie (1.9) is sufficient for the present discussion and is used here as a working description: -

> "A glass is any isotropic material, organic or inorganic, in which three dimensional atomic periodicity is absent and the viscosity of which is greater than 10^{14} poise".

The technique of rapid cooling employed in glass production results in a "freezing in" of liquid disorder, and the resulting lack of periodicity of the basic structural units distinguishes a glass from a crystal. Debye has pointed out (1.10) that a regular crystal environment is not, in fact, necessary for X-ray diffraction, but, whereas crystals produce sharp lines in X-ray powder diffraction, amorphous materials such as liquids and glasses in general produce several diffuse halos. This is, of

course, to be expected, as the well-defined lattice parameters, requisite for sharp diffraction lines, are absent in glasses.

The most common glass systems are based on silicon, phosphorous and boron, together with oxygen, and in many cases the glass will also contain amounts of alkali metals and/or alkaline earth metals. A useful review of glass types can be found in reference 1.11.

Most of the early work on glass was empirical until Zachariasen (1.12) introduced the random network theory in 1932. The oxides : B_2O_3, SiO_2, GeO_2, P_2O_5 and As_2O_5 were designated "glass formers" while the alkali metal oxides and the alkaline earth metal oxides were designated "network modifiers". Intermediate roles could be played by oxides such as Al_2O_3. The glass formers were postulated as essential for the formation of vitreous compounds. Glass is envisaged as a disordered network in which all atoms are placed differently in relation to others so that one may only speak of statistical order (Fig 1.1a).

A more detailed examination of ionic environments led Valenkov and Poray-Koshitz (1.13) to develop a new "crystallite theory". This, in contrast to Zachariasen's ideas, favours a high degree of ordering in localised domains or crystallites. These small, slightly distorted crystals, it is suggested, are then separated by zones of less order. It should be emphasised that neither theory fits all glasses in all details, but each is capable of many experimental predictions. The extent of their validity depends very much on the system under consideration.

The degree of difficulty of determining glass structure may be inferred from the fact that even the nature of pure vitreous silica is not yet fully understood. Most modern theories, however, do incorporate

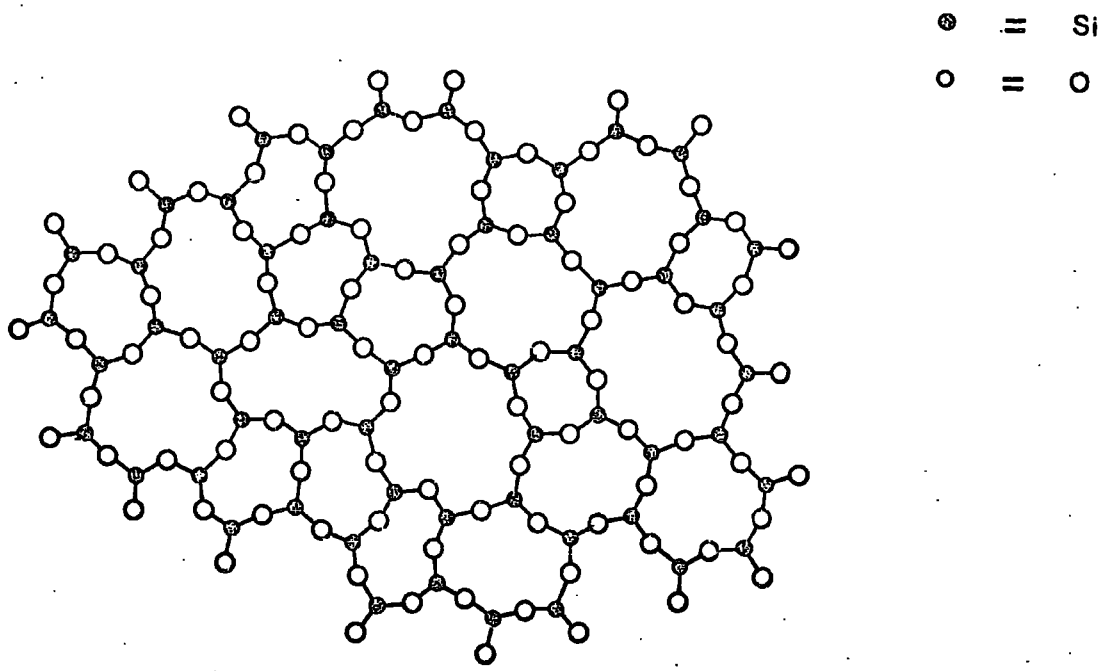

Fig 1.1a

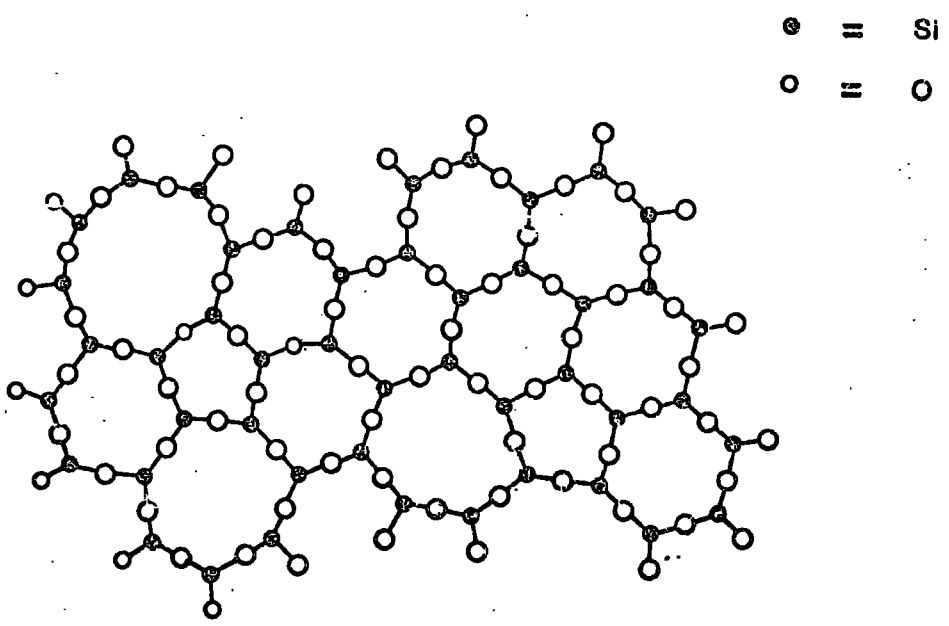

Fig 1.1b

Fig 1.1 Models of glass structure after
(a) Zachariasen (1932), random network theory
(b) Valenkov and Poray-Koshitz (1936), crystallite theory

some form of short-range order (1.14) of typically 10Å to 100Å, together with long-range disorder. The silicon tetrahedra in silicate glasses are pictured as forming "rings". Oberlies (1.15) has calculated the probability of the formation of rings with four, five, six, seven and eight silicon atoms, and finds a maximum for hexagons (see Figure 1.1b).

For various specialist purposes, certain other ions are often incorporated into a glass matrix, usually as the oxide. These are often transition metals or rare earths. For instance, the ion Ti^{4+} (1.16) is used in the nucleation process for forming glass ceramics, and Ce^{3+} finds application in photo-sensitive glasses (1.17).

In this work we are concerned with the optical properties of one of the rare earths, terbium, when incorporated into various inorganic glasses. The work is concentrated on silicate glasses, as these constitute almost all commercially manufactured glasses.

1.3 Energy Levels in Glass

All simple forms of calculation predict that the familiar energy band structure in crystalline solids depends explicitly upon the periodic arrangement of atoms in some form of lattice. Theoretical work (1.18) has shown, however, that the essential idea of band theory can be predicted assuming only local symmetry sites. In more recent work, Inglis and Williams (1.19) consider local symmetries extending over a range of 100Å in an amorphous semiconductor and conclude that the energy bands are not so smeared out as to overlap, but that a reasonably well-defined energy gap exists. However, it is not yet certain for what degree of inhomogeneity the model remains valid. When there is no long-range

order, any structure in the optical spectra characteristic of translational symmetry is absent.

From an experimental standpoint, the transparency in the infrared region in amorphous materials implies that there exists a gap between valence and conduction bands. Thus we see that the existence of short-range order permits the description of the energy bands in glasses in a somewhat similar manner to crystalline solids.

1.4 The Rare Earths

According to Hund's rules, the electron configurations of the elements in the ground state are built up sequentially by placing electrons in hydrogen like orbitals, beginning with those of lowest energy. However, lowest energy is not necessarily equivalent to smallest radial expectation values, so that inner orbitals may be unoccupied in low atomic number elements and then filled at some subsequent stage in the periodic table. This is illustrated by the various series of transition elements where the d orbitals are filled, while the outer electron configuration remains constant. A similar situation occurs with the 4f orbitals, the stepwise filling of which produces the rare earths or lanthanides. These highest energy electrons are shielded by outer electron clouds which results in the very similar chemical properties of the lanthanides. Because of this screening effect, the 4f electrons are particularly insensitive to changes in the external environment.

Some of the basic properties of the rare earths are shown in Table 1.1. It should be noted that the element yttrium (Y) is included because, although it is not a rare earth, it is very similar in many of its physical

TABLE 1.1

General Properties of the Rare Earth Elements

Element and symbol	Atomic number Z	Electronic structure (outer electrons only)		Colour due to absorption in Ln^{3+}	Ionic radius Ln^{3+}
		Ln	Ln^{3+}		
Yttrium Y	39	$4d^1 5s^2$	(Kr)	colourless	0.880
Lanthanum La	57	$5d^1 6s^2$	(Xe)	colourless	1.061
Cerium Ce	58	$4f^1 5d^1 6s^2$	$4f^1$	colourless	1.034
Praseodymium Pr	59	$4f^3 6s^2$	$4f^2$	yellow/green	1.013
Neodymium Nd	60	$4f^4 6s^2$	$4f^3$	reddish	0.995
Promethium Pm	61	$4f^5 6s^2$	$4f^4$	pink/yellow	0.979
Samarium Sm	62	$4f^6 6s^2$	$4f^5$	yellow	0.964
Europium Eu	63	$4f^7 6s^2$	$4f^6$	nearly colourless	0.950
Gadolinium Gd	64	$4f^7 5d^1 6s^2$	$4f^7$	colourless	0.938
Terbium Tb	65	$4f^9 6s^2$	$4f^8$	nearly colourless	0.923
Dysprosium Dy	66	$4f^{10} 6s^2$	$4f^9$	yellow	0.908
Holmium Ho	67	$4f^{11} 6s^2$	$4f^{10}$	pink/yellow	0.894
Erbium Er	68	$4f^{12} 6s^2$	$4f^{11}$	pink	0.881
Thulium Tm	69	$4f^{13} 6s^2$	$4f^{12}$	pale green	0.869
Ytterbium Yb	70	$4f^{14} 6s^2$	$4f^{13}$	colourless	0.858
Lutetium Lu	71	$4f^{14} 5d^1 6s^2$	$4f^{14}$	colourless	0.848

and chemical properties. Also it should be noted that in some respects the first (La) and the last (Lu) elements of the series do not exhibit entirely typical properties because they correspond to an empty and a filled 4f subshell respectively. The electronic configurations of both the neutral and the trivalent ions are shown together with the principal colour associated with the triply charged lanthanide ion, Ln^{3+}, and its ionic radius. The only electrons tabulated are those existing outside the common xenon configuration which is:-

$$1s^2 2s^2 2p^6 3s^2 3p^6 3d^{10} 4s^2 4p^6 4d^{10} 5s^2 5p^6 6s^2.$$

(Yttrium is an exception in this respect; the appropriate structure is that of krypton.) Again notice that, while the 4f shell is filled sequentially in the tripositive ions, the same is not true for the neutral atoms. This is because the first electron in the 5d shell has a very similar energy to the 4f electrons. Indeed, lutetium may be regarded as the beginning of the 5d transition series.

Many of the rare earths show multiple valency, especially towards the beginning and end of the series, and also to some extent in the middle. In general the configurations $4f^0$, $4f^7$ and $4f^{14}$ tend to be slightly more stable than the others, so that terbium, for instance, can show quadruple valency, under modest oxidation, when it achieves the $4f^7$ configuration. Europium, on the other hand, will, under reducing conditions, form Eu^{2+} to achieve the same electronic state. However, for all elements the most stable valency is three.

1.5 The Co-ordination of the Rare Earths

The shrinkage of the ionic radius as the 4f subshell is filled (see Table 1.1), commonly referred to as the "lanthanide contraction", is largely due to the imperfect shielding from the nuclear potential of one f electron followed by another f electron. Also, since these orbitals are shielded by outer electrons in the n = 5 shell, they contribute but little to any chemical bonding (1.20). The rare earth ions are strongly electropositive, so that bonding to ligands is essentially electrostatic. The poor screening by f electrons of the nuclear charge also determines the high polarising power of these cations. Unlike the d-transition elements, the rare earths show a gradual monotonic variation in ionic radii (which totals about 20%) for ions in six-fold co-ordination (1.21). This variation in ionic size influences both the co-ordination number and the geometry of rare earth bonding (1.22).

The rare earth silicates, borates and phosphates tend to have structures in which the rare earth cation is surrounded by the appropriate polyhedra of $(MO_x)^{n-}$, where M = Si, P or B, and x, n are defined by the stoichiometry of the polyhedra. It is reasonable to assume that a similar situation pertains in glasses (1.23).

The oxygen co-ordination around a rare earth cation is chiefly controlled by the principle of achieving as much spherical shielding as may be allowed by the repulsive forces between the co-ordinating oxygens and by the degree of distortion possible in, for example, $(SiO_4)^{4-}$ tetrahedra. Thus the co-ordination number of rare earth cations is determined by the size of the ion and the geometrical quality of the ligand polyhedra.

Co-ordination numbers observed in crystalline rare earth silicate

structures vary from six to nine for trivalent cations (1.22). The variation in rare earth-oxygen distances is quite large, since all coordinating oxygens in the first shell around the rare earth ion do not represent totally independent spheres. They are usually part of relatively rigid units, such as $(SiO_4)^{4-}$ or $(Si_2O_7)^{6-}$.

1.6 The Nature of the Rare Earth Ion Site in Glass

The structural role of rare earth oxides in glass is basically the same, since they are all glass modifier oxides. This is clear not only from the similarity of the properties of these oxides in glasses to those in various crystalline matrices, but also from the analogy with various rare earth silicates. Work by Toropov et al (1.24) indicates that most rare earth silicates are of a quasi-olivine structure.

Kan Fu-Hsi et al (1.25) show that it is impossible for the rare earth ions, Ln^{3+}, to replace Si^{4+} in the frame structure of silicate glasses, and that, in fact, the trivalent ion remains in the interspace between silicon-oxygen tetrahedra. It was found impossible to obtain glasses in the Ln_2O_3 - SiO_2 system, even with rapid cooling, implying that the rare earth ions must block the connection between the tetrahedra.

The addition of Al_2O_3 produced more stable glasses, showing that the rare earth ions have a totally different function from that of Al^{3+} ions. Al_2O_3 is an intermediate oxide and enters into the structural network of the glass.

Since a glass is lacking in any long-range order, it is reasonable to assume that a dopant ion will affect only its immediate surroundings (1.26). The strong electropositivity of a rare earth ion affects its

immediate anionic environment, but any long-range effect is greatly reduced by shielding produced by the electrons of the ligands. Thus, while the cation may be expected to produce some degree of local ordering, this will not extend beyond the first few neighbours. In addition, the near surroundings of all rare earth ions will not vary significantly from one site to another, and all sites will have a definite micro-symmetry.

Previous workers (1.27) have assumed a model for the lanthanide ion site in oxide glasses where the average cation environment approximates to the appropriate site(s) in the equivalent rare earth sesquioxide. Mann (1.28) showed that the energy levels of Nd^{3+} in silicate glasses have a close correlation with those in oxide crystals, and concludes that the ions occupy sites of low symmetry.

Rice and DeSchazer (1.27) compare the absorption and fluorescence of Eu^{3+} ions in borosilicate glass with spectra of Eu^{3+} in single crystals of Gd_2O_3. Certain absorption lines of Eu^{3+} in Gd_2O_3 (for instance, the $^7F_0$ to $^5D_2$ transition) reveal a group of three lines. This, it is argued, implies that there are three preferential sites for Eu^{3+}, which agrees with the three sites in europium sesquioxide (which has point group symmetry C_3). A similar situation arises in europium doped glasses. By direct comparison, Hunt (1.29) has suggested three sites for the Gd^{3+} ion in glass as Gd_2O_3 has three sites for the Gd^{3+} ion, since it also crystallises in the monoclinic system.

Neodymium sesquioxide has trigonal symmetry, so that Mann and DeSchazer (1.30) reason that the Nd^{3+} ion in glass has only one average environment. Snitzer (1.31) has, in fact, proposed a distorted icosahedral site symmetry for Nd^{3+} ions in alkali-alkali earth-silicate

TABLE 1.2

Structures of the Lanthanide Sesquioxides (Ln_2O_3).
After Goldschmidt et al (1925)

Lanthanide	Structure Types Known*		
(Y)			C
La	A		
Ce	A		C
Pr	A	B	C
Nd	A		
Pm		---	
Sm	A	B	C
Eu		B	C
Gd		B	C
Tb		B	C
Dy		B (?)	C
Ho			C
Er			C
Tm			C
Yb			C
Lu			C

* A = hexagonal type; B = monoclinic type; C = cubic type.

Where an oxide has several possible structures, the temperature at which the crystal type is stable increases in the order C < B < A.

glasses.

The appropriate crystal structure for the sesquioxide is, however, difficult to choose, as most show several temperature modifications. Whether the high temperature structure form is "frozen in" as the glass cools, or whether the low temperature structure form develops is decided by rigidity of the structural group.

Goldschmidt et al (1.32) showed that there are three main polymorphic groups for rare earth oxides, hexagonal or A-type, monoclinic or B-type and cubic or C-type. These structures are listed for the corresponding rare earths in Table 1.2.

Terbium oxide is usually supplied after having been ignited in air to give a compound with the nominal formula, Tb_4O_7. However, it has been shown (1.33) that careful measurement reveals the stoichiometry to be $TbO_{1.76}$.

Measurements of the partial pressure of oxygen above terbium oxide (1.34) show that there are actually three stable oxides of terbium : $TbO_{1.5}$ (the sesquioxide) which has a body centered cubic structure, $TbO_{1.71}$ with a trigonal (rhombohedral) structure, and $TbO_{1.81}$ with a face centered cubic (CaF_2 type) lattice. It is believed that the approximate compound, Tb_4O_7, is formed when $TbO_{1.71}$ is cooled slowly in air. The very slow reaction rate prevents oxidation all the way to $TbO_{1.81}$.

It has been shown by Hubbert-Paletta et al (1.35) that Tb_4O_7, when melted with MgO, is converted to the sesquioxide Tb_2O_3. It is believed that a similar event takes place in glass melts, especially where such melts are performed in moderately reducing conditions.

Hence the appropriate oxide structure to consider is that of Tb_2O_3. This is usually of the C-type (cubic), although there is a B-type (monoclinic) crystal form at high temperatures. Thus, the most likely approximation at this stage is that the terbium ion environment in oxide glasses is similar to C-type Tb_2O_3.

It is worth noting that the degree of reorganisation a cubic environment about Tb^{3+} ions would require is likely to be small, as many rare earth glass systems crystallise in the cubic system. For instance, SiO_2:Tb crystallises, in one form, as crystobalite (f c c lattice) (1.36). Cubic lattices are, however, by no means predominant.

In rare earth oxides which crystallise in the cubic form, Ln^{3+} is located in a hexahedron (co-ordination number = 6) and the interspace of the cubic unit cell occupies nearly 30% of the whole space (1.37).

In silicate crystals a part of the interspace in the cube is occupied by silicon-oxygen tetrahedra so as to make the structure compact. In silicate glasses the rare earth ions fill up the network interspace framed by silicon-oxygen tetrahedra with co-ordination number 6 to 8, making the structure even more compact.

Little use has been made of optical spectra, interpreted by ligand field theory, to describe rare earth ion sites in glass. This is due, in the main, to the amorphous nature of these materials which makes the application of symmetry concepts seem impracticable. However, due to the similarity between properties of rare earth doped crystals and glasses, the optical properties of lanthanide glasses may be explained in terms similar to those used for impure crystals. The principal difference is that the amorphous disorder produces a perturbation on

the average site, which leads to inhomogeneous broadening.

In principle, the site symmetry can be deduced from group theoretical considerations applied to the emission and absorption spectra. However, the number of Stark levels into which the free ion energy levels are split is often quite large, and they are confused by the glassy broadening.

Wybourne (1.38) shows that optical transitions of rare earth ions in a medium are largely electric dipole in character. In a free ion, electric dipole transitions between states of the same configuration (as in intra-f^n transitions) are forbidden by the parity rule. Hence, the observed spectra in condensed matter result from non-centrosymmetric interactions leading to a mixing of opposite parity states.

Reisfeld et al (1.39, 1.40, 1.41) have used the fluorescence of Eu^{3+} ions as an indicator of site symmetry of rare earth ions in glass. They show that there is a slight change in frequency of the luminescence emission bands of order a few cm^{-1} when changing from phosphate to silicate to germanate glasses, from which it is shown that the asymmetric part of the "crystalline" field is greater in the order:germanate > silicate > phosphate.

Magnetic dipole transitions may take place only between states of the same parity, and, hence, should not be as sensitive to the host matrix as electric dipole transitions.

By comparison of various terms in the spectra, Rice and DeSchazer (1.27) estimated the percentages due to electric and magnetic dipole transitions and deduced a C_s symmetry for Eu^{3+} ions in silicate glass. Also, the half band width for emission or absorption of Eu^{3+} is approx-

Fig 1.2 Structure of the rare earth ion site in silicate glass. After Reisfeld et al (1972)

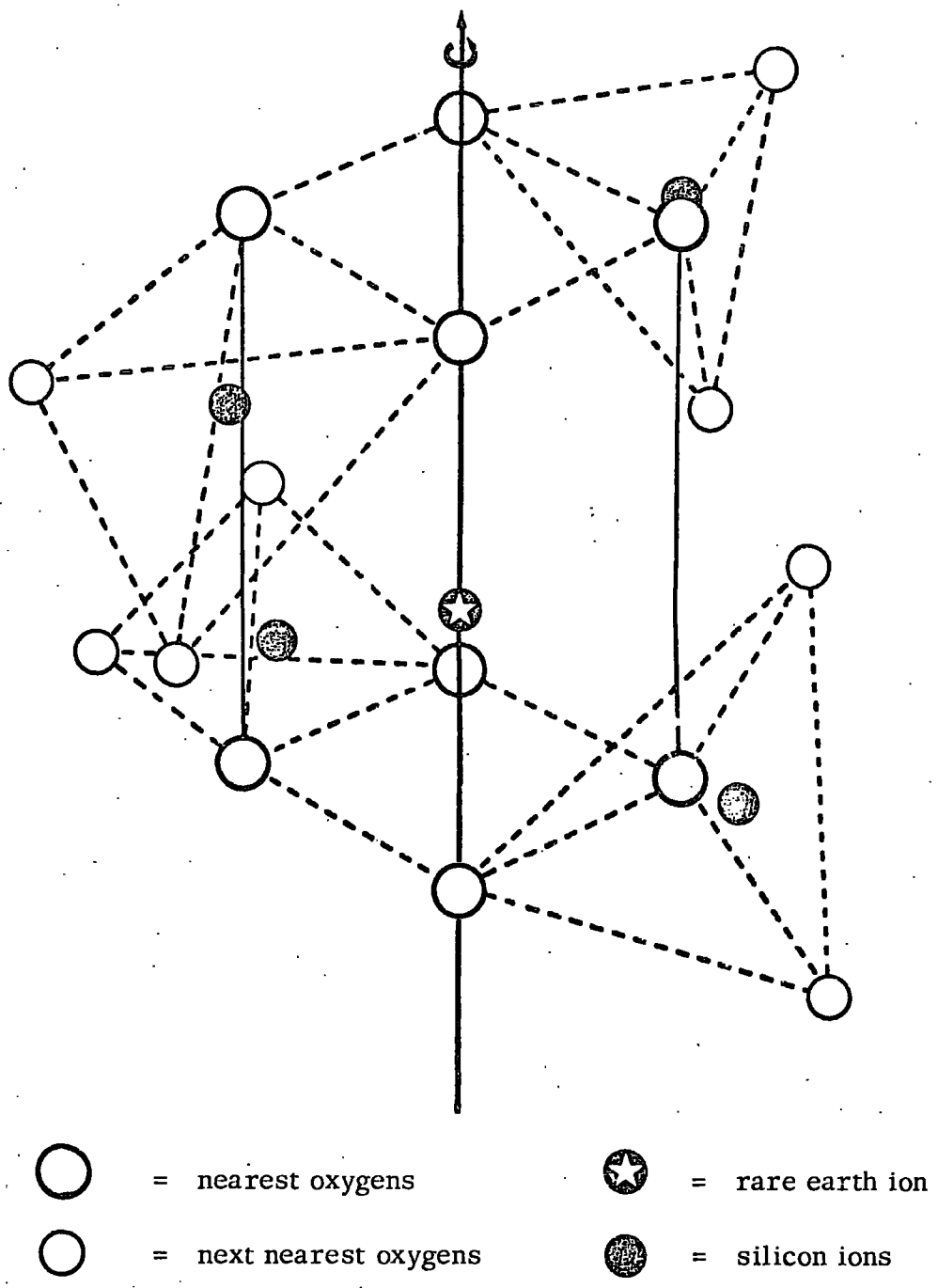

imately 75 times greater in glass than in the sesquioxide, so that there are at least this number of sites in the glass. Slight differences are caused by a small variation in crystal field parameters.

In a series of papers, Reisfeld et al have shown that in glasses the rare earth ion is surrounded by non-bridging oxygens of phosphate (1.39), borate (1.23), silicate (1.42) and germanate (1.41) tetrahedra. The MO_4 (M = B, P, Ge, Si) tetrahedra are relatively undistorted, since their covalent bonding strongly favours preservation of tetrahedral geometry. It should be pointed out that, while the bonding of the lanthanide ion to these tetrahedra is predominantly electrostatic, there is some degree of covalency in the cation-tetrahedron bonding. The relative positions of the tetrahedra are still free to change in relation to the cation.

Reisfeld and Eckstein (1.23) propose that the rare earth ion in glass is co-ordinated by four MO_4 tetrahedra; each tetrahedron contributes two oxygens to the co-ordination with the rare earth. The overall co-ordination is eight, which is the most typical co-ordination for Ln^{3+} in oxidic environments.

Accordingly, Ln^{3+} occupies the centre of a distorted cube of four tetrahedra; two oxygens produce each edge of the cube, see Figure 1.2.

Site differences are shown to arise from the existence of non-uniform, non-identical ligand fields caused by small differences in rare earth-oxygen distances.

Actual symmetries are found to be C_s for Eu^{3+} in phosphate glass (1.39), and C_2 for Tm^{3+} in phosphate and borate glasses (1.23). That is to say, the symmetry is lower than simple cubic, so that forced electric dipole transitions become possible, and absorption and fluorescence

are observed.

1.7 Rare Earth Spectra

The optical spectra of rare earth ions in various media display modifications in energy level structure caused by the electrostatic "crystal" field. In order to estimate the effect of this, one must compare the results in the various media with those for the free ion, not subject to any external fields. However, as the free ion levels seem to be largely unknown empirically, this direct procedure is only possible in a few cases (1,43).

The spectra in condensed materials usually consist of transitions between levels of the $4f^n$ configuration, which are forbidden, with oscillator strengths of order 10^{-6}. Other low energy configurations are $4f^{n-1}5d$, $4f^{n-1}6s$ and $4f^{n-1}6p$, and in the fourth spectra (i.e., those due to Ln^{3+}) their energy is always in this order (1,44). The lines originating from transitions between two configurations are not always easy to observe and may spread over a very wide spectral region.

For the majority of trivalent rare earths, only the intra-$4f^n$ and the 4f-5d transitions lie at wavelengths longer than the vacuum ultraviolet. The separation of these configurations is always large relative to the divalent lanthanides (Ln^{2+}). Thus, the degree of configurational mixing is small, which results in the sharp line spectra observed. In a perfect crystal the natural line width of intra-$4f^n$ transitions is less than 10^{-3} cm^{-1} at low temperatures (1,45).

Because of the large number of representative wave functions for each configuration, especially near the centre of the lanthanide series,

energy level calculations are far from complete. Systematic methods developed by Racah (1.46) have simplified the calculations considerably, so that they are now complete in all cases, at least for the lower lying levels ($<40,000\,cm^{-1}$).

Comparison between these computed levels and those reported in crystals is quite good, especially for the lower lying levels, as here the shift in levels produced by the crystal field is usually less than their spacing. This is a result of the shielding of the 4f electrons by the outer filled orbitals, with which there is no considerable wave function overlap.

This comparison has allowed the identification of many of the energy levels observed in crystals and other media, so that the correlation is now likely to be permanently accepted for all levels below $20,000\,cm^{-1}$. With the exception of Pm^{3+} and the $^6F_{\frac{1}{2}}$ level of Dy^{3+}, all levels predicted by theory have been observed in this region.

The observed energy levels of Ln^{3+} ions in $LaCl_3$ are shown diagrammatically in Figure 1.3, after Dieke et al (1.44). The thickness of each level is meant to represent the total crystal field splitting. The levels where known are identified in Table 1.3. This table also indicates the known luminescence levels. These levels have not been observed to differ in any significant respect for lanthanides in other media.

Some transitions between the various $4f^n$ configurations are forbidden in the free ion by the parity rule for electric dipole transitions. In a crystal or glass, forced electric transitions become allowed as a consequence of the coupling of odd electronic wave functions due to the

Figure 1.3 Schematic representation of the energy levels of the triply charged lanthanide ions in $LaCl_3$. After Dieke et al (1961).

indicates fluorescent levels

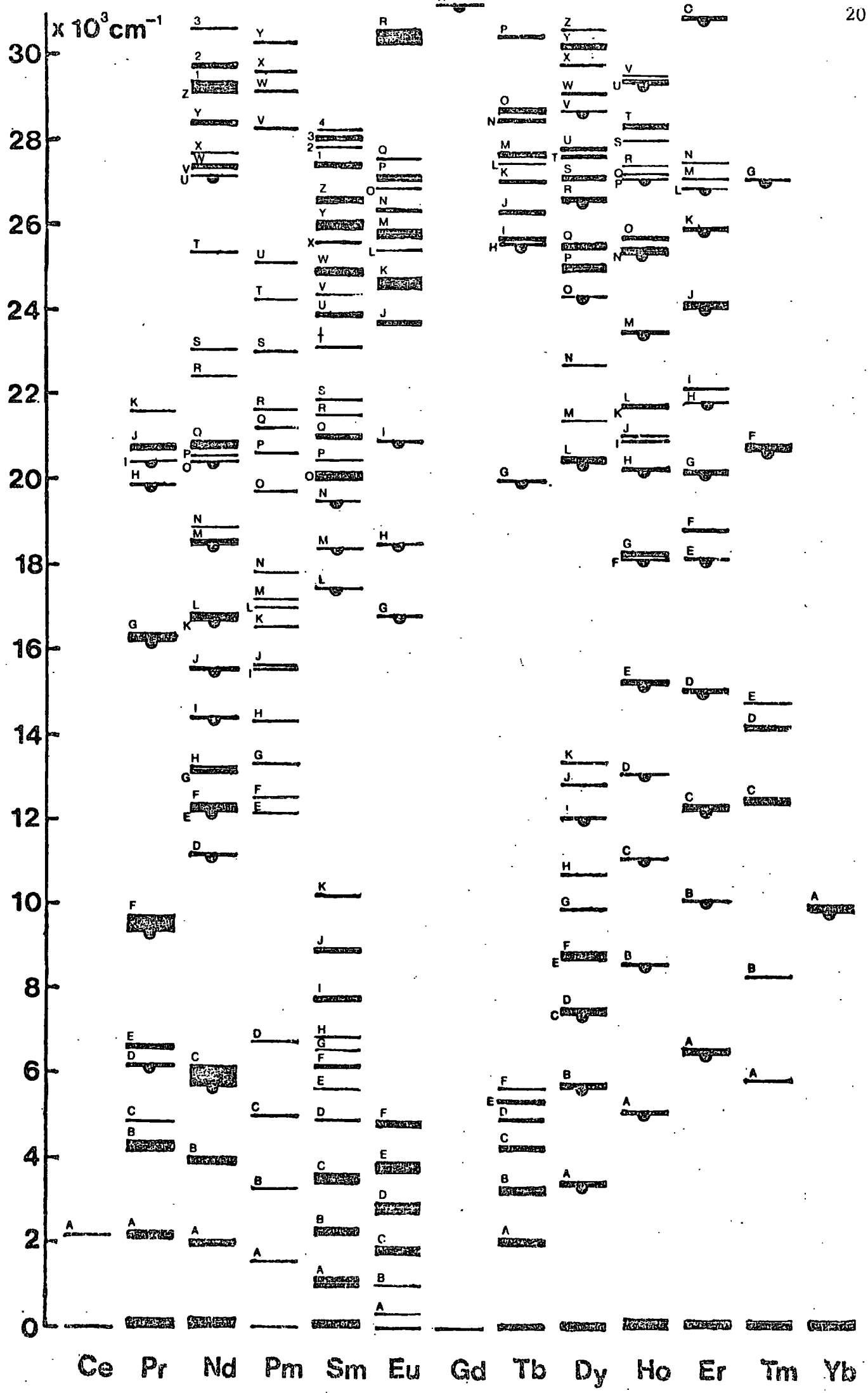
x 10³cm⁻¹
30
28
26
24
22
20
18
16
14
12
10
8
6
4
2
0
Ce
Pr
Nd
Pm
Sm
Eu
Gd
Tb
Dy
Ho
Er
Tm
Yb

TABLE 1.3

Spectroscopic Notation and Fluorescence Levels of the Trivalent Rare Earths (after Dieke)

Ion	Ce^{3+}	Pr^{3+}	Nd^{3+}	Pm^{3+}	Sm^{3+}	Eu^{3+}	Gd^{3+}	Tb^{3+}	Dy^{3+}	Ho^{3+}	Er^{3+}	Tm^{3+}	Yb^{3+}
Ground State	$^2F_{5/2}$	$^3H_4$	$^4I_{9/2}$	$^5I_4$	$^6H_{5/2}$	$^7F_0$	$^8S_{7/2}$	$^7F_6$	$^6H_{15/2}$	$^5I_8$	$^4I_{15/2}$	$^3H_6$	$^2F_{7/2}$
Level A	$^2F_{7/2}$	$^3H_5$	$^4I_{11/2}$	$^5I_5$	$^6H_{7/2}$	$^7F_1$	$^6P_{7/2}$	$^7F_5$	$^6H_{13/2}$	$^5I_7$	$^4I_{13/2}$	$^3H_4$	$^2F_{5/2}$
Level B		$^3H_6$	$^4I_{13/2}$	$^5I_6$	$^6H_{9/2}$	$^7F_2$		$^7F_4$	$^6H_{11/2}$	$^5I_6$	$^4I_{11/2}$	$^3H_5$	
Level C		$^3F_2$	$^4I_{15/2}$	$^5I_7$	$^6H_{11/2}$	$^7F_3$		$^7F_3$	$^6H_{9/2}$	$^5I_5$	$^4I_{9/2}$	$^3F_4$	
Level D		$^3F_3$	$^4F_{3/2}$	$^5I_8$	$^6H_{13/2}$	$^7F_4$		$^7F_2$	$^6F_{11/2}$	$^5I_4$	$^4F_{9/2}$	$^3F_3$	
Level E		$^3F_4$	$^4F_{5/2}$	$^5F_1$	$^6F_{1/2}$	$^7F_5$		$^7F_1$	$^6H_{7/2}$	$^5F_5$	$^4S_{3/2}$	$^3F_2$	

Table 1.3 (Continued)

Level F		$^1G_4$	$^2H_{9/2}$	$^5F_2$	$^6F_{3/2}$	$^7F_6$		$^7F_0$	$^6F_{9/2}$	$^5S_2$	$^2H_{11/2}$	$^1G_4$	
Level G		$^1D_2$	$^4F_{7/2}$	$^5F_3$	$^6H_{15/2}$	$^5D_0$		$^5D_4$	$^6H_{5/2}$	$^5F_4$	$^4F_{7/2}$	$^1D_2$	
Level H		$^3P_0$	$^4S_{3/2}$	$^5S_2$	$^6F_{5/2}$	$^5D_1$		$^5D_3$	$^6F_{7/2}$	$^5F_3$	$^4F_{5/2}$		
Level I		$^3P_1$	$^4F_{9/2}$	$^5F_4$	$^6F_{7/2}$	$^5D_2$		$^5L_{10}$	$^6F_{5/2}$	$^5F_2$	$^4F_{3/2}$		
Level J		$^1I_6$	$^2H_{11/2}$	$^3K_6$	$^6F_{9/2}$	$^5D_3$		.	$^6F_{3/2}$	$^3K_8$	$^2H_{9/2}$		
Level K		$^3P_2$	$^4G_{5/2}$	$^5F_5$	$^6F_{11/2}$	.		.	$^6F_{1/2}$	$^5G_6$	$^4G_{11/2}$		
Level L			$^2G_{7/2}$	$^3K_7$	$^4G_{5/2}$	.		$^5D_2$	$^4F_{9/2}$	$^5F_1$	$^2G_{9/2}$		

Table 1.3 (Continued)

Level M			$^4G_{7/2}$	$^3H_4$	$^4F_{3/2}$	.		.	$^4I_{15/2}$	$^5G_5$	$^2K_{15/2}$			
Level N			$^2G_{9/2}$	$^5G_2$	$^4G_{7/2}$	.		.	$^4G_{11/2}$	$^5G_4$	$^2G_{7/2}$			
Level O			$^4G_{9/2}$	$^5G_3$	$^4I_{9/2}$	$^5D_4$		.	.	$^3K_7$	$^2P_{3/2}$			
Level P			$^2D_{3/2}$	$^5G_4$	$^4I_{11/2}$	.		.	.	$^3H_5$				
Level Q			$^4G_{11/2}$	$^3G_3$	$^4I_{13/2}$	.			.	$^3H_6$				
Level R			$^2P_{1/2}$	$^3D_2$	$^4F_{5/2}$	.			.	$^5G_2$				
Level S			$^2D_{5/2}$	$^5G_5$	$^4G_{9/2}$				.	$^5G_3$				

Table 1.3 (Continued)

Level T			$^2P_{3/2}$	$^3L_8$	$^6P_{5/2}$				·	$^3L_9$			
Level U			$^4D_{3/2}$	$^3P_0$	·				·	·			
Level V			$^2I_{11/2}$	$^1D_2$	·				·	·			
Level W			$^4D_{5/2}$	$^3F_2$	·				·				
Level X			$^4D_{1/2}$	$^5D_0$	·				·				
Level Y			$^2L_{15/2}$	$^5D_1$	·				·				
Level Z			$^4D_{7/2}$		·				·				

Table 1.3 (Continued)

Level 1			$^2I_{13/2}$		.								
Level 2			$^2L_{17/2}$		.								
Level 3			$^2H_{9/2}$		.								
Level 4					.								

= fluorescent level

odd parity terms in the crystal field expansion (1.47).

The positions of absorption bands of Ln^{3+} ions in glass are essentially similar to those observed in crystals and solutions. However, as a result of the increase of covalent bonding in glass, the effect of the glass base on the absorption spectra is somewhat intensified. Greatest effects are seen for anion groups with highest polarisation capabilities (1.37).

At this stage it would be instructive to discuss the principal features of the fourth terbium spectrum. The calculations have been performed by Judd (1.48) and Ofelt (1.49). The treatment is semi-empirical, using fitting parameters obtained by experiment. The agreement is quite good up to 27,000 cm^{-1}. The discussion is best achieved by dividing the band scheme of Figure 1.3 into three parts, plus one other division not shown in the diagram.

(1) The ground state multiplet (ground state plus levels A to F). Tb^{3+} has a ground state electronic configuration of $4f^8$. The electron spins are aligned according to Hund's rules to give seven electrons "spin-up" and one electron "spin-down". The resultant total spin is:-

$$S = \sum_i s_i = 3$$

(the sum is taken vectorially)

The angular momenta also couple to give a total angular momentum quantum number, L = 3.

Then $J_{max} = L + S = 6$, and the ground state multiplet, $^{(2S+1)}L_J$, is ^7F_J (J = 0, 1, 2, 3, 4, 5, 6).

The ground state is $^7F_6$, and the other levels are spread out in

order of decreasing J to about 6,000 cm^{-1}.

(2) The luminescent levels (levels G, H).

The next two levels above the ground state are interpreted as $^5D_4$ at about 20,000 cm^{-1}, and $^5D_3$ at about 26,000 cm^{-1}. These levels are metastable, having lifetimes of the order of a few milliseconds. The luminescence results from transitions from both of these levels to the seven levels of the ground state multiplet. Thus, the characteristic emission from Tb^{3+} ions consists of 14 bands in the visible spectrum.

Sometimes not all these bands are observed because of partial overlap between the two emission regions and also because of the low emission intensities of transitions to the higher energy levels of the ground state multiplet.

(3) Higher $4f^8$ levels (levels I onwards).

The intra-$4f^n$ configuration levels extend to above 150,000 cm^{-1} in the case of Tb^{3+}, and there are a total of 198 levels. Identification of levels above 26,000 cm^{-1} is complicated by the small separation of a large number of levels. Absorption spectra data are often lacking because:-

(a) the absorption edge of the medium containing the ions is often in the near ultra-violet;

(b) the oscillator strengths are quite low (of order 10^{-6} and less);

(c) the shifts in the peaks of the absorption due to crystal field effects are often comparable with the level separations.

Very little is known of intra-$4f^n$ spectra above 40,000 cm^{-1}.

(4) Transitions from $4f^n$ to higher order configurations.

Reisfeld et al (1,50) in their investigations of excitation spectra of rare

earths showed that there are strong excitation bands for Eu^{3+} and Tb^{3+} emission which cannot be explained by intra-$4f^n$ transitions. For europium this is believed to be due to charge transfer processes, but for terbium it is due to a 4f-5d transition (1.51). Tb^{3+} has been shown to have the lowest 4f-5d excitation energy and the highest charge transfer energy among all the trivalent rare earths (1.52).

The $4f^7 5d$ configuration for Tb^{3+} lies in the region 40,000 to 50,000 cm^{-1} in both oxide and fluoride crystals (1.53). Further transitions are believed to occur above 60,000 cm^{-1}.

Blasse and Bril (1.54) report excitation bands in oxidic phosphors containing Tb^{3+} ions at 220-230nm, which they attribute to a ^7F to ^7D transition, and also a weaker band at 260-270nm attributed to the spin-forbidden ^7F to ^9D transition.

Shionoya and Nakazawa (1.55) show that, whereas f-f transition probabilities of Tb^{3+} ions in $Ca(PO_3)_2$ glass are of the order 10^{-7}, for f-d transitions they are of the order 10^{-2}. For this reason it is believed that these transitions are very important in the luminescence of Tb^{3+} ions.

1.8 Spectra in Glass

Glass is not in a state of thermodynamic equilibrium, since its free energy is higher than that of its crystalline counterpart. A glass of given composition can exist in different energy states depending on its structure (1.56).

The properties of a glass are dependent upon the different energy states it may assume as a result of its thermal history. The structural state is a function of the rate of cooling and determines such properties

as density (and hence refractive index).

Because of the lack of periodicity in the structure of glasses, luminescence centres find themselves in a variety of energetically different environments. This leads to a broadening of the luminescence bands relative to similar emission centres in crystals or vapours.

Some ions in glass give rise to luminescence which is influenced by the anisotropy of the surrounding binding forces. Thus, it is of interest to observe the changes in luminescence as a function of changes in the host glass composition.

In the case of the rare earth ions, luminescence results from the inner 4f electrons, and changes in the structure and composition of the glass host do not lead to large changes in the emission characteristics. This is in contrast to the situation in the transition metal series, where considerable changes in spectra may be produced by the effect of the glass environment (1.57). Conversely, it should be noted that the transition metals produce larger rearrangements of the glass micro-structure. Consequently their use as probes into glass structure is correspondingly limited (1.58).

Luminescent centres due to structural impurities do not arise in glasses. No matter what is put into a glass (at least in small quantities), it can be incorporated into the glass structure by suitable rearrangements of the local ionic environment (1.59). Many glasses have an absorption edge in the near ultra-violet region of the spectrum (say 250 to 350nm). This can affect the excitation spectra of luminescent centres by providing competition for absorbed photons. For instance, the absorption edge of silicate glasses is shifted to higher wavelengths by the addition

of alkali or alkali-earth metal oxides. Fused silica transmits reasonably well, down as far as 200 nm, but incorporation of only moderate amounts of sodium or potassium into the glass gives large absorption coefficients up to 300 nm. Any excitation processes due to absorption in this region are likely to be reduced by the addition of Na_2O or K_2O to the glass, especially where there is little transfer of energy between the matrix and the luminescent bands.

CHAPTER 2

THEORETICAL CONSIDERATIONS

2.1 Luminescence Theory

2.1.1 Definitions

The term "luminescence" is defined by Curie (2.1) as luminous emission which is not purely thermal in origin. There is some confusion between the terms "fluorescence" and "phosphorescence"; here we adopt the definitions given by J and F Perrin (2.2).

The phenomenon is fluorescence if the emission takes place by one or more spontaneous transitions. If, on the contrary, the emission occurs with the intervention of a metastable state followed by a return to the excited state due to addition of energy, this is phosphorescence.

Phosphorescence, then, involves a metastable state from which energy cannot be released by a direct transition to the ground state.

Lifetimes of excited states are usually of the order 10^{-8} s for atomic dipole emission, so that this is a typical lifetime of a state in fluorescence. In phosphorescence the lifetime is dependent on the much more lengthy process of excitation from the metastable level and, since this is usually of a thermal nature, the lifetime, τ, is generally of the form

$$\frac{1}{\tau} = b \exp\left(-\frac{E}{kT}\right) \qquad (2.1)$$

where b is a constant, k is Boltzmann's contant, and E is the energy difference between the metastable and excited states.

Such lifetimes are often longer than a second.

For intermediate durations, say 10^{-1} to 10^{-5} s, it is difficult to distinguish, on evidence of luminescence decay alone, between a long fluorescence due to "forbidden" transitions and a short phosphorescence due to very shallow traps. However, since fluorescent lifetimes are almost temperature independent at room temperature, and phosphorescence lifetimes are very strongly temperature dependent, the two phenomena can easily be distinguished.

F Perrin also showed that, in fluorescence, the lifetime, τ, of fluorescence is generally of the form shown in Figure 2.1, and that the efficiency, η, of the fluorescence also shows a similar temperature dependence. Such behaviour can best be explained by a competition between radiative transitions, with a probability, p_r, which is essentially temperature independent, and non-radiative transitions, due to thermal de-excitation by the matrix, with a probability, p_{nr}, which increases with temperature.

Hence,

$$\frac{1}{\tau} = p_r + p_{nr} \qquad (2.2)$$

This thermal de-excitation will decrease the observed lifetime of the state at temperatures where p_{nr} is significant compared with p_n.

In general, if $\tau = \tau(T)$ and $\eta = \eta(T)$, then:-

$$\frac{\tau(T)}{\tau(O)} = \frac{\eta(T)}{\eta(O)} \qquad (2.3)$$

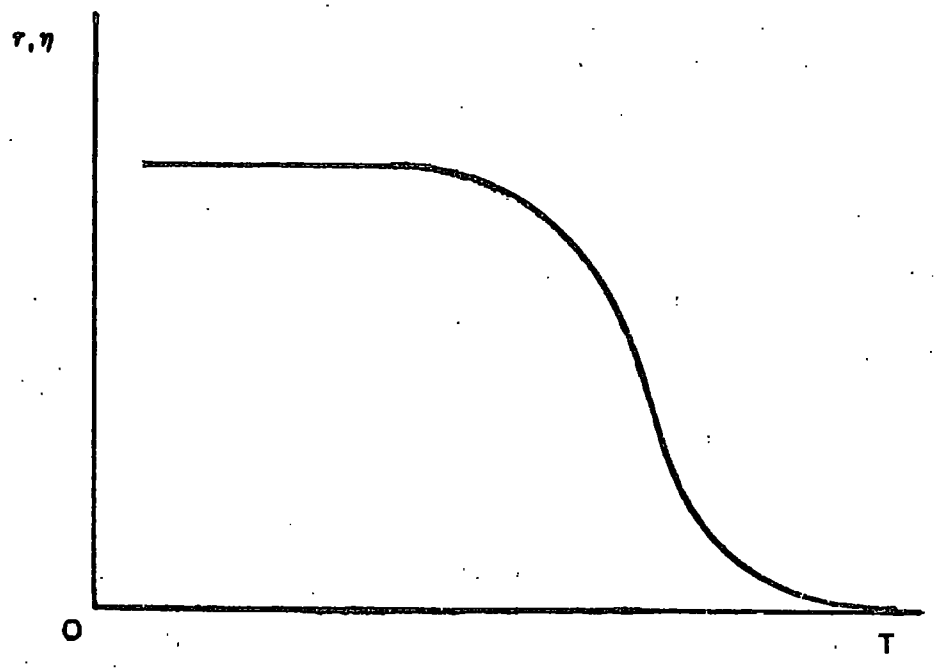

Fig 2.1 Lifetimes, τ, and efficiencies, η, as a function of temperature

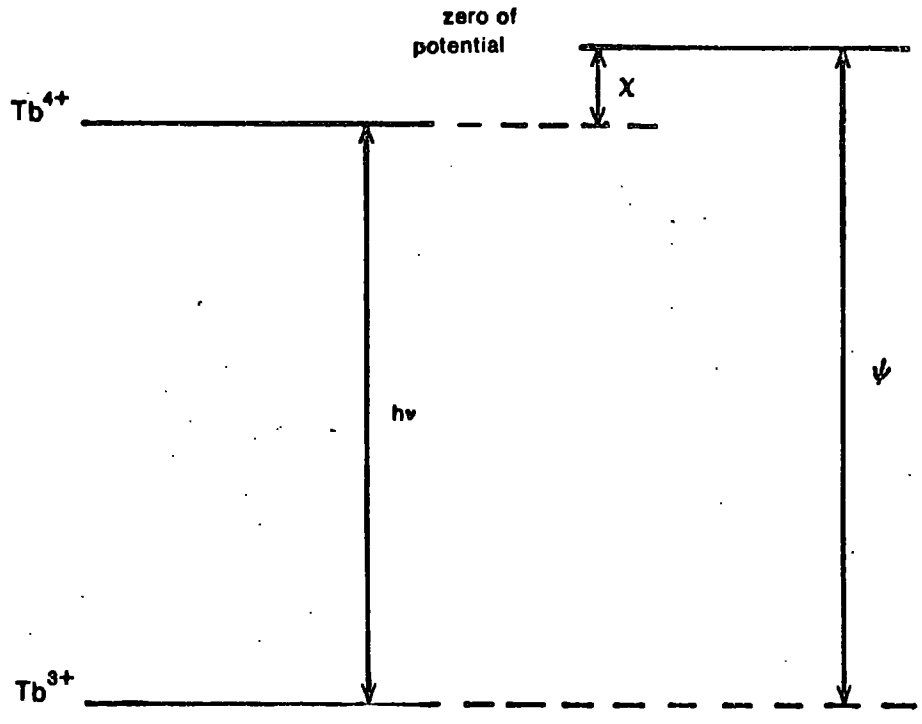

Fig 2.2 System of potentials of terbium ions in solids

2.1.2 Radiative Transitions

It is useful in discussing luminescent phenomena to consider some elementary theory of multipole radiation. In general, the probability of emission for various multipole orders falls off by a factor of roughly $\left(\frac{a}{\lambda}\right)^2$ for each successive order; where a is the dimension of the source and λ is the wavelength emitted. In the visible region of the spectrum:-

$$\frac{a}{\lambda} \simeq 2 \times 10^{-6}$$

so that quadrupole emissions are quite weak compared with dipole emissions. It should be noted that this argument only applies to radiative transitions between electron energy levels and does not apply to energy transfer processes where the transitions are non-radiative.

Electric dipole transitions have lifetimes of order 10^{-8} to 10^{-7} s, whereas magnetic dipole transitions decay after 10^{-3} to 10^{-1} s. Higher order transitions last even longer.

When multipolar emissions result from transitions between different electronic configurations they are subject to the following selection rules, expressed in terms of the total angular momentum operator J:-

Dipole emission $\Delta J = 0, \pm 1$

Quadrupole emission $\Delta J = 0, \pm 1, \pm 2$

The multipolar characteristic is, to some extent, influenced by the presence or absence of a parity change involved in the electron transition. Electric dipole emission requires a parity change, whilst electric quadrupole and magnetic dipole emission requires that there be no change in parity. If the parity remains constant, then magnetic dipole emission usually predominates. In crystals, the parity of

electron eigenfunctions is partly mixed with parity states arising from the ligands.

Transitions between electron states of different multiplicities, for instance between triplet and singlet states, where the symmetry of the spatial wave functions differ, are "forbidden". This condition is partially lifted by the spin-orbit interaction, especially in ions of high atomic number.

2.1.3 Configuration Co-ordinates

Luminescent spectra differ from free ion spectra in that they consist of much wider bands (of order $100\,cm^{-1}$ for rare earth ions in glass) and the emission is usually shifted, to some extent, to longer wavelengths (the Stokes' shift). Both phenomena are a result of interaction between the luminescent ion and the containing matrix.

The interaction is usually represented by means of the configurational co-ordinate model, which represents the interaction by means of a single configurational co-ordinate involving (and as a first approximation equalling) the average distance between the luminescent centre and its ligands. This has been extensively used in the study of KCl:Tl luminophors (2.3).

The transition of an electron from the valence band to the conduction band corresponds to a further oxidation of the Ln^{3+} ion to Ln^{4+}. If we take the zero of potential as the electron at infinite distance from the matrix, the energy positions of the levels due to Ln^{3+} and Ln^{4+} can be written as ψ and χ respectively (Fig 2.2).

χ is the electron affinity of the material, it is the work required to remove an electron from the bottom of the conduction band to the

zero of potential. ψ is the separation energy : the work done in removing an electron from the top of the valence band to the zero potential.

The width of the forbidden energy gap is:-

$$h\nu = \psi - \chi \qquad (2.4)$$

and corresponds to the absorption edge which, for rare earths, is in the ultra-violet. This "cut-off" is usually beyond the limit for absorption by the matrix and so is not accessible experimentally.

The ionisation energy of Ln^{3+} in a material:-

$$Ln^{3+} \longrightarrow Ln^{4+} + \text{conduction electron}$$

is likely to be much less than the fourth ionisation potential of the free ion:-

$$Ln^{3+} \longrightarrow Ln^{4+} + \text{free electron}$$

(see reference 2.4).

This is because the extra charge on the ion increases the binding energy between the ion and the lattice. It is further reduced because of the different polarisabilities of lattice ions. This difference has been calculated for ionic levels in crystals (2.5), but the problem is complicated in glass by the lack of knowledge of the microstructure around the ion, and further by the inhomogeneity of different sites.

We shall see in Chapter 5 that most of the spectral width of emission lines of Ln^{3+} ions in glass is due to inhomogeneous broadening, but that some of the width is due to thermal broadening. To account for this width and also for the difference in wavelength of absorption and emission

spectra (the Stokes' shift) requires the introduction of the interaction between the ion and the glass matrix. This interaction is also responsible for the nephelauxetic effect where the absorption lines in condensed media are shifted (usually to longer wavelengths) compared with those of the free ion.

To a first approximation we can consider the Ln^{3+} ion surrounded by a number of oxygen ions vibrating about a mean distance, r, called the configurational co-ordinate. Clearly a consideration of next nearest neighbours would lead to a modification of our definition of r. Even in crystals, it is rarely possible to give a precise physical definition of r, or to calculate the configurational curves. Usually it is merely shown that a set of curves can be drawn to explain the experimental results.

The expression for the ground state describing the interaction between Ln^{3+} and 0^- is:-

$$U_g = E_R + E_{vW} + E_M + E_I \qquad (2.5)$$

and for an excited state:-

$$U_g = E'_R + E'_{vW} + E'_M + E'_I + E_C + E_e \qquad (2.6)$$

where E_R is the exchange repulsion energy,

E_{vW} is the Van der Waals attraction energy,

E_M is the Madelung electrostatic energy, and

E_I is a correction to E_{vW} for the attraction between dipoles induced on the 0^- ligands by the introduction of Ln^{3+} into the matrix.

In general, the above terms will change with the state of excitation of the Ln^{3+} ion.

For the excited state, E_C is a change in the electrostatic energy produced by overlap of charge distributions around the different ions, and E_e is the excitation energy of the upper level.

The Stokes' shift and nephelauxetic effect arise from the correction term, E_C. This results largely from the reduction of electron repulsions between ions, produced by overlap of spatial wavefunctions. The overlap of charge distributions is much higher for an excited state, which fact is largely responsible for a shift in the spatial equilibrium positions of the 0^- ligands in excited states of the Ln^{3+} ion. The change in radial displacement is typically of order a few tenths of an Ångstrom (2.6).

The curve $U_e(r)$ is generally less sharp than $U_g(r)$, corresponding to smaller vibrational quanta for ions in an excited state. The curves are drawn in terms of the parameter

$$\Delta r = r - r_o \qquad (2.7)$$

where r_o is the equilibrium distance between Ln^{3+} ions in the ground state and the ligands. Δr is used here because r_o is often unknown.

The functions, $U(\Delta r)$, are approximately quadratic in terms of Δr

$$U_{e,g}(\Delta r) = a_{e,g}(\Delta r - \Delta r_o)^2 + \text{constant} \qquad (2.8)$$

Here, Δr_o is a displacement representing the change produced in the lattice by including the luminescent ion. In glasses this term is

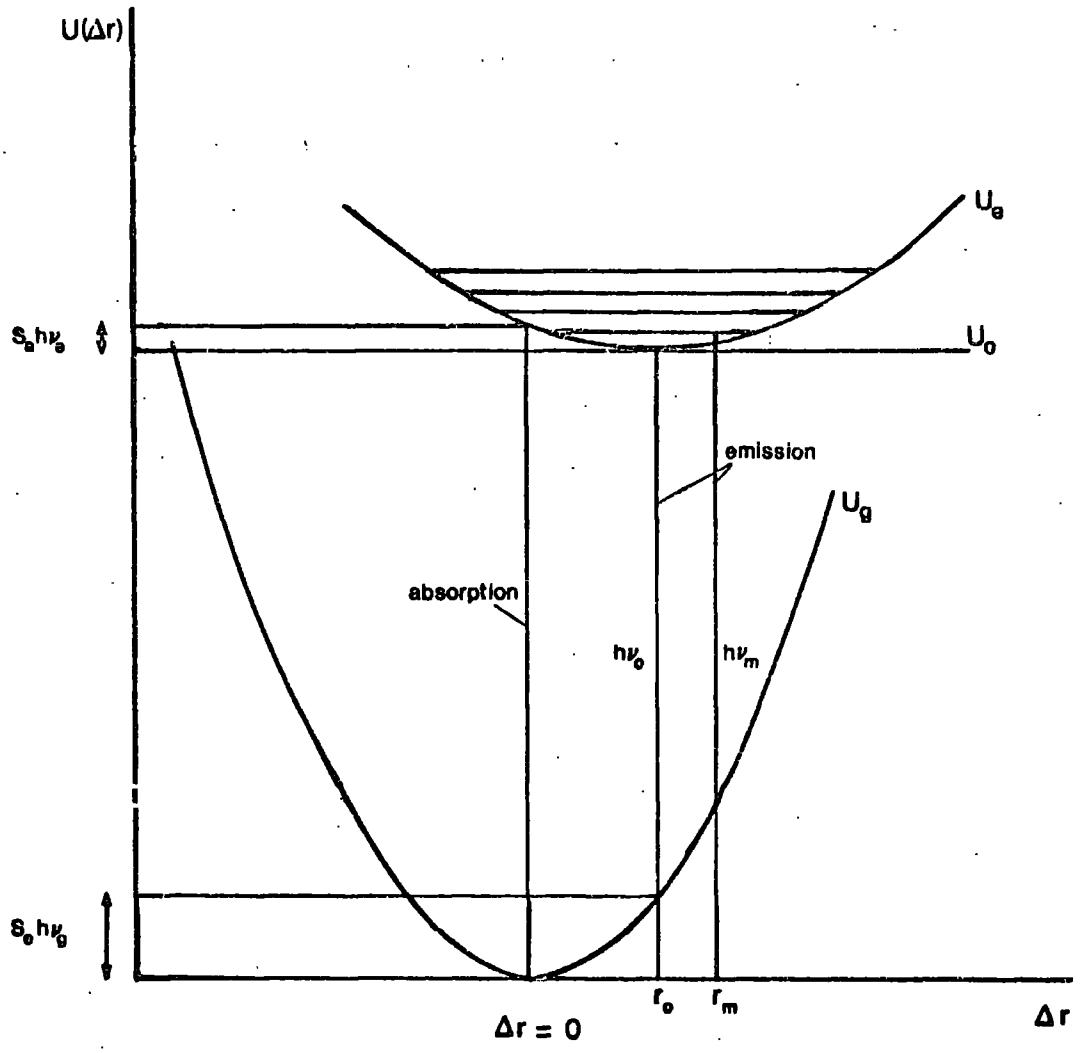

Fig 2.3 The configurational co-ordinate model of luminescence

unknown.

The general form of the configurational co-ordinate diagram is shown in Figure 2.3. We obtain the mean frequencies of absorption and emission from this diagram by calculating $h\nu = \Delta U$ for vertical transitions from the minima of each curve (i.e., using the Franck-Condon principle). The remaining energy after each transition is converted into phonons of energy, $h\upsilon_g$, for the ground state and $h\upsilon_e$ for the excited state. These give rise to vibrational levels which we denote by m for the ground state and by n for the excited state. Thus, a transition from the nth level of the excited state to the mth level of the ground state will result in emission of frequency, υ_{nm} where

$$h\upsilon_{nm} = E_{ne} - E_{mg} \tag{2.9}$$

The total emission band then results from a superposition of all such emission lines for all values of n and m.

2.1.4 Transition Probabilities and Cross-Sections

The transition probability per unit time, P, is related to the interaction Hamiltonian by

$$P = \frac{4\pi^2}{h} \left| \int \Psi_f^* H_{int} \Psi_i \, d\tau \right|^2 \rho(E) \tag{2.10}$$

where Ψ_f and Ψ_i are the final and initial electron states respectively

$H_{int} = \frac{e}{mc} \cdot \frac{h}{i} (\underline{A} \cdot \underline{\nabla})$ is the interaction Hamiltonian for an electron in an electromagnetic field; $\underline{A}$ is the vector potential $\Box \underline{A} = 4\pi \underline{j}$

and $\rho(E)$ is the density of oscillator states for the photons of energy, $h\upsilon$, in the volume, V

$$\rho(E)dE = V\frac{8\pi\upsilon^2}{c^3}\,d\upsilon \qquad (2.11)$$

The solution of this expression is quite complicated, so here we give only an outline of the results (2.1).

If we assume a constant vector potential, $\underline{A}$, at all points within the source of charge, then we obtain matrix elements of the form

$$\frac{\hbar}{i}\int[\psi_f^* - \psi_i]\,d\tau = m\frac{d}{dt}\int\psi_f^*\,\underline{r}\,\psi_i\,d\tau \qquad (2.12)$$

where $\psi_f(r)$ and $\psi_i(r)$ are eigenfunctions of the electron co-ordinates.

Also we can obtain matrix elements for the electric dipole moment:-

$$\underline{\mu}_{if} = e\underline{r}_{if}$$

$$= e\int\psi_f^*\,\underline{r}\,\psi_i\,d\tau \qquad (2.13)$$

Then the probability per second of an interaction with the photon flux is:-

$$P = M\frac{64\pi^4\upsilon^3}{3hc^3}\left|\underline{\mu}_{if}\right|^2 \qquad (2.14)$$

where M = N + 1 for emission

= N for absorption

and N is the mean number of photons.

So the emission intensity per second from the ion is:-

$$I(h\upsilon) = \frac{64\pi^4\upsilon^4}{3c^2}\left|\underline{\mu}_{if}\right|^2 \qquad (2.15)$$

The photon flux per second is:-

$$S = cN \frac{8\pi\upsilon^2}{c^3} d\upsilon \qquad (2.16)$$

Dividing equation 2.14 by equation 2.16 gives the effective absorption cross-section:-

$$\sigma(\upsilon) = \frac{P_{abs}}{S} = \frac{8\pi^3\upsilon}{3hc} \left|\underline{\mu}_{if}\right|^2 \cdot \frac{1}{d\upsilon} \qquad (2.17)$$

So the effective cross-section for absorbed photons, integrated over all possible neighbouring energies to $h\upsilon$, is:-

$$\int \sigma(\nu)d\nu = \frac{8\pi^3\nu}{3hc} \left|\underline{\mu}_{if}\right|^2 \qquad (2.18)$$

In practice, one usually considers:-

$$\int \sigma(E)dE = \frac{8\pi^3\nu}{3c} \left|\underline{\mu}_{if}\right|^2 \qquad (2.19)$$

The absorption coefficient is:-

$$K(E) = \sigma(E)\times C \qquad (2.20$$

where C is the concentration of the absorbing ions.

2.1.5 Temperature Effects

Even at absolute zero there is a finite width to the emission band. Although the transition begins from the level n = 0, the zero point energy of vibration allows transitions to various of the m levels.

Experiment has shown (2.7) that the shapes of the emission bands,

$I(h\nu)$, and the absorption bands, $A(h\nu)$, are well fitted by a gaussian distribution:-

$$I(h\nu) = \frac{1}{\sigma\sqrt{2\pi}} \exp\left(\frac{-(h\nu - h\nu_o)^2}{2\sigma^2}\right) \qquad (2.21)$$

where ν_o is the mean frequency of emission and normalisation requires:-

$$\int I(h\nu)\, d(h\nu) = 1 \qquad (2.22)$$

$A(h\nu)$ is similarly defined.

We wish now to calculate the distribution of energy in the emission and absorption spectra and determine the changes in width of these bands as a function of temperature. We proceed along the lines used by Curie (2.1).

The quantum mechanical expression for the intensity of light emitted by dipole radiation, given in equation 2.15, is:-

$$I(h\nu_{nm}) = \frac{64\pi^4 \nu_{nm}^4}{3c^3} \left|\mu_{nm}\right|^2 \qquad (2.23)$$

where μ_{nm} is the matrix element for the electric dipole moment.

Then we make use of the Condon approximation, which assumes that μ_{nm} is proportional to the overlap integral. We can separate the electron wave function, $\phi(\underline{x})$ and the vibration wave function, $\psi(r)$, where $\underline{x}$ represents the electron co-ordinates. Thus we can write:-

$$\mu_{nm} = \int \phi_e^*(\underline{x})\, \psi_{ne}^*(r - r_o)\, e\, \underline{x}\, \phi_g(\underline{x})\, \psi_{mg}(r)\, d\underline{x}\, dr \qquad (2.24)$$

Writing:-

$$\mu_{eg} = \int \phi_e^*(\underline{x})\ e\,\underline{x}\ \phi_g(\underline{x})\ dx \qquad (2.25)$$

then μ_{eg} depends only on the electronic states, e and g, and so can be taken out of the integral as a factor. Thus:-

$$\mu_{nm} = \mu_{eg}\int \psi_{ne}^*(r - r_o)\ \psi_{mg}(r)\ dr \qquad (2.26)$$

If we now take the form of $U_{e,g}(r)$ as quadratic in r, with reference to Figure 2.3, we can write:-

$$U_g(r) = \tfrac{1}{2} k_g r^2 \qquad (2.27)$$

and:-

$$U_e(r) = \tfrac{1}{2} k_e (r - r_o)^2 + U_o \qquad (2.28)$$

where U_o is the energy difference between the minima of the curves, $U_e(r)$ and $U_g(r)$.

Hence, the wave functions $\psi_{mg}(r)$ and $\psi_{ne}(r - r_o)$ are eigenfunctions of the harmonic oscillators, and

$$\psi_{mg}(r) = N_m \exp\left[-\tfrac{1}{2}\left(\frac{r}{a_g}\right)^2\right] H_m\left(\frac{r}{a_g}\right) \qquad (2.29)$$

where H_m is the Hermitian polynomial

N_m is the normalising factor

and a_g is the classical amplitude of the zero point vibration:-

$$a_g^2 = \frac{\hbar}{\sqrt{k_g M}} = \frac{\hbar}{M\omega_g} \qquad (2.30)$$

Also, $$\upsilon_g = \frac{1}{2\pi}\sqrt{\frac{k_g}{M}} \; ; \; \omega_g = \sqrt{\frac{k_g}{M}} \qquad (2.31)$$

Here, $h\upsilon_g$ is the energy quantum of vibration of ions in the ground state (phonon energy). M is the mass of those ions vibrating, that is the ligand oxygen ions to first approximation.

M is modified by:-

(a) the coupling between Ln^{3+} and the ligands

(b) the partial covalent nature of the rare earth-oxygen bond

(c) the effect of next nearest neighbours.

We can similarly define the wave function for the excited state.

The quantum numbers, m and n, usually run up to fairly large numbers (about 50), so that $\left|\psi_{mg}(r)\right|^2$ tends towards the classical density distribution, and so we can use a semi-classical approximation technique. The distribution is well localised in the vicinity of the classical amplitude, r_m, which is given by:-

$$U_g(r_m) = \tfrac{1}{2} k_g r_m^2 = (m + \tfrac{1}{2})h\upsilon_g \qquad (2.32)$$

However, because the initial state of the transition is a single eigenstate, it must be treated quantum mechancially.

At low temperatures the Boltzmann distribution of electrons in states $n > 0$ will be insignificant and so:-

$$\mu_{nm} \simeq \text{constant} \times \psi_{oe}(r_m - r_o) \qquad (2.33)$$

But we have seen that ψ_{oe} is a gaussian function, hence so is μ_{nm}:-

$$\left|\psi_{oe}(r - r_o)\right|^2 = N_o^2 \exp\left[-\left(\frac{r - r_o}{a_e}\right)^2\right] \qquad (2.34)$$

whence:-

$$\left|\mu_{om}\right|^2 = \text{constant} \times \exp\left[-\left(\frac{r_m - r_o}{a_e}\right)^2\right] \qquad (2.35)$$

where a_e is defined as for a_g:-

$$a_e^2 = \sqrt{\frac{\hbar}{k_e M}} = \frac{\hbar}{M\omega_e} \qquad (2.36)$$

and is the amplitude of vibration at 0°K.

Differentiating $U_g(r)$ in the region $r = r_o$ gives:-

$$U_g(r_m) - U_g(r_o) = -h(\upsilon_{om} - \upsilon_o)$$

$$= k_g r_o (r_m - r_o) \qquad (2.37)$$

Hence, combining equation 2.35 and 2.37:-

$$\mu_{om}^2 = \text{constant} \times \exp\left[-\left(\frac{h(\upsilon_{om} - \upsilon_o)}{k_g r_o a_e}\right)^2\right] \qquad (2.38)$$

So, the moment, σ_e, of the emission band is:-

$$2\sigma_e^2 = (k_g r_o a_e)^2 \qquad (2.39)$$

and for the absorption band:-

$$2\sigma_a^2 = (k_e r_o a_g)^2 \qquad (2.40)$$

If we introduce S_e and S_a as the number of phonons produced after a photon has been emitted or absorbed respectively, then for emission:-

$$h\nu_o = U_o - S_e h\nu_g \tag{2.41}$$

and:-

$$\tfrac{1}{2} k_g r_o^2 = S_e h\nu_g \tag{2.42}$$

Thus:-

$$\sigma_e^2 = \frac{S_e (h\nu_g)^3}{h\nu_e} \tag{2.43}$$

And for absorption:-

$$h\nu_o = U_o + S_a h\nu_e \tag{2.44}$$

and:-

$$\tfrac{1}{2} k_e r_o^2 = S_a h\nu_e \tag{2.45}$$

Thus:-

$$\sigma_a^2 = \frac{S_a (h\nu_e)^3}{h\nu_g} \tag{2.46}$$

For higher temperatures, there is a distribution of electrons within the vibrational states. The fraction of electrons in an excited state, n, if the system is in thermal equilibrium, is:-

$$p_n = \frac{\exp\left(-\frac{nh\nu_e}{kT}\right)}{\sum_{n=o}^{\infty} \exp\left(-\frac{nh\nu_e}{kT}\right)} \tag{2.47}$$

Hence, $\left|\mu_{nm}\right|^2$ is affected by the factor, p_n, and:-

$$I(h\nu_{nm}) \propto p_n \left|\psi_{ne}(r_m - r_o)\right|^2 \tag{2.48}$$

The intensity of emission at frequency, ν, where $h\nu = E_{ne} - E_{mg}$ can be written as:-

$$I(h\nu) \propto \sum_n \sum_m p_n \left|\psi_{ne}(r_m - r_o)\right|^2 \delta(E_{ne} - E_{mg} - h\nu) \tag{2.49}$$

If the emission occurs in a time shorter than the relaxation time of the lattice, then we can assume that transitions are vertical (Franck-Condon principle). Then:-

$$\delta(E_{ne} - E_{mg} - h\nu) = \delta(U_e(r_m) - U_g(r_m) - h\nu) \qquad (2.50)$$

Also, using the semi-classical approach, we can replace the sum over m by an integral. Thus:-

$$I(h\upsilon) \propto \int \left[\sum_n p_n \left| \psi_{ne}(r_m - r_o) \right|^2 \delta(U_e(r_m) - U_g(r_m) - h\upsilon) \right] dr_m \qquad (2.51)$$

To perform the summation we make use of the Mehler formula:-

$$\sum_{n=o}^{\infty} \frac{e^{-(n+1)\alpha}}{\sqrt{\pi}\ 2^n n!} H_n^2(x)\, e^{-x^2} = \frac{1}{\sqrt{2\pi \sinh\alpha}} \cdot \exp\left[-x^2 \tanh\left(\frac{\alpha}{2}\right) \right] \qquad (2.52)$$

where $\alpha = \dfrac{h\upsilon_e}{kT}$

Thus we can write:-

$$\sum_{n=o}^{\infty} p_n \left| \psi_{ne}(r_m - r_o) \right|^2 = \frac{e^{\alpha/2}(1 - e^{-\alpha})}{\sqrt{2\pi \sinh\alpha}} \cdot \exp\left[-\left(\frac{r_m - r_o}{a_e} \right)^2 \cdot \tanh\left(\frac{\alpha}{2}\right) \right] \qquad (2.53)$$

Substituting this in our expression for $I(h\upsilon)$ gives:-

$$I(h\upsilon) \propto \int \exp\left[-\tfrac{1}{2} k_e (r_m - r_o)^2 \cdot \frac{2}{h\nu_e} \tanh\left(\frac{h\upsilon_e}{2kT} \right) \right] \cdot \delta(U_e(r_m) - U_g(r_m) - h\upsilon)\, dr_m \qquad (2.54)$$

If we select a new variable:-

$$x = U_e(r_m) - U_g(r_m) \tag{2.55}$$

then:-

$$I(h\nu) \propto \int \exp\left[-\tfrac{1}{2} k_e (r_m - r_o)^2 \cdot \frac{2}{h\nu_e} \tanh\left(\frac{h\nu_e}{2kT}\right)\right] \delta(x - h\nu) \frac{dr_m}{dx} \cdot dx \tag{2.56}$$

Now, since $\int f(x)\, \delta(x - h\nu)\, dx = f(h\nu)$ (2.57)

we have:-

$$I(h\nu) \propto \left\{ \exp\left[-\tfrac{1}{2} k_e (r - r_o)^2 \cdot \frac{2}{h\nu_e} \tanh\left(\frac{h\nu_e}{2kT}\right)\right] \frac{dr}{dx} \right\}_{x=h} \tag{2.58}$$

Note that r is linearly proportional to the emission frequency

since $-h(\upsilon - \upsilon_o) = k_g r_o (r - r_o)$ (2.59)

and the exponential factor gives an essentially gaussian form to $I(h\nu)$.

At high temperatures:-

$$I(h\nu) \propto \exp\left[-\tfrac{1}{2} k_e (r - r_o)^2 \cdot \frac{1}{kT}\right] \frac{dr}{dx} \tag{2.60}$$

At $T = 0$ the term:-

$$\tanh\left(\frac{h\nu_e}{2kT}\right) = 1 \tag{2.61}$$

so that the band width, L_e, varies with temperature according to the expression:-

$$L_e(T) = L_e(0) \sqrt{\tanh\left(\frac{h\upsilon_e}{2kT}\right)} \tag{2.62}$$

The width of the absorption band has an identical temperature dependence except that υ_e is replaced by υ_g.

2.1.6 Oscillator Strengths

Oscillator strengths can be determined experimentally from the Smakula formula (2.8), the derivation of which follows.

If there are N absorbing atoms per unit volume, the absorption cross-section for photons, integrated over as an assembly of states with the same matrix element, is (from equation 2.19):-

$$\int \sigma(E)dE = \frac{8\pi \nu^3}{3c} \left|\mu_{if}\right|^2 \qquad (2.63)$$

where μ_{if} is the matrix element for the electric dipole moment between the initial and final state. Experimentally it is more convenient to measure absorption coefficient, K(E), so we write instead:-

$$\int K(E)dE = N\frac{8\pi \nu^3}{3c} \left|\mu_{if}\right|^2 \qquad (2.64)$$

Then, the oscillator strength, f_{if}, is defined by:-

$$f_{if} = \frac{8\pi^2 m\nu}{3h} \left|r_{if}\right|^2 \qquad (2.65)$$

and is normalised as $$\sum_{i,f} f_{if} = 1 \qquad (2.66)$$

The above arguments apply to ions in vacuo; we must therefore make the following alterations for ions in a medium.

(a) For a medium of refractive index n, c must be replaced by $\frac{c}{n}$.

(b) We should introduce the ratio of the effective field (due to the electromagnetic field) E_{eff} to the applied field, E. The ratio occurs as a squared term, since $E \propto \mu$.

(c) We should divide by the dielectric constant, κ.

The result of these corrections is:-

$$\int K(E)dE = N\frac{\pi ne^2h}{\kappa mc}\left[\frac{E_{eff}}{E}\right]^2 . f_{if} \qquad (2.67)$$

Now, since the frequency of the applied field is large, we can approximate

$$\kappa = n^2 = 1 + 4\pi\alpha \qquad (2.68)$$

where α is the electric permeability of the ions.

Consequently:-

$$\frac{E_{eff}}{E} = 1 + \frac{4\pi}{3}\alpha = \frac{n^2 + 2}{3} \qquad (2.69)$$

and:-

$$\int K(E)dE = N\frac{\pi e^2h}{nmc}\left(\frac{n^2 + 2}{3}\right)^2 f_{if} \qquad (2.70)$$

so that, numerically:-

$$N = 0.821\times10^{17}.\frac{n}{(n^2 + 2)^2}\cdot\frac{1}{f_{if}}\int K(E)dE \qquad (2.71)$$

The units of N are cm^{-3} if K is in cm^{-1} and E is in eV.

Equation 2.71 is known as Smakula's formula and was originally developed to determine concentrations of impurities from their absorption spectra. We shall, of course, be concerned with using this formula to determine the oscillator strengths, f_{if}. Dexter (2.9) shows that the above expression is valid only for the highly localised centres we are dealing with, and must be modified for extensive centre luminescence.

Smakula's formula can be put into a more useful form by using the approximation developed by Hoogschagen (2.10):-

$$f_{if} = \frac{2303\ mc^2}{N\pi e^2}\int \epsilon(k)\,dk \qquad (2.72)$$

where ϵ is the molar absorptivity as a function of the wave-number k.

Then:-

$$\epsilon = \frac{1}{c\ b} \cdot \log\left(\frac{I_o}{I}\right) \tag{2.73}$$

where $\frac{I_o}{I}$ = the ratio of incident to transmitted light intensity;

c = the concentration of ions in moles per litre;

and b = the sample thickness in cm.

Numerically (2.11) this is:-

$$f_{if} = 4.318\times10^{-9}\int\epsilon(k)dk = A\int\epsilon(k)dk \tag{2.74}$$

The incident light intensity, I_o, is related to the transmitted and absorbed intensities (I and I_a respectively) by:-

$$I_o = I_a + I \tag{2.75}$$

Hence,

$$f_{if} = \frac{A}{c\ b}\int\log\left[\frac{I_o}{I_o - I_a}\right].\ dk \tag{2.76}$$

Since spectrophotometers usually give output which is linear in wavelength λ, it was necessary to derive a formula relating f_{if} to $\int(I_a/I_o)d\lambda$. For rare earths the absorption bands are very narrow and Δk or $\Delta\lambda$ is small. Then:-

$$dk = -\frac{1}{\lambda^2}\ d\lambda \tag{2.77}$$

and so:-

$$f_{if} = \frac{-kA}{cb\ \lambda^2}\int\log\left[\frac{I_o}{(I_o - I_a)}\right]\ d\lambda \tag{2.78}$$

Rearranging this gives:-

$$f_{if} = \frac{-kMA}{cb\,\lambda^2}\int -\ln\left[1 - \frac{I_a}{I_o}\right] d\lambda \qquad (2.79)$$

where $M = \log_{10} e = 0.4343$.

Then since:-

$$\ln x = (x - 1) - \tfrac{1}{2}(x - 1)^2 + ... \text{ for } 2 \geq x > 0 \qquad (2.80)$$

and since for rare earths the absorption coefficient, $\frac{I_a}{I_o}$, is small,

we can write:-

$$f_{if} \simeq \frac{-kMA}{cb\,\lambda^2}\int \frac{I_a}{I_o}\, d\lambda \qquad (2.81)$$

The minus sign is merely a consequence of λ increasing as k decreases.

The validity of this equation is entirely dependent on the fact that the absorption bands of rare earths are weak, narrow lines.

2.1.7 Quantum Efficiencies

The apparent quantum efficiency, $\eta'(\lambda)$, is the ratio of the number of photons emitted in fluorescence to the number of incident exciting photons, while the fluorescence quantum number, $\eta(\lambda)$, is defined as the ratio of the number of emitted photons to the number of exciting photons absorbed. These terms are related by the expression:-

$$\eta(\lambda) = \frac{\eta'(\lambda)}{\alpha(\lambda)} = \frac{\eta'(\lambda)}{1 - \rho(\lambda)} \qquad (2.82)$$

where $\alpha(\lambda)$ and $\rho(\lambda)$ are the absorption and reflection coefficients respectively. In most solids, however, part of the luminescence emission is absorbed. To evaluate the real efficiency, η_v, these losses must be

determined. Bril and Klasens (2.12) have connected $\eta_v(\lambda)$ to $\eta(\lambda)$ with the reflection factor, R, of the phosphor for its own luminescence by the relation:-

$$\eta_v(\lambda) = \frac{2\eta(\lambda)}{1 + R} \qquad (2.83)$$

Absolute efficiencies are most easily measured by comparison with a phosphor whose efficiencies have already been determined (2.13). Apparent quantum efficiencies are corrected for the different detector photocurrents by the equation:-

$$\frac{\eta' p(\lambda)}{\eta' s(\lambda)} = \frac{I_p(\lambda)}{I_s(\lambda)} \cdot \frac{K_s}{K_p} \qquad (2.84)$$

where the subscripts, s and p, refer to the standard phosphor and the experimental specimen respectively $I(\lambda)$ is the detector photocurrent. $\frac{K_s}{K_p}$ is a correction factor for the photodectector since the luminescence emission of the two phosphors is generally in different regions of the spectrum. The real quantum efficiency can then be determined from the expression:-

$$\frac{\eta_{vp}(\lambda)}{\eta_{vs}(\lambda)} = \frac{I_p(\lambda)}{I_s(\lambda)} \cdot \frac{K_s}{K_p} \cdot \frac{1 - \rho_s(\lambda)}{1 - \rho_p(\lambda)} \cdot \frac{1 + R_s}{1 + R_p} \qquad (2.85)$$

2.1.8 The Nephelauxetic Effect

Comparison of absorption spectra of rare earths in crystals and glasses with those of the aqueous ion demonstrates the existence of three effects, all of which are related to variations in the crystal field (2.14):-

(1) Small shifts, usually towards longer wavelengths, but occasionally towards shorter wavelengths (2.15);

(2) Frequent splitting of certain bands into several subsidiary maxima.

(3) Changes in the specific absorptivity of individual absorption peaks.

Some of these alterations are perhaps due to a measure of covalency in the ion to ligand bond. Jørgensen (2.16, 2.17) has described the wavelength shifts in terms of the nephelauxetic effect. The existence of this effect has been attributed to the overlap of the wavefunctions of the central ion and its ligands (2.18).

The parameter, $d\beta$, was used to express the wavelength shifts relative to those in aqueous ions averaged over all observed transitions. The values for $d\beta$ were obtained from the expression:-

$$k - k_a = dk - (d\beta).k_a \qquad (2.86)$$

where k is the baricentre of the absorption spectra of the central ion in a given medium; k_a is the baricentre of the absorption spectra of the aqueous ion; and dk represents the ligand-field stabilisation of the lowest sub-level of the ion in a solid medium, relative to the aqueous ion. It accounts for the difference between the average sub-level population of the lowest sub-level of the material studied, at some definite temperature, and the energy of the lowest sub-level of the aqueous ion relative to the baricentre of the ground state J multiplet. Experimentally the relationship gives a plot which is very nearly linear in k_a (2.19).

Sinha (2.20) has suggested that, whenever possible, the wavenumber of the free ion, k_f, should be used, as the aquo complex does produce a slight nephelauxetic effect. This also removes the possibility of shifts to higher energies.

Reisfeld (2.21) has calculated the nephelauxetic parameter, β, from the expression:-

$$\beta = \frac{k_f - k}{k_f} \qquad (2.87)$$

Comparisons of β for different hosts is most reliable when only one ion is considered, and the host lattice is changed. The nephelauxetic series obtained in this way is analogous to the tendency of increase of both covalent bonding and the reducing nature of the glass polyhedra.

Duffy and Ingram (2.22) show that in various glass types, the nephelauxetic constant, β, and the degree of ionicity in the ligand bond increase in the order:-

sulphate > phosphate > silicate glass.

Jørgensen (2.23) has shown that β can be factorised as:

$$(1 - \beta) = H.K \qquad (2.88)$$

where H and K are parameters appropriate to the ligand environment and the central ion respectively. The value of H is roughly a linear function of the Pauling electronegativity values for the ligand complex.

Good agreement is obtained with experiment if one Pauling unit is made equal to $30,000\,cm^{-1}$ (2.24). Then the observed wavenumber of the absorption peak is given by:-

$$k = 3 \times 10^4 \left[\varkappa_{opt}(X) - \varkappa_{unc}(M) \right] \qquad (2.89)$$

where $\varkappa_{unc}(M)$ is the uncorrected optical electronegativity of the metal ion and $\varkappa_{opt}(X)$ is the electronegativity of the ligand.

This gives good agreement with experiment for at least the charge transfer spectra of Eu^{3+} ions in glass (2.21).

2.1.9 Energy Level Calculations

For the free ion, the Hamiltonian representing the interactions of the 4f electrons can be written:-

$$H \simeq H_0 + H_1 + H_2 \qquad (2.90)$$

where $H_0 = \sum_i \frac{Z'e^2}{4\pi\epsilon_o r_i}$ is the Hamiltonian representing the Coulombic potential for an effective nuclear charge, Z'.

$H_1 = \sum_{ij} \frac{e^2}{r_{ij}}$ is the Hamiltonian due to electrostatic repulsion between the outer electrons, summed over all the electron pairs.

$H_2 = \sum_i \zeta_i(\underline{l}_i \cdot \underline{s}_i)$ is the Hamiltonian due to the spin-orbit interaction.

The parameter $\zeta_i = \frac{\alpha^2 RZ''}{r_i^3}$, where α is the fine structure constant; R is the Rydberg constant; s and l are the spin and angular momentum quantum numbers respectively. The effective charge, Z'', is generally different from Z'.

The theory of angular momentum and group theory makes the calculations less difficult (2.25, 2.26). Such considerations enable a reference system to be chosen which makes the perturbation matrices as simple as possible.

The energies and wavefunctions of these electron states may be expressed in terms of the Slater integrals (2.27), F^k, which are given by:-

$$F^k = \int_0^\infty \int_0^\infty \frac{r_l^k}{r_g^{k+1}} R_i^2(r_i)\, R_j(r_j)\, r_i^2 r_j^2\, dr_i\, dr_j$$

where r_l is the lesser and r_g is the greater of r_i and r_j and the R(r) are the radial parts of the electronic wave functions. The Slater integrals are usually expressed as the parameters, F_k (2.28), which, for f electrons, are related by:-

$$F_2 = F^2 / 225$$
$$F_4 = F^4 / 1809$$
$$F_6 = F^6 / 7361.64$$

Judd (2.29) has shown that for Ln^{3+} ions the ratios of the F_k are approximately the same as the hydrogenic ratios, and are given by:-

$$\left.\begin{aligned} F_4 &= 0.145\ F_2 \\ F_6 &= 0.0164\ F_2 \end{aligned}\right\} \qquad (2.91)$$

and, also for trivalent lanthanides, that:-

$$\left.\begin{aligned} Z' &= Z - 34 \\ \text{and}\quad F_2 &\sim 12.3\ Z' \end{aligned}\right\} \qquad (2.92)$$

Only the even terms are non-zero, and F_0 is a common additive constant to all levels. The splitting due to spin-orbit interaction leaves degenerate all levels differing only in m_J, the magnetic quantum number.

The parameter, $\chi = \frac{\zeta}{F_2}$, is used to describe the separations of the various J levels (2.30); pure LS coupling is represented by $\chi = 0$.

Ofelt (2.31) has performed the calculation for the equivalent $4f^6$ and $4f^8$ configurations. The number of multiplets is 119, which through the spin-orbit interaction results in 295 levels.

For rare earths, reasonable agreement of calculated and experimental energy levels requires the inclusion of the spin-orbit interactions

with the states of the next lower and higher spins than those of the multiplet of interest (2.32).

In the case of Tb^{3+}, the inclusion of the quintet states in the calculations gives reasonable agreement for the ^7F multiplet. Ofelt includes the triplet states and discusses the effect of neglecting the interaction with singlet states.

With the aid of experimental data from Thomas et al (2.33) reasonable agreement with calculated levels(2.34) was obtained by choosing:-

$F_2 = 434$ and $\zeta = 1705\,cm^{-1}$ (thus $\chi = 3.93$).

The 4f-4f transitions which produce the luminescence of Tb^{3+} ions are spin and parity fobidden to a first approximation. The spin selection rule is lifted by the spin-orbit mixing of the ground state ^7F multiplet with the upper ^5D levels. The parity selection rule is lifted by the mixing of the $4f^8$ configuration with configurations of opposite symmetry. Thus, if the Tb^{3+} ion occupies a site with inversion symmetry, only magnetic dipole transitions ($\Delta J = 0, \pm 1$) and vibronically induced electric dipole transitions can occur.

From the eigenfunctions of the free ion it is possible to calculate the relative intensities of emission bands for purely magnetic dipole transitions. The $^5D_4$ to $^7F_5$ transition has the highest transition probability (2.31) because this is the only transition for which the contribution of the matrix element between the ^7F states is not counteracted by the contribution of the matrix elements between the ^5D states.

The results of this calculation (2.35) show that the relative contributions of the $^5D_4$ to $^7F_5$, $^7F_4$ and $^7F_3$ transitions, is 89, 1, and 10

respectively, for magnetic dipole radiation only. Deviations from these ratios, in results from some media, were ascribed to electric dipole transitions, and were most noticeable in lattices lacking inversion symmetry.

2.1.10 Crystal Field Splitting

The Hamiltonian expressed in equation 2.90 for a free ion is only an approximation, and further terms should be added to take account of the hyperfine interaction and exchange effects. In a magnetic field another term is required to account for the Zeeman effect.

If the ion is included in condensed matter, the ionic potential is further influenced by the electromagnetic field due to the ligand ions. The situation can be represented as an electrostatic field of symmetry determined by the crystal lattice.

This static crystal field surrounding the rare earth ion may be written as a series of spherical harmonics. The representative Hamiltonian is:-

$$H_3 = \sum_i \sum_{k,q} A_k^q \, r_i^k \, P_k^q(\cos \theta_i) \exp(iq \phi_i) \qquad (2.93)$$

The summation is over $0 \leq k < \infty$ and $|q| \leq k$, and over all 4f electrons (i). The coefficients, A_k^q, depend on the normalisation of the spherical harmonics.

For transition metals this interaction is much larger than the spin-orbit interaction. The reverse is true for the lanthanides; so that perturbation theory can be used, taking the crystal field as a perturbation on the LS coupling.

Thus for rare earths only:-

$$H_3 < H_2 \tag{2.94}$$

which is entirely due to the shielding of the 4f electrons by the outer electron orbitals.

In the free ion each L, S, J, level is (2J + 1) fold degenerate, but this condition is partially lifted by the crystal field. In general each level is split into a number of levels of lesser degeneracy, and the number of levels into which a single free ion level can be split is determined only by the site symmetry.

The crystal field is often expressed as a combination of two fields, one of which is cubic in symmetry. The Hamiltonian may then also be separated into two parts as:-

$$H_3 = H_{cubic} + H_{non\text{-}cubic} \tag{2.95}$$

First solutions of these equations (2.36) made use of "operator equivalents" (2.37). The technique is to substitute the components of the angular momentum operator, J_x, J_y, J_z, for the spatial coordinates x, y, z occurring in the potential of the crystal field. The theory of angular momentum can then be applied to obtain the matrix elements of these operators.

The operator equivalents have lost some of their applicability since Rotenberg et al (2.38) simplified the more direct theory by making the so-called 3-j coefficients available in tabulated form.

In principle, one can predict the emission characteristics of a given ion in a given lattice; or, alternatively, by measuring the lumin-

escence, one can determine the site symmetry.

In crystals the Stark components are easily resolved and the site symmetries are known, so that experiment and theoretical predictions are readily compared (2,39).

In glasses the inhomogeneous broadening is usually larger than the Stark splitting, complicating the discrimination of these levels even at temperatures near absolute zero. Since the symmetry of the ionic site is also poorly known, approach from the other standpoint is equally difficult. It is more useful to compare the resultant spectra with those in crystals of known symmetry to determine the site structure, at least in general terms.

2.2 Thermoluminescence Theory

Thermoluminescence (hereafter abbreviated as TL) is the process whereby electrons and/or holes are thermally activated out of trapping states in such a way that their recombination is radiative.

Energy gaps in condensed matter are a phenomenon usually associated with a regular periodicity of lattice arrangement, and consequently are associated with crystals. That an equivalent energy gap exists in glasses is readily seen from optical absorption measurements. Fritzsche (2,40) has attempted to derive band-gaps in amorphous materials by theoretical arguments. However, the theory required the existence of material inhomogeneities within the glass. The density of states falls off gradually into the band-gap and produces ill-defined band edges, as the band-gap is only forbidden when there is perfect order.

Electronic transitions occur when electrons are raised from the valence band to the conduction band after the application of radiation of sufficiently high energy. The production of electrons in the conduction band gives rise to holes in the valence band. Electrons, upon excitation, may either directly recombine with the holes or may remain in traps near the conduction band (Fig 2.4).

With increase in temperature of the irradiated sample, sufficient thermal energy can be supplied to the electrons such that their Boltzman distribution of energies can carry them into the conduction band. The trapped electrons, after release, may recombine with holes to produce emission of optical frequency radiation. The intensity of this radiation is a measure of the trap population, and the temperature required for the recombination indicates the trap depth.

Electron traps in crystals are known to be located at point defects, impurity defects, etc. Also, after production, the electrons may migrate in the lattice, so that the recombination may not occur at the production site. It is assumed that an analogous situation arises in a glass because of local ordering (2.41).

A further possibility arises in that the absorbed energy may be transferred non-radiatively by means of, for example, multipolar energy transfer processes. If energy is transferred to excited states of rare earth ions within the glass, the characteristic line spectra of the rare earth will result. Since the main emission line of Tb^{3+} ions is known to be in the green region of the spectrum, which is close to the maximum efficiency of normal photomultiplier types, the detection efficiency of TL may be increased. This would find application in

dosimetry, where dose levels of harmful radiation are measured by such techniques (2.42).

In order to have a practical theory of TL, both the number and population of electron and hole traps must be known, and also the degree of charge transfer between them. Inadequate knowledge of these data has led to several approximation methods, notably the "U R W" formalism due to Urbach (2.43) and Randall and Wilkins (2.44) which is adopted here.

The escape of electrons from trapping centres and subsequent emission of radiation is assumed to be a thermally activated process. In this event we can write the probability per unit time of this process as:-

$$P = b \exp\left(-\frac{E}{kT}\right) \qquad (2.96)$$

where E is an activation energy, and b is termed the frequency factor (2.43). This is because the thermal excitation of charge carriers from metastable or trapping states is a multiphonon process.

For materials with uniform trap depths, the luminescent decay is governed by simple reaction kinetics. If the association between the trapping states and the activator is such that each activator decays separately, then the intensity of the decay is given by first order kinetics.

If n(t) represents the number of filled traps at time t, then:-

$$-\frac{dn}{dt} = b \exp\left(-\frac{E}{kT}\right) \cdot n \qquad (2.97)$$

For an initial number, n_o, of traps at a constant temperature T_o

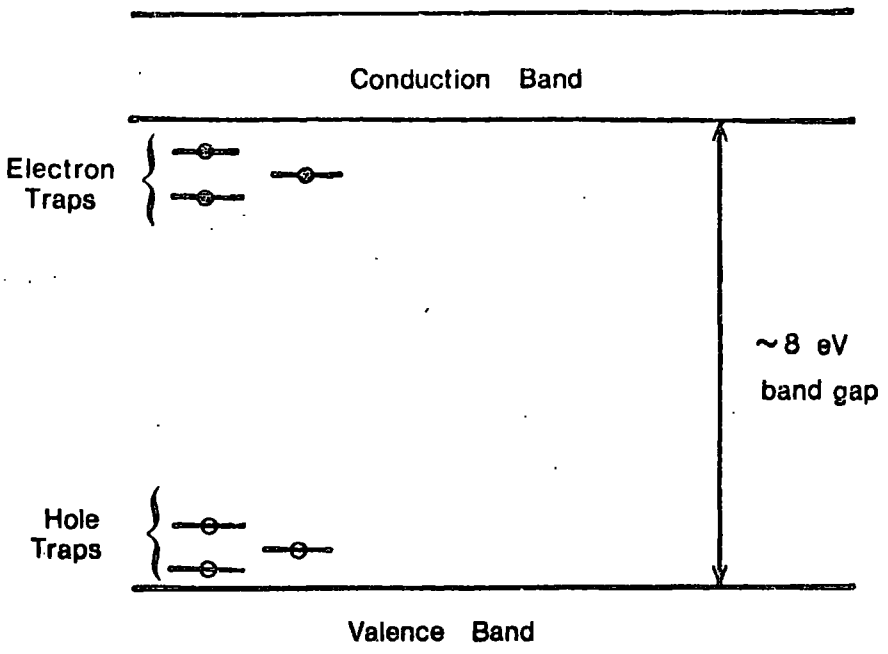

Fig 2.4 Electron and hole traps in silicate glasses (TL theory)

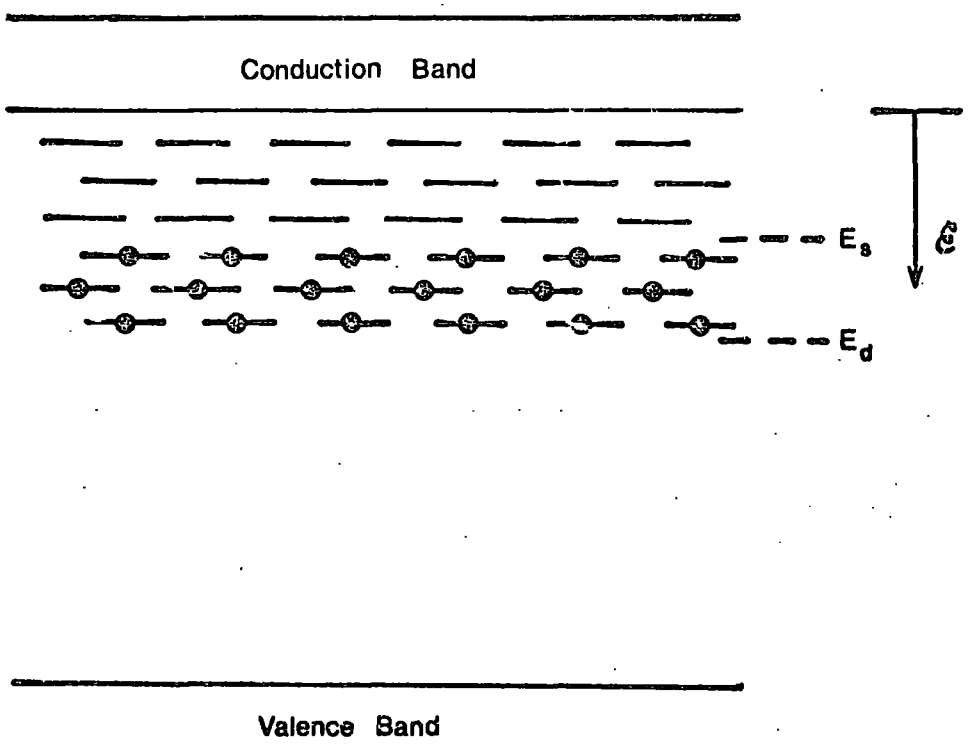

Fig 2.5 Distribution model for trapped electrons, after Kikuchi (1963)

$$n(t, T_o) = n_o \exp(-P_o t) \tag{2.98}$$

where we define:-

$$P_o = b \exp\left(-\frac{E}{kT_o}\right) \tag{2.99}$$

Hence, the rate of change with respect to time is:-

$$-\frac{dn}{dt} = P_o n_o \exp(-P_o t) \tag{2.100}$$

This represents the intensity of light emitted after a time interval, t, and so an exponential decay is predicted.

Integration of equation 2.97 for a linear temperature increase will produce the shape of the glow curve. The solution given by Bonfiglioli (2.45) is:-

$$\frac{\beta E}{kT^{*2}} = \exp\left(-\frac{E}{kT^*}\right) \tag{2.101}$$

where the temperature, T^*, corresponds to the maximum of the glow curve peak, and β is the linear heating rate

$$\beta = \frac{dT}{dt} \tag{2.102}$$

An exponential increase in the emission is produced by the thermal depopulation of defects, and ceases when the population of electron traps becomes small. The light ouput is zero when the traps are empty.

It is important to note that the above calculation assumes the existence of a single electron and a single hole trap. However, especially when considering glasses, there is no a priori reason why the number of electron and hole traps should be limited to one.

If the trapping sites are separated from the activator sites and there is equal probability that a charge carrier will recombine radiatively with any of the activators, then the decay is determined by second order kinetics. The rate equation is:-

$$-\frac{dn}{dt} = \frac{P_o n_o^2}{(1 + P_o n_o t)^2} \qquad (2.103)$$

and the decay shape depends on the intensity of excitation.

Yokota (2.46) used TL techniques in the investigation of fused quartz. Later, Kikuchi (2.47) noted a broad low temperature peak in fused quartz and other silicate glasses, which is not found in crystalline quartz. This broad peak began immediately on heating after irradiation, even at the lowest temperatures available (~77°K). This led to the suggestion of many shallow electron traps with levels distributed over wide ranges.

The rate of decay of luminescence after the removal of incident radiation is not exponential, as is typical of bimolecular processes. Various attempts have been made to fit these curves (2.48).

Kikuchi proceeds as follows.

Let ϵ represent the depth of a trapping level from the bottom of the conduction band, and let $z(\epsilon)d\epsilon$ represent the density of electron occupied trapping levels from ϵ to $\epsilon + d\epsilon$ immediately after the removal of x-ray irradiation. Then the intensity of the luminescence, I(t), after a time interval, t, is given by:-

$$I(t) = \int_0^\infty Cb \exp\left[-bt \exp\left(-\frac{\epsilon}{kT}\right)\right] z(\epsilon)\, d\epsilon \qquad (2.104)$$

where b is the frequency factor as before, and C is a constant.

Assume a distribution of trapped electrons which is uniform from arbitrary chosen levels, E_d and E_s, as shown in Figure 2.5.

Mathematically, we can write:-

$$\left.\begin{aligned} 0 < \epsilon < E_s \;;\quad & z(\epsilon) = 0 \\ E_s \leqslant \epsilon \leqslant E_d \;;\quad & z(\epsilon) = A \\ E_d < \epsilon \;;\quad & z(\epsilon) = 0 \end{aligned}\right\} \qquad (2.105)$$

E_s and E_d represent the shallowest and deepest trapping levels occupied by electrons at $t = 0$.

Subsitution of equation 2.105 into equation 2.104 gives:-

$$I(t) = \int_{E_s}^{E_d} ACb \exp\left(-\frac{\epsilon}{kT}\right) \cdot \exp\left[-bt \exp\left(-\frac{\epsilon}{kT}\right)\right] d\epsilon \qquad (2.106)$$

which on integration yields:-

$$I(t) = I_o \frac{\exp(-bx_d t)(1 - \exp(-b(x_s - x_d)t))}{b(x_s - x_d)t} \qquad (2.107)$$

where the parameters, x_s and x_d, are defined by:-

$$\left.\begin{aligned} x_s &= \exp\left(-\frac{E_s}{kT}\right) \\ x_d &= \exp\left(-\frac{E_d}{kT}\right) \end{aligned}\right\} \qquad (2.108)$$

and I_o is the intensity of luminescence at $t = 0$.

Since $x_s \gg x_d$ this may be further approximated as:-

$$I(t) = I_o \frac{1 - \exp(-bx_s t)}{bx_s t} \qquad (2.109)$$

An estimate of the trap depth can be made by finding a best fit for E_s and T if the frequency factor, b, is fixed.

However, the agreement of equation 2.109 with experimental decay curves is not very good. Kikuchi ascribes this discrepancy to the assumption of only one type of trapping site, and also to the assumption of a uniform distribution of traps. If, instead, the integration is performed for a gaussian distribution of traps, one finds much the same result is obtained for the predicted form of the decay curve.

Broser and Warminsky (2.49) have analysed various trap distribution systems and have derived relationships between phosphorescence and steady state luminescence.

A non-uniform distribution of electrons over many traps is a realistic model to choose for glasses, as the perturbation of local, short-range structures makes possible a series of discrete traps with a relatively narrow range of energies. Calculations assuming such distributions of electrons become rapidly very complicated, but do not take into account the possibility that the traps are filled by energy transfer processes. Later in this work it is shown that a more accurate prediction of decay curves can be obtained by using the formalism of resonant transfer. Indeed the assumption of Kikuchi's, that the emission centre and the absorption or defect centre are one and the same, was not justified experimentally.

We turn now to the problem of estimating trap depths from glow curve measurements. In a recent article Shalgaonkar and Narlikar

review more than twelve different methods of attacking this problem (2.50). Since several of the different methods have not been applied to the same specimen, no estimate was given of the range of trap depths derived from the various approaches.

The broad glow curves obtained from glass and the difficulties in interpretation mentioned above suggest that an approximate formalism is adequate for the discussion here. Returning then to the U R W treatment, the equation representing the rate of change of filled traps is:-

$$-\frac{dn}{dt} = b \exp\left(-\frac{E}{kT}\right).n \qquad (2.110)$$

where the symbols have the same meaning as before. For a heating rate, β, the solution becomes:-

$$\{\ln n\}_{n_o}^{n} = -\frac{b}{\beta}\int_{T_o}^{T} \exp\left(-\frac{E}{kT}\right)dT \qquad (2.111)$$

or:-

$$n = n_o \exp\left[\left(-\frac{b}{\beta}\right)\int_{T_o}^{T} \exp(-E/kT)\, dT\right] \qquad (2.112)$$

Also, the intensity, I, of the TL peak is given by:-

$$I = -C\frac{dn}{dt} = Cbn \exp\left(-\frac{E}{kT}\right) \qquad (2.113)$$

where C is a proportionality constant.

Substituting in this from equation 2.112 leads to:-

$$I = Cbn_o \exp\left(-\frac{E}{kT}\right).\exp\left[-\frac{b}{\beta}\int_{T_o}^{T} \exp\left(-\frac{E}{kT}\right)dT\right] \qquad (2.114)$$

The position of maximum intensity is obtained from the above equation by differentiation with respect to T and setting the result equal to zero. After cancellation, the result is:-

$$\frac{E}{kT_m^2} = \frac{b}{\beta} \exp\left(-\frac{E}{kT_m}\right) \qquad (2.115)$$

which, on rewriting, gives:-

$$E = kT_m \cdot \ln\left[\frac{bkT_m^2}{\beta E}\right] \qquad (2.116)$$

Equation 2.116 can be solved numerically to give the trap depth, E, from a knowledge of the peak temperature, T_m, and an estimation of b, the escape factor frequency. However, for glasses it is reasonable to apply an approximation to allow the direct solution of this equation.

To first order:-

$$E \simeq kT_m \qquad (2.117)$$

which, upon substitution in the logarithmic term of equation 2.116, gives:-

$$E = kT_m \ln\left[\frac{bT_m}{\beta}\right] \qquad (2.118)$$

2.3 Energy Transfer

Energy transfer was first observed in gases, between different isotopes of a gas (2.51) and between different gases (2.52). The transfer processes are based on quantum mechanical resonances of the excited state of the primary excited ion with states of the ion from which

emission is finally observed. Even optically forbidden transitions may occur through these resonance processes, and emission may be either enhanced or quenched.

In solids, excitation at wavelengths within the region of base lattice absorption produces emission due to added centres or "activators". Two possibilities have been considered : firstly that the absorption may be at special centres produced by the inclusion of the activator ions and then the energy transferred straight to the emission centre. Alternatively, energy may be transported from the absorption site via the lattice to the neighbourhood of the emission site, then transferred to the emission centre.

It is important to distinguish between energy transport and energy transfer, although both may occur by the same mechanism. The term "energy transport" is correct for the case where energy is transported from one centre to another via the base lattice or via other centres, while "energy transfer" is pertinent to the direct transfer of energy from one centre to another.

There are four methods by which energy transfer or transport has been shown to take place:-

(a) By self absorption. The ion excited first emits its characteristic luminescence, which is absorbed by a second ion. This then emits its own luminescence.

(b) By the excitation of an electron-hole pair. Both the electron and hole can then move separately through the lattice to recombine elsewhere giving emission. (2.53).

(c) By transfer of energy in a quantum mechanical resonance

process. Resonance can occur over much greater distances than neighbouring ions, even in solids. The excitation energy is transferred directly from the primary excited ion to another ion some distance away, without being transported via the base lattice.

(d) By excitons (2.54). Strongly bound electron-hole pairs move through the lattice and recombine somewhere. This is also a quantum mechanical resonance phenomenon.

The process (c) is the one relevant to rare earth ions in transparent media, and is dealt with below, but first it is necessary to distinguish between:-

(1) Processes in which excitation occurs in the base lattice and the excitation energy is then transferred to the activator, or transported through the lattice via excitons (2.55).

and (2) Processes where the excitation energy is absorbed at particular added ions ("sensitisers"). Energy is then transferred to other added ions ("activators") from which luminescence takes place (2.56). The activators may or may not be similar ions, and usually energy transport does not take place via the base lattice, the latter serving largely as a suspensive medium.

One practical implication of energy transfer is that some phosphors can be excited by short wavelength ultra violet but not by lower frequency radiation. The range of the excitation bands can then be extended to more useful wavelengths by the addition of sensitiser ions. Losses do occur, however, because luminescence is often observed in bands characteristic of the sensitiser ions.

Space does not permit a complete review of earlier theories of energy transfer, but since they have been shown not to be appropriate to rare earths in crystals, they are unlikely to have relevance here (2.57, 2.58, 2.59).

When the sensitiser and activator have excited states of roughly equal energy, it is possible for the activator to be brought into the excited state by a resonance process, even though this transition may be forbidden. The probability of this transfer will decrease rapidly as the distance between the two ions increases. It is this question of distance over which transfer can take place which led to two rival theories.

Botden and Kröger (2.60) considered the possibility that transfer could only occur between ions situated at adjacent sites, that is in "pairs". With a statistical distribution of ions, the fraction of pairs is too low to explain the high transfer efficiencies observed. Hence it was assumed that some influence exists to promote the production of these pairs. For example, if the matrix ions are intermediate in size between the sensitiser and activator ions, then pairs might be created to minimise potential energy. Chemical analysis was unsuccessful in proving the existence of pairs. Also, the rate of cooling during the preparation of samples should affect the proportion of pairs produced. No such effect was discovered.

Schulman and co-workers (2.61) assumed a random distribution of centres, so that energy is transferred over much larger distances (many cation sites). Energy may be transported to the activator via several sensitiser sites, or may be transferred directly. This theory is now generally accepted for rare earth phosphors.

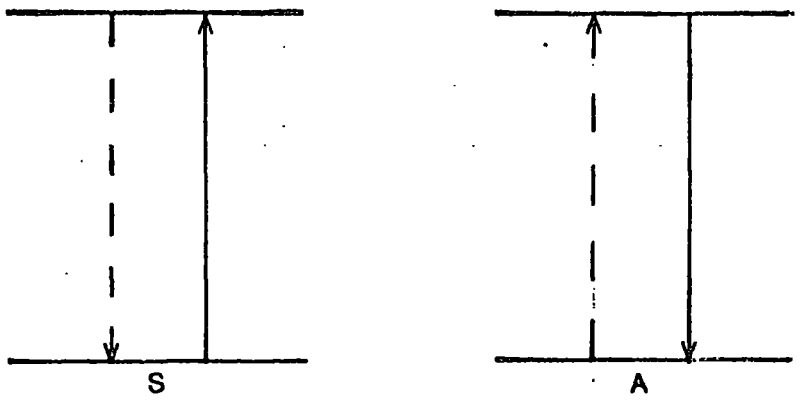

a. Multipolar Resonance

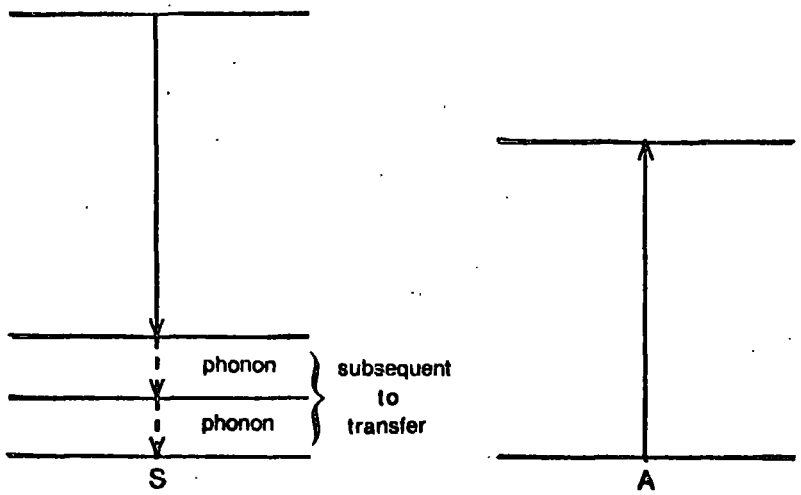

b. Multipolar Transfer

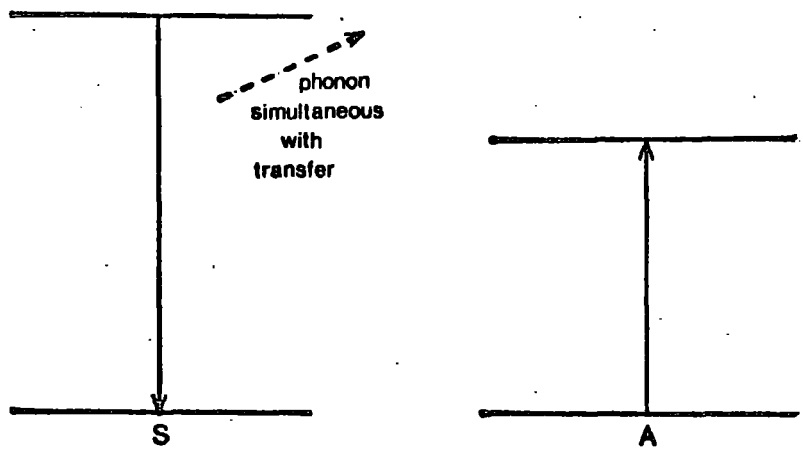

c. Non-Resonant Transfer

Fig 2.6 Multipolar energy transfer processes

The sharp line spectra of the tripositive rare earth ions are ideal for the study of transfer of excitation between ions. Energy transfer processes in rare earth crystals are either radiative or non-radiative and usually result in quenching of at least one of the emission processes. Radiative transfer is not an efficient emission quenching process for rare earth ions. Such transfer can only occur if an emission transition of one ion overlaps in energy with an absorption transition of a second ion. Only the emission of the second ion is affected. On the other hand, non-radiative transfer is characterised by all transitions from a given manifold being equally quenched (or enhanced) by energy transfer interactions under the same conditions. Non-radiative transfer can take place via multipolar or exchange interactions.

Multipolar interactions have been divided into three categories (2.62):-

(a) Multipolar resonance

(b) Multipolar transfer

(c) Non-resonant transfer interactions.

These are illustrated in Figure 2.6. Multipolar resonances are reversible energy transfer transitions between two ions which are matched in energy. In principle the upper levels need not lie at exactly the same energy for excitation to move freely through the lattice. Effective lifetimes of all levels involved are increased by this process.

Multipolar transfer excites a lower lying level of the second ion by a transition which is matched in energy. The process is accompanied by the production of phonons and is non-reversible when the

lifetime of the terminal level of the first ion is less than the transfer time.

Transfer of energy can also occur between two levels which are not matched in energy. The difference in energy is simultaneously transferred to a third ion and/or the phonon spectrum. Non-resonant transfer is always non-reversible. The probability for this third method of transfer is generally small compared with transitions which are matched in energy, except when part of the energy is transferred between ions which are coupled by exchange (2.62).

A quantum mechanical formalism for energy transfer processes was first developed by Perrin (2.63) and Förster (2.64) for solutions containing organic molecules. In 1953 Dexter (2.65) applied the theory to luminescence in solids and extended it.

The probability that energy is transferred from a particular sensitiser, S, to a particular activator, A, was given as:-

$$P_{sa} = \frac{2\pi}{\hbar} \cdot \rho_E \left| \int \Psi_i H_1 \Psi_f \, d\tau \right|^2 \qquad (2.119)$$

where ρ_E is the density of electron states

H_1 is the interaction Hamiltonian between Ψ_i and Ψ_f, the initial and final states respectively.

The Hamiltonian H_1 (and hence P_{sa}) is the sum of a series of terms each due to successive multipolar approximations. The first term in this series for the interaction between the dipole fields of each ion is:-

$$P_{sa}(dd) = \frac{3\hbar^4 c^4 Q_a}{4\pi R^6 n^4 \tau_s} \cdot \left(\frac{\xi}{K^{\frac{1}{2}} \xi_c} \right)^4 \cdot \int \frac{f_s(E) F_a(E)}{E^4} \, dE \qquad (2.120)$$

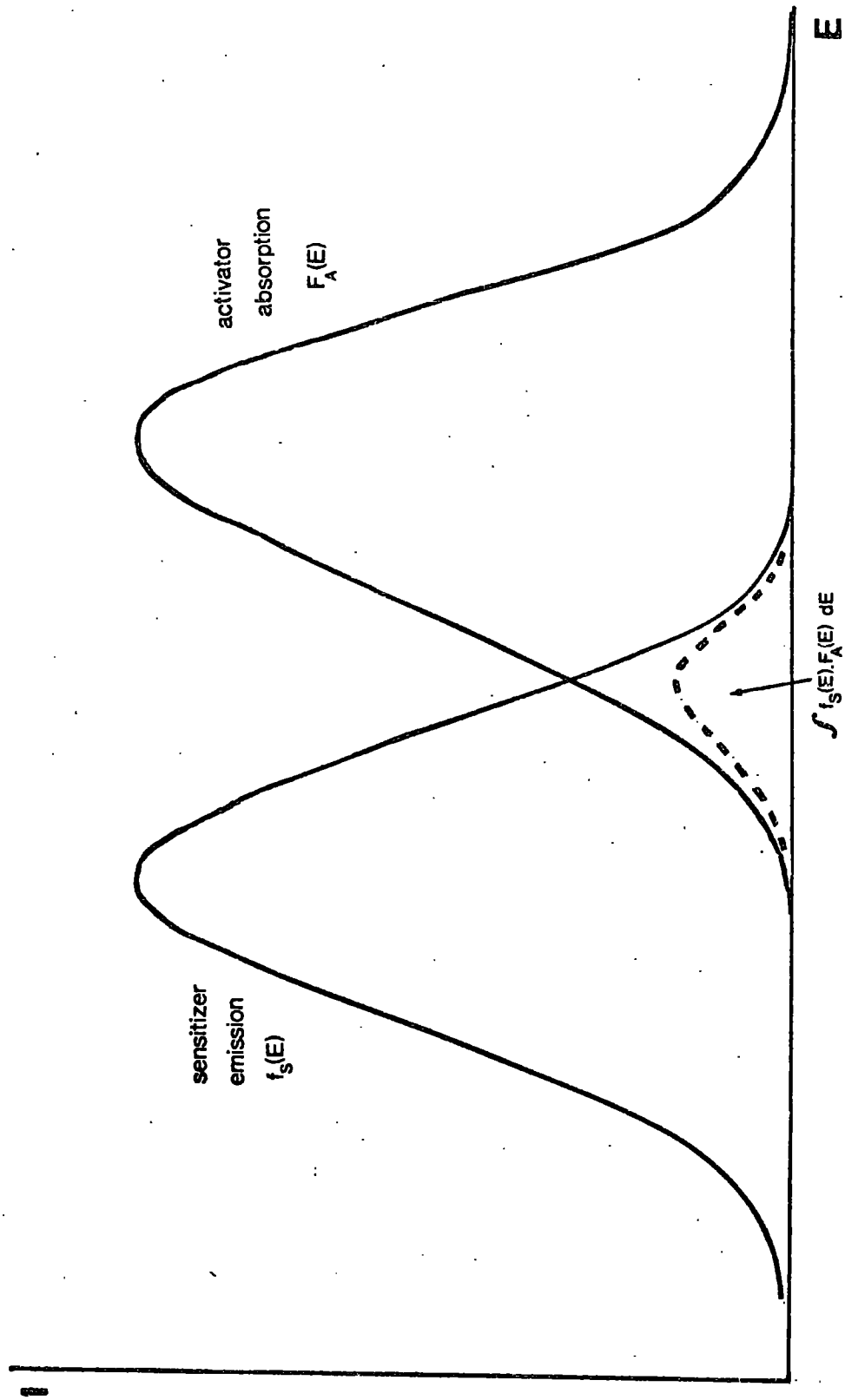

Fig 2.7 Schematic representation of the overlap integral used in the theory of energy transfer processes

where Q_a is the absorption cross-section for the acceptor,

τ_s is the lifetime of the sensitiser,

K is the effective dielectric constant,

$\frac{\xi_c}{\xi}$ is the ratio of the field strength within the medium to that due to the isolated ion,

n is the refractive index,

R is the spatial separation of the ions,

f_s is the shape of the emission spectrum of the sensitiser,

and F_a is the shape of the absorption spectrum of the acceptor.

F_a and f_s are normalised as:-

$$\left.\begin{aligned} \int F_a(E)\, dE &= 1 \\ \int f_s(E)\, dE &= 1 \end{aligned}\right\} \qquad (2.121)$$

The integral:-

$$\int \frac{f_s(E)\, F_a(E)}{E^4}\, dE \qquad (2.122)$$

takes into account the overlap of the respective spectra; the larger this overlap, the more efficient is the transfer process (see Fig 2.7).

The dipole quadrupole term is:-

$$P_{sa}(dq) = \frac{135\, \pi\, \alpha\, \hbar^9\, c^8}{4\, n^6\, R^8\, \tau_s\, \tau_a} \cdot \frac{g'_a}{g_a} \left(\frac{\xi}{K^{\frac{1}{2}}\, \xi_c} \right)^4 \int \frac{f_s(E)\, F_a(E)}{E^8}\, dE \qquad (2.123)$$

where $\alpha = 1.266$ is a constant to account for all states of both ions, and $\frac{g'_a}{g_a}$ is a factor to take account of the degeneracy of the acceptor level.

Except for the next term, $P_{sa}(qq)$, the remaining terms in this

series are not important in this discussion.

A useful parameter is R_c, the critical distance of energy transfer from the sensitiser to the acceptor. R_c is defined as the distance for which the probability of transfer equals the probability of radiative emission of the sensitiser; that is, the distance for which:-

$$P_{sa}\ \tau_s = 1 \qquad (2.124)$$

Numerically, R_c can be determined from:-

$$R_c^6 = 0.63 \times 10^{28} \cdot \frac{Q_a}{E^4} \int f_s(E)\, F_a(E)\, dE \qquad (2.125)$$

Blasse (2.66) has derived the alternative formula:-

$$R_c \simeq 2\left(\frac{3\,V}{4\pi\, x_c\, N}\right)^{1/3} \qquad (2.126)$$

where V is the volume of the unit cell,

x_c is the critical concentration,

and N is the number of ions in V.

Typical values for R_c quoted by Blasse range from about 15Å to 35Å, and the two formulae compare favourably.

In luminescence sensitisation experiments, the quantum efficiency of energy transfer is:-

$$\eta_{ET} = \sqrt{\pi}\, e^{\gamma^2}\left[1 - \mathrm{erf}(\gamma)\right] \qquad (2.127)$$

where $\gamma = \frac{x}{x_c}$ for the acceptor.

Resonances between spin functions of the electrons lead to an exchange interaction which was expressed by Dexter (2.65) as:-

$$P_{sa}(ex) = \frac{2\pi}{\hbar} Z_2 \int f_s(E)\, F_a(E)\, dE \qquad (2.128)$$

where Z_2 is a quantity which is not directly related to experiment and is defined by:-

$$Z_2 = \sum_I \sum_F \frac{e^4}{g_s' g_a K^2} \left| \int Q'(\underline{r}_1) \frac{1}{r_{12}} Q(\underline{r}_2) \, d\tau_{12} \right|^2_{IF} \qquad (2.129)$$

where the $Q(\underline{r})$ are functions of the radial displacement from the respective ions which in turn are separated by a distance, r_{12}. Suffixes I and F refer to the initial and final states respectively. The $Q(\underline{r})$ are products of two functions, both of which decay exponentially with distance, $\underline{r}$, from each ion. Thus Q is very small unless the ionic separation is very small. The critical distance, R_c, for the case of the exchange interaction, is typically of the order 10Å to 15Å (2.67).

The decay equation for the donor ion in the presence of an acceptor is affected by these transfer processes, and is quoted by Nakazawa and Shionoya (2.68) as:-

$$\phi(t) = \frac{I(t)}{I(0)} = \exp\left[-\frac{t}{\tau_s} - \Gamma\left(1 - \frac{3}{s}\right) \cdot \gamma \left(\frac{t}{\tau_s}\right)^{3/s} \right] \qquad (2.130)$$

where S = 6, 8, 10 corresponding to dipole-dipole, dipole-quadrupole, and quadrupole-quadrupole interactions respectively, and Γ is the gamma function; $\Gamma\left(1 - \frac{3}{s}\right)$ = 1.77, 1.43 and 1.30 for s = 6, 8 and 10 respectively.

The emission intensity of the donor under continuous excitation is described by:-

$$\frac{I}{I_o} = \tau_s^{-1} \int_0^\infty \phi(t) \, dt \qquad (2.131)$$

where I_o is the intensity of luminescence in the absence of the acceptor (2.69).

The emission intensity of the donor ion varies with concentration as:-

$$I(x) \propto (a + x^{-s/3})^{-1} \qquad (2.132)$$

and the variation with ionic separation is:-

$$I(r) \propto (a + r^{-s})^{-1} \qquad (2.133)$$

where a is a constant (2.70).

Energy transfer processes between rare earth ions have been studied extensively in both crystals (2.71) and glasses (2.72). The importance of such effects lies in the enhancement of certain emission bands and a broadening of excitation spectra. In considerations of the practicability of terbium glass lasers, for instance, appropriate transfer to the bands of the Tb^{3+} ions is necessary since absorption bands (and consequently the excitation spectrum) are not very pronounced for this ion.

The existence of vibronic levels in rare earth crystals shows that the rare earth ions are coupled with the vibronic quanta of the lattice. Reisfeld et al (2.73) have studied energy transfer from terbium to gadolinium in borate glasses. They consider that such coupling to the lattice also plays a dominant role in the energy transfer processes between rare earth ions in glass.

CHAPTER 3

EXPERIMENTAL METHODS AND APPARATUS

3.1 Sample Preparation

All samples were prepared in a specially constructed furnace, built from Johns-Mansville JM3000 insulating bricks. The bricks were built into a two foot cube asbestos and steel frame, with a side entrance. The furnace was electrically heated by eight Morganite 'crystolon' heating elements, grouped in two rows, 15 cm apart.

The rods were connected in series to give a total resistance of 10.4 Ω. Voltage was supplied from a Eurotherm control system and FM-2 filter unit. The maximum r m s voltage was 240 V, the system operating on the principle of phase angle control. Temperature was measured by means of a platinum/rhodium thermocouple and could be maintained within 10°C of the preset value. The furnace was capable of reaching 1600°C; the actual temperatures required for melting or annealing vary with the glass type and are considered later (Table 3.8).

Before melting, the appropriate oxides were ground together to assist dispersion. Except when high concentrations of terbium oxide were required, samples were prepared in 100 g batches.

Silicate glasses were prepared in a 95% platinum - 5% rhodium crucible, with a lid of the same material. The crucible was an Engelhard model number 110 with a reinforced rim and capacity 70 cm^3. The lid prevented the surface of the powdered sample from heating first and erupting over the crucible side.

No attempt was made to change the atmospheric conditions dur-

ing the melt, the constant air environment was considered to be an oxidising atmosphere.

If visible inhomogeneities appeared in the glass, it was reground and remelted. This was only necessary for the high terbium concentration glasses, where batch sizes were 20g. After melting, the glasses were poured out on to a stainless steel plate, preheated to around 300°C.

Non-silicate glasses were melted in alumina or quartz crucibles and allowed to solidify in situ.

Initially, samples were shown to be glassy by means of X-ray powder diffraction. The presence of a diffuse halo in Debye-Scherrer powder photographs is characteristic of the glassy state. The diffraction pattern was so diffuse that no differences were observed for glasses of varying terbium concentration.

From this procedure, it was learned that the presence of a crystalline phase is betrayed by translucent material. Presumably this is because the rate of cooling is too rapid to allow the growth of sizeable crystals. Such 'seeding' could occasionally be seen before the melt had cooled.

Before the samples could be cut they had to be annealed in a muffle oven, to remove internal stresses, which would shatter the glass if subjected to any mechanical shock. Stress patterns seen in polarised light were completely removed by the annealing process (see Table 3.8).

For optical absorption work, samples were cut to the requisite thickness (usually 3 to 5 mm) and polished with various grades of diamond paste, to a 1 micron finish, on a felt cloth lap.

No attempt was made to melt samples of pure silica (SiO_2), as this requires temperatures in excess of 1800 °C, which was beyond the capabilities of the furnace. Instead, the work was concentrated on alkali-metal silicates and alkali-metal aluminium silicates. Sodium silicate (hereafter abbreviated as NS) glass was chosen to represent the binary system, and lithium aluminium silicate (hereafter abbreviated as LAS) was chosen in the ternary glass system.

The LAS glasses were formed by mixing appropriate weights of the various oxides. The silica used was finely ground, acid washed, Brazilian quartz, and the alumina was finely ground, spectroscopically pure sapphire. Both were supplied by James A Jobling Ltd. The alkali metals were incorporated as the anhydrous carbonates, as their oxides are not stable in air at room temperature. On heating the carbonates decompose to the oxide by the usual reaction:-

$$M_2CO_3 \longrightarrow M_2O + CO_2$$

where M = Li, Na, K. The reaction is essentially complete at the temperatures of melting. The silica and alumina do not themselves melt at these temperatures, but dissolve in the molten alkali oxide.

The NS glasses were prepared from soda glass which had been premelted and reground. Their purity was consequently not high (see Table 3.1), but the concentration of impurity metals with optically active electrons was low.

Table 3.1 lists the composition of the NS and LAS base glasses and the principal metal impurities, where known, are also given. The base glasses were doped with rare earth oxides of at least 99.9% purity,

TABLE 3.1

Composition of Silicate Base Glass, Types NS and LAS

Oxide	Weight Percentages	
	NS*	LAS
SiO_2	70.8	60.0
Na_2O	16.4	
Al_2O_3	2.4	20.0
Li_2O		20.0
CaO	5.0	
MgO	2.4	
BaO	1.8	
K_2O	1.6	
PbO	0.1	
Trace elements < 20 ppm	Fe, Mn, Ti, Cu	Fe, Pb

* The quantitative analysis was carried out by Mr J Sanderson at the British Steel Corporation (Consett) laboratories, using standard wet chemical techniques

the principal impurities being other rare earth oxides. In the case of terbium oxide (Tb_4O_7), the principal impurity was gadolinium oxide (Gd_2O_3). The concentration of other rare earths was considered to be low enough for energy transfer processes, between the impurity ions and the desired ions, to be insignificant.

Table 3.2 lists weight percentages of the terbium doped NS and LAS glasses prepared, together with their mole percentages. The latter are calculated on the basis of terbium ion concentration and not on the concentration of Tb_4O_7, since:-

(a) the luminescence properties are an ionic phenomenon, so that comparison between oxides such as Tb_4O_7 and Gd_2O_3 is not realistic in terms of the formulae molarities.

(b) Tb_4O_7, in any case, is not a stoichiometric formula (see note in Chapter 1).

The weight and mole percentages of other rare earths incorporated into NS and LAS glasses are given in Table 3.3. These samples were chosen for comparison of luminescence intensity (Sm and Dy) and for comparison in thermoluminescence measurements.

For energy transfer investigations, NS samples of higher purity were prepared from the acid washed quartz, used in the preparation of the LAS glasses, and anhydrous sodium carbonate. The concentration of other alkali metals and alkali-earth metals together was less than 0.1%. The samples prepared are listed in Table 3.4. Various other silicate glasses prepared are listed in Table 3.5.

The representative phosphate glass chosen was calcium phosphate,

TABLE 3.2

Doped Samples Prepared (NS and LAS Glasses)

Terbium in NS Glass

Weight Percent	Mole Percent
0.095	0.031
0.900	0.297
3.000	1.009
4.350	1.481
8.160	2.880
11.600	4.250
15.800	6.030

Terbium in LAS Glass

Weight Percent	Mole Percent
1.12	0.364
2.22	0.728
5.36	1.810

TABLE 3.3

Other Samples Melted (NS and LAS Glasses)

Other Rare Earths in NS Glass

Rare Earth Oxide	Weight Percent	Mole Percent
Nd_2O_3	4.35	1.62
Sm_2O_3	4.35	1.56
Dy_2O_3	4.35	1.47

Other Rare Earths in LAS Glass

Rare Earth Oxide	Weight Percent	Mole Percent
Nd_2O_3	5.24	2.00
Gd_2O_3	5.62	2.00

TABLE 3.4

Silicate Glasses (NS) Prepared for Energy Transfer Studies

Base Glass

Constituant	Weight %	Mole %
SiO_2	75·33	74·75
Na_2O	24·67	25·25

Singly Doped Glasses

Dopant Ion	Weight %	Mole %
Y^{3+}	0·902	0·487
La^{3+}	1·296	0·487
Pr^{3+} *	1·354	0·488
Nd^{3+}	1·337	0·486
Sm^{3+}	1·386	0·487
Tb^{3+}	1·484	0·487
Dy^{3+}	1·480	0·487
Er^{3+}	1·518	0·487

* Note: Pr was added as the oxide Pr_6O_{11}

Doubly Doped Glasses

Co-dopant	Weight % Tb	Weight % Ln	Mole % Tb	Mole % Ln
Y	1·471	0·889	0·486	0·486
La	1·466	1·278	0·486	0·486
Pr*	1·465	1·335	0·487	0·487
Nd	1·465	1·318	0·486	0·486
Sm	1·464	1·365	0·486	0·486
Tb	2·925	-	0·974	-
Dy	1·463	1·459	0·486	0·486
Er	1·462	1·499	0·486	0·486

* Note: Pr was added as the oxide Pr_6O_{11}

TABLE 3.5

Other Silicate Glasses Prepared (to Investigate IRQC Effect in Rare Earth Glasses - see Chapter 7)

Oxide	1		2		3		4		5	
	weight %	mole %	weight %	mole %	weight %	mole %	weight %	mole %	weight %	mole %
SiO_2	61.28	72.73	61.27	72.73	61.27	72.73	62.43	80.00	62.41	80.00
Na_2O*	19.76	22.73	19.75	22.73	19.75	22.73	12.08	15.00	12.07	15.00
Y_2O_3	8.20	2.59	8.20	2.59	8.20	2.59	--	--	--	--
Yb_2O_3	9.80	1.77	9.80	1.77	9.79	1.77	23.29	4.55	23.28	4.55
Ho_2O_3	0.96	0.17	--	--	--	--	2.21	0.45	--	--
Er_2O_3	--	--	0.97	0.18	--	--	--	--	2.23	0.45
Tm_2O_3	--	--	--	--	0.98	0.18	--	--	--	--

* added in the form of Na_2CO_3

which was prepared from the thermal decomposition of calcium tetra-hydrogen diorthophosphate, by the reactions:-

$$CaH_4(PO_4)_2.H_2O \longrightarrow CaH_4(PO_4)_2 + H_2O$$

$$CaH_4(PO_4)_2 \longrightarrow Ca(PO_3)_2 + 2H_2O$$

The water of crystallisation is lost at 109°C, and the second reaction begins at 203°C. On cooling, the calcium phosphate solidifies at 975°C.

The representative borate glass chosen was sodium borate (borax), which was prepared from the solid by fusion:-

$$Na_2B_4O_7.10H_2O \longrightarrow Na_2B_4O_7 + 10H_2O$$

The water of crystallisation is lost at 320°C, and the anhydrous borax melts at 741°C.

The terbium concentrations in the phosphate and borate glasses melted are listed in Table 3.6, and the principal impurities are given in Table 3.7.

Table 3.8 gives the thermal histories of all samples melted, together with the temperatures at which the samples were annealed.

The practical applications of both phosphate and borate glass phosphors are considered to be limited, particularly as the latter had to be kept in vacuo to prevent devitrification. However, no attempt was made in this study to evaluate the properties of mixed network

TABLE 3.6

Phosphate and Borate Glasses Prepared

Phosphate Glasses

Weight %	Mole %
0·117	0·126
1·241	1·328
5·015	5·517

Borate Glass

Weight %	Mole %
4·943	5·54%

TABLE 3.7

Purity of Chemicals used in the Production of Borate and Phosphate Glasses (Suppliers' Specifications)

Impurity	sodium tetraborate $Na_2B_4O_7.10H_2O$ ppm	calcium tetrahydrogen di-ortho phosphate $CaH_4(PO_4)_2.H_2O$ ppm
As	1	2
Ca	50	---
Cl	10	50
Pb	5	---
Fe	5	50
PO_4	10	---
SO_4	50	500

TABLE 3.8

Thermal Histories of the Samples Prepared

Sample Type	Melting Conditions	Annealing Conditions
NS	Three hours at 1300°C	Three hours at 600°C
LAS	Five hours at 1450°C	Three hours at 580°C
Energy transfer glasses	Four hours at 1400°C	Three hours at 600°C
IRQC glasses	Four hours at 1400°C	----
Phosphate	Three hours at 1050°C	----
Borate	Three hours at 900°C	----

glasses (for example, borosillicate glasses) which are more stable. The applications of these latter glasses may be significant.

3.2 Spectrophotometers and Associated Equipment

Most of the luminescence and visible region absorption measurements were made on an Optica CF4DR/CF4NI double-beam grating spectrophotometer. Absorption spectra from 200nm to 40 microns were taken on various spectrometers which are listed in the appropriate sections of Chapter 4.

The Optica spectrophotometer consists of a monochromator, a detector head and the electronics system. The monochromator grating can be turned by a motor at speeds of 3, 6 or 12 Å/sec. The wavelength is given by a direct-reading scale. The monochromator can be fitted with either a single- or double-beam head. The single-beam head employs an RCA 1P28 photomultiplier tube, supplied with a maximum operating potential of 850V. The monochromator slit width may be varied manually, up to a maximum of 0.18mm.

The double-beam head divides the monochromator beam into two equal parts, and then recombines them on to the photodetector, by a pair of rotating mirrors, which are driven by the same motor. One beam is a reference beam, the other is the sample beam. Two separate compartments allow access to each beam, before recombination. Two photodetectors are employed; an EMI 6256B photomultiplier for wavelengths between 185 and 690nm, and a Dumont 6911 Pb S infrared detector for wavelengths from 600 to 1,000nm. These photodetectors may be supplied with any voltage up to 1,000 V. The monochromator

slit may be adjusted either manually or by a servo motor. The servo mechanism is driven by the output of a transistorised pre-amplifier fitted to the photodetector. Thus the beam from the monochromator produces a constant detector response due to the reference beam.

The photodetector signal is fed to a double-beam ratio amplifier, which produces an output proportional to the ratio of the sample beam to the reference beam. The amplifier switching frequency is synchronised with the mirror chopping frequency. The electronics can also be used as a simple amplifier when the single-beam mode is employed. The output of the amplifier is fed to a strip chart recorder, which has a speed of 480 inches/hour.

The electronic system also includes stabilised supplies for the photodetectors and for tungsten and deuterium lamps which are fitted to the instrument. The tungsten lamp (50W) supplies continuum radiation in the visible region of the spectrum, and the deuterium lamp (30W) has a quartz envelope to supply continuum ultra-violet radiation.

The spectral response of the 6256B photomultiplier tube is shown in Figure 3.1. This response is similar to that of the 6097B photomultiplier tube which was used in thermoluminescence experiments.

For low temperature measurements, a specially designed cryostat was used. The cryostat had two chambers which were separated from each other, and from the outside, by vacuum. The inner chamber was filled with either liquid nitrogen or liquid helium, and could be pumped to reduce the temperature of the liquid. The temperature of the system could be increased by a small electric heater, placed inside the cryo-

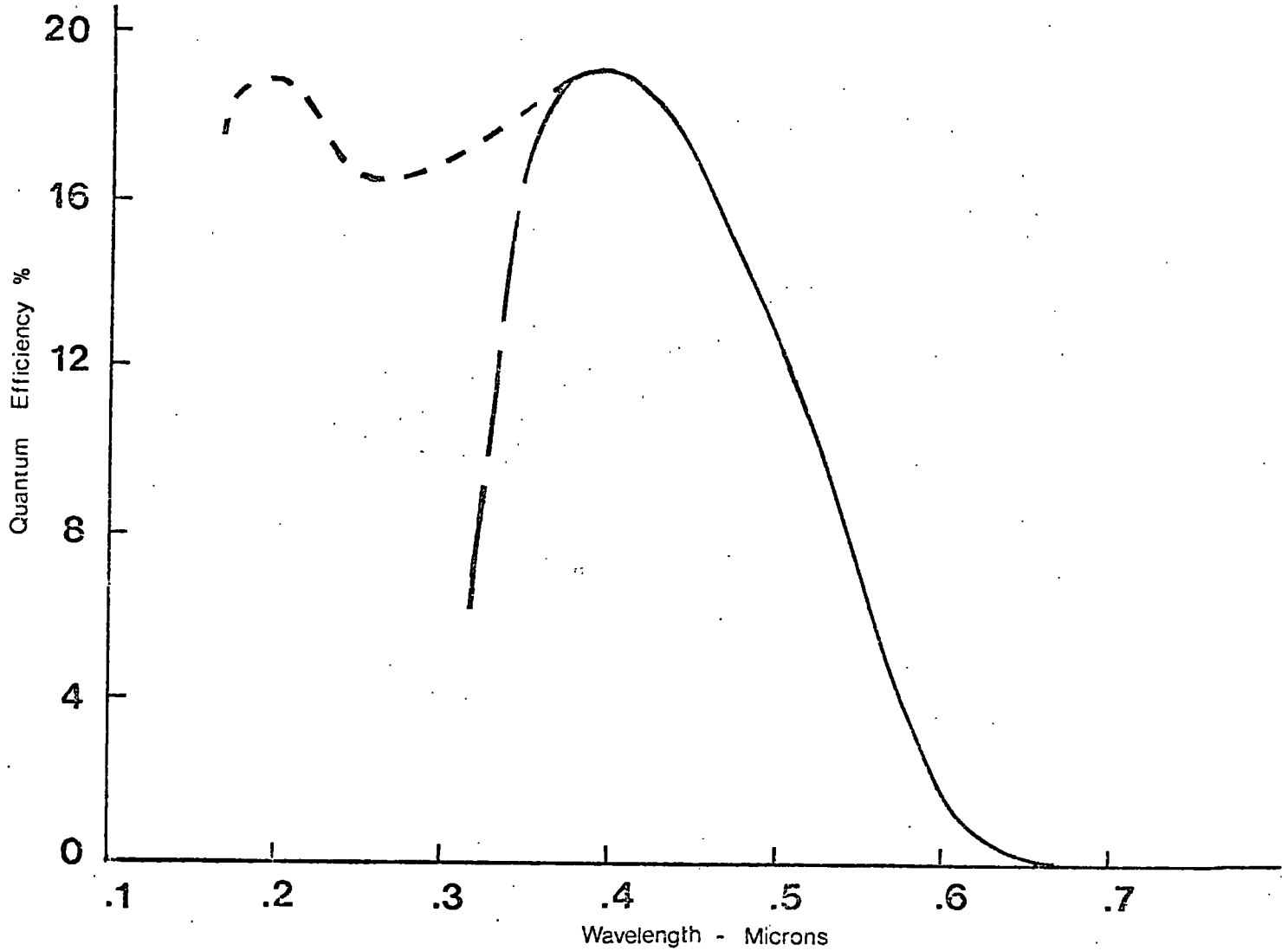

Fig 3.1 Photomultiplier quantum efficiency, EMI 6097B and 6256B, as a function of wavelength

stat.

The sample was mounted on a copper block, projecting from the bottom of the inner chamber. Temperatures were measured by direct contact with a gold/iron thermocouple. The sample was irradiated through a perspex window. The resulting luminescence emerged through a glass window and was focussed on to the entrance of the spectrophotometer by a concave mirror.

Ultra-violet excitation was achieved using an Osram, 125W, MBW/U mercury vapour lamp. This lamp has a Philips ultra-violet filter which was found to have similar transmission properties to the 26-3012 filter described in section 3.4. A 250W compact source mercury lamp was also used and, in addition, the deuterium lamp described above.

In the measurement of luminescence decay times, a xenon flash tube was used for ultra-violet excitation. The system is shown in Figure 3.2. The photomultiplier response was displayed on an oscilloscope and the resulting trace was photographed. As the decay times measured were all of order milliseconds or slower, the effect of oscilloscope and photomultiplier response times were not considered.

When X-ray excitation was employed, it was found impractical to use the Optica spectrophotometer, and so an alternative system was devised. A Grubb-Parsons' PM2 single-beam monochromator was adapted into a low resolution spectrophotometer. The optical system is shown in Figure 3.3. This monochromator produces its dispersion by means of a quartz prism, which is rotated by a micrometer screw gauge, hence the system must be calibrated. The calibration and res-

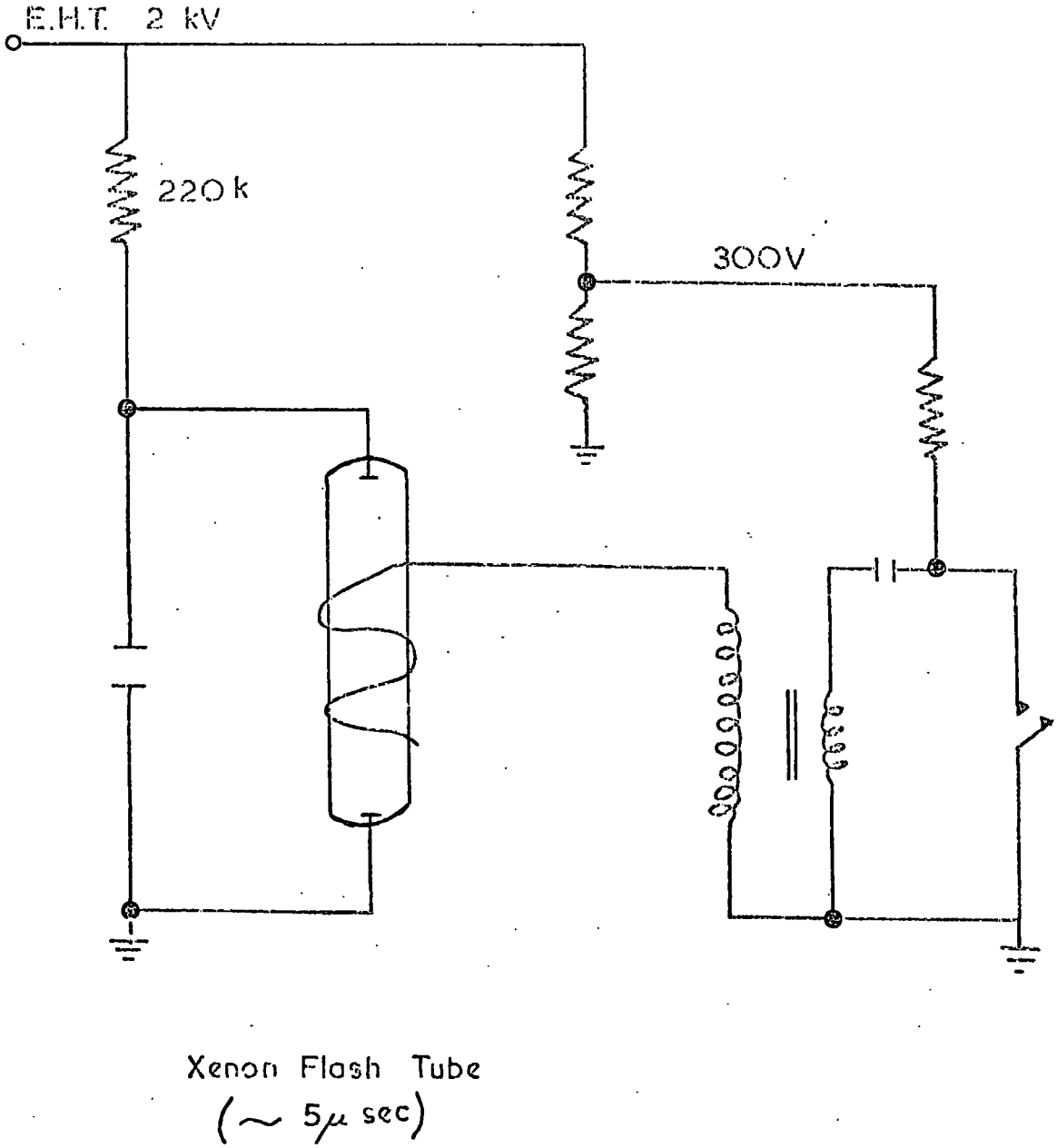

Fig 3.2 Circuit diagram of Xenon flash tube used in determining the decay curves of ultra-violet excited luminescence

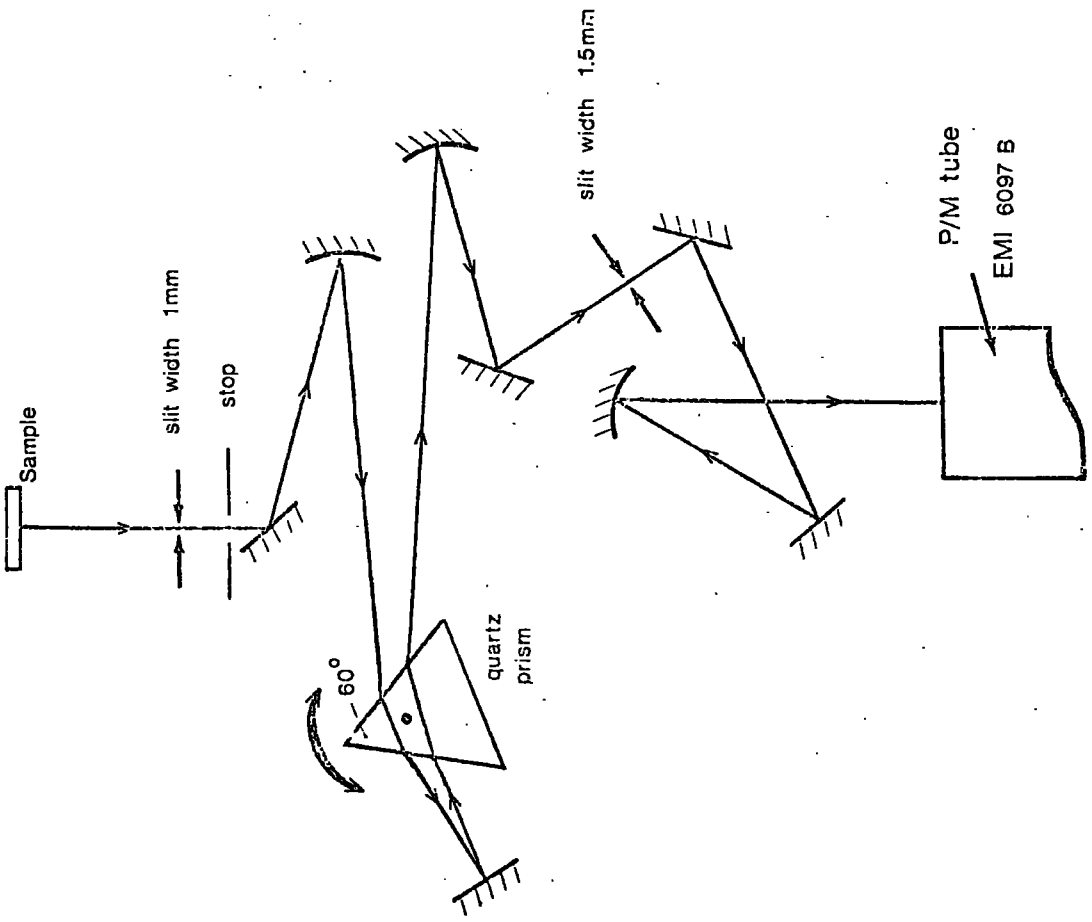

To Scale
1:3

Fig 3.3 Modified Grubb-Parsons' PM2 monochromator for use in X-ray excited luminescence

olution are described in the experimental section.

The monochromator output was measured with an EMI 6097B photomultiplier tube, the base circuit of which is described in the section of this chapter on thermoluminescence. Details of the X-ray equipment used are also given in this section. Some X-ray luminescence measurements, for example of decay times and the temperature dependence of luminous intensity, were also carried out with the thermoluminescence equipment.

3.3 Thermoluminescence Equipment

Glow-curves were obtained using the specially designed cryostat shown in Figure 3.4. The equipment included an EMI 6097B photomultiplier tube and had a working temperature range from 100°K to 600°K.

The samples used were 2 mm thick and approximately 0.5 cm wide by 1 cm long. Irradiation was performed with a Philips PW 1009 X-ray set which has an exit slot size of 1.2 mm by 7 mm.

The samples were subjected to various periods of irradiation at set temperatures, while mounted inside the cryostat. For thermoluminescence from room temperature, samples were also irradiated adjacent to the exit slot of the X-ray set to obtain a better signal.

The X-ray beam was from a water cooled cobalt target, which produces K-line radiation as follows:-

$K_{\alpha 1}$	1.7889 Å
$K_{\alpha 2}$	1.7928 Å
$K_{\beta 1}$	1.6208 Å

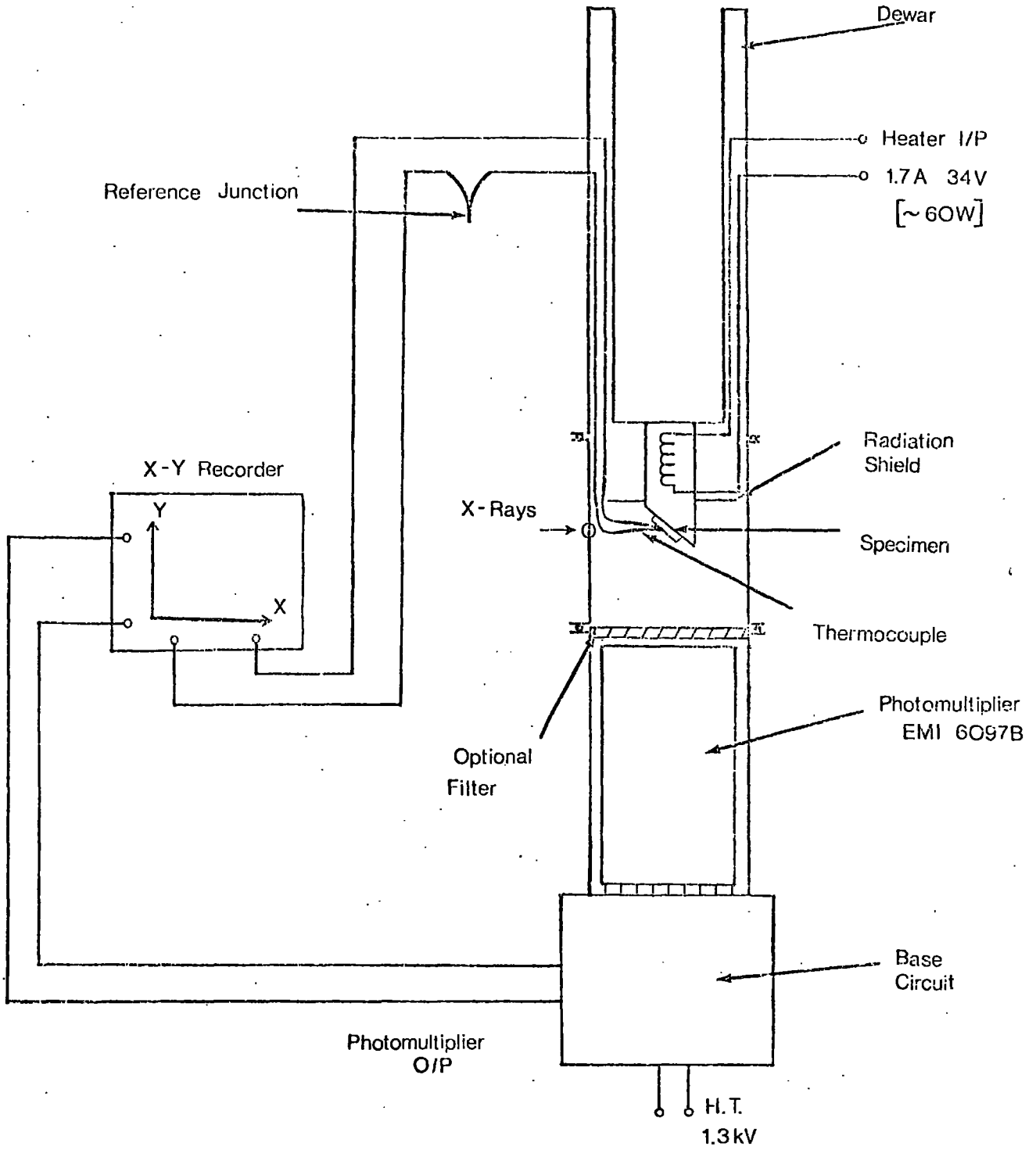

Fig 3.4 Diagram of the apparatus used to measure the thermo-luminescence glow curves of silicate glasses.

To improve the beam intensity no filter was used to select from these lines.

The samples were irradiated through a quarter-inch diameter mylar window, 0.1 mm thick, to permit evacuation of the cryostat when glow-curves were to be measured beginning at low temperatures. Specimens were mounted on a copper "cold finger", and their temperature was measured by direct contact of a copper/constantan thermocouple with the surface of the glass. The X-rays produced solarisation as an essentially surface phenomenon; the brown discolouration penetrated perhaps 1 mm into the glass. After irradiation, the solarisation was greatest on the side of the specimen away from the copper mount. Since glass has a fairly low thermal conductivity, there was a small temperature difference between the two surfaces of the specimen. The thermocouple was fastened to the side on which the solarisation was produced, as this was nearer the actual temperature of the defects.

After an appropriate irradiation period, the samples were warmed at a roughly constant rate of 11°C per minute, using a 20 Ω 32 W Kanthal wire-wound heater. An aluminium shield was incorporated to prevent the detection of photons from the heater, as the latter at times became red hot.

The T L was detected by the photomultiplier which had the base circuit shown in Figure 3.5. The glow-curves were displayed on an X-Y recorder. The ouput from the photomultiplier tube was fed to the Y-terminals and the voltage from the thermocouple supplied the drive on the X-axis. The reference junction of the thermocouple was kept at 77°K in liquid nitrogen.

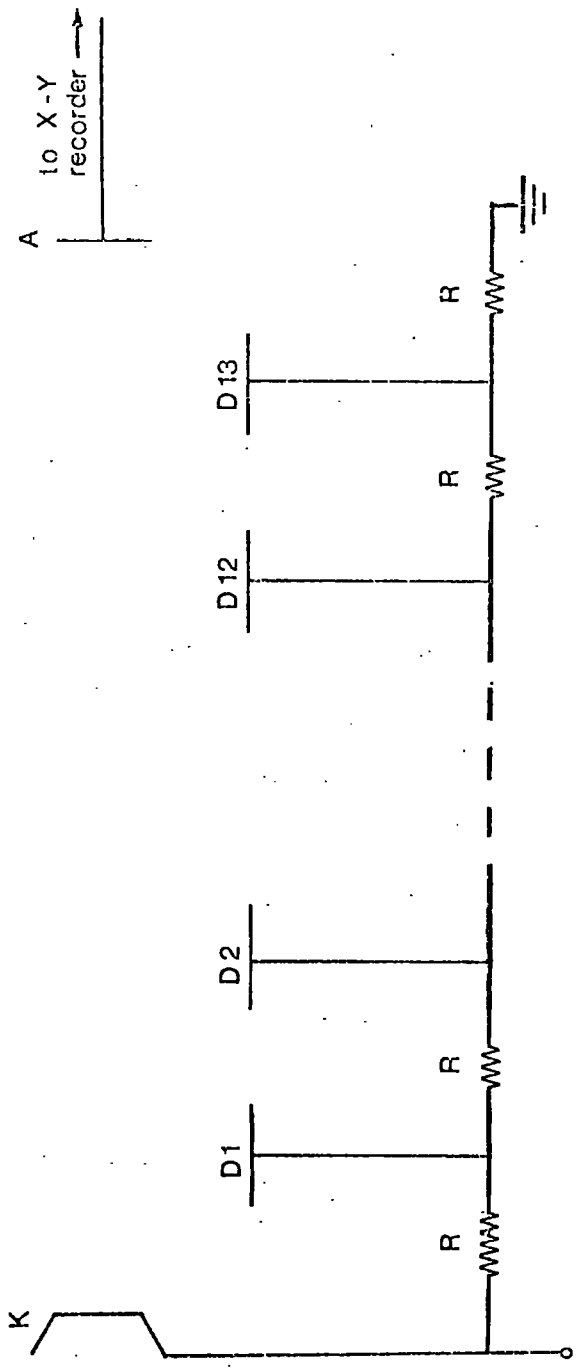

Fig 3.5 Base circuit of EMI 6097B photomultiplier tube, used in thermoluminescence measurements

The heating rate was determined by superimposing small marker pulses at approximately 45 second intervals on to the glow-curve. The pulses were generated by an RC network charging a uni-junction transistor. The circuit is shown in Figure 3.6.

By employing the internal time base, the X-Y recorder could also be used to display the decay curves of X-ray excited luminescence at various temperatures.

3.4 Filters

In the thermoluminescence measurements, emission spectra were determined by comparing glow-curves taken through various optical filters. All the filters were ground into circular discs, two inches in diameter, to fit the thermoluminescence equipment. The end of the photomultiplier tube was completely covered.

All filters used were Ealing colour filters, except the yellow, which was an Actina DBD colour filter. Their transmission characteristics were measured on the Optica spectrophotometer and are shown in Figure 3.7. The results are consistent with the manufacturers' specifications(3.1). The filter number 26-3012 was also used to isolate the 365 nm emission line from the mercury lamps when this was required for fluorescence measurements.

The actual intensity of the glow-curve peak must, of course, be corrected for the photomultiplier tube response. The wavelength and the effective photodetector sensitivity of the resultant peaks, after correction for the appropriate filter, are listed in Table 3.9. Also listed are the pass ranges, which are taken as the ranges of wave-

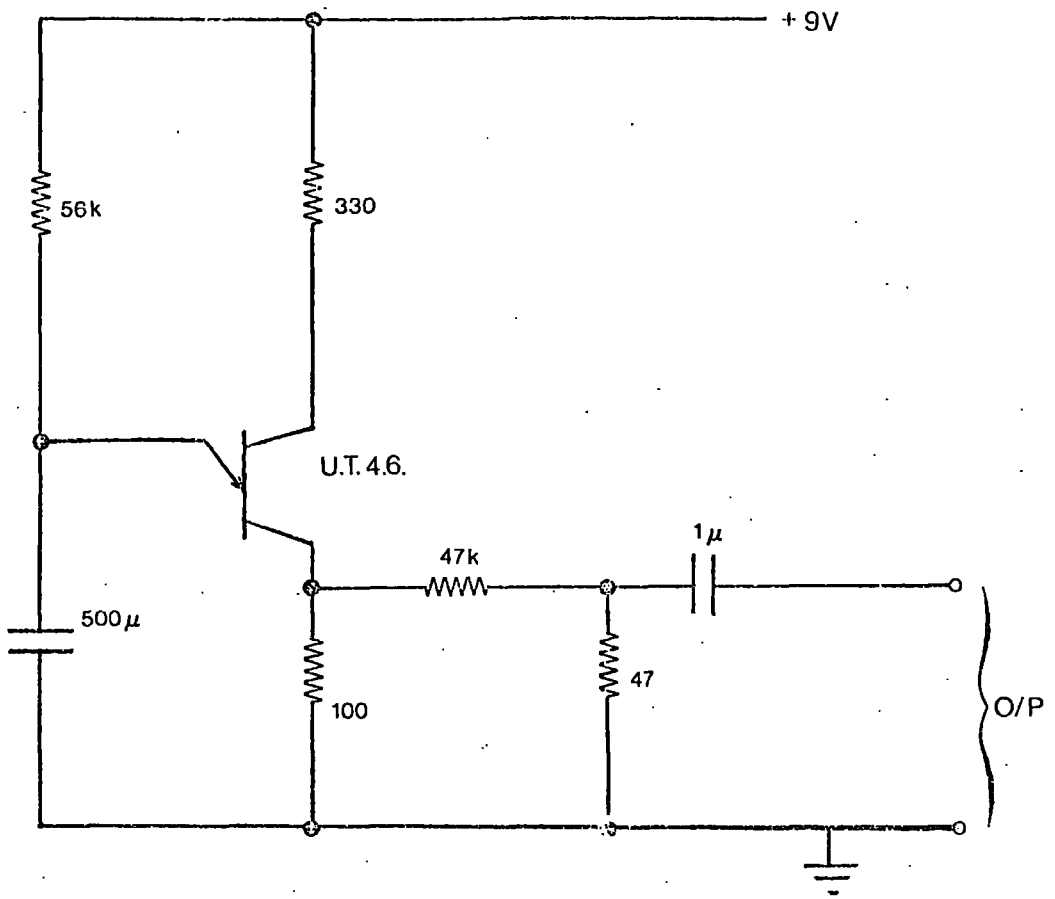

Fig 3.6 Unijunction transistor circuit generating 5 mV pulses at 44.2 second intervals, used to determine the heating rate in thermoluminescence measurements.

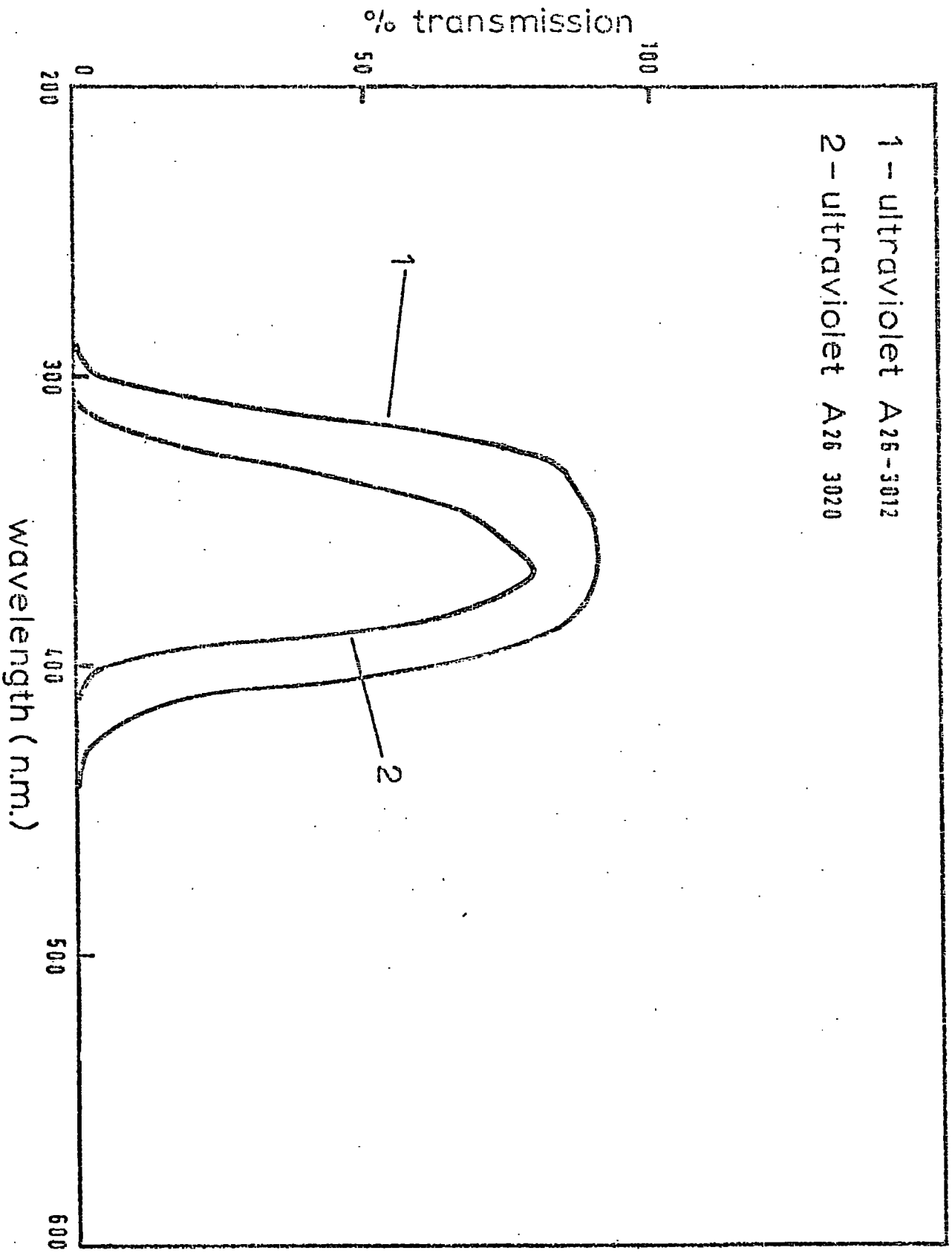

Fig 3.7a

Percentage Transmission of Filters

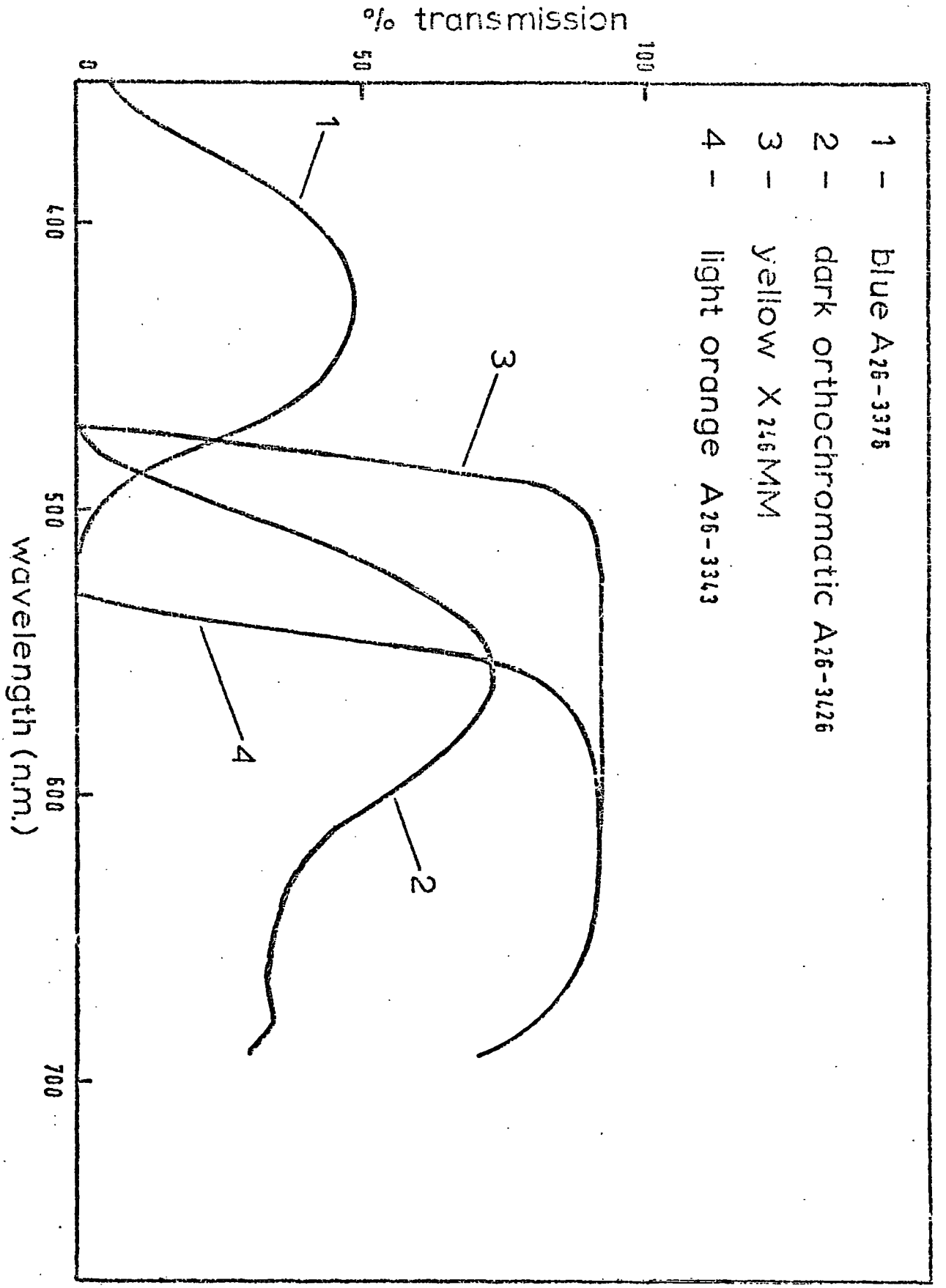

Fig 3.7b

Percentage Transmission of Filters (continued)

TABLE 3.9

Resultant Sensitivity of the Photomultiplier Tube used in Conjunction with Various Filters

Filter	Colour	Peak Wavelength ± 2nm	Pass Range ± 3nm	Maximum Sensitivity (relative units)
26-3012	ultra-violet	372	348 - 386	5.75
26-3020	ultra-violet	375	336 - 401	6.60
26-3376	blue	423	387 - 464	3.80
X 246 MM	yellow	502	485 - 544	3.15
26-3426	dark orthochromatic	536	507 - 562	5.65
26-3343	light orange	553	543 - 578	2.65

lengths for which the effective sensitivity is $\frac{1}{\sqrt{2}}$ times that at maximum.

3.5 Refractive Indices

Although the refractive index of a material does not give much information about its physical nature, nevertheless it is a useful parameter in many types of optical calculation. The glass samples prepared were all cut in thin sections so that direct measurement of refractive indices by the method of real and apparent depth would be inaccurate. A central illumination method, known as the Becke line method (3.2), which involves the use of powder samples, was employed. With monochromatic illumination, the method is capable of distinguishing between indices of refraction differing by as little as one part in a thousand. The phenomenon used depends upon the total internal reflection of light incident at more than the critical angle when passing from a material of greater to a material of lesser index. The test is employed for comparing indices of refraction of fragments of material with various immersion media of known refractive index in which they may be mounted.

Light entering from below will strike an inclined boundary at some point at greater than the critical angle and a portion of the beam will be deflected towards the material of greater refractive index. It forms an irregular white line called the "Becke line", which may be viewed under a microscope with a magnification of 80. If the microscope tube is raised, the line appears to move towards the medium of higher refractive index (see Figure 3.8). By comparing a sample

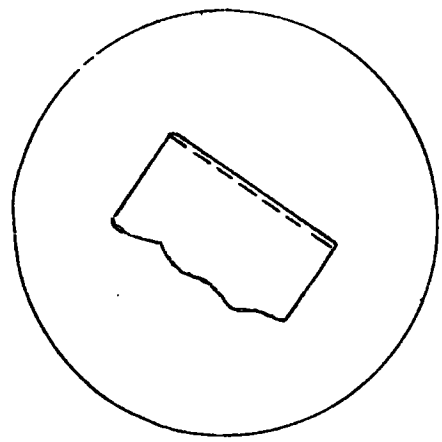

Tube at focus

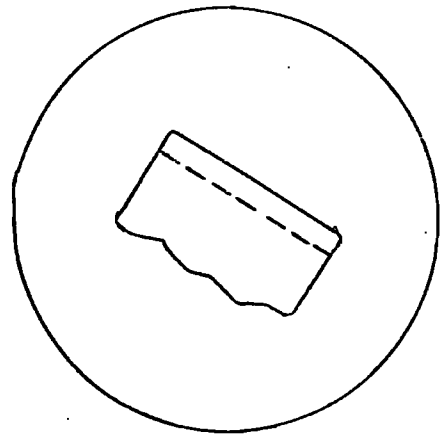

Tube raised

Fig 3.8 The appearance of a specimen under central illumination for the case n(specimen) > n(immersion medium), furnishing the illusion of the Becke line moving to the optically dense material

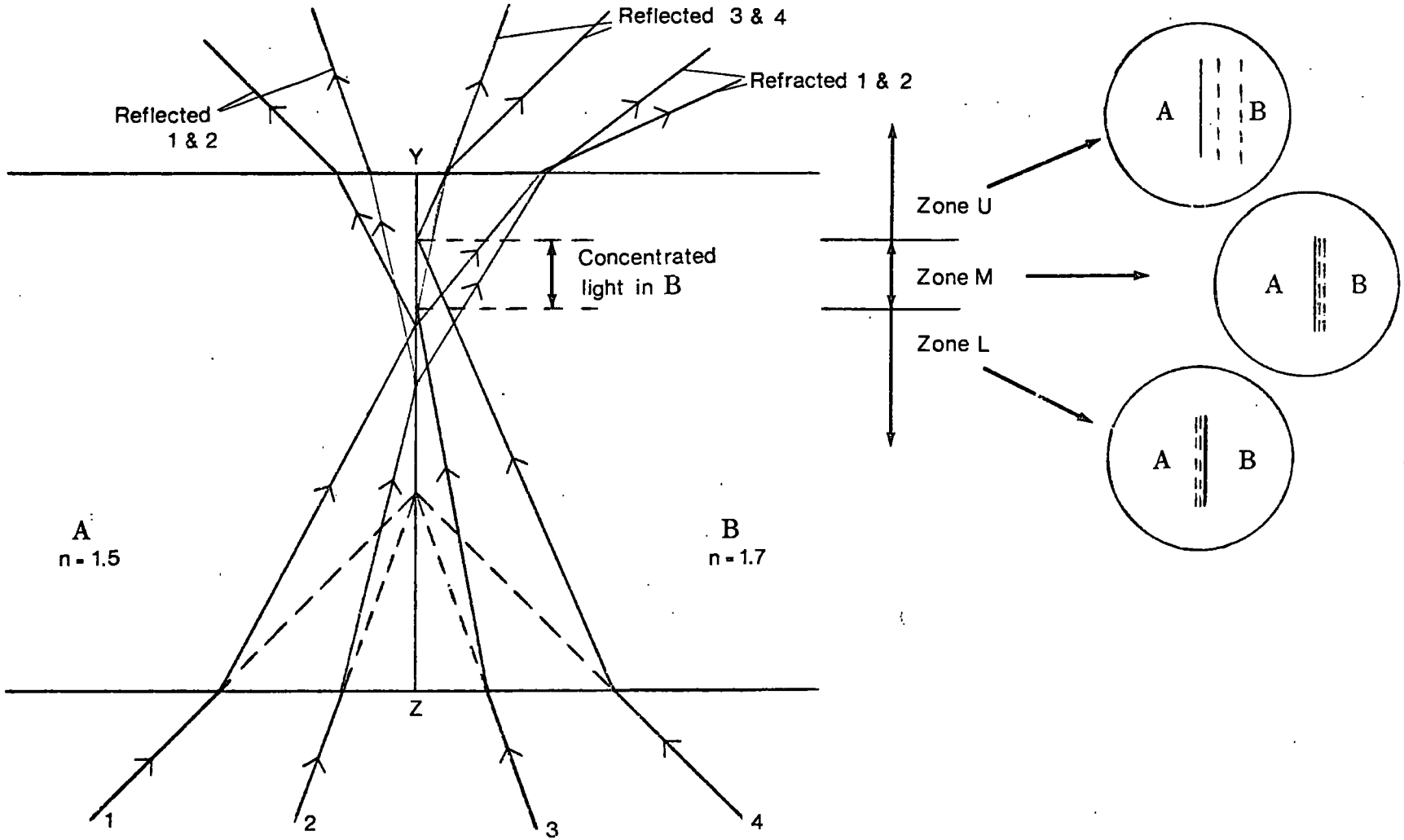

Fig 3.9 Explanatory diagram of the Becke line effect used to determine refractive indices. After Hotchkiss (1905)

with various immersion media the refractive index of glass powders was determined to an accuracy of about one part in 200.

Hotchkiss (3.3) has given an explanation of this effect. The construction is shown in Figure 3.9. The glass, B, is assumed to be in contact with a liquid, A, with a vertical bounding plane, YZ. A is assumed to have a lesser index (n = 1.50), and B has a greater index, 1.70. The cone of light entering from below may be represented by the rays, 1, 2, 3, 4, with angles of inclination as indicated in the diagram. The critical angle of B with respect to A is, in this case, about 62°. The rays of light within B (3 and 4) which strike the surface YZ at greater than the critical angle, are totally reflected. The rays of light within A are split at the boundary surface, part being refracted into B. A band of light appears in the material of higher index at level M. If the plane of focus is elevated to level U, the band becomes broader and furnishes the illusion of moving towards the centre of B.

CHAPTER 4

ABSORPTION AND REFRACTIVE INDICES

4.1 Refractive Indices

Refractive indices of the NS and LAS glasses were measured using the Becke line method, which was outlined in Chapter 3.5. The results are shown graphically in Figure 4.1. The index of refraction is a linear function of molar concentration of the rare earth oxide. This is in agreement with Beer's law, which states that the absorption coefficient (and hence the refractive index) of a solution of an absorbing ion is directly proportional to the concentration of that ion. The concept of a solution is here extended to the glassy state.

The slope of both graphs is:-

$$(7.4 \pm 0.5) \times 10^{-3} \quad (\text{mole } \%)^{-1}$$

The density of the 2.88 mole % NS glass was determined directly from a bulk sample by suspension in water. For this glass, the result was 2.42 ± 0.03 g/cm^3.

The molecular volume, V, of the Tb_4O_7 oxide (but see the note on stoichiometry in Chapter 1) in aqueous solution is defined as the ratio of the molecular weight, M, of Tb_4O_7 to the sample density, ρ, multiplied by the weight fraction. In a glassy solution we can assume a similar definition, and determine the molecular volume from:-

$$V = \frac{M}{\rho} \cdot \frac{W}{100} \qquad (4.1)$$

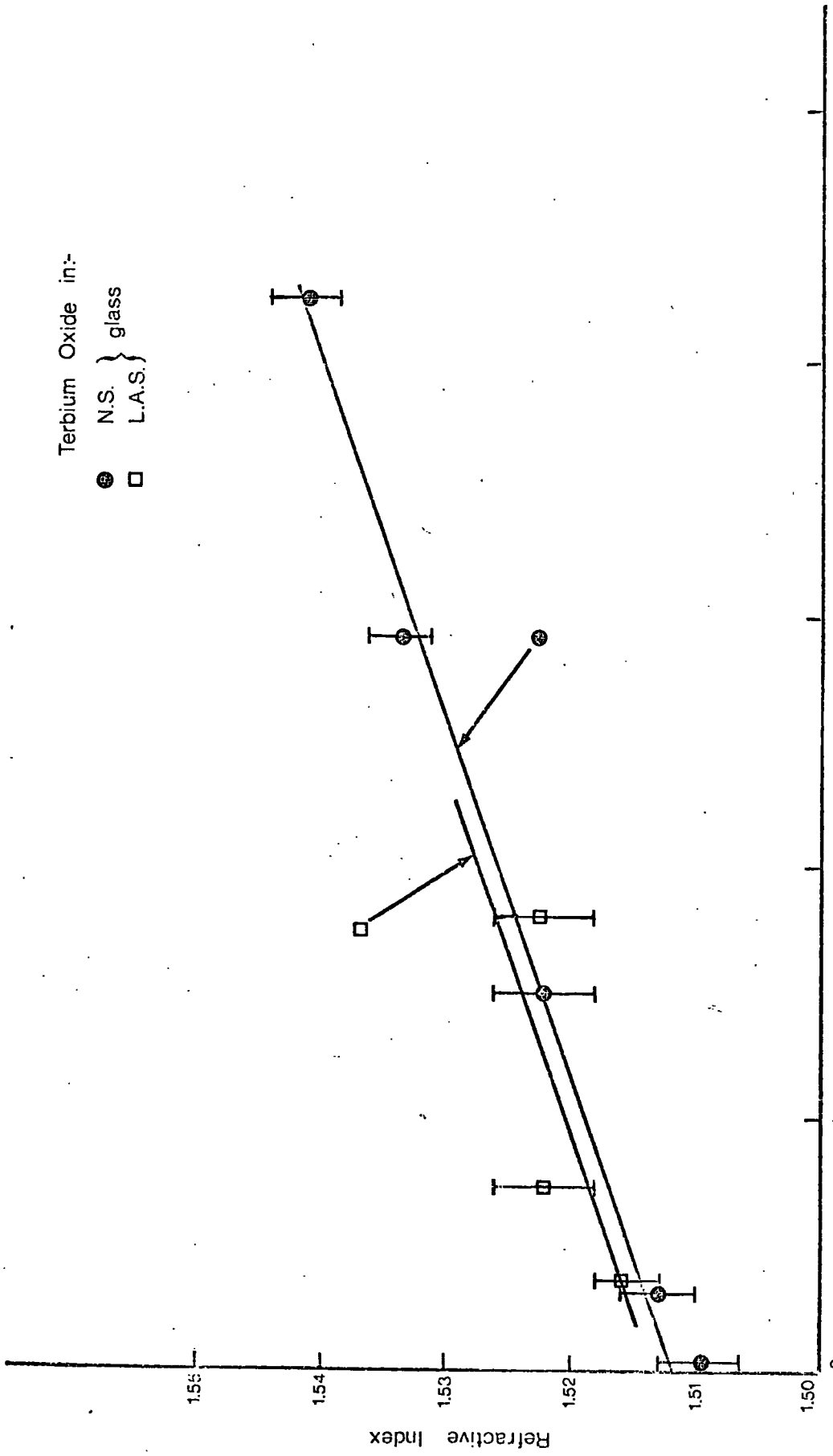

Fig 4.1 Effect of terbium concentration on the refractive index of silicate glasses

where W is the weight percent of Tb_4O_7 concentration. For the 2.88 mole % sample the result was:-

$$V = 25.6 \pm 0.04$$

The Lorenz-Lorentz law (for gases) defines the specific refraction, N, as:-

$$N = \frac{(n^2 - 1)}{(n^2 + 2)\rho} \qquad (4.2)$$

where n is the refractive index. The product of N with the molecular weight is known as the molar refraction, $[n]$, and:-

$$[n] = \frac{(n^2 - 1)}{(n^2 + 2)} \cdot \frac{M}{\rho} \qquad (4.3)$$

For aqueous and glassy solutions, we can still apply this same formalism if we again multiply by the weight fraction:-

$$[n] = \frac{(n^2 - 1)}{(n^2 + 2)} \cdot \frac{M}{\rho} \cdot \frac{W}{100} \qquad (4.4)$$

For the 2.88 mole % NS sample the result is:-

$$[n] = 7.9 \pm 0.2$$

It is interesting to compare these figures with those quoted by Kan Fu-Hsi et al (4.1) for 8 mole % Gd^{3+} in a sodium silicate glass, namely:-

$$V = 25.61 \qquad [n] = 8.01$$

Values for other rare earths were similar.

The agreement appears to be good, until it is realised that to a first approximation both V and [n] are proportional to the weight percentage of rare earth oxide included. So there is a discrepancy of at least a factor of two. This is explained by the fact that, for terbium oxide (Tb_4O_7), the molecular weight (747.7) is approximately twice that for gadolinium oxide (Gd_2O_3 = 362.5). If we make the calculation on the basis of a molecular formula, Tb_2O_3, and correct for concentration, the results are:-

$$V = 34.3 \qquad [n] = 10.8$$

These figures are still slightly high, but this can be accounted for by the higher density of the glasses used by Kan Fu-Hsi and coworkers.

Values for the density, molecular volume and molecular refraction for a range of NS and LAS glasses are given in Table 4.1.

4.2 Optical Absorption

The optical absorption spectra of the silicate glass types, NS and LAS, were measured on various spectrometers in the range 250nm to 40μ. The results are most usefully discussed in three sections : the far infra-red, the near infra-red, and the visible and near ultraviolet regions of the spectrum.

4.2.1 Far Infra-red Sepctra

The absorption of both NS and LAS glasses in the far infra-red spectral region was measured on a Perkin Elmer 457 grating spectrophotometer.

TABLE 4.1

Density, Molecular Volume and Molecular Refraction

of NS and LAS glasses

Base glass	Mole %	Density $\rho\left(g/cm^3\right)$ $\pm$ 0.03	Molecular volume V $\pm$ 2%	Molecular refraction [n] $\pm$ 3%
NS	0.031	2.38	0.30	0.09
	0.297	2.38	2.83	0.85
	1.481	2.40	13.60	4.13
	2.880	2.42	25.60	7.93
	4.250	2.45	35.40	11..10
LAS	0.364	2.56	3.27	0.99
	0.728	2.56	6.48	1.97
	1.810	2.60	15.40	4.73

Because of the high lattice absorption in this region, very thin specimens must be used. Measurements were taken on both thin blown films of glass and on specially prepared discs. The results from both types of sample were similar.

The thin films were blown to a thickness of approximately 1/100 to 1/10 mm on the end of soda glass tubes. Sufficient glass was melted on the end of the tube to ensure very little intermixing of the two glasses.

Spectra were also taken from 0.2 mm thick disc shaped samples. These were prepared by mixing powdered glass with KBr in the proportion 1:30 (glass:KBr). 100 mg portions of the resulting mixture were then compressed in vacuum at a pressure of four tons per square inch in 1 cm diameter moulds.

Comparison of the two methods shows that there was no appreciable absorption by KBr in this region except above 35 μ.

The resulting spectrum for NS glass containing 8.16 wt % terbium is shown in Figure 4.2. The results were very similar for all (silicate) glasses investigated and show three absorption peaks, one of which has two components. These peaks are labelled A, B, C, D, and their wavelengths and the full widths at half height are given in Table 4.2 for both this sample and the undoped NS glass.

Since the samples were very thin, no attempt was made to determine their actual thicknesses. Thus the approximate heights of the absorption peaks are given, in the table, relative to the main peak at about 10 microns.

No attempt has been made to determine the oscillator strengths

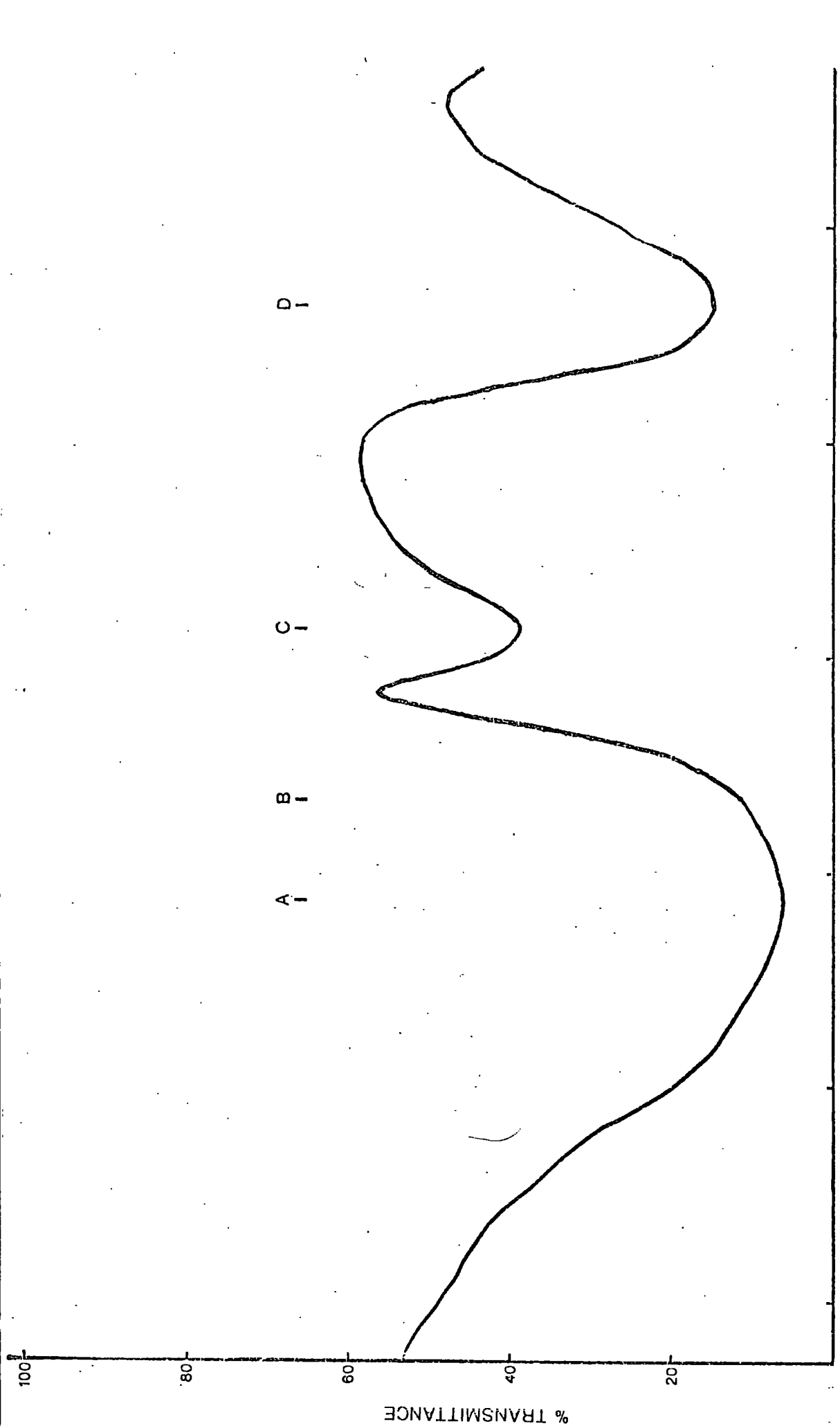

Fig 4.2 Infra-red region absorption spectrum of 2.83 mole % terbium in NS glass. Sample mixed with K Br

TABLE 4.2

Far Infra-red Absorption Data

Glass	Peak	Wavelength Microns	$\Delta\lambda$* Microns	Relative Absorption at Peak
NS	A	9.7	3.1	1.00
	B	10.7		0.81
	C	12.9	1.5	0.32
	D	22.8	9.4	0.86
NS + 2.88 mole % Tb^{3+}	A	9.7	2.7	1.00
	B	10.7		0.91
	C	12.9	1.5	0.34
	D	21.5	9.2	0.83

* half weight full width

of these peaks, but they were much larger than those due to Tb^{3+} ions in the visible spectrum. The spectra are similar to those observed in silica gel (4.2) and quartz (4.3). The absorption bands must therefore be associated with vibrations in the silica tetrahedra.

Although it may be incorrect to characterise an absorption band by a particular type of vibration in an amorphous material, nevertheless by analogy with crystal spectra, the peaks are identified as follows (4.4, 4.5).

A ~ $1100\,cm^{-1}$, stretching of the Si-O bond within the tetrahedra (4.6).

B ~ $950\,cm^{-1}$, stretching modes in non-bridging Si-O bonds (4.7). Here there is no covalent bonding between a corner of one of the silica tetrahedra and an adjacent silica group.

C ~ $800\,cm^{-1}$, stretching of Si-O-Si chains, bridging between tetrahedra (4.8).

D ~ $450\,cm^{-1}$, bending modes involving the chains Si-O-Si and O-Si-O (4.9).

Note that peak B increases in relative intensity with terbium concentration. This is consistent with the idea that Tb^{3+} ions enter the lattice as network modifiers. The rare earth ion is thought to attract oxygen ions as its ligands and so reduce the number of bridging oxygens. This is similar to the function of Na^{+} ions. Ferraro and Manghnani (4.9) report a considerable increase in the intensity of peak B as the proportion of Na_2O in sodium silicate glass is increased from 10 mole % to 45 mole %.

Very little difference in the position of the peaks was produced

by the inclusion of terbium oxide. Ferraro et al (4.10) found that with 8 mole % of terbium in soda-lime glass ($75SiO_2.15Na_2O.10CaO$) the position of peak A was shifted by about 25 cm^{-1} to longer wavelengths relative to the base glass. This shift to lower energy is consistent with the network modifier lengthening the average Si-O bond length and is also produced by the inclusion of Na_2O in the glass (4.9).

Effects in L A S glasses were not so pronounced, but a similar relationship of Tb^{3+} ions with the $(SiO)^{2-}$ tetrahedra is believed to exist. No absorption bands which could be attributed to Al-O bonding were seen in this region.

4.2.2 Near Infra-red Spectra

Absorption spectra in the region one to five microns were taken on a Grubb Parsons' 'Spectromaster' spectrophotometer. Figure 4.3 shows a typical spectrum, taken from a 0.5 cm thick sample of 1.81 mole % terbium in L A S glass. Absorption peaks due to atmospheric carbon dioxide at about 4.6 microns have been subtracted from the curve.

The base glass spectra for both N S and L A S glasses show a strong absorption band beginning at about 2.7 and 3.4 microns respectively. The results are similar to those reported by Scholze and Dietzel (4.11) and the 3.4 to 3.6 micron band is attributed to absorption at bound hydroxyl groups. These groups were shown to be present in alkali-rich glasses up to quite high temperatures.

Similar bands are reported in phosphovanadate glasses (4.12), but they are then due to P-O and V-O bond absorptions (4.13). A

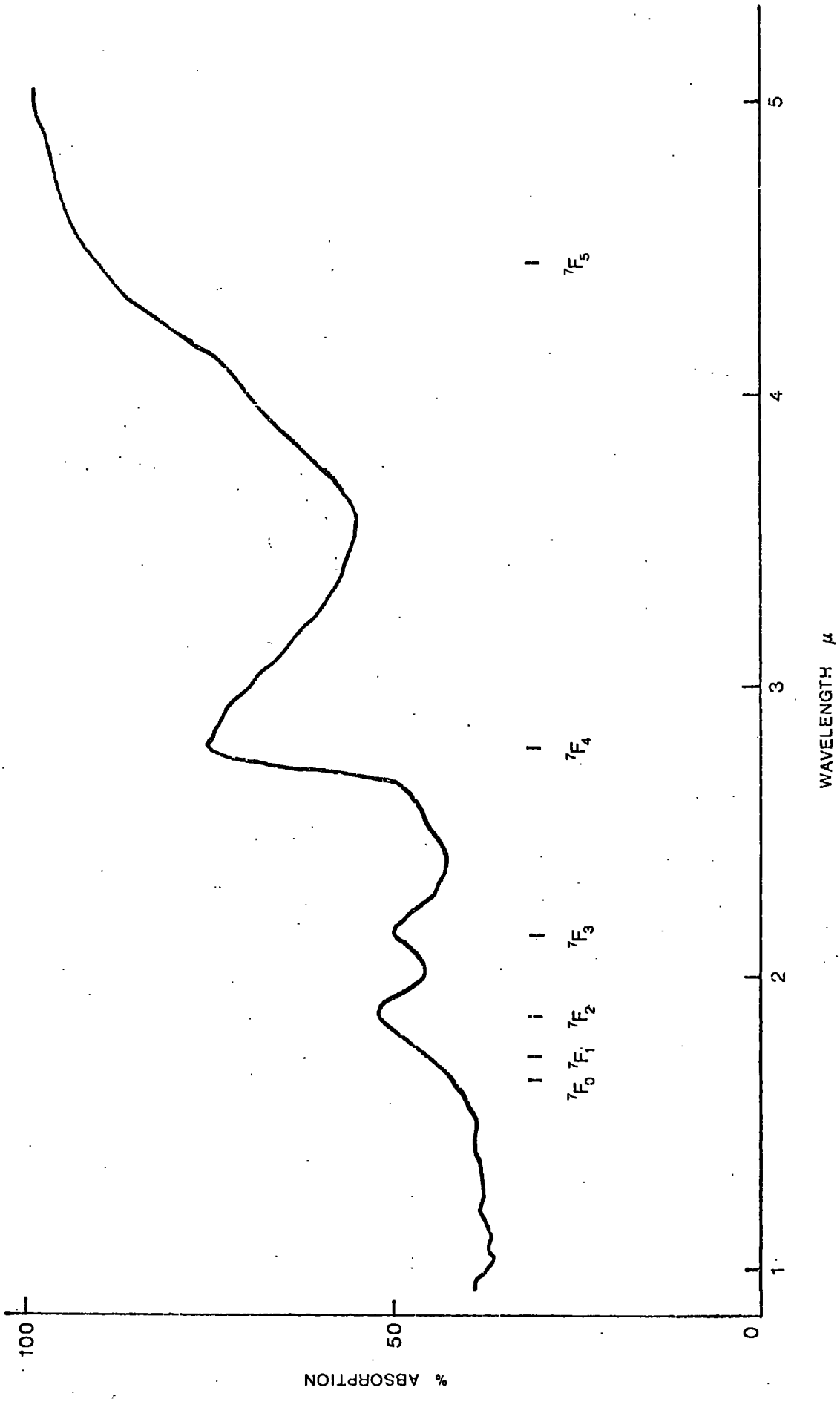
100
50
0
% ABSORPTION
1
2
3
4
5
WAVELENGTH μ
$^7F_0$ $^7F_1$ $^7F_2$
$^7F_3$
$^7F_4$
$^7F_5$

series of narrow absorption bands was also observed in both NS and LAS glasses containing terbium ions. These are tabulated in Table 4.3 for the 0.5 cm thick sample of 1.81 mole % Tb^{3+} in LAS glass. By comparison with absorption data from Tb^{3+} ions in $LaCl_3$ (4.14) and Tb^{3+} in a similar silicate glass (4.15), these bands are assigned to transitions in the ground state multiplet of terbium. The levels are identified by reference to theoretical predictions due to Ofelt (4.16), and the bands arise from transitions from the $^7F_6$ state to all the other ^7F_J (J = 0 to 5) states.

The absorption associated with Tb^{3+} in both $LaCl_3$ (4.14) and aqueous solution (4.17) is similar to that of the free ion (4.16).

The ratios of the wavenumbers of the terbium absorption peaks in LAS glass to the respective wavenumbers for absorption in aqueous solution (figures taken from Ref 4.17) are given in Table 4.4. It will be seen that this ratio is constant within experimental error, and the average value found was 1.064. Thus the peaks are found to have the same relative spacings as in other media, but displaced to higher energies.

Similar shifts of these bands to higher wavenumbers are reported by Nelson et al (4.18) in fused silica and by Karapetyan and Lunter (4.15) in sodium calcium silicate glasses. However, the latter's results show no constant ratio to the levels in crystal and aquo spectra of the type found here. In particular, the $^7F_0$ level was displaced to much higher energies. This may be due to incorrect assignment, as the $^7F_0$ level was determined from luminescence data and may in fact result from transitions to the ground state from higher

TABLE 4.3

Comparison of Near Infra-red Absorption of Tb^{3+} Ions in LAS with Absorption in Other Media

Terminal level	In Glass (this work)		In Glass (reference 4.15)		In $LaCl_3$ (reference 4.14)	
	$\pm .05\mu$	$\pm 40 cm^{-1}$	μ	cm^{-1}	μ	cm^{-1}
$^7F_5$	4.45	2250	--	--	4.75	2104
$^7F_4$	2.80	3550	{2.84 / 2.60}	{3530 / 3850}	2.98	3356
$^7F_3$	2.15	4650	2.20	4550	2.30	4348
$^7F_2$	1.85	5400	1.98	5030	1.99	5024
$^7F_1$	1.73	5780	1.90	5230	1.83	5472
$^7F_0$	1.65	6060	1.45	6900	1.75	5701

TABLE 4.4

Near Infra-red Absorption Data for 1.81 Mole % Tb^{3+} in LAS Glass, 0.5 cm Thick Sample

Level	Ratio of Absorption Peak Wavenumbers $\frac{\text{glass}}{\text{aquo ion}}$ $\pm$ 0.007	% Absorption (maximum) $\pm$ 1%	Oscillator Strength $f_{if} \times 10^7$ $\pm$ 0.5	Half Height Full Width $\Delta\nu$ cm^{-1} $\pm$ 50
$^7F_5$	1.072	21%	3.8	300
$^7F_4$	1.056	31%	9.9	600
$^7F_3$	1.057	9%	1.8	400
$^7F_2$	1.072	12%	3.8	600
$^7F_1$	1.063	5%		
$^7F_0$	1.063	2%		
Average = 1.064				

levels than the $^5D_3$ level they describe.

This effect of large J state splitting may be explained in terms of the model of the terbium ion site outlined in Chapter 1. The displacement is considered to be due to the partially covalent nature of the bonding between Tb^{3+} ions and the ligands. The covalent component of the bonds in, for instance, $LaCl_3$: Tb is likely to be far smaller. This 'sharing' of electrons permits a greater mixing of the 4f states with higher states in the terbium ion and, perhaps, also with the electron configurations of the ligand. This mixing of wavefunctions increases the effect of the perturbation Hamiltonian on the ground state levels, which are degenerate in all but the J quantum number. The effect will be to increase the separation of the resulting multiplet. The ratio 1.064 is thus an indication of the extent of covalency in the terbium-ligand bond.

The levels are broadened somewhat relative to those observed in crystals (4.19), half widths being of the order $400\,cm^{-1}$. This is believed to be a result simply of the inhomogeneous crystalline field in the glass matrix; the broadening is referred to in Chapter 1. The splitting of these levels is not well resolved in absorption work and is discussed further in the section on luminescence (Chapter 5). It is noted here that, in general, the splitting is larger for levels of higher multiplicity (higher J).

Also given in Table 4.4 are the maximum percentage absorptions associated with each absorption band, and the corresponding oscillator strengths determined from equation 2.74. The values found for the oscillator strengths are in the region 10^{-7} to 10^{-6}, which is typical for the 'forbidden' 4f-4f transitions in the rare earths.

As expected , for non-interacting absorption centres, the strengths of the absorption bands due to Tb^{3+} ions were found to be roughly proportional to the ionic concentration.

4.2.3 Visible Region and Ultra-violet Spectra

Optical absorption spectra of silicate glasses in the region 200nm to 1000nm were taken on both the Optica spectrophotometer, described in Chapter 3, and on a Unicam SP 800 spectrophotometer. No differences were seen in spectra obtained from the two instruments.

Figure 4.4 shows the absorption spectrum from 350nm to 650nm of a 0.25 cm thick sample of 2.88 mole % terbium in NS glass. The results obtained were similar to those reported by Herring et al (4.20) in a sodium calcium silicate glass. The absorption observed again fell into two classes; with features due to the base glass and to the terbium ions. The wavelengths and wavenumbers of the various peaks are given in Table 4.5, where the terbium absorption is also compared with data from the aqueous Tb^{3+} ions (4.17, 4.21).

Two distinct bands arise which are attributed to the base glass, as only these peaks were observed in undoped samples of NS glass. These have been labelled A (at about 630nm) and B (at about 440nm) and have also been reported by Herring et al. However, these absorption peaks were not observed in the LAS glasses. They may therefore be due to low concentrations of impurity ions rather than the base glass. Ferric or ferrous iron (Fe^{3+} or Fe^{2+}) would be a likely possibility. Alternatively, they may be due to structural properties of the glass. Defects akin to the F and V centres seen in some ionic crystals

0.25 cm thick sample

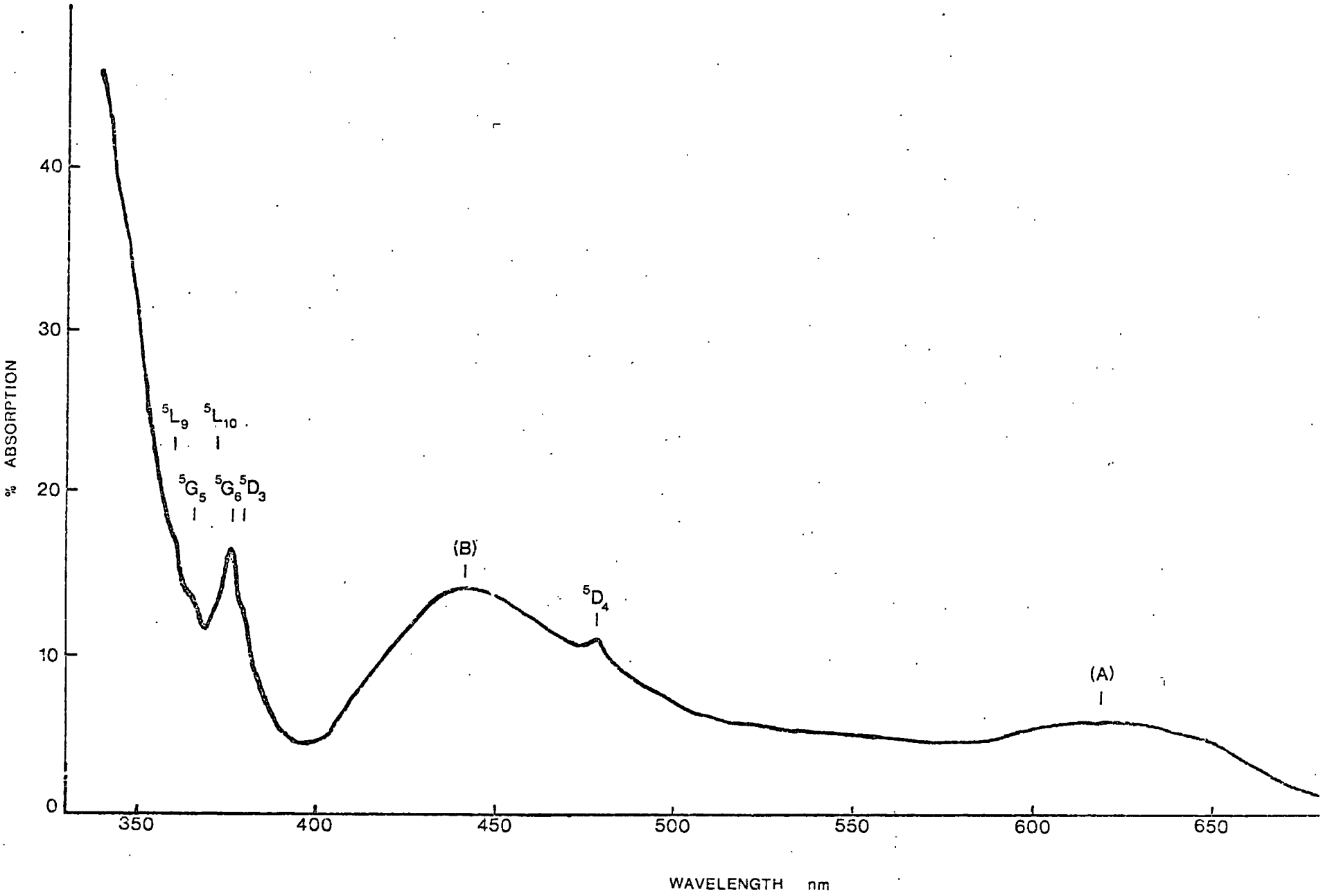

TABLE 4.5

Wavelengths of Visible Region Absorption Spectra of 2.88 Mole % Tb^{3+} in NS Glass and Comparison with the Aquo Ion

Terminal Level	In Glass (this work)		Aqueous Ions (reference 4.17)	
	± 1 nm	± 70 cm^{-1}	nm	cm^{-1}
(A)	629	15900	--	--
$^5D_4$	479	20900	472*	21200*
(B)	441	22700	--	--
$^5D_3$	380	26300	--	--
$^5G_6$	376	26600	377	26500
$^5L_{10}$	373	26800	369	27100
$^5G_5$	365	27400	360	27800
$^5L_9$	358	27900	352	28400

* From reference 4.21

may exist even in glass not subjected to ionising radiation. This question is returned to in greater detail in the section on thermoluminescence (Chapter 6).

A further feature which is associated with absorption in the glass matrix is the so-called ultra-violet 'cut-off'. This absorption began at around 360nm for the NS glass, while for the LAS glasses (see Figure 4.5) it occurred at about 280nm. In consequence, the absorption of the terbium ions in the region from 280nm to 360nm could only be studied in the LAS glasses.

The glassy absorption cut-off was very pronounced; percentage transmission fell to less than 1% at wavelengths 50nm to 100nm below the upper wavelength limit of the band. The absorption is probably due to either the excitation of electrons into the glass conduction band, or holes being created in the valence band, and is found in all glass types (phosphates, Ref 4.22; germanates, Ref 4.23; silicates, Ref 4.24; borates, Ref 4.25).

The absorption spectrum of a 0.5 cm thick sample of 1.81 mole % Tb^{3+} in LAS glass is shown in Figure 4.5. A large number of weak absorption bands were seen, the wavelengths of which are compared with data from the aqueous Tb^{3+} ions (4.17) in Table 4.6.

The aqueous Tb^{3+} ion was chosen for comparison for the following reasons:-

(1) The nephelauxetic shifts in the aquo ion relative to the free ion are small.

(2) The liquid disorder is similar in many ways to the inhomogeneity in glass.

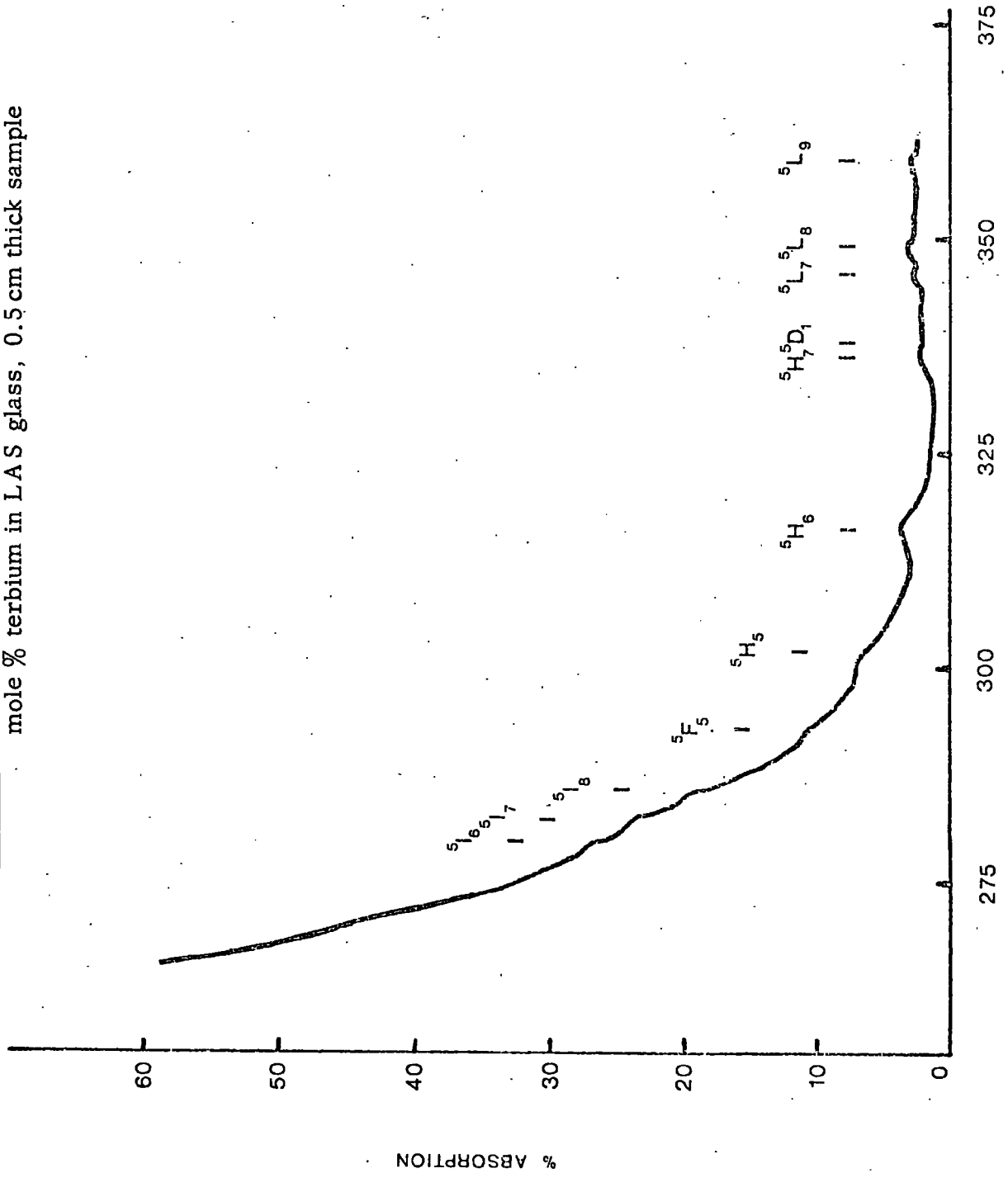

Fig 4.5 Ultra-violet region absorption spectrum of 1.81 mole % terbium in L A S glass, 0.5 cm thick sample

TABLE 4.6

Wavelengths of Ultraviolet Region Absorption Spectra of 1.81 Mole % Tb^{3+} in LAS Glass and Comparison with the Aquo Ion

Terminal Level	In Glass (this work)		Aqueous Ions (reference 4.17)	
	± 1 nm	± 100 cm^{-1}	nm	cm^{-1}
$^5L_9$	359	27860	352	28400
$^5L_8$	349	28650	341	29300
$^5L_7$	346	28900	339	29400
$^5D_1$	338	29590	326	30650
$^5H_7$	336	29760	317	31600
$^5H_6$	316	31650	303	33000
$^5H_5$	302	33110	295	33900
$^5F_5$	293	34130	287	34900
$^5I_8$	290	34480	284	35200
$^5I_7$	282	35460	273	36700
$^5I_6$	280	35710	265	37760

(3) The ligands will be oxygen ions in both water and the glass. Thus to a first approximation the difference in electonegativity between Tb^{3+} ions and the ligand ions will be the same in both systems.

(4) The environment of rare earth ions in the presence of water is similar to the site model chosen to represent the terbium ion site in glass and outlined in Chapter 1. In the solid state, all trivalent lanthanides, Ln^{3+}, can give rise only to nonanhydrates, $Ln(H_2O)_9^{3+}$, or octahydrates, $Ln(H_2O)_8^{3+}$ (4.26). The ligand oxygens will thus have co-ordination numbers 8 or 9 and have a spatial arrangement which is approximately cubic. In aqueous solution a similar situation is thought to arise, making the lanthanide ion site very similar to the proposed site in glass.

(5) The absorption spectrum of aquo Tb^{3+} ions is known (4.17), and the levels have been identified. By comparison it is hoped to identify the absorption bands due to Tb^{3+} in glass.

If allowance is made for concentration by using the Lambert-Beer law, the absorption spectra of Tb^{3+} ions in both binary (NS) and ternary (LAS) glasses are the same. If now these levels are compared with those found in aqueous solution, the peaks fall into a one-to-one correspondence. The levels have thus been identified in a similar manner, that is by comparison with the calculated figures due to Ofelt (4.16). Not all the calculated levels produce absorption discernible by this experiment, the 'missing' peaks are thought to have very low oscillator strengths.

The absorption peaks in glass are all shifted to a lower energy relative to the aquo ions (or the free ions). These shifts are listed

in Table 4.7 in terms of the nephelauxetic parameter, β, determined from equation 2.87. The mean value for β was 0.023.

Also listed in Table 4.7 are the half widths of the various peaks, the maximum percentage absorption and the oscillator strengths as determined from equation 2.81. The oscillator strengths (typically 10^{-9} to 10^{-7}) are similar in relative magnitude to those determined for the aquo ion. They are generally much lower than the oscillator strengths of the ^7F_J multiplet in the near infra-red (section 4.2.2).

Note that all transitions arise from the $^7F_6$ ground state, and the negative value found for the $^5G_6$ level may be due to incorrect identification.

The extreme similarity of the absorption spectra of Tb^{3+} ions in glass and in aqueous solution is taken as evidence of the similarity of site structure. Thus, although direct determination of the site geometry is impossible, by comparison some of the features of the ionic environment can be deduced.

The value of β (= 0.023) is a further measure of the covalent interaction between Tb^{3+} ions and the ligands. The bond in glass is much less ionic than the Tb-O bond in aqueous solution.

Reisfeld (4.27) quotes values found for β from 4f-5d ("rydberg") transitions of Tb^{3+} ions in various glasses. The figures quoted are:-

borate glass	β	= 0.0430
phosphate glass	β	= 0.0108
germanate glass	β	= 0.2322

If comparison is permissible between shifts in 4f-4f transitions and those in 4f-5d transitions, it will be seen that the covalency of the

TABLE 4.7

Optical Constants of the Visible and Ultraviolet Absorption of Tb^{3+} Ions in Silicate Glasses

Level	Nephelauxetic parameter β (1) $\pm$ 0.003	Width $\Delta\lambda$ nm $\pm$ 0.3 nm	Percent Absorption (maximum) $\pm$ 0.3%	Oscillator Strength x 10^9 (2) $\pm$ 2
$^5D_4$	0.014	4.0	1.5	24
$^5D_3$	0.019			
$^5G_6$	-0.038	8.0	8.5	261
$^5L_{10}$	0.011			
$^5G_5$	0.014	1.0	0.5	6
$^5L_9$	0.019	1.0	0.5	5
$^5L_8$	0.022	1.0	0.5	6

TABLE 4.7 (Continued)

Level	Nephelauxetic parameter β (1) $\pm$ 0.003	Width $\Delta\lambda$ nm $\pm$ 0.3 nm	Percent Absorption (maximum) $\pm$ 0.3%	Oscillator Strength x 10^9 (2) $\pm$ 2
$^5L_7$	0.017	1.0	0.5	3
$^5D_1$	0.035	1.0	0.5	7
$^5H_7$	0.058	1.0	1.0	10
$^5H_6$	0.041	4.0	2.0	47
$^5H_5$	0.023	3.0	1.0	13
$^5F_5$	0.022	1.0	0.5	5
$^5I_8$	0.020	1.0	0.5	5
$^5I_7$	0.034	1.0	0.5	5

TABLE 4.7 (Continued)

Level	Nephelauxetic parameter β (1) $\pm$ 0.003	Width $\Delta\lambda$ nm $\pm$ 0.3 nm	Percent Absorption (maximum) $\pm$ 0.3%	Oscillator Strength x 10^9 (2) $\pm$ 2
$^5I_6$	0.054 Average β = 0.023	1.0	0.5	5

(1) Calculated from equation 2.87

(2) Calculated from equation 2.81

Tb-O bond in silicate glass is intermediate between borate and phosphate glasses.

Reisfeld also quotes figures for β in cerium containing glasses. The nephelauxetic shifts are very similar in silicate, phosphate and borate glasses. This is consistent with the idea of Ln^{3+} ion sites being similar in these glasses. The much higher figure for germanate glass may mean that a totally different lanthanide ion site is appropriate here.

4.3 The Valence of Terbium Ions in Glass

Since it is possible for terbium to exist in reduced (Tb^{2+}) and oxidised (Tb^{4+}) ionic states, the contamination due to these ions must be considered.

The optical absorption of Tb^{2+} ions in CaF_2 has been studied by McClure and Kiss (4.28). Various broad absorption peaks were observed, in particular one at about $18,000\,cm^{-1}$ (~ 550 nm). This absorption band was not detected in any of the terbium glass samples studied.

Blasse and Bril (4.29) refer to a light grey colouration being characteristic of Tb^{4+} ions. However, no data could be found in the literature on the absorption spectra of this ion. Since Tb^{4+} is isoelectronic with Gd^{3+} and Eu^{2+}, the absorption of terbium is expected to be in bands above $30,000\,cm^{-1}$. Thus the absorption of Tb^{4+} may be confused with the glassy cut-off.

Tb^{4+} also shows electron paramagnetic resonance at room temperature (as do Gd^{3+} and Eu^{2+}) (4.30). Attempts to measure

resonance due to Tb^{4+} by Hunt (4.31), in the specimens used, were unsuccessful. Epr due to Gd^{3+} ions could easily be seen, even at low concentrations ($< 10^{-2}$ mole %).

Thus the concentrations of Tb^{2+} and Tb^{4+} in the samples used are considered to be negligible. No luminescence has been reported from either of these valence states of terbium, so that their inclusion in a glass would lead to less efficient luminophors.

CHAPTER 5

PHOTOLUMINESCENCE

5.1 Ultra-Violet Excited Luminescence in Glasses

5.1.1 Introduction

Trivalent terbium ions in many transparent media produce green or greenish-blue luminescence under ultra-violet excitation. The number of papers in the literature is very extensive, and space does not permit a comprehensive survey. Details of the luminescence spectra of Tb^{3+} ions in several crystalline solids may be found in references 5.1 to 5.10, and organic complexes of terbium are also reported to give visible emission (5.11 to 5.14).

The photoluminescence spectra of terbium glasses excited by ultra-violet irradiation were measured with the Optica spectrophotometer system. Details of the spectrophotometer are given in Chapter 3. The accuracy of the system was tested by measuring the emission spectrum from an unfiltered mercury lamp and also by measuring the absorption spectrum of a standard holmium glass filter. The wavelength positions of the peaks were found to be accurate to within 0.5 nm, and the half widths of the mercury lines as measured on the spectrometer were slightly less than 2 nm.

The mercury lamp used for the excitation of the luminescence was also examined with the spectrometer. By using an optical filter the lamp emission was essentially restricted to a single line at 365 nm. Without this filter a second intense line at 254 nm was also observed.

A further emission line in the mercury source at 405 nm could not be completely eliminated by the filter, but its intensity was more than a factor of 10^3 less than the main line at 365 nm. While it is not thought that the 405 nm line excites luminescence in terbium luminophors, scattered light of this wavelength was troublesome when measuring luminescent spectra in the region 380 nm to 420 nm.

The filter was very effective in removing all emission from the lamp in the range from 420 nm to 620 nm, but in the red region of the spectrum small peaks above 620 nm were transmitted.

The work on ultra-violet excited luminescence was concentrated on silicate glasses doped with terbium, but some work was also done on other glass systems containing Tb^{3+} ions. To limit this work to manageable proportions, luminophors of glasses with mixed network formers were not investigated.

For the purpose of comparison, the luminescence spectra of other rare earth ions in glass were also investigated, notably of the elements samarium and dysprosium, which are known to give intense visible luminescence.

5.1.2 General Luminescence Characteristics

Of the 14 possible emission bands (see Chapter 1) from the $^5D_3$ and $^5D_4$ levels of Tb^{3+} ions to the ^7F_J ground state multiplet, only eight were seen in silicate glasses. These eight emission lines correspond to transitions terminating in the levels of the ground state with highest J values ($^7F_6$ to $^7F_3$). It is thought that the other possible transitions were not seen because:-

1) They are, in any case, much weaker.

2) The $^5D_3$ to $^7F_{2,1,0}$ emissions overlap with the more intense $^5D_4$ to $^7F_6$ band.

3) The $^5D_4$ to $^7F_{2,1,0}$ emissions lie in the orange-red region of the spectrum where the photomultiplier sensitivity was very low.

The transitions $^5D_3$ to $^7F_4$, $^5D_4$ to $^7F_6$, $^5D_4$ to $^7F_5$ and $^5D_4$ to $^7F_4$ all showed a doublet structure, and consequently these bands are often referred to as two separate emission lines in this analysis. The subject of line-shape is returned to later in this chapter. A typical emission spectrum of Tb^{3+} ions in silicate glass is shown in Figure 5.1 for 4.25 mole % Tb^{3+} in NS glass at room temperature. The level scheme is also given in this diagram.

The concentration of the terbium ions in the glass greatly affects the relative intensities of the various emission bands. This is dealt with in detail in the next section. In contrast, the widths of the emission bands and the wavelength positions of the peaks were not found to differ significantly in any of the silicate glasses studied. The widths (typically 5 to 10 nm) and wavelengths of the emissions bands are given in Table 5.1 for NS glass specimens, and in Table 5.2 for LAS glasses excited by ultra-violet radiation at room temperature. Note that the widths of the emission bands are slightly less in the case of the ternary glass.

5.1.3 Relative Intensities of the Emission Bands and Effects of Concentration

The relative intensities of the emission peaks for various concen-

TABLE 5.1

Wavelength Positions and Widths at Half Height of the Luminescence from Tb^{3+} Ions in NS Glasses at Room Temperature

Wavelength at Peak of Emission Band (nm)	Width of Emission Band at Half Height (nm)	Transition Responsible for Emission
382	10	$^5D_3 - {}^7F_6$
416	9	$^5D_3 - {}^7F_5$
436	6.5 } 11	$^5D_3 - {}^7F_4$
442	7.5 }	
457	8.5	$^5D_3 - {}^7F_3$
487	9 } 17	$^5D_4 - {}^7F_6$
495	10 }	
542	3 } 11	$^5D_4 - {}^7F_5$
549	8 }	
583	10 } 16	$^5D_4 - {}^7F_4$
594	11 }	
619	14	$^5D_4 - {}^7F_3$

TABLE 5.2

Wavelength Positions and Widths at Half Height of the Luminescence from Tb^{3+} Ions in LAS Glasses at Room Temperature

Wavelength at Peak of Emission Band (nm)	Width of Emission Band at Half Height (nm)	Transition Responsible for Emission
382	11	$^5D_3 - {}^7F_6$
416	11	$^5D_3 - {}^7F_5$
438	5	$^5D_3 - {}^7F_4$
443	6 (10)	
459	7.5	$^5D_3 - {}^7F_3$
489	10	$^5D_4 - {}^7F_6$
498	10 (17)	
543	3	$^5D_4 - {}^7F_5$
549	7 (10)	
586	10	$^5D_4 - {}^7F_4$
594	10 (15)	
623	13	$^5D_4 - {}^7F_3$

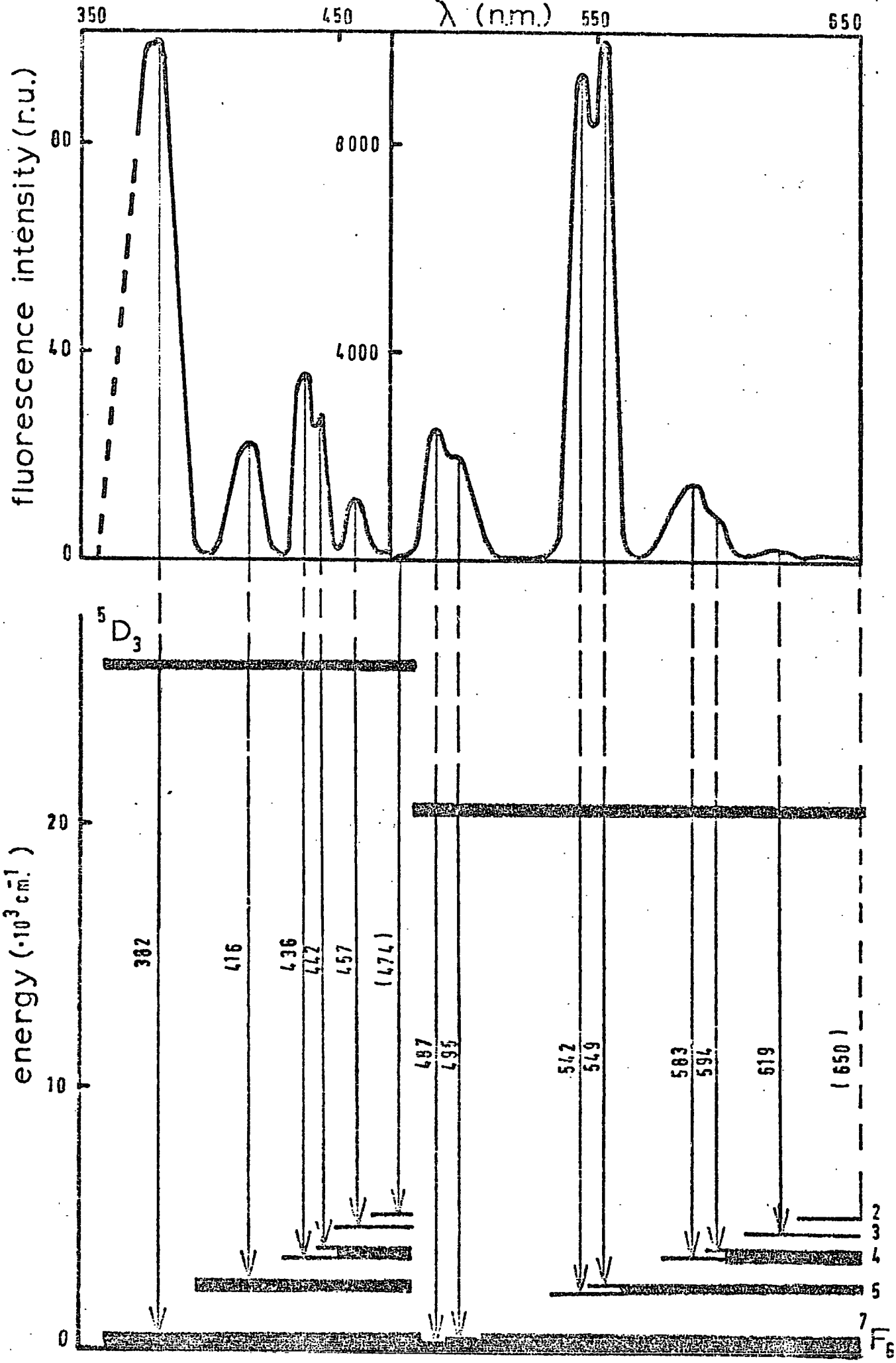

Fig 5.1 A typical emission spectrum of silicate glass containing Tb^{3+} ions and the level diagram showing the observed transitions

trations of Tb^{3+} ions in NS glass excited by the 365 nm line of the mercury lamp are listed in Table 5.3. Similar data for various concentrations of Tb^{3+} ions in LAS glass are given in Table 5.4 on the same relative scale.

The concentration dependence of the emission has very different characteristics for the bands which result from transitions from each of the two metastable (luminescing) levels. The shortwave bands from the $^5D_3$ level at first increase in intensity slowly but then remain at roughly the same intensity above about 0.5 mole %. This variation in NS glass is shown graphically in Figure 5.2 for the 436 nm line, normalised to unit intensity at the lowest concentration for which results were obtained (0.031 mole %). The behaviour is characteristic of many rare earth ions (for example, Eu^{3+} - ref 5.15) which show concentration quenching.

The behaviour of the emission intensity associated transitions from the $^5D_4$ level is rather different. This is shown in Figure 5.3 for the 549 nm line for NS glass also normalised to unit at the lowest concentration. The luminescence becomes slightly more intense with concentration up to about 0.5 mole %. At this point the emissions become rapidly more intense up to about 5 mole % when they also appear to be subject to concentration quenching.

A similar concentration dependence was found for terbium doped LAS glass, as is shown in Figure 5.4 However, results were only taken for intermediate concentrations (0.36 to 1.81 mole %) of Tb^{3+} ions in this glass, and consequently the concentration quenching of $^5D_4$ bands was not observed.

TABLE 5.3

Relative Intensities of the Emission Bands of Various Concentrations of Tb^{3+} Ions in NS Glass

Wavelength (nm)	Relative Intensity at the Following Concentrations (mole %)							Level Assignments
	0.031	0.30	1.01	1.48	2.88	4.25	6.03	
382	---	--	--	17	16	20	21	$^5D_3 - {}^7F_6$
416	4.2	5.6	7.0	8.7	8.5	9.1	9.8	$^5D_3 - {}^7F_5$
436	4.8	7.1	9.7	11	10.5	11.6	11.7	$^5D_3 - {}^7F_4$
442	2.8	3.7	4.7	6	5.8	6.5	5.9	
457	1.1	1.4	1.9	2.2	1.8	1.8	1.8	$^5D_3 - {}^7F_3$
487	1.6	2.5	17	48	166	510	345	$^5D_4 - {}^7F_6$
495	1.0	1.4	9.4	24	83	230	150	
542	6.6	9.3	64	155	630	1750	1300	$^5D_4 - {}^7F_5$
549	6.7	9.8	67	170	640	1820	1350	
583	2.9	3.3	17	38	103	300	290	$^5D_4 - {}^7F_4$
594	2.2	3.1	12	24	86	245	250	
619	1.7	2.0	10	22	62	165	170	$^5D_4 - {}^7F_3$

TABLE 5.4

Relative Intensities of the Emission Bands of Various Concentrations of Tb^{3+} in LAS Glass

Wavelength (nm)	Relative Intensity at the Following Concentrations (mole %)			Level Assignments
	0.364	0.728	1.81	
415	13.6	20.3	25.6	$^5D_3 - {}^7F_5$
436	14.7	21.8	27.6	$^5D_3 - {}^7F_4$
441	9.8	13.5	11.5	
457	2.5	3.1	5.1	$^5D_3 - {}^7F_3$
487	10.2	32.6	170	$^5D_4 - {}^7F_6$
494	5.4	17.7	96.5	
541	28.6	104.6	597	$^5D_4 - {}^7F_5$
548	26.8	95.5	507	
583	6.3	18.3	83.3	$^5D_4 - {}^7F_4$
593	5.0	12.5	86.3	
618	2.3	9.7	60.0	$^5D_4 - {}^7F_3$

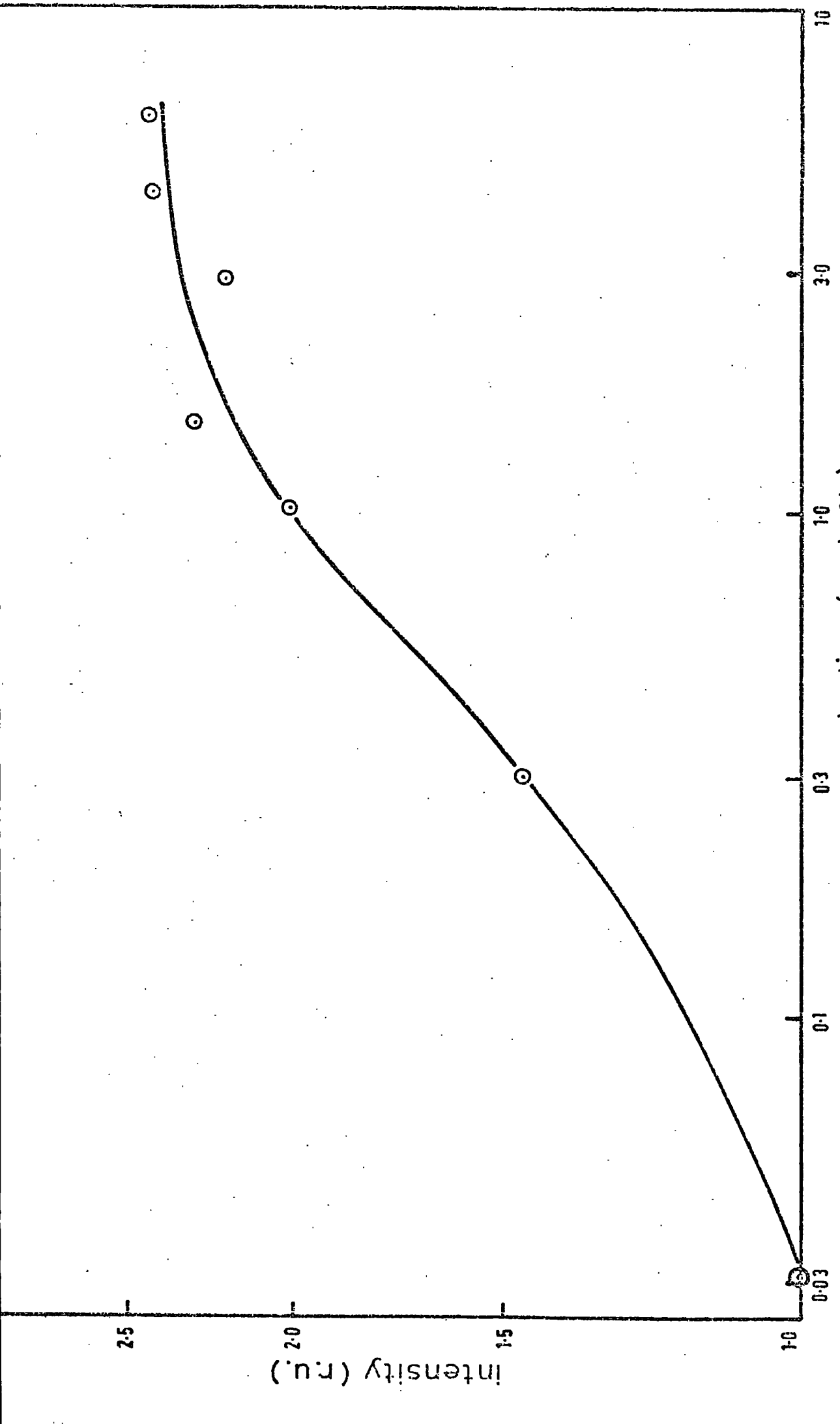

Fig 5.2 Emission intensity of the 442 nm line of Tb^{3+} ions in NS glass as a function of concentration, normalised to 1.0 at 0.03 mole %

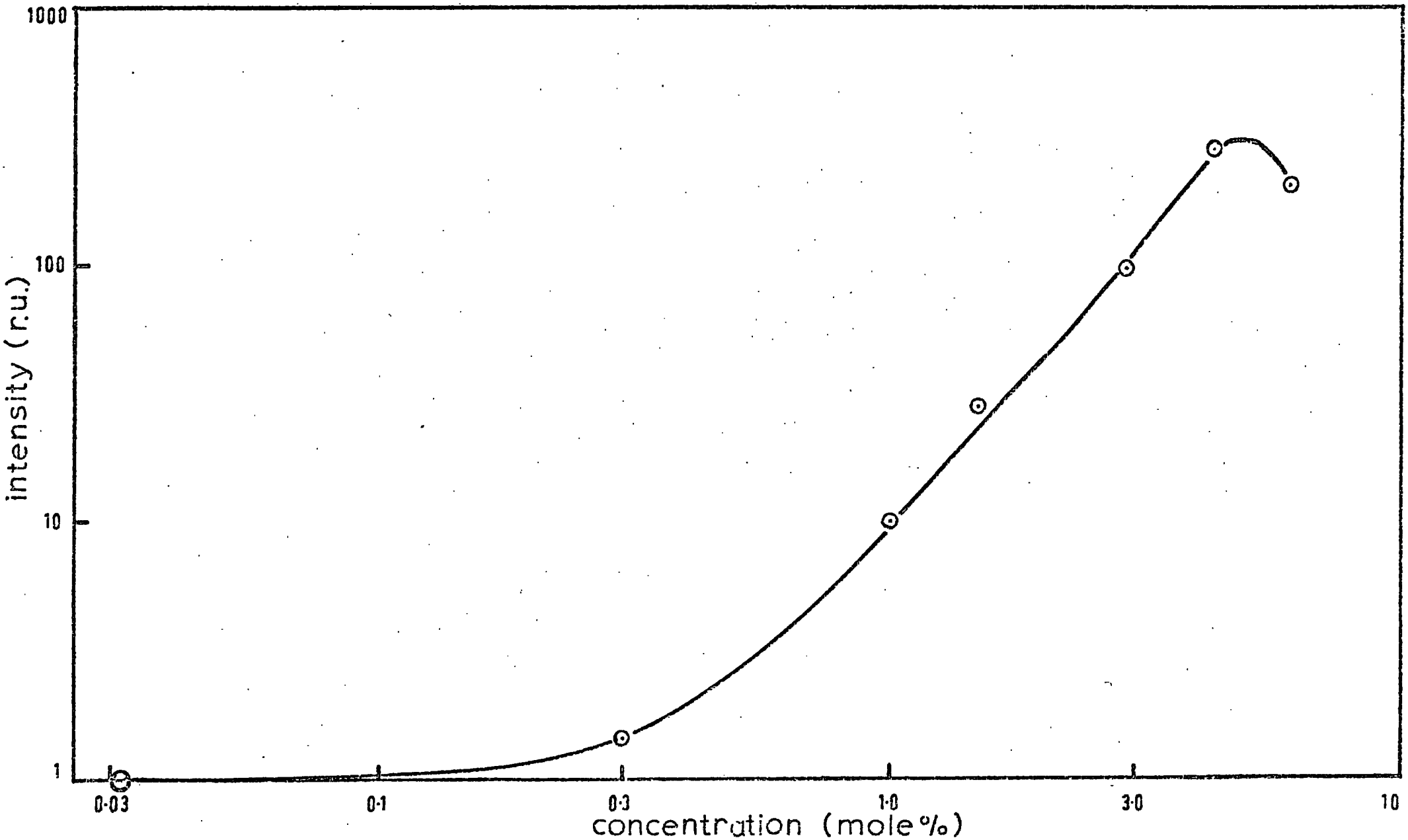

Fig 5.3 Emission intensity of the 549 nm line of Tb^{3+} in N3 glass as a function of concentration, normalised to 1.0 at 0.03 mole %

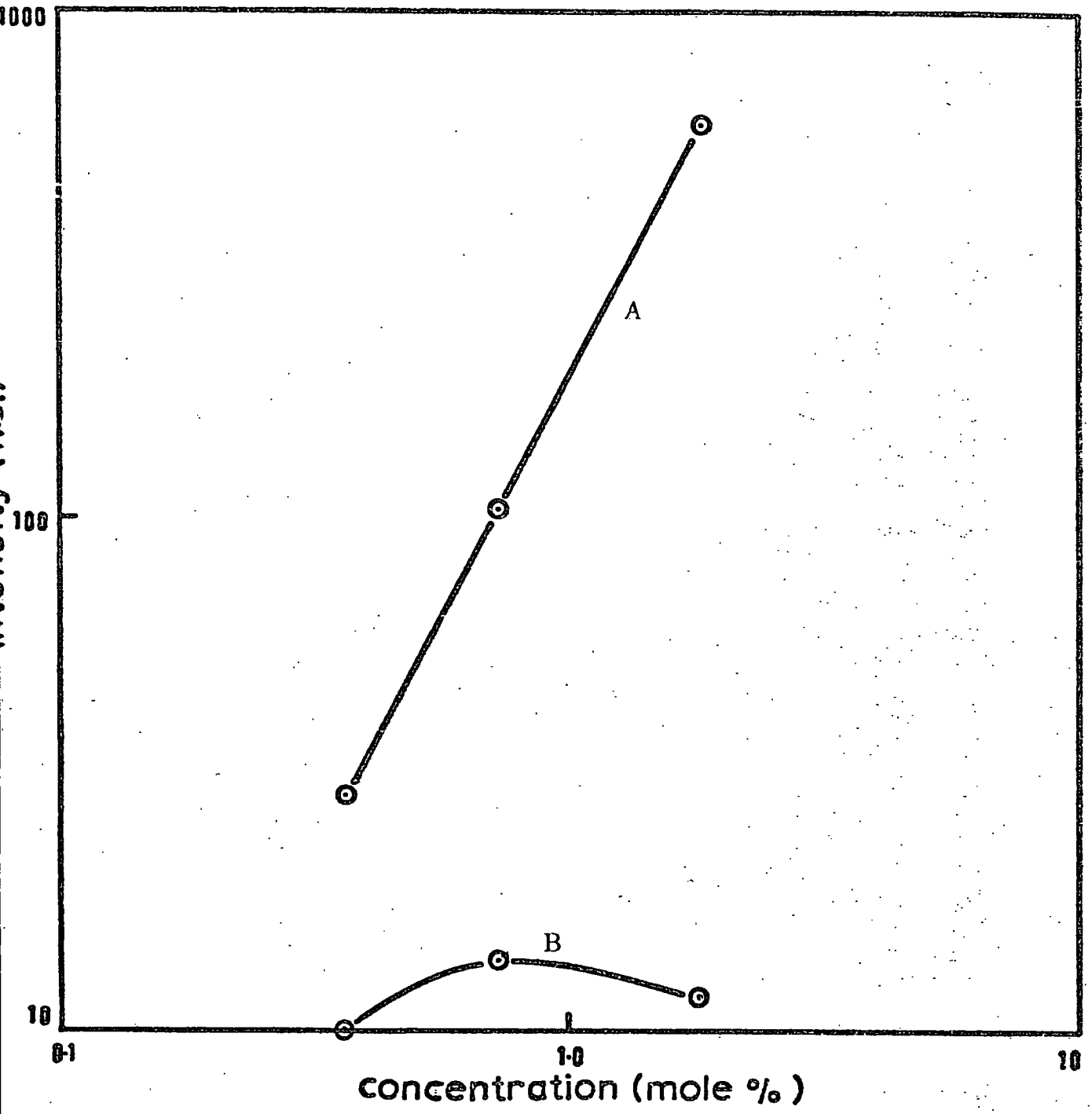

Fig 5.4

Emission intensity of the 548 nm (A) and 441 nm (B) lines of Tb^{3+} ions in LAS glass as a function of concentration

Figure 5.5 shows the sum:-

$$\sum \text{(relative intensity x half height full width)}$$

for all lines in each of the two groups ($^5D_3$ and $^5D_4$) of the emission bands in LAS glass as a function of concentration. These graphs are essentially the total intensity for each of the multiplets after allowance for the photomultiplier efficiency. The third graph in this figure shows the ratio of these two intensities and may be regarded as a measure of the efficiency of energy transfer for the process $^5D_3 \longrightarrow {}^5D_4$. Note that the emission from the transition $^5D_3 \longrightarrow {}^7F_6$ at 382 nm has not been included in these graphs, and this will tend to reduce slightly the energy transfer efficiency as estimated in the third curve in Figure 5.5. The lowest curve shows clearly that the emission intensity from the $^5D_3$ level saturates at concentrations a little above 0.5 mole %, which is similar to the results for NS glass.

Van Uitert (5.16), in studies of sodium yttrium tungstate doped with trivalent terbium, has demonstrated that such concentration quenching can be explained by energy transfer processes between Tb^{3+} ions.

The quenching of the shortwave bands can be explained by a multipolar transfer of electrons from the $^5D_3$ level to the $^5D_4$ level. Thus the long wavelength bands are enhanced at concentrations above 0.5 mole % at the expense of the shortwave bands. Van Uitert characterised the transfer process in $NaYWO_4$ as dipole - quadrupole in character.

Van Uitert has also proposed that the concentration quenching of

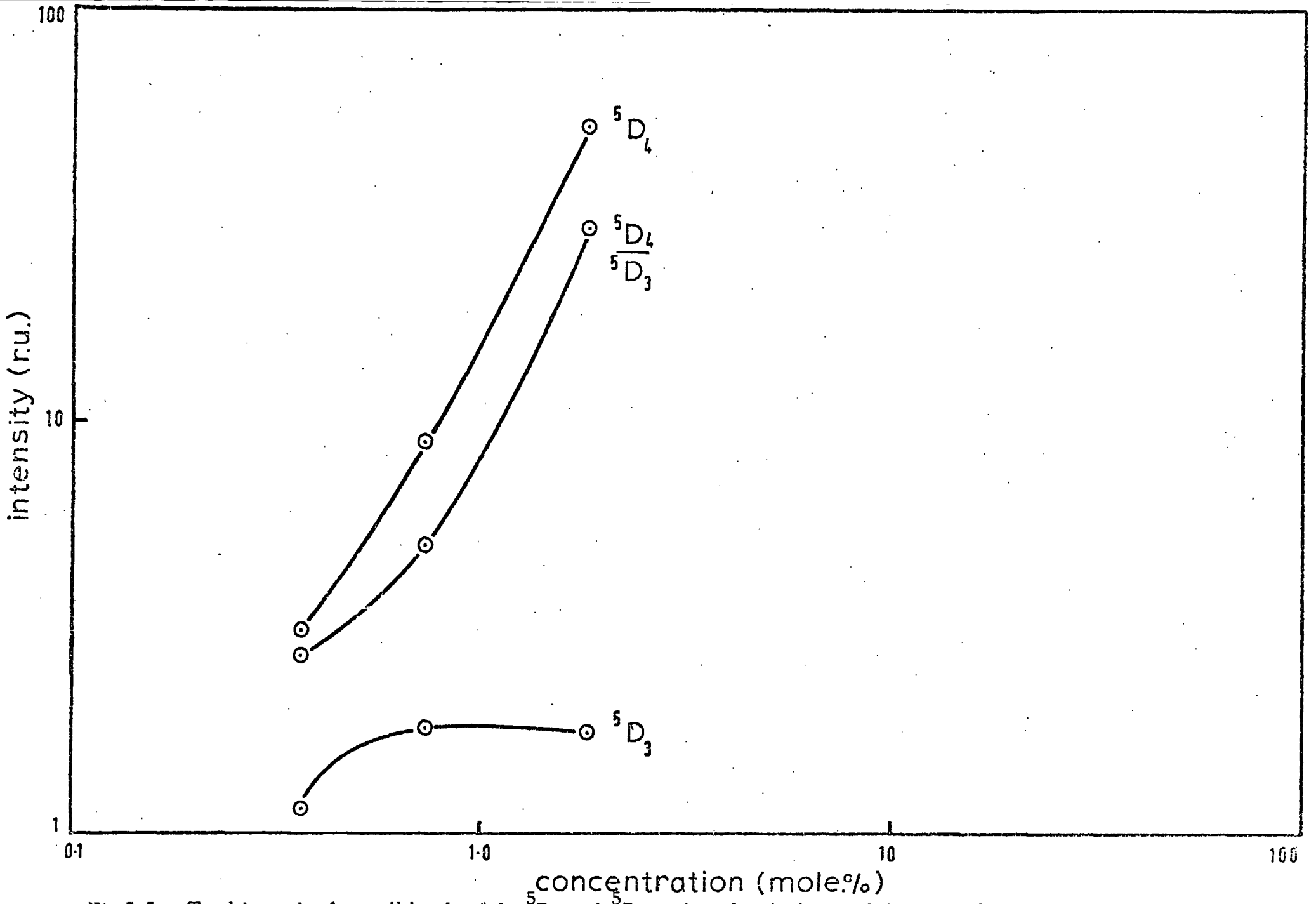

Fig 5.5 Total intensity from all bands of the $^5D_4$ and $^5D_3$ series of emissions and the ratio of these as a function of concentration of Tb^{3+} ions in LAS glass

the $^5D_4$ bands is due to an exchange mechanism wherein the $^7F_{0,1}$ components of the ground state multiplet of an excited ion and those of three neighbouring ions are filled.

The separation, r, of Tb^{3+} ions at the critical concentration at which these energy transfer phenomena become significant was estimated from the expression:-

$$r = \left(\frac{M}{N \rho x}\right)^{1/3} \qquad (5.1)$$

where M is the average gram-molecular weight of the glass, N is Avogadro's number, ρ is the bulk density, and x is the ionic concentration of Tb^{3+}.

Using the values M = 60 and ρ = 2.4 g/cm^3 (see Chapter 4), and taking the critical concentration for quenching as 0.5 mole % ($^5D_3$) and 5 mole % ($^5D_4$) gives separations, r, of 20Å and 9.5Å respectively.

These values are much larger than those given by Van Uitert (5.16) and Nakazawa and Shionoya (5.17) for Tb^{3+} in crystalline host materials (see section 5.5). The critical concentrations, however, agree quite well with those taken from the results of Herring et al (5.15) and Karapetyan and Lunter (5.18) in glassy hosts. Similar values of r may be imputed from these latter results. The difference between glassy and crystalline media is believed to be due to the inhomogeneous broadening in glass, which widens the spectral lines, thus increasing the value of the overlap integral (see Chapter 2) and consequently increasing the efficiency of energy transfer. It is proposed that energy transfer will, in general, be a more efficient process

in glasses because of these effects of local disorder.

The extent of local disordering may thus be estimated, at least qualitatively, from the plots of intensity versus concentration. Thus the addition of Al_2O_3 to a glass, which is believed to reduce inhomogeneous broadening, should produce concentration quenching at higher doping levels. The results presented here are inconclusive on this point, but they do show a slight tendency for saturation of the $^5D_3$ emissions to occur at slightly higher concentrations in LAS glass.

Figure 5.6 shows the energy level diagram of Tb^{3+} ions and possible energy transfer mechanisms between two ions. The excitation at 365 nm is thought to promote electrons to higher levels of the Tb^{3+} ions (for example, the $^5G_5$ level), which relax, either non-radiatively or with the emission of infra-red quanta, to the $^5D_3$ level.

In general, the larger the energy difference between two electronic states, the smaller the non-radiative transition probability between them (5.19). For rare earths, the energy difference between the electronic levels, below which considerable non-radiative de-excitation occurs in glass, has been shown to be about four phonons (5.20). This corresponds to about $4000\,cm^{-1}$ in silicate glasses, since the phonons are thought to be due to stretching in Si-O bonds. (The absorption due to this mode of vibration occurs at about $1000\,cm^{-1}$ - see Chapter 4.) Thus the $^5D_4$ level, which is separated from the next highest ($^5D_3$) level by some $5400\,cm^{-1}$, is unlikely to be significantly populated by the non-radiative de-excitation

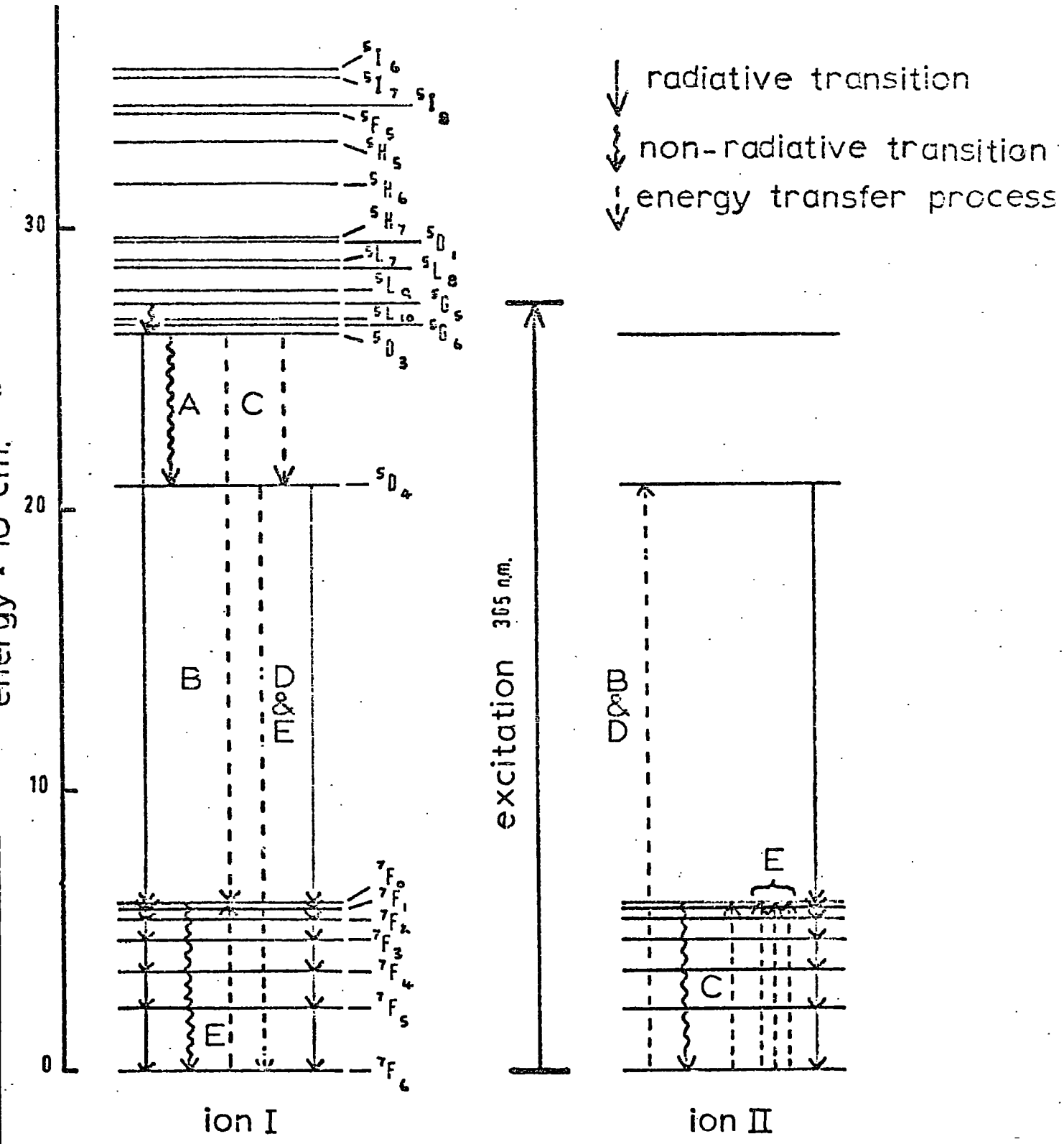

Fig 5.6

Some energy transfer processes between Tb^{3+} ions in silicate glasses:-

A: Non-radiative excitation $^5D_3 \longrightarrow {}^5D_4$

B and C : Alternative multipolar energy-transfer mechanisms for $^5D_3 \longrightarrow {}^5D_4$

D : Resonant transfer $^5D_4 \longrightarrow {}^5D_4$

E : Exchange-dipole quenching of $^5D_4$

shown as A in Figure 5.6.

Note that the value 5400 cm^{-1} is very close to the separation of the $^7F_{0,1}$ and $^7F_6$ levels. This implies that the two energy transfer processes B and C shown in Figure 5.6 are possible mechanisms for the population of the $^5D_4$ level. However, these two mechanisms cannot be discriminated between at this stage, and process B will be taken as the energy transfer mechanism responsible for the excitation of the $^5D_4$ level. Process C may be regarded as equivalent to the non-radiative de-excitation of the $^5D_3$ level and will be treated as an extra contribution to process A.

The probability of the transfer process will be strongly dependent on the ionic separation and hence on concentration. The experimental results suggest that below about 0.5 mole % Tb^{3+}, the transfer mechanism is weak and both the shortwave ($^5D_3$) and the longwave ($^5D_4$) emission intensities increase with concentration. Above 0.5 mole % the transfer process becomes progressively more efficient, and the longwave bands become very intense at the expense of the shortwave bands.

A simplified version of the energy level diagram is shown in Figure 5.7, where A represents an isolated Tb^{3+} ion and B a pair of coupled Tb^{3+} ions (see also ref 5.19).

In what follows, N_{ja} and N_{jb} (j = 1,2,3) represent the number of Tb^{3+} ions in the different excited states. The subscripts a and b are used to distinguish isolated pairs of ions. The transitions between the different excited states are indicated by arrows, and the radiative transitions are labelled L_A and L_B. In the case of a non-interacting

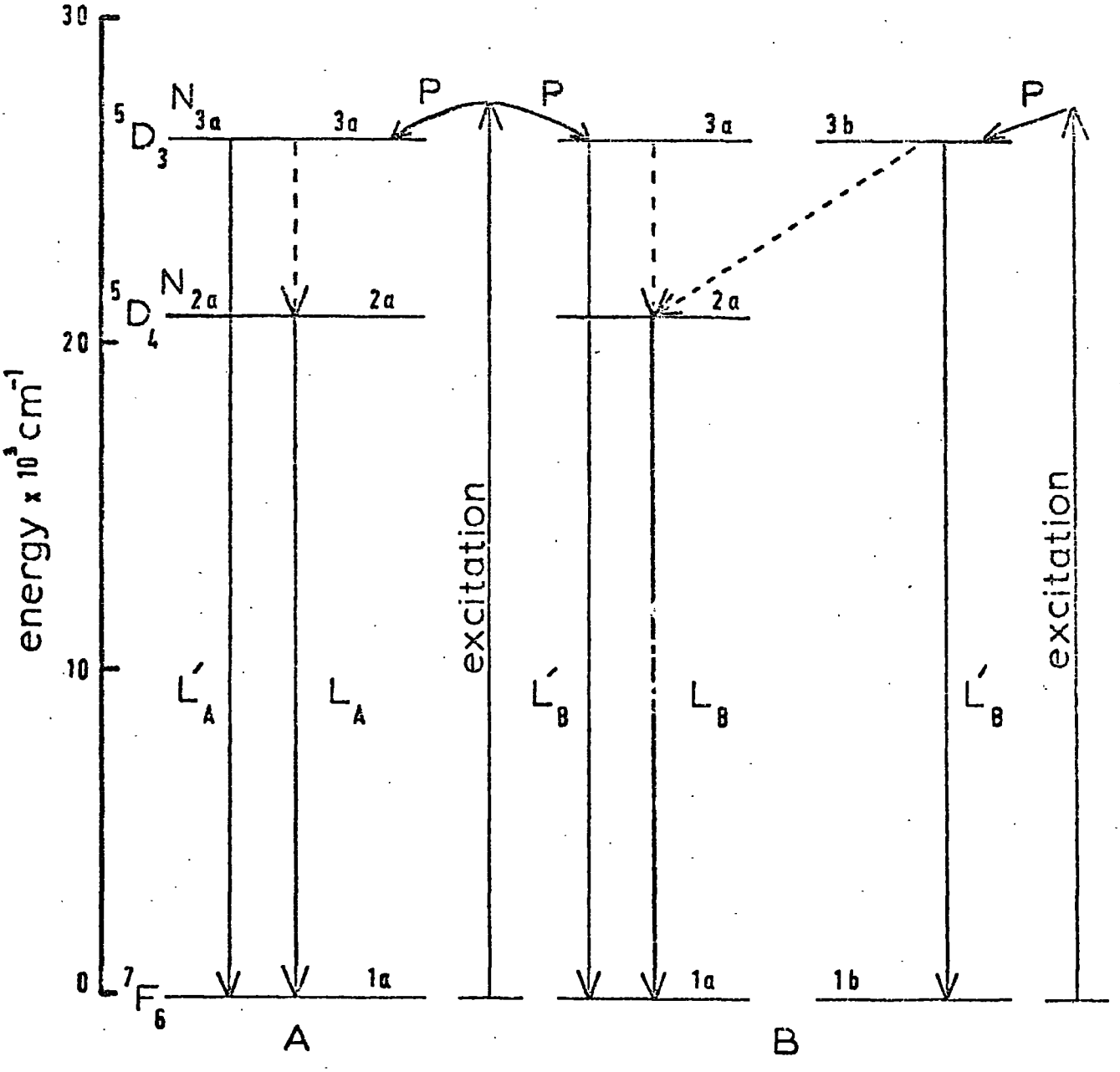

Fig 5.7

Simplified energy level model for Tb^{3+} ions in silicate glasses

ion, the basic kinetic equation describing level 2a is:-

$$\frac{dN^{A}_{2a}}{dt} = A_{3a2a}\, N_{3a} - A_{2ala}\, N_{2a} \qquad (5.2)$$

where the A_{ja} describe the transition probabilities between the various levels. In the case of a pair of interacting ions this becomes:-

$$\frac{dN^{B}_{2a}}{dt} = A_{3b2a}\, N_{3b} + A_{3a2a}\, N_{3a} - A_{2ala}\, N_{2a} \qquad (5.3)$$

Here the A_{3b2a} term describes the energy transfer process.

If now we assume $N_{3a} = N_{3b}$, then:-

$$L_A \simeq A_{2ala}\, N_{2a}$$

$$= A_{3a2a}\, N_{3a} \qquad (5.4)$$

and

$$L_B \simeq A_{3a2a}\, N_{3a} + A_{3b2a}\, N_{3b} \qquad (5.5)$$

$$= L_A \left[1 + \frac{A_{3b2a}}{A_{3a2a}}\right] \qquad (5.6)$$

$$= K'_p\, L_A \qquad (5.7)$$

where K'_p is the pair interaction coefficient.

For a terbium concentration, c, we can write:-

$$L_B(c) = K'_{pair}\,(c).\, L_A(c)$$

and taking into account the concentration quenching above 5 mole %,

we have in general:-

$$L_B(c) = L_A(c) . K'_p(c) . K'_q(c) \qquad (5.8)$$

where K'_q is the interaction coefficient for the quenching process.

Karapetyan and Lunter (5.18) also report concentration quenching of the longwave emissions in silicate glasses at approximately 15 weight % of terbium oxide (~5.6 mole %). The variation of the coefficients $K'_p(c)$ and $K'_q(c)$ can be obtained from the present experimental data and the data of Karapetyan and Lunter. For small terbium concentration (<0.5 mole %) $K'_p \simeq 1$, but with increasing concentration its value increases non-linearly, as shown in Figure 5.8. The variation of $K'_q(c)$ is also shown in this figure, along with the concentration dependence of the longwave luminescence.

A similar mathematical expression can be derived to describe the concentration quenching of the $^5D_3$ level. For an isolated ion, A, in equilibrium with the photon flux:-

$$\frac{dN^A_{3a}}{dt} = 0$$

$$= P - A_{3a1a} N_{3a} - A_{3a2a} N_{3a} \qquad (5.9)$$

where P is the "pump" rate which describes the excitation rate of the $^5D_3$ level by all processes, thus:-

$$P = A_{3a1a} N_{3a} + A_{3a2a} N_{3a} \qquad (5.10)$$

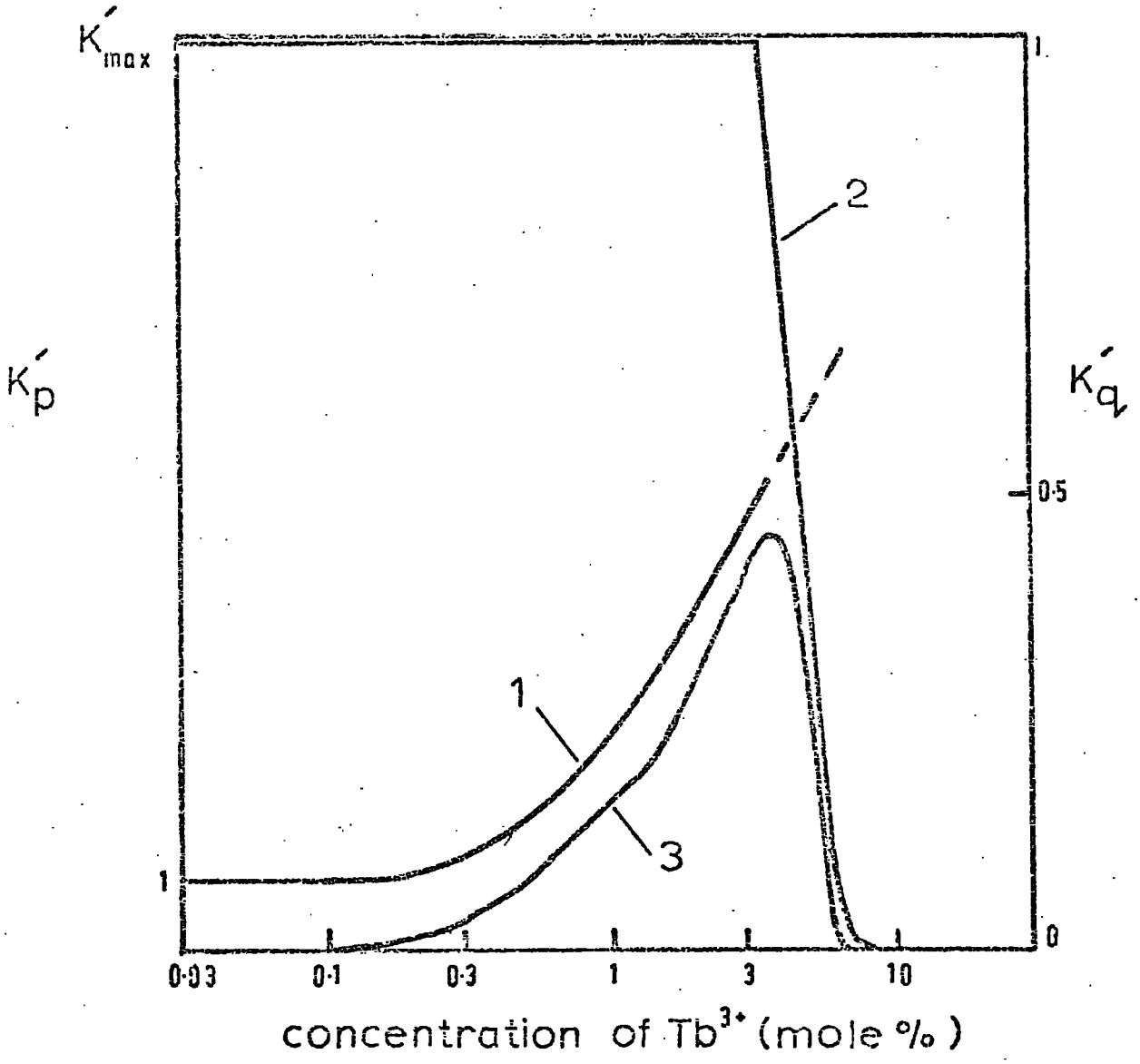

Fig 5.8

The parameters K'_p (1) and K'_q (2) and the emission intensity of the $^5D_4 - {}^7F_J$ transitions (3) as a function of concentration in NS glass

For a pair of coupled ions, B, the expression becomes:-

$$\frac{dN_{3a}^{B}}{dt} = 0$$

$$= P - A_{3a1a} \; N_{3a} - A_{3a2a} \; N_{3a} - A_{3a2b} \; N_{3a} \qquad (5.11)$$

and the expression for the pump rate is similarly modified to:-

$$P = A_{3a1a} \; N_{3a} + A_{3a2a} \; N_{3a} + A_{3a2a} \; N_{3a} \qquad (5.12)$$

Then, the intensity of emission with no energy transfer is:-

$$L_{A}^{'} = A_{3a1a} \; N_{3a} = P - A_{3a2a} \; N_{3a} \qquad (5.13)$$

and the intensity allowing for energy transfer is:-

$$L_{B}^{'} = A_{3a1a} \; N_{3a} \qquad (5.14)$$

$$= P - A_{3a2a} \; N_{3a} - A_{3a2b} \; N_{3a} \qquad (5.15)$$

Thus:-

$$L_{B}^{'} = L_{A}^{'} - A_{3a2b} \; N_{3a} \qquad (5.16)$$

Then, the ratio of luminescence intensities with and without energy transfer is:-

$$T = \frac{L_{B}^{'}}{L_{A}^{'}} = \frac{A_{3a1a} \; N_{3a} - A_{3a2b} \; N_{3a}}{A_{3a1a} \; N_{3a}} \qquad (5.17)$$

Whence:-

$$L'_B = L'_A \left[1 - \frac{A_{3a2b}}{A_{3a1a}} \right] \qquad (5.18)$$

If the emission rate of the $^5D_3$ level is assumed, in the absence of energy transfer, to be proportional to the number of emitting species, then:-

$$L'_A(c) \propto c \qquad (5.19)$$

or

$$\frac{L'_A(c)}{c} = K \qquad (5.20)$$

with K a constant.

Consequently, combining equations 5.17 and 5.20,

$$T = \frac{L'_B(c)}{c} \cdot K$$

At low concentrations T = 1.0. Figure 5.9 shows a plot of T against the concentration of Tb^{3+} in NS glass which has been derived by assuming $T \simeq 1$ at the lowest concentration available for study.

An approximate relationship exists between the parameter T and the efficiency of energy transfer η. If the excitation of the $^5D_4$ level is assumed to be entirely by transfer of electrons from the $^5D_3$ level, either by non-radiative relaxation or by energy transfer, then the emission intensity from the $^5D_4$ level is given by:-

$$A_{2a1b} N_{2b} \simeq A_{3b2b} N_{3a} \qquad (5.21)$$

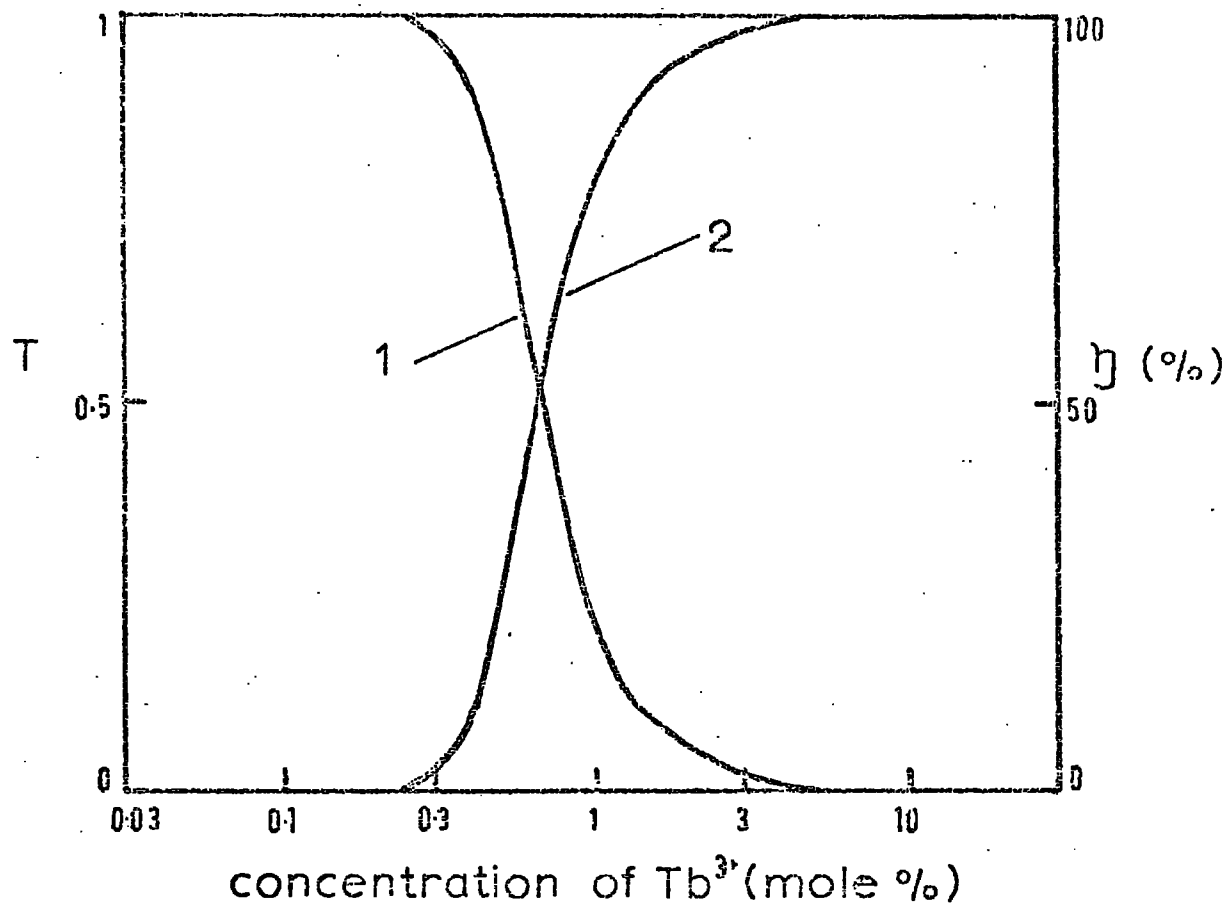

Fig 5.9

The parameters T (1) and η (2) as a function of concentration in NS glass

The efficiency of energy transfer, η , is given by:-

$$\eta \simeq \frac{A_{2b1b} N_{2b}}{A_{3a1a} N_{3a}} \qquad (5.22)$$

Thus

$$\eta \simeq \frac{A_{3a2b}}{A_{3a1a}} \qquad (5.23)$$

which on comparison with equation 5.18 gives:-

$$T \simeq 1 - \eta$$

Figure 5.9 also give a plot of η derived from this expression as a function of concentration.

The relationship between T and η is approximate because it takes little or no account of the following:-

1. Resonant transfer between neighbouring ions.
2. Excitation of the $^5D_4$ level direct from higher levels (such as ^5G_J).
3. Concentration quenching of the $^5D_4$ level (probably by an exchange dipole mechanism).
4. Non-radiative de-excitation, particularly of the $^5D_4$ level.

The approximation is thought to be quite good, as these effects are all likely to be small except at such concentrations where '3' becomes significant ($\sim$ 5 mole %).

5.1.4 Relative Intensities within the Emission Band Series

The relative intensities of the two series of emission bands have

been explained in terms of an energy transfer model. The relative intensities of the individual bands are now described, and an attempt is made to explain the broad features in terms of magnetic- and electric-dipole transitions. There is still further detail to be explained, such as, for example, the structure of each emission band. Discussion of line-shapes, however, will be deferred until section 5.1.6, after the presentation of the low temperature data.

The inter-4f transitions, responsible for the Tb^{3+} luminescence, are to a first approximation both spin- and parity-forbidden. The spin selection rule is relaxed by the mixing of the ^5D_J and ^7F_J wavefunctions by spin-orbit coupling. However, the parity selection rules may only be relaxed by a mixing of the 4f wavefunctions with eigenstates of the opposite symmetry. Thus, if the Tb^{3+} ion occupies a site with strict inversion symmetry, only magetic-dipole transitions (with $\Delta J = 0, \pm 1$) and vibronically induced electric-dipole transitions can occur.

For the $^5D_4$ - ^7F_J series of emission bands, the transition $^5D_4$ - $^7F_5$ will be most intense, as only for this transition is the contribution of the matrix element between the ^7F states not counteracted by the contribution of the matrix elements between the ^5D states (5.2). Calculation has shown the relative contribution of the emissions from the magnetic-dipole transitions $^5D_4$ - $^7F_5$ ($\Delta J = +1$), $^5D_4$ - $^7F_4$ ($\Delta J = 0$), and $^5D_4$ - $^7F_3$ ($\Delta J = -1$) to be 89, 1 and 10 respectively, if the total intensity is put equal to 100. In Table 5.5 below, these theoretical values are compared with the average values obtained in this work for Tb^{3+} in NS and LAS glasses.

TABLE 5.5

Relative Contributions to the Emission Intensity from $^5D_4$ Transitions with $\Delta J = 0, \pm 1$

System	$\Delta J = +1$	$\Delta J = 0$	$\Delta J = -1$
Theoretical (md only)	89	1	10
NS glass : Tb	71	18	11
LAS glass : Tb	79	14	7

The disparity of the figures for Tb^{3+} ions in glass together with the presence of an intense $^5D_4$ - $^7F_6$ transition leads to the conclusion that there is a significant electric-dipole contribution to the emission. This additional intensity component appears to imply a partial lack of symmetry of the ligands about the Tb^{3+} ion due to local disordering. However, Blasse and Bril (5.2) and Avella et al (5.22) have shown that the intensity distribution among the $^5D_4$ - ^7F_J transitions in materials containing Tb^{3+} is particularly insensitive to the ligand field symmetry.

In Table 5.6 the relative intensities of the transitions $^5D_4$ - ^7F_J (J = 3,4,5,6) given by Blasse and Bril are compared with those determined for silicate glasses in this work. Only those crystalline materials containing potential glass-network formers have been used for comparison. Note that the values obtained in this work are very similar to those taken from the literature. Also note that some of these

TABLE 5.6

Distribution of Emission Intensity from the Transitions $^5D_4 - {}^7F_J$ (J = 3,4,5,6) in Several Media

- After Blasse and Bril (1967)

Material	Relative Intensity* of the Transitions from $^5D_4$ to :			
	$^7F_6$	$^7F_5$	$^7F_4$	$^7F_3$
Sc BO_3 : Tb	11	75	4	10
Sc Si_2O_7 : Tb	12.5	64	15	8.5
Li $YGeO_4$: Tb	15	73	5	7
$YAl_3B_4O_{12}$: Tb	12.5	71	11	5.5
NS glass : Tb (a)	15.5	60	15.5	9
LAS glass : Tb (a)	20	63	11	6

* Total intensity of the emission intensities is put at 100.

(a) This work.

crystalline materials have inversion symmetry and some do not. For example, $ScBO_3$: Tb has definite inversion symmetry, while $LiYGeO_4$: Tb has not.

The insensitivity of the distribution of intensity among the emission bands of Tb^{3+} is in striking contrast to the situation for the similar ion Eu^{3+} (5.22). With Eu^{3+} ions, quite small deviations from strict inversion symmetry are sufficient to induce strong electric-dipole transitions. This is thought by Blasse and Bril to be because the eigenstate mixing involved in the removal of the parity selection rule for Eu^{3+} is between the 4f levels and the charge transfer configuration, which is much lower in energy for Eu^{3+} than for Tb^{3+}. In the case of Tb^{3+}, the wavefunction of opposite symmetry involved in the removal of parity restrictions is thought to be the 4f - 5d configuration.

Experiment (5.2) suggests that 4f-ligand mixing is more effective in removing the parity selection rule than is 4f - 5d mixing. This is further emphasised by the particular behaviour of the emission from the transition $^5D_4$ - $^7F_6$ which is expected to be "hypersensitive" to changes in the ligand field. The change in the total angular momentum quantum number for this transition is $\Delta J = +2$, and consequently this is forbidden as a magnetic dipole transition. This line is thus a vibronically induced electric-dipole transition only, and is expected to be very sensitive to crystal field perturbations. However, as the results recorded in Table 5.6 and others quoted by Blasse and Bril (5.2) show, the intensity of this emission band is very insensitive to environment.

The general theory has thus proved to be a reasonable description

of the distribution of intensities within the $^5D_4$ - ^7F_J series, but has proved inadequate to infer the symmetry of the Tb^{3+} ion site. The study of line-shape leads to more definite conclusions, and this is dealt with later in this chapter.

5.1.5 Decay Times in NS Glass

Luminescence decay times were measured using the Optica spectrophotometer in monochromator mode. The single beam head was used to avoid modulation effects from the rotating mirrors of the double beam system. The photomultiplier output was amplified and displayed on an oscilloscope, the trace of which was photographed for later examination. Excitation was by means of a filtered mercury source (365 nm) modulated with a rotating shutter (pulse duration 0.4 msec) or a Xenon flash tube (pulse duration 5 μsec). Results from both experimental methods were entirely similar, so that the results presented are not referred to any particular excitation method.

The measurements for transitions from the $^5D_4$ level showed two clearly defined decay regions which are well represented by an exponential decay equation of the type:-

$$I = I_o \exp\left(\frac{-t}{\tau}\right) \qquad (5.24)$$

At a concentration of 2.88 mole % Tb^{3+} in NS glass the first of these regions had a decay time, τ, of 2.5 $\pm$ 0.2 msec (see Figure 5.10 (a)) and accounted for the majority of the fall in intensity. The second decay component for this specimen had a much longer characteristic time of 1.4 $\pm$ 0.1 sec (see Figure 5.10 (b)).

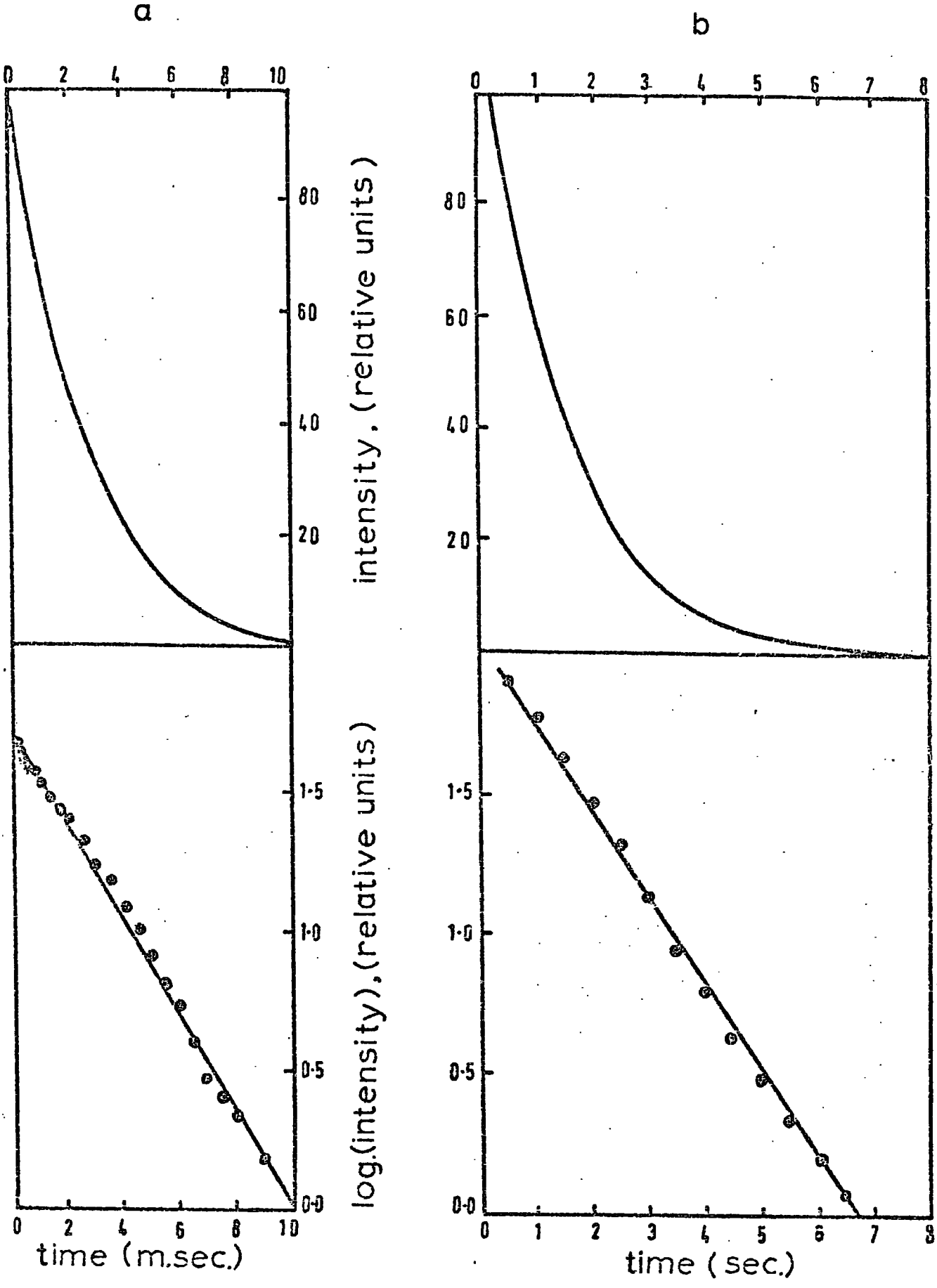

Fig 5.10

The short (a) and long (b) decay components of the afterglow of the luminescence at 549nm from NS glass activated with 2.88 mole % of Tb^{3+} ions

The short decay time compares well with a value of 3.0 msec in borate glasses reported by Reisfeld et al (5.23) and values of 2.4 msec and 2.5 msec for a sodium calcium borate glass and a zinc phosphate glass respectively reported by Karapetyan and Lunter (5.18).

The concentration dependence of the faster decay process is shown graphically in Figure 5.11, where the decay times are plotted for all the specimens examined. The curve shows that the duration of the afterglow decreases slowly with increasing terbium concentration in this glass. There was no detectable change in the longer decay time as the concentration increased, although this could only be detected for concentrations $\gtrsim 1$ mole%.

The value of 2 to 3 msec is typical for the decay of the inter - 4f transitions $^5D_4 - {}^7F_J$ in materials containing Tb^{3+} but, although similar values have been found in a variety of crystalline materials (5.24), some crystals can have values an order of magnitude lower (5.25).

The decay times of Tb^{3+} ions in a condensed medium are likely to be longer than those of the free ion (5.26) because of the influence of energy transfer processes. The $^5D_3$ level interacts with the $^5D_4$ level in such a way as to transfer electrons from the more energetic to the less energetic state. Thus, the afterglow of the lower luminescing level is protracted; the more efficient the energy transfer, the longer the decay time observed.

A similar explanation is proposed for the shortening of decay times observed with increasing terbium concentration. In this case, the energy transfer leads to a quenching of the luminescence of the

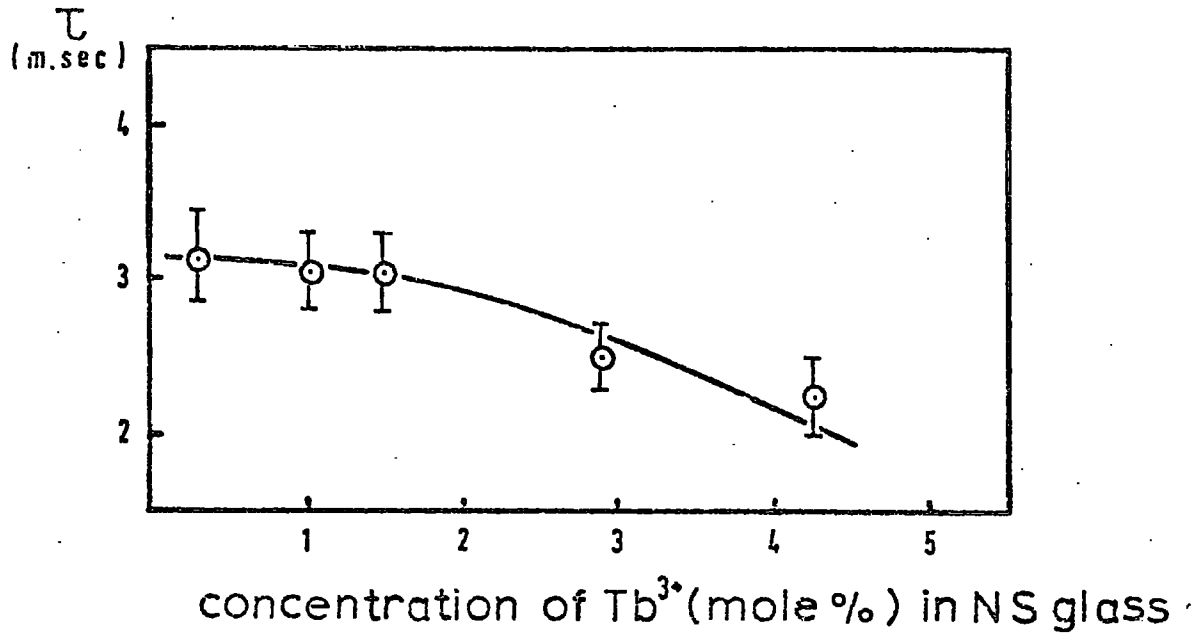

Fig 5.11 The concentration dependence of the faster decay process in NS glass

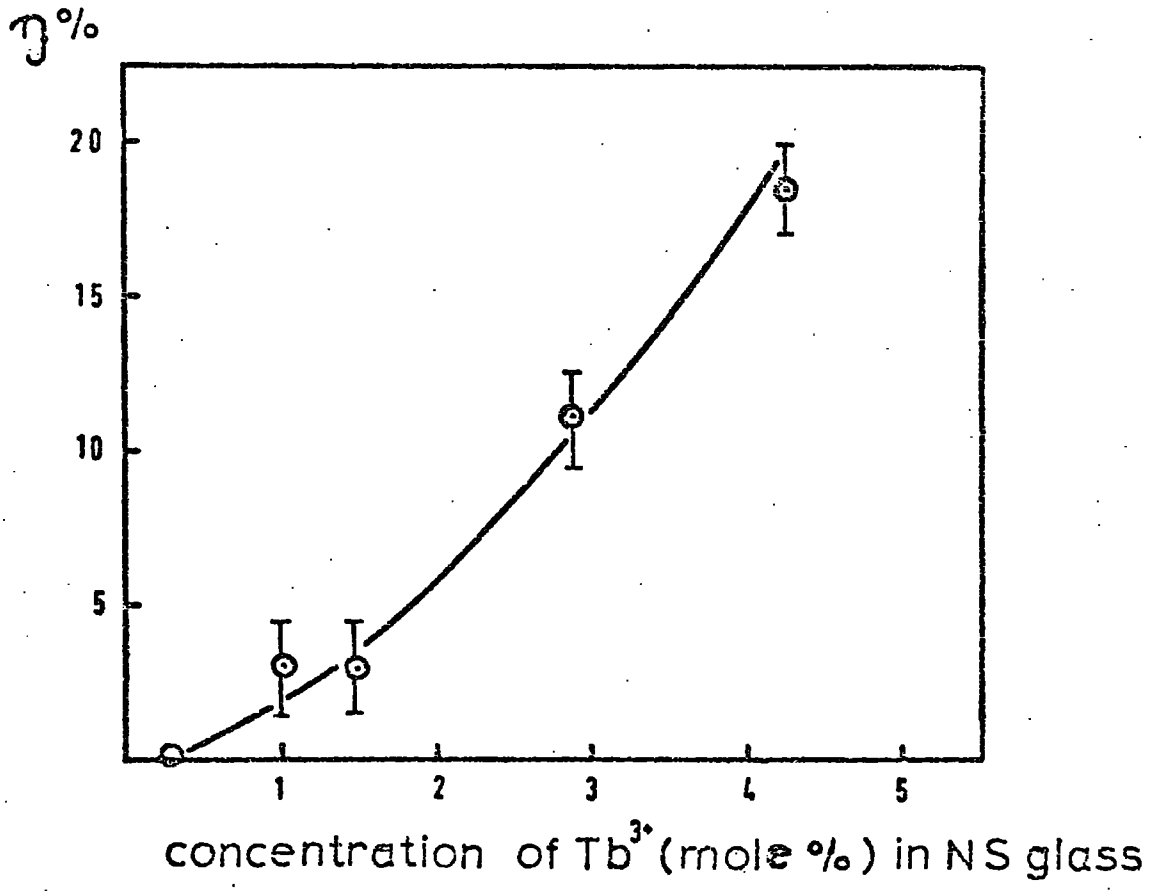

Fig 5.12 The efficiency of energy transfer as a function of concentration as derived from Fig 5.11

$^5D_4$ level. A higher probability of non-radiative de-excitation results in a reduction of the intensity of the afterglow.

The efficiency, η, of this quenching process resulting from interactions between Tb^{3+} ions may be determined from the relation:-

$$\eta = 1 - \frac{\tau}{\tau_o} \qquad (5.25)$$

which is applicable to any type of interaction. Here τ_o is the decay time for the terbium luminescence in the case of no interaction between the Tb^{3+} ions (i.e., in the case of low concentrations). The dependence of η on concentration is shown in Figure 5.12, where η has been assumed to be approximately zero at the lowest concentration studied.

The efficiency derived in this way is small (~11% for the 2.88 mole % Tb^{3+} sample), but increases rapidly above, say, 5 mole % when concentration quenching becomes significant (see previous section). Thus, it is proposed that the mechanism responsible for the reduction in the luminescence decay time of the $^5D_4$ level in silicate glasses is a non-radiative de-excitation process which is likely to take place via an exchange dipole interaction.

Similar measurements were made for luminescence resulting from transitions from the $^5D_3$ level, principally the emission from the more intense $^5D_3$ - $^7F_4$ transition at around 440nm. Results gave a decay time $\tau = 1.7 \pm 0.1$ msec at 0.031 mole % which was reduced considerably at concentrations above 0.5 mole %. The results for those concentrations of terbium which were studied are given in Figure 5.13. Note that the reduction in lifetime begins at the same concentrations as

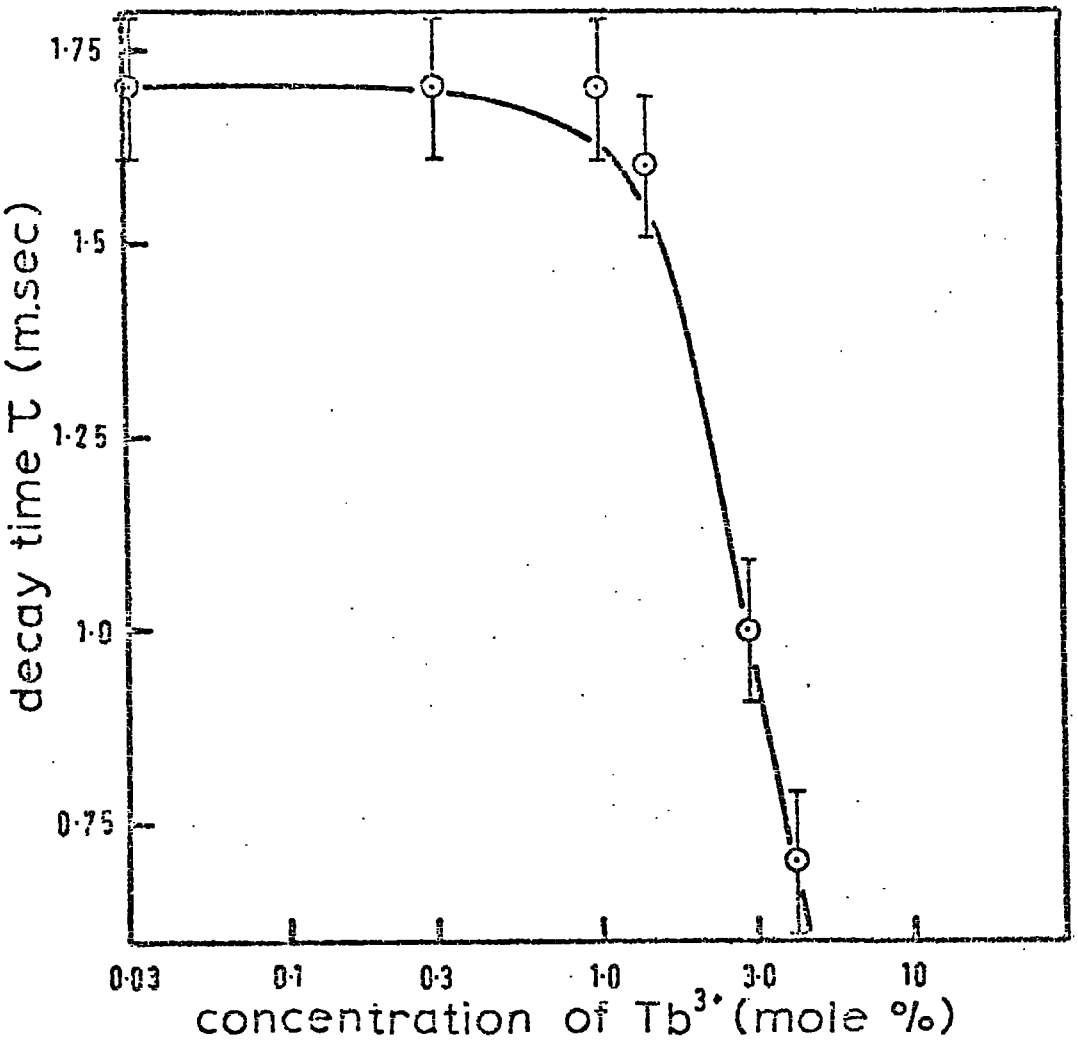

Fig 5. 13

The decay time of the 442 nm emission band from Tb^{3+} ions in NS glass as a function of concentration

the transfer process $^5D_3 \longrightarrow {}^5D_4$ was observed (see previous sections). The lifetime is thought to be reduced in a similar fashion to the $^5D_4$ transition except that in this case a multipolar transfer process is responsible for the depopulation of the luminescing level.

The long decay component discovered in the measurements of the afterglow of the $^5D_4$ emissions was absent in the shorter wavelength luminescence. Probably this was because of the much lower intensity of the blue ($^5D_3$) emissions.

It is interesting to note that the values obtained for the decay times of the $^5D_3$ and $^5D_4$ levels were both longer than those quoted by Nelson et al (5.27) in pure vitreous silica. These authors obtained values of τ = 0.9 m sec and τ = 1.7 m sec for the $^5D_3$ and $^5D_4$ levels respectively at concentrations up to 0.1 mole %. No explanation of this difference could be decided, although the results of Nelson et al were not in good agreement also with the work of Karapetyan and Lunter (5.18) especially for the lower wavelength emissions.

Temperature was also found to be an important parameter influencing the rate of luminescence decay, but the presentation and discussion of the relevant results will be deferred to the next section, which deals explicitly with the various effects of temperature on the luminescence characteristics.

5.1.6 The Temperature Dependence of the Luminescence from Rare Earth Doped Silicate Glasses

The change with temperature of the structure and shape of luminescence emission bands can be qualitatively predicted by reference to

the appropriate configurational co-ordinate model. The changes observed reflect the interaction of the excited states of the luminescing centres with the phonon flux of the material, which increases with increasing temperature. The configurational co-ordinate model, however, can but rarely give a quantitative representation of these temperature effects. In consequence, the usual procedure is to use experimental measurements of the luminescent spectra at various temperatures in order to infer the configurational co-ordinates of the system.

In this section, details are given of the variation of the luminescence intensity of the various emission bands of Tb^{3+} ions with temperature in glasses excited by the 365 nm mercury line. Also the effect of temperature on decay times is considered, together with the variation of width and peak wavelengths of the emission bands. Finally, since the widths of the emissions bands are reduced at very low temperatures, the more pronounced line structure is considered.

Measurements of these various effects are then used to discuss the symmetry of the site of Tb^{3+} ions in silicate glasses, and some deductions about the configurational co-ordinate model are also presented.

(a) Luminescence Intensity as a Function of Temperature

In assessing the general characteristics of a luminophor, it is important to consider the effect of temperature on the emission intensity and wavelength. Such measurements can give an indication of the strength of any interactions between the emission centre and the host matrix. Further, by reducing the temperature to near absolute zero,

the effect of thermal broadening on the emission line-shape can be considerably reduced, due to a suppression of phonon interactions. The line-shape at lower temperatures is thus of great interest from a theoretical standpoint, since the splitting of the Stark levels due to the electrostatic crystal field is more easily resolved.

The equipment designed for use in thermoluminescence measurements (for a description, see Chapter 3) was employed to give an indication of the total emission intensity as a function of temperature. The total emission from a sample of NS glass containing 1.48 mole % of Tb^{3+} was measured and compared with the behaviour of NS glass containing Sm^{3+} and Dy^{3+}, and LAS glass containing Gd^{3+} at roughly similar molar concentrations. The specimens were excited by the 365 nm emission line of a mercury vapour lamp. The wavelengths of the resulting emission bands are given in Table 5.7.

TABLE 5.7

Ultra-violet Excited Luminescence Characteristics of Several Trivalent Lanthanide Ions

Activator Ion	Wavelengths of the Main Emission Bands nm		
Tb^{3+}	490	550*	590
Sm^{3+}	560	604	650*
Dy^{3+}	485	490	587*
Gd^{3+}	313-315		

* = most intense emission band

It must be realised that such measurements are limited in their generality because no account is taken of changes in the spectral distribution of the luminescence which may result from the temperature change. For rare earth ions this is in part justified, since the emission results from transitions among the 4f electrons which are well shielded from the external environment. The wavelengths of the peaks in the various emission lines are thus expected to have little temperature dependence. However, there is still another feature, namely that no account was taken of the relative intensities of the emission bands, which (especially in the case of terbium) may be prone to changes due to thermal effects on the multipolar energy transfer processes. This latter point is returned to later in this section.

Figure 5.14a shows the relative emission intensities (normalised to 100 at low temperatures for each ion) as a function of temperature in the range 100°K to 700°K for the ions Tb^{3+}, Dy^{3+} and Gd^{3+} in silicate glasses. The results for Sm^{3+} are not presented as they are similar to those for Dy^{3+}. The observed intensity was still appreciable in all cases at temperatures up to about 600°K or 700°K. In extended measurements the luminescence of Tb^{3+} ions in NS glass was found to persist to well above 500°C (770°K).

The data for Gd^{3+} and Dy^{3+} are re-plotted in Figure 5.14b as a function of reciprocal temperature, and it is evident that the thermal quenching of the luminescence is given by the relation (see reference 5.28):-

$$I(T) = I_o \left[1 + C \exp \left(\frac{-W}{kT} \right) \right]^{-1} \qquad (5.26)$$

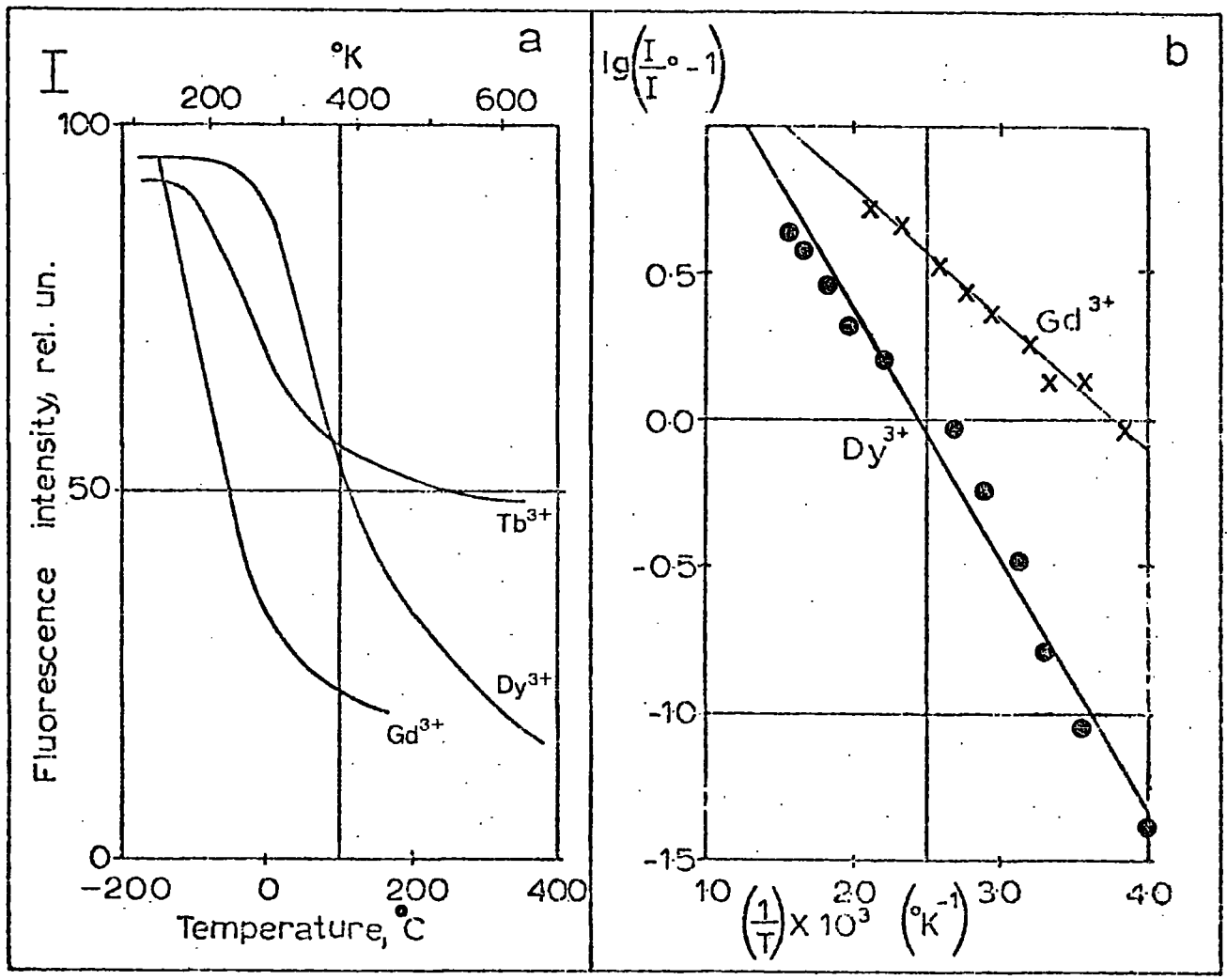

Fig 5.14

(a) The variation with temperature of the total emission intensity from Tb^{3+}, Dy^{3+} and Gd^{3+} ions in silicate glasses

(b) The data from (a) transferred to a plot of log (relative intensity) versus reciprocal intensity

where W is the activation energy of the quenching process. For the present case of Dy^{3+} in NS glass, the data give $W = 0.20 \pm 0.03$ eV, and for Gd^{3+} in LAS glass $W = 0.10 \pm 0.03$ eV. These small values of W result in the persistence of the luminescence emission to the high temperatures observed. In the case of Tb^{3+}, the results do not follow this classical behaviour.

The luminescence intensity of Tb^{3+} follows expression 5.26 only up to about 400°K; above this temperature, the emission is more intense than would be predicted by extrapolation from lower temperatures. This behaviour is thought to be a further manifestation of the efficient transfer of energy between the ^5D_J levels.

The increased width of the emission bands at elevated temperatures is discussed later in this section. This thermal broadening may be attributed to an interaction of the 4f levels of the Tb^{3+} ion with the phonon spectrum, leading to an increase in the overlap integral (see Chapter 2) between emission and absorption bands. The resulting increase in efficiency of energy transfer would then enhance the emission intensity at high temperatures.

Note that in this case the phonon interactions give rise to two competing processes. The increased phonon flux increases the probability of non-radiative de-excitation, reducing the emission intensity, and at the same time increases the efficiency of energy transfer resulting in an increased luminescence output, at least from the (intense) $^5D_4 - {}^7F_J$ transitions.

A converse effect was noted for X-ray excited luminescence (see section 5.2.4), and also for individual bands with ultra-violet

excitation. Here the emission intensity at low temperatures is thought to be reduced by a narrowing of the spectral lines which decreases the efficiency of energy transfer.

The variation of intensity with temperature of the three most intense groups of emissions (corresponding to the transitions $^5D_4 - {}^7F_{6,5,4}$) is shown in Figures 5.15 a and b. The effect of decreasing intensity with temperature is clearly seen, particularly for the $^5D_4 - {}^7F_4$ transition group. In this respect, the emission at 542 nm is seen to be an anomaly, being almost three times as intense at 10°K as at room temperature. The graphs also show results for a third component of the emission from the transition $^5D_4 - {}^7F_6$. This has been ignored in the previous discussion of room temperature characteristics as at such temperatures it is ill-defined, only becoming noticeably distinct below about 100°K. The datum at 300°K for this emission peak is therefore estimated.

The data used in Figure 5.15 are for 2.88 mole % Tb^{3+} in NS glass and were measured using the Optica spectrophotometer and dewar system described in Chapter 3. Liquid nitrogen produced temperatures of approximately 85°K and down to 70°K on pumping. Using liquid helium, temperatures of 20°K and 10°K were attained.

The behaviour and origin of the intense emission peak at 542 nm is somewhat enigmatic; not only does this line show markedly different temperature behaviour from the others in the $^5D_4 - {}^7F_J$ series, but it is also a much narrower emission line (3 nm as opposed to 8 to 10 nm for the others). The latter point may indicate that the emission originates from Tb^{3+} ions which lie in more ordered sites,

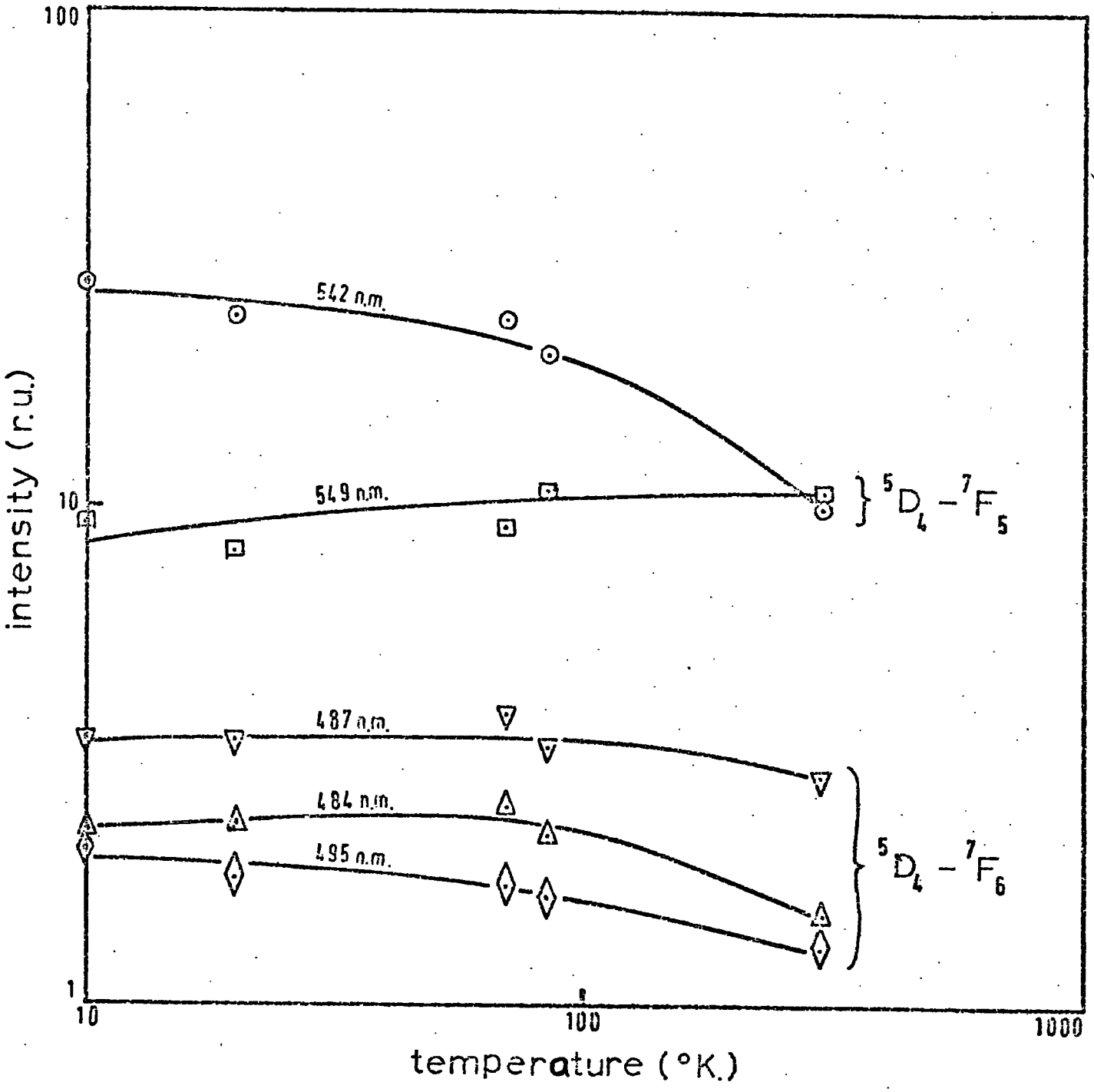

Fig 5. 15a

The low temperature behaviour of the emission intensity of the $^5D_4$ - $^7F_5$ and $^5D_4$ - $^7F_6$ lines, 2.88 mole % Tb^{3+} ions in NS glass

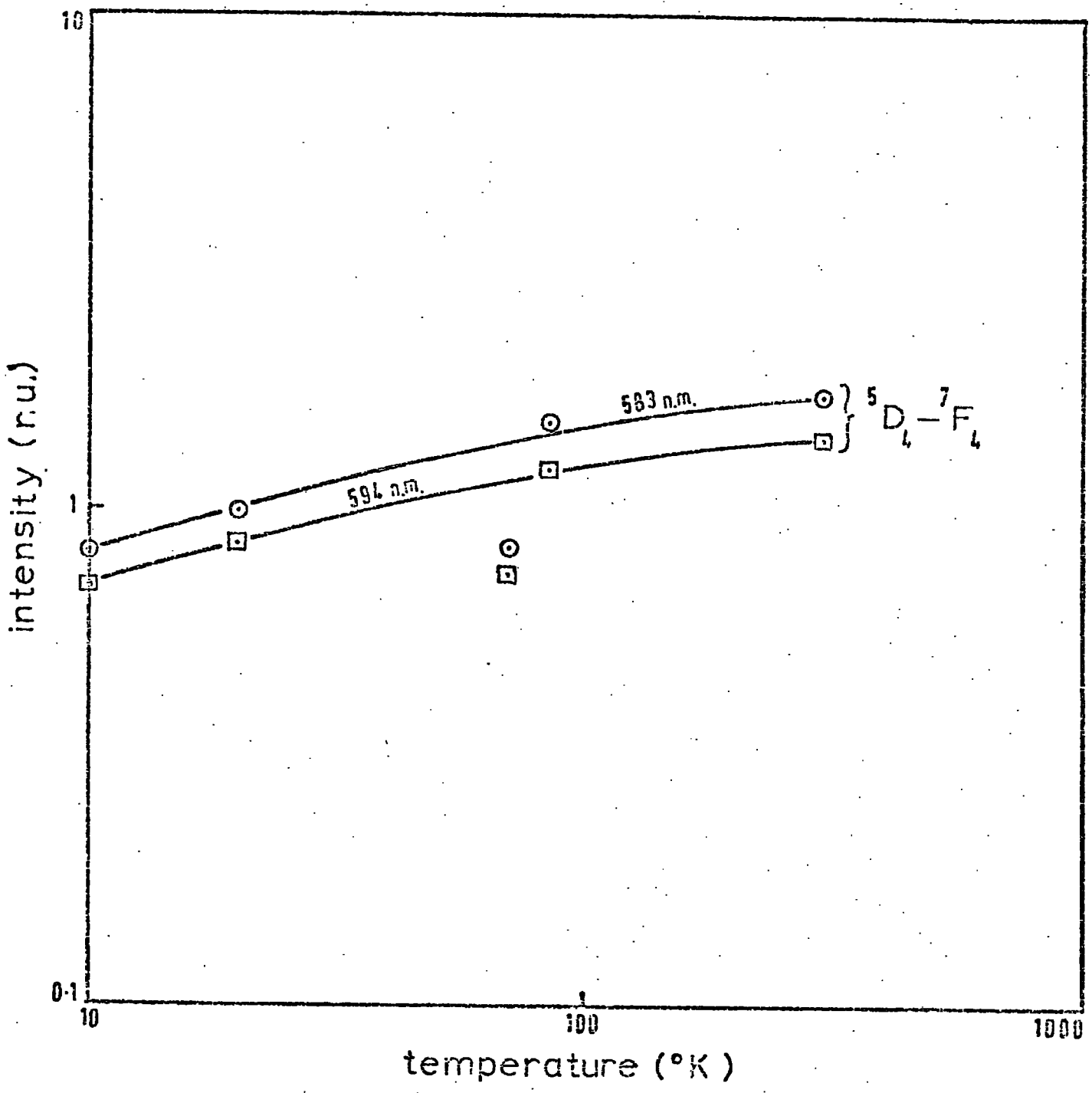

Fig 5. 15b

The low temperature behaviour of the emission intensity of the $^5D_4$ - $^7F_4$ line, 2.88 mole % Tb^{3+} ions in NS glass

but similar peaks were not found in the other emission bands, nor in the absorption spectra. Conceivably, if such a band were a result of a more ordered site in the glass, the particular transition $^5D_4 - {}^7F_5$ may for some reason favour a high emission intensity. The reason why, however, this line does not follow the behaviour of the others vis-a-vis energy transfer remains unknown.

(b) The Effect of Temperature on Decay Times

The determination of the decay times of the ^5D_J levels of the Tb^{3+} ions in the NS glass was described in the previous section. The effect of temperature on the shorter decay times (~1m sec) was investigated at 120°K by cooling the specimen on a "cold finger" with liquid nitrogen. No significant changes could be measured in the decay time of the green ($^5D_4$) emissions, but the decay time of the blue ($^5D_3$) emissions was increased by about 20% at the higher concentrations (2.88 mole %).

This again can be explained in terms of the energy transfer model. As the temperature is reduced, the consequent reduction in line-width and reduction of transfer efficiency results in a higher population of the upper level ($^5D_3$) at such times, after irradiation has ceased, as are characteristic of the transfer process. This predicts a higher intensity (as was demonstrated in section 5.1.3) and a longer decay time from this level.

This change in decay time of the $^5D_3$ level was also reported by Nelson et al (5.27), who determined values of τ = 0.87 m sec at 300°K and τ = 1.02 m sec at 77°K for 0.02 mole % terbium in fused silica.

Komura (5.29) reports a slight decrease in the decay time of the

$^5D_4$ level of Tb^{3+} with temperature in a glass of the composition $K_2O.BaO.3SiO_2$:O. $12Tb_2O_3$. Komura also reports a lengthening of the decay time if the sample is continuously illuminated with infra-red light of wavelength 0.8 to 1.0 μ, the effect being least noticeable at lower temperatures. No explanation of the latter effect was given. If it is assumed that the infra-red illumination used had a considerable intensity at 2 to 5μ, the the result may have been a significant population of the higher ^7F_J levels. These are not normally thermally populated to any appreciable extent at room temperature (5.15). Thus the population of these levels is likely to change the nature of the energy transfer processes and the transition probabilities for the transitions $^5D_4$ - ^7F_J. This is evidently a phenomenon which requires further study.

(c) Variation of Line-width and Emission Wavelength with Temperature

The form of the temperature dependence of the line-width of luminescence emission bands was derived in section2.1.5 from the configurational co-ordinate model. Equation 2.62 gives the width of an emission band, at temperature T, as:-

$$L_e(T) = L_e(O) \sqrt{\tanh\left(\frac{h\nu_e}{2kT}\right)} \qquad (5.27)$$

Thus, measurements of line-widths at various temperatures give the average energy $h\nu_e$ of the phonons interacting with the appropriate excited state of Tb^{3+} ions.

Measurements of emission spectra from samples of NS glass containing 2.88 mole % Tb^{3+} were made at five temperatures down to about

10°K using the Optica spectrophotometer and the dewar system which was described in Chapter 3. The results are tabulated in Table 5.8 for the $^5D_4$ - $^7F_5$ transition at 542 nm.

TABLE 5.8

Width of the 542 nm Emission Line from NS Glass Containing 2.88 mole % Tb^{3+} Ions as a Function of Temperature (Ultra-violet Excitation)

Temperature °K	Relative Width $\left[\frac{L_e(T)}{L_e(O)}\right] \pm 0.08$	$\left[\frac{L_e(T)}{L_e(O)}\right]^2 \pm 0.1$
10	1.0	1.0
20	1.0	1.0
70	1.0	1.0
85	1.1	1.2
300	1.8	3.2

Figure 5.16 shows a plot of measured values of $\left[\frac{L_e(T)}{L_e(O)}\right]^2$ against temperature from these data, and a curve representing the function given by equation 5.27. A best fit was found for:-

$$h\nu_e = 2.8 \times 10^{-21} J$$

$$= 1.7 \times 10^{-2} eV$$

Thus, the corresponding average frequency associated with the phonons is:-

$$\nu_e = 4.2 \times 10^{12} \text{ sec}^{-1}$$

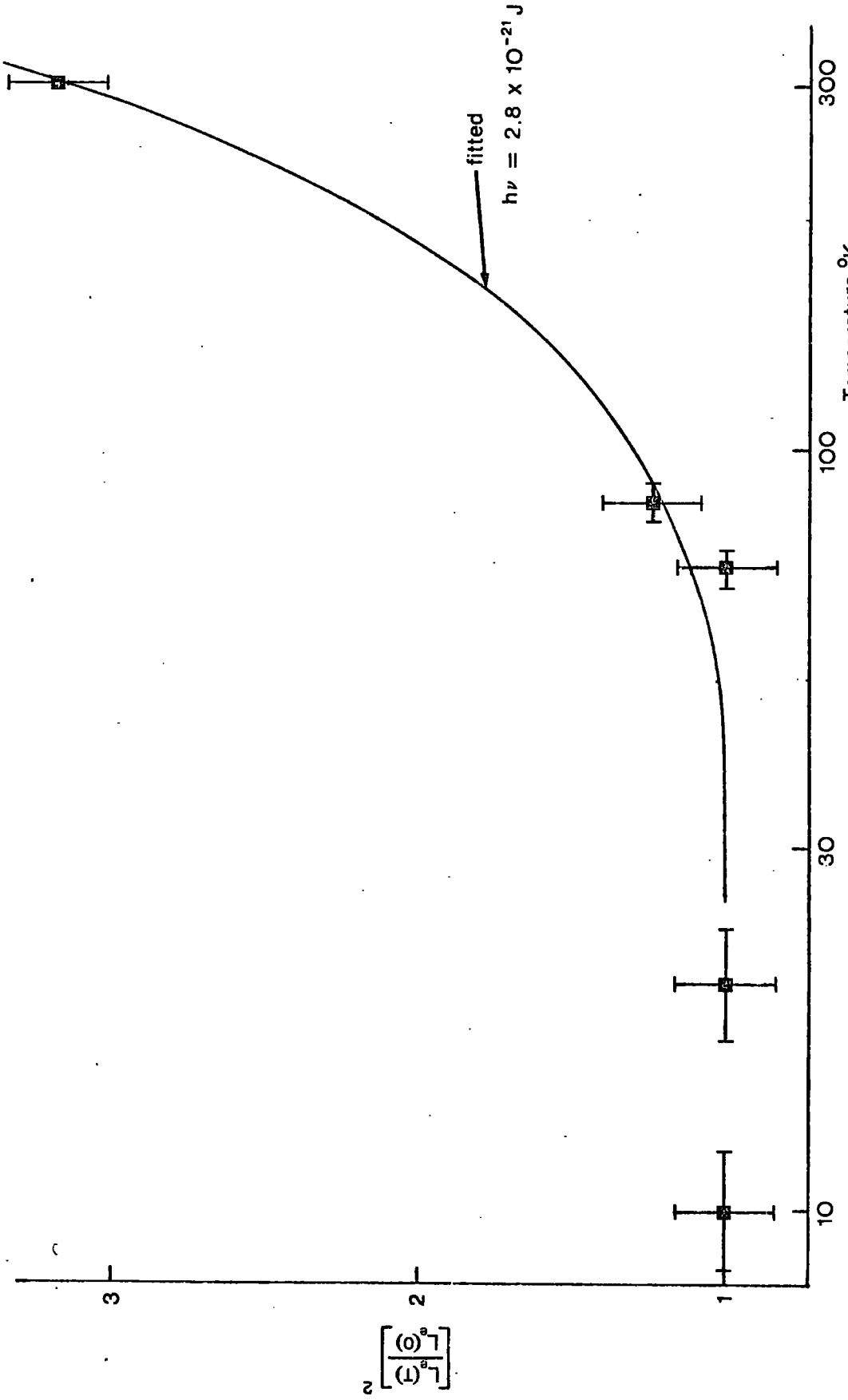

Fig 5.16

The square of the relative width of the 542 nm line as a function of temperature, 2.88 mole % Tb^{3+} ions in NS glass

and the corresponding wavelength of a photon with this energy is

$$\lambda = 72\,\mu$$

Similar measurements have been made by Parke and Webb (5.30, 5.31) for Tl^{+}, Pb^{2+} and Bi^{3+} ions in calcium phosphate glasses. They found the variation in half width with temperature of the emission from these ions to be the same in absorption measurements and a best fit was found to correspond to:-

$$h\nu_e = 0.07 \pm 0.01 \text{ eV}$$

and hence the corresponding wavelength of a photon with this energy is:-

$$\lambda = 18 \pm 2\,\mu$$

Calcium phosphate, $Ca_2(PO_4)_3$ has been found (5.32) to have an absorption band at 15.5μ which may correspond to the phonon modes responsible for the thermal broadening. Wide absorption bands in the region of $500cm^{-1}$ in phosphates are now known (5.33) to be caused by antisymmetrical deformation of PO_4 tetrahedra of the form:-

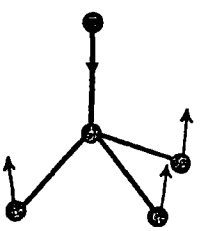

A similar description of the processes involved in silicate glasses would require absorption measurements up to, say, 80μ. Since such measurements have not apparently been made, indeed none have been found in the literature, it is postulated that similar absorption bands exist in silicate glasses, and that the phonon spectrum responsible for

the thermal broadening is associated with the bending modes in $(SiO_4)^{4-}$ tetrahedra. Further, as is evident from Chapter 4, stretching modes are not found below, say, 700cm^{-1} (above, say, 15μ). Thus, it is likely that the phonons which produce an increase in the width of spectral emission lines of metallic ions in an inorganic glass are associated with the bending modes of the network-forming polyhedra.

Similar measurements were attempted for the 436 nm line corresponding to the $^5D_3$ - $^7F_4$ transition. However, no significant change in line width could be detected. This was due, in part, to the lower intensities of the transitions from the $^5D_3$ level. Thus, in the consideration of the configurational co-ordinate model, the actual nature of the $^5D_3$ level must be implied from its interactions with other levels rather than by direct measurement.

Dieke (5.34, page 347 et seq) has pointed out that, in general, ions near the middle of the lanthanide group (Eu^{3+}, Gd^{3+}, Tb^{3+}) show least thermal broadening, as with these ions there is a tendency towards less interaction of the rare earth ion with the crystal or glass matrix. However, even in crystals, the extent of the thermal broadening was found also to depend very much on the lattice structure.

Although the absolute determination of wavelength using the Optica spectrophotometer was only accurate to about 1 nm, relative wavelengths of similar spectra could be determined to within 3Å. However, at this accuracy, no change could be determined in the peak wavelengths in the spectra measured at 10°K and 300°K.

Dieke and Leopold (5.35) succeeded in measuring an effect of temperature in the shift of luminescence from Gd^{3+} ions in $GdCl_3 . 6H_2O$.

The shifts were typically of order 1 to 3 cm^{-1} for the $^6P_{7/2}$ emission lines, corresponding to 0.1 to 0.3Å, between 4°K and 300°K. The shifts were attributed to thermal expansion of the crystal lattice which reduces the magnitude of the crystal field potential at higher temperatures, thus producing reduced Stark component separation. The failure to observe a similar effect in this work is thought to be due to the inadequate resolution available.

Another trivalent lanthanide ion which is known to change the wavelength of its emission spectrum with differing crystal field strengths is Eu^{3+}. Kurkjian et al (5.36) have shown that the position of the $^5D_0$ - $^7F_0$ peak in sodium silicate glasses at around 579 nm changes by 4Å on increasing the mole % of Na_2O from 20% to 40%. The effect was explained on the basis of an increased interaction between europium and oxygen ions, and was associated with a commensurate increase in luminescent efficiency.

(d) Line Structure and Site Symmetry

The obvious doublet structure found for most of the emission bands resolves itself into a more complex situation when the spectra are examined at 10°K. Details of the three most intense bands ($^5D_4$ - $^7F_{6,5,4}$) for 2.88 mole % Tb^{3+} in NS glass are given in Table 5.9. The bands split into four or five discernible sub-bands although the essential doublet structure remains. Figure 5.17 is a sketch of the $^5D_4$ - $^7F_6$ group of emissions which will now be discussed in detail.

From the magnitude of the oscillator strengths derived from optical absorption measurements (see Chapter 4), it was postulated

TABLE 5.9

Relative Intensities of the Split Stark Levels Corresponding to the Transitions $^5D_4 - {}^7F_J$ (J = 6,5,4) for 2.88 mole % Tb^{3+} in NS Glass

Wavelength ± 1 nm	Relative Intensity	Transition Designation
484	37	$^5D_4 - {}^7F_6$
487	55	
491	37	
495	45	
500	26	
542	532	$^5D_4 - {}^7F_5$
551	67	
553	122	
557	20	
583	6	$^5D_4 - {}^7F_4$
588	3	
594	3	
600	1	

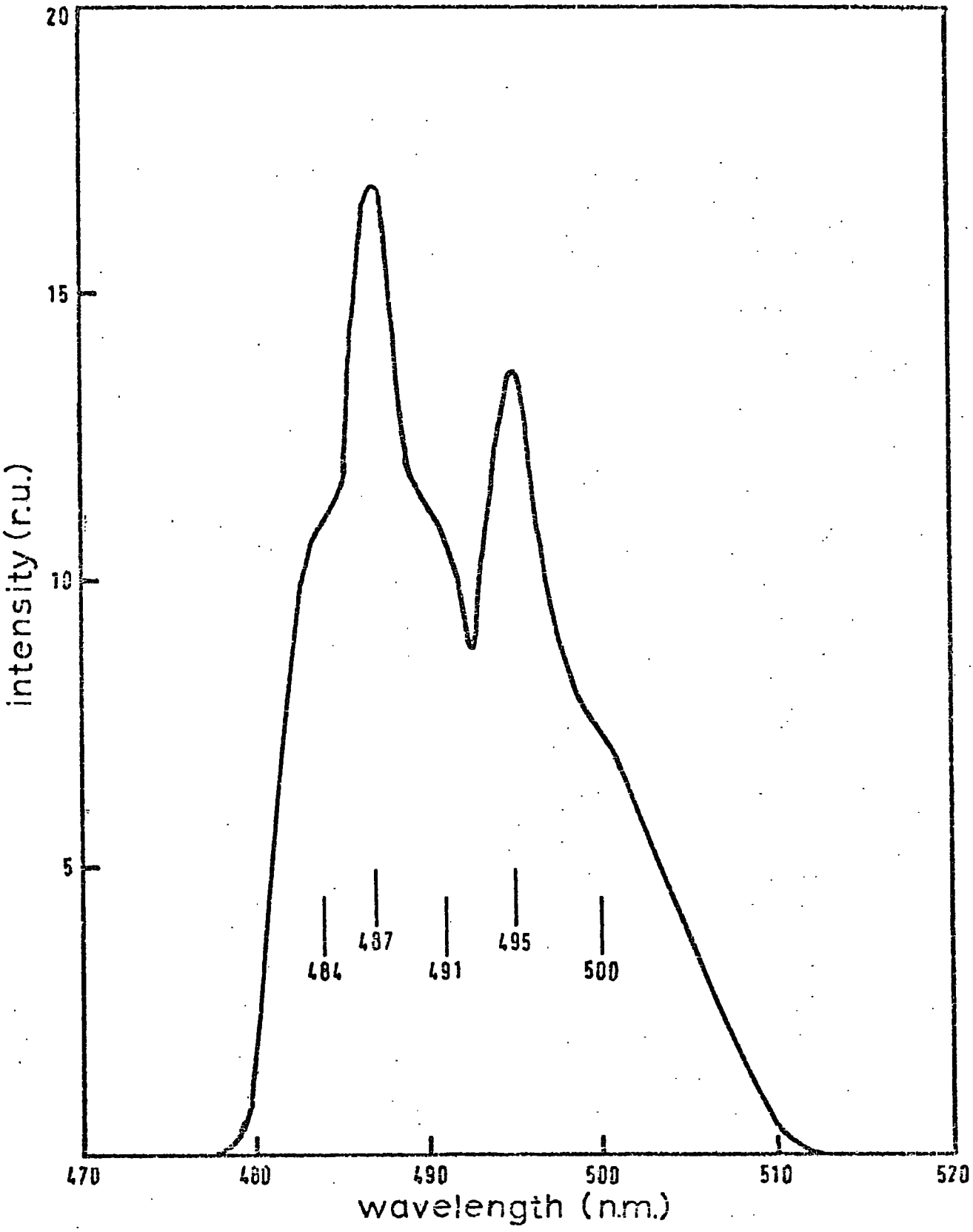

Fig 5.17

The line-shape of the $^5D_4$ - $^7F_6$ emission band of NS glass doped with 2.88 mole % Tb^{3+} ions at approximately 10°K

that the Tb^{3+} ion is likely to occupy a site with approximate cubic symmetry in silicate glasses. The Tb^{3+} ion has been extensively studied in cubic environments (5.37). In crystalline materials with cubic symmetry, Tb^{3+} often shows a doublet structure, particularly from the $^5D_4$ - ^7F_J emissions - for example, Sc BO_3:Tb (5%) (5.2).

With an even number of 4f electrons in a Ln^{3+} ion in a non-cubic field, every free ion level is capable of splitting into 2J+1 components. Because of degeneracies in higher symmetry crystal fields, the number of components is generally lower and can be determined if the field symmetry is known. In the case of the $^5D_4$ - $^7F_6$ transition in the Tb^{3+} ion (which has the structure of $4f^8$), the number of possible components in the excited state is 2J+1 = 9 and in the ground state is 2J+1 = 13. This gives a possible combination of 117 components to the luminescence spectrum. Even though this number is considerably reduced by the application of selection rules, the system is too complex to deal with other than empirically at this stage. Thus the procedure adopted by Mann (5.38) of fitting multi-component Gaussian curves to spectra for Nd^{3+} ions in glass has been rejected here.

Regarding the $^5D_4$ - $^7F_6$ transition as a basic doublet, and assuming that each doublet is derived from two dissimilar sites for Tb^{3+} ions, does give some insight into the fundamental line-shape. The argument was developed in Chapter 1 that rare earth ions in glass tend to adopt an environment which is similar to that of the appropriate sesquioxide. With terbium the oxide has the approximate formula Tb_4O_7 which is thought to be a mixture of the non-stoichiometric

oxides, $TbO_{1.71}$ and $TbO_{1.81}$, with rhombohedral and cubic symmetries respectively. This implies sites of similar symmetry should exist for Tb^{3+} ions in oxide glasses.

Since the two Tb^{3+} ion environments are conjectured to be rhombohedral and cubic, the co-ordination is eight-fold in both cases. The two sites designated type 'A' and type 'B' are illustrated below.

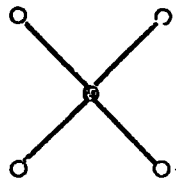

Type 'A' site
(cubic)

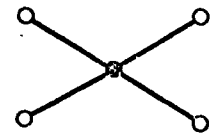

Type 'B' site
(rhombohedral)

The optically active electron in each case will be attracted by the more electro-positive Tb^{3+} ion and repelled by the O^{-} ligands. The ligand repulsion will increase with decreasing interionic distance. The rhombohedral structure, being a more closely packed structure than cubic, is assumed to have the smaller anion - cation displacement.

The $^5D_4$ - $^7F_6$ transition of Tb^{3+} ions requires a change of total angular momentum quantum number $\Delta J = 2$. This transition therefore is expected to be "hypersensitive" to the symmetry of the ionic site, as this must be a forced electric dipole transition. The various intensities of the components of this emission band are thus expected to reflect the symmetry of the sites appropriate to each component. However, it must be noted that this situation will be modified

if the relative occurrence of the various sites differ. Since the occurrence of cubic and rhombohedral sites in the Tb_4O_7 oxide are nearly equal, it will be assumed that this pertains also in the glass.

The argument above may be summarised for the rhombohedral site as follows:

A rhombohedral site implies a

closer spacing between the Tb^{3+} ions and the ligands, and

a higher repulsive term in the expression for the potential

of the optically active electron, leading to

a lower emission wavelength.

This type of site also implies a lower symmetry, and

a higher emission intensity (when $\Delta J = 2$).

Thus the low-wavelength component of the doublet is expected to be of higher intensity in agreement with observation.

The above argument by necessity contains many assumptions, some of which bear further discussion. The two alternative sites in the glass have been assumed to be similar to those of Tb^{3+} ions in the oxide Tb_4O_7. This is only secondary to the argument, as any two sites with differing ion-ligand spacing would serve equally well, especially if these sites led to large cubic terms appearing in the corresponding crystal field expansions.

Another assumption was that the $^5D_4 - {}^7F_6$ transition is in fact hypersensitive to variations in the crystal field parameters. In section 5.1.3, however, it was demonstrated that the mixing between the 4f orbitals and the ligand wavefunctions is weak in the case of the $^5D_4$ level of Tb^{3+}, but this argument applies best to the ion in differ-

ing crystals. The mixing is likely to be more noticeable in the situation postulated here, as the comparison is between ions in two sites which are much more nearly identical. Also, the next nearest neighbours (Si ions) are the same for both sites, which removes any differences which may occur as a result of the varying electronegativity of the other cation in the several solids.

Note that a similar situation is expected to occur for the $^5D_3 - {}^7F_5$ transition, which also has $\Delta J = 2$. However, it was not possible to determine the line-shape of this band because of interference from scattered light from the excitation source. Herring et al (5.15) have determined the shape of this band and show the two components to be almost equally intense. However, their results show that for the $^5D_3 - {}^7F_6$ transition (with $\Delta J = 3$), which is also expected to be forced electric dipole in origin, a similar line-shape does apply, with the higher energy component the more intense.

5.1.7 Borate and Phosphate Glasses

A list of the phosphate and borate glasses prepared is contained in Table 3.6. The preparation of these glasses has been described in Chapter 3. Both types of glass were found to have luminescence properties fairly similar to those of silicate based glasses when excited with mercury light. The visual appearance of the luminescence was, however, somewhat more blue in the phosphate glass than in similar silicate glasses. Both the borate and phosphate glasses produced less intense luminescence than silicate glasses at similar terbium concentrations. This was particularly true of the borate glass, the

TABLE 5.10

Relative Intensities of the Emission Bands of Various Concentrations of Tb^{3+} Ions in Calcium Phosphate

Wavelength ± 1 nm	Relative Intensity at the Following Concentrations (mole %) 0.126	1.328	5.517	Level Assignments
414	0.95	400	6.05	$^5D_3 - {}^7F_5$
435	2.10	9.13	20.20	$^5D_3 - {}^7F_4$
439	0.59	2.54	4.27	
456	0.17	0.71	1.09	$^5D_3 - {}^7F_3$
473	0.13	0.56	1.03	$^5D_3 - {}^7F_2$
488	0.22	4.09	43.20	$^5D_4 - {}^7F_6$
544	1.00	17.90	190.50	$^5D_4 - {}^7F_5$
584	0.40	6.54	31.80	$^5D_4 - {}^7F_4$
620	0.20	3.23	16.50	$^5D_4 - {}^7F_3$

TABLE 5.11

Relative Intensities of the Emission Bands of Tb^{3+} Ions in Sodium Borate Glass

Wavelength (nm)	Relative Intensities at 5.542 mole %	Level Assignments
415	0.47	$^5D_3 - {}^7F_5$
436	1.00	$^5D_3 - {}^7F_4$
456	0.07	$^5D_3 - {}^7F_3$
487	830	$^5D_4 - {}^7F_6$
543	1800	$^5D_4 - {}^7F_5$
586	105	$^5D_4 - {}^7F_4$
623	115	$^5D_4 - {}^7F_3$

emission from which was approximately 15 times less than that from sodium silicate glasses under similar conditions, even for the $^5D_4 - {}^7F_J$ set of emissions.

The wavelengths and relative intensities of the emission from calcium phosphate glasses are given in Table 5. 10 for the three different concentrations of terbium which were studied. The values of intensity are all relative to the emission at 544 nm at the lowest concentration. The wavelengths of the emission peaks and the relative intensities are in good agreement with the data of Shionoya and Nakazawa (5.39) for a similar glass.

The corresponding data for the borate glass are recorded in Table 5. 11. In this glass the emissions from the $^5D_3$ level were so weak that the relative intensity between the two sets of emission lines ($^5D_3$ and $^5D_4$) is only approximate. These data also compare well with values reported in the literature (5.40).

The variation of luminescence intensity of phosphate glasses with terbium concentration shows behaviour characteristic of the energy transfer process $^5D_3 \longrightarrow {}^5D_4$ similar to that determined for silicate glasses. However, the ratio of intensities $^5D_4 : {}^5D_3$ is not so large for the phosphate glass, which implies a lower efficiency of energy transfer.

5.2 X-ray Excited Luminescence in Silicate Glasses activated with Terbium

5.2.1 Introduction

Little work has been reported in the literature on X-ray

excitation of rare earth phosphors and almost none on rare earths in glass. This, it is thought, may be due in part to a lack of commercial interest, as few applications have been suggested for such processes. Glasses do have the advantage of transparency, so that possible applications could arise where it is necessary to view a radiograph before a permanent photographic record is made. However, this could be achieved more economically by the use of a thin paint of more conventional (even opaque) crystal phosphors.

All the terbium doped glasses which were prepared for luminescence studies under ultra-violet excitation were found to luminesce strongly under X-ray irradiation. Since the emission spectra have similar characteristics for both forms of excitation, they were studied in an attempt to relate the photoluminescence of silicate glasses with their thermoluminescence properties (which are discussed in Chapter 6).

The emission of the X-ray excited luminescence was found to occur in the intra-4f transition bands of the Tb^{3+} ions as for the longer wavelength excitation. One advantage was that there were no troublesome additional peaks (such as the 405 nm line from mercury vapour lamps) so that emission lines such as the $^5D_3$ - $^7F_6$ line (at about 380 nm) could more easily be determined.

5.2.2 Monochromator Calibration

The spectral distribution of the X-ray excited luminescence of silicate glasses doped with terbium was measured using the modified Grubb-Parsons' PM2 monochromator described in section 3.2 (see

also Figure 3.3). The detector was an EMI 6097B photomultiplier tube operating at voltages up to 1.3 kV. Wavelength selection was by means of a prism mounted on a turntable rotated by a gear system and micrometer screw gauge, the reading on which was related to the wavelength of light emerging through the exit slit of the monochromator. Thus, before spectra could be measured, the screw gauge had to be calibrated in terms of wavelength. This was achieved using cadmium and sodium discharge lamps and an unfiltered mercury vapour lamp as wavelength reference sources. The photomultiplier output was measured on an X-Y recorder as a function of the micrometer setting and peaks in the resulting spectrum were calibrated using wavelength tables. Peaks were found corresponding to the line spectra of the lamps as follows:-

Sodium	589 nm
Cadmium	480, 509 nm
Mercury	405, 436, 577 nm

The resulting calibration chart is shown in Figure 5.18 and includes a point corresponding to the maximum intensity peak of the luminescence spectrum from one of the terbium glass specimens. This peak was found to be at 546 nm, which is very similar to the wavelength of the most intense peak found in ultra-violet excited luminescence.

A measure of the spectrometer resolution was also obtained from the calibration spectra. The half-height full width of the sodium 'D lines' corresponded to 5.5 nm and that of the 405 nm mercury line corresponded

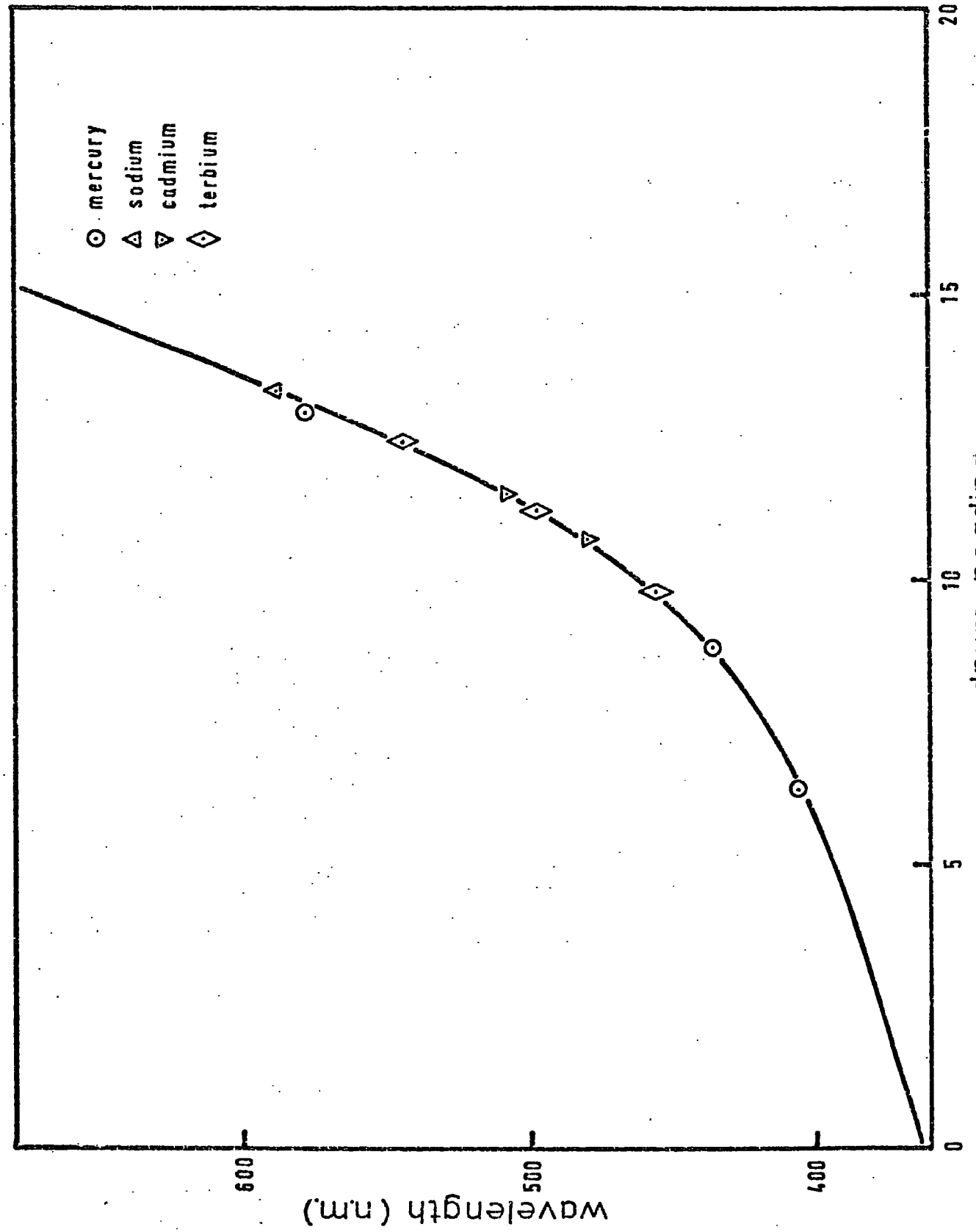

Fig 5.18. Wavelength calibration of the spectrometer used to determine X-ray excited luminescence spectra

to 10 nm. Since the measured widths of these lines were much greater than their accepted values (~ 1Å), these widths relate to the resolution of the monochromator. The resolution is not, therefore, linear and increases with decreasing wavelength.

It should be noted that these measured widths relate only to the ability of the apparatus to resolve closely spaced spectral lines, and not to the accuracy of determining the wavelength of the intensity peaks. The monochromator was used to measure the wavelengths of the emission spectrum from the ultra-violet excited luminescence of silicate glasses doped with terbium, and the results compared with those determined using the Optica spectrophotometer. The values found were in agreement to within 3 nm, which was thus assumed to be the wavelength accuracy of the apparatus.

All spectra measured were found to be superimposed on a roughly constant background level, also detected by the photomultiplier tube. This was attributed to scattered light within the monochromator and did not appear to be dependent upon the wavelength being measured. All data in this work have been corrected for this by the subtraction of the appropriate background level.

5.2.3 General Characteristics of the Spectra

Luminescence of terbium doped silicate glasses was produced by excitation with unfiltered X-rays from a cobalt target. The X-ray set is described in section 3.3 and was operated at 15mA, 20kV, unless otherwise stated.

Typical spectra of the X-ray excited luminescence of terbium in

NS glass (1.009 mole % Tb^{3+}) and LAS glass (0.364 mole % Tb^{3+}) are shown in Figures 5.19 and 5.20 respectively. The spectra show three distinct peaks in the binary glass and five in the ternary glass. The wavelengths of these peaks are listed in Table 5.12, and were not found to change significantly as a function of the concentration of terbium ions within the accuracy of the experiment.

As with the ultra-violet excited spectra, the emission lines were identified by reference to the free ion spectra (5.41). The general form of the spectra is similar in both cases, the most intense line being observed for the transition $^5D_4 - {}^7F_5$.

The emission bands are more sharply defined in LAS glass. This is thought to be due to a greater degree of local ordering around the Tb^{3+} ion site in the ternary silicate glass. The effect is likely to be produced by the inclusion of the intermediate oxide Al_2O_3 into the glass matrix. This point is discussed in greater detail in section 6.9.

The selected power settings of the X-ray tube (15 mA, 20kV) were chosen arbitrarily. In order to assess the importance of these conditions on the luminescence, the intensity of the 546 nm line of 2.88 mole % Tb^{3+} in NS glass was measured as a function of tube voltage. Figure 5.21 shows the results for a constant tube current of 5mA. The intensity is almost a linear function of voltage (and hence power). Complete spectra were also taken for a series of voltage-current combinations and the results are given in Table 5.13. The combinations were chosen so as to give a nearly constant power through the X-ray tube. The intensities of both the 546 and 498 nm lines were found to increase proportionately with the tube voltage so

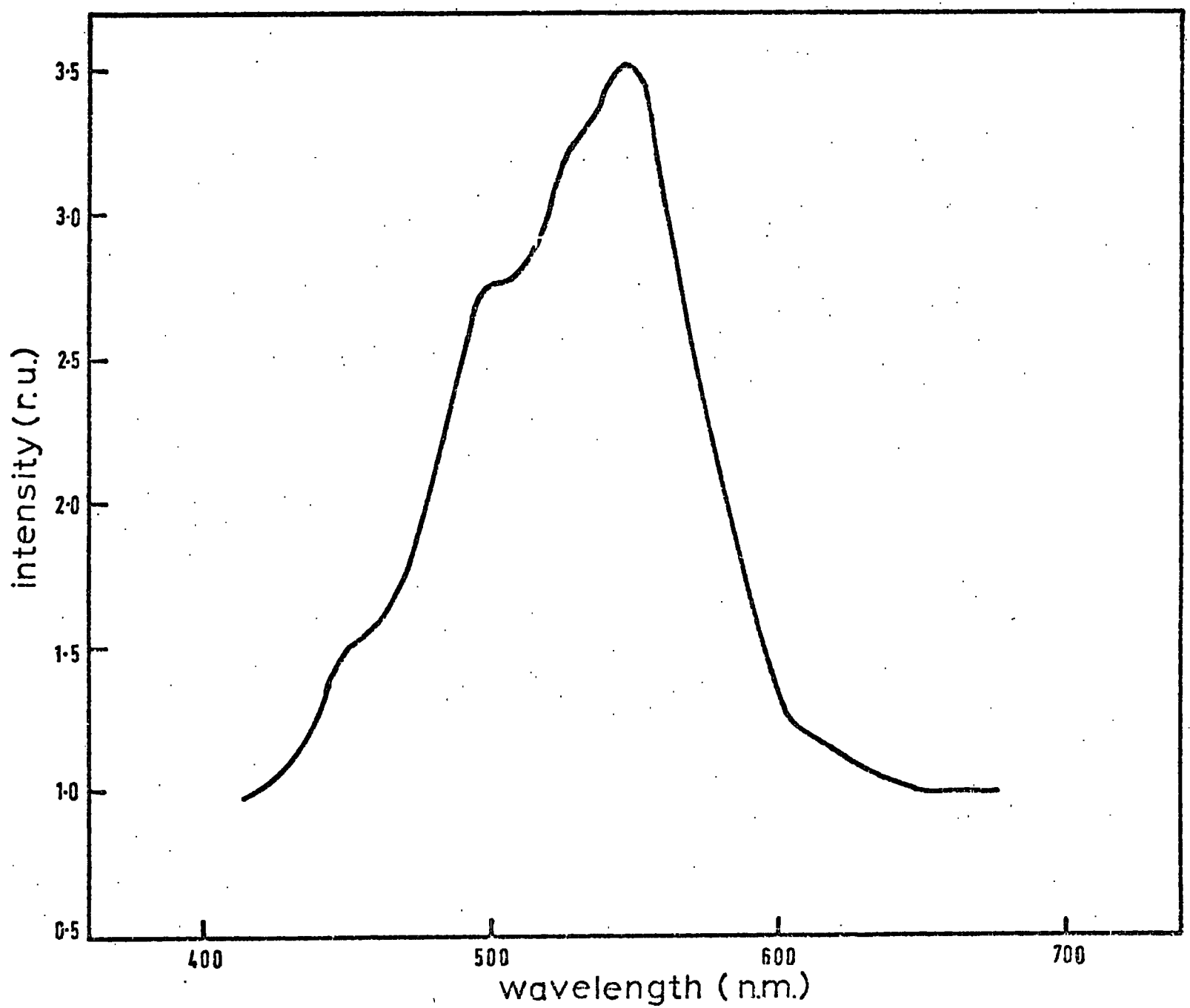

Fig 5.19 Typical luminescence spectrum for Tb^{3+} activated NS glass (1.009 mole % Tb^{3+}) - X-ray excitation

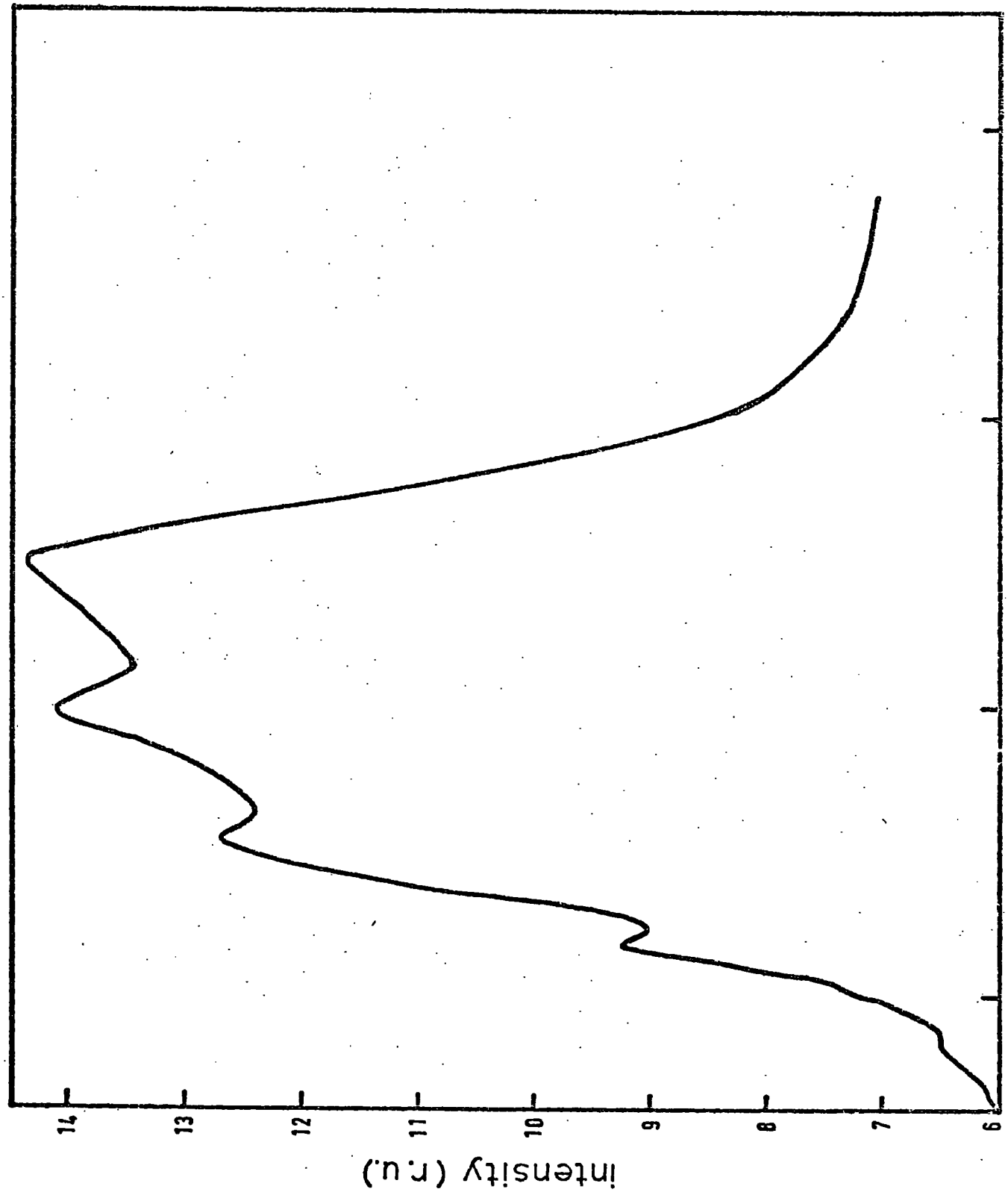

Fig 5.20 Typical luminescence spectrum for Tb^{3+} activated LAS glass (0.364 mole % Tb^{3+}) - X-ray excitation

TABLE 5.12

Wavelengths of the Peaks in the X-ray Excited Spectra of Silicate Glasses Containing Tb^{3+}

Glass Type	Micrometer Reading ± 0.05	Wavelength nm ± 3 nm	Energy Level Transition Responsible for Emission Band
NS	9.8	457	$^5D_3 - {}^7F_5$
	11.2	498	$^5D_4 - {}^7F_5$
	12.4	546	$^5D_4 - {}^7F_5$
LAS	3.4	383	$^5D_3 - {}^7F_6$
	7.4	417	$^5D_3 - {}^7F_5$
	9.7	455	$^5D_3 - {}^7F_3$
	11.2	498	$^5D_4 - {}^7F_6$
	12.4	546	$^5D_4 - {}^7F_5$

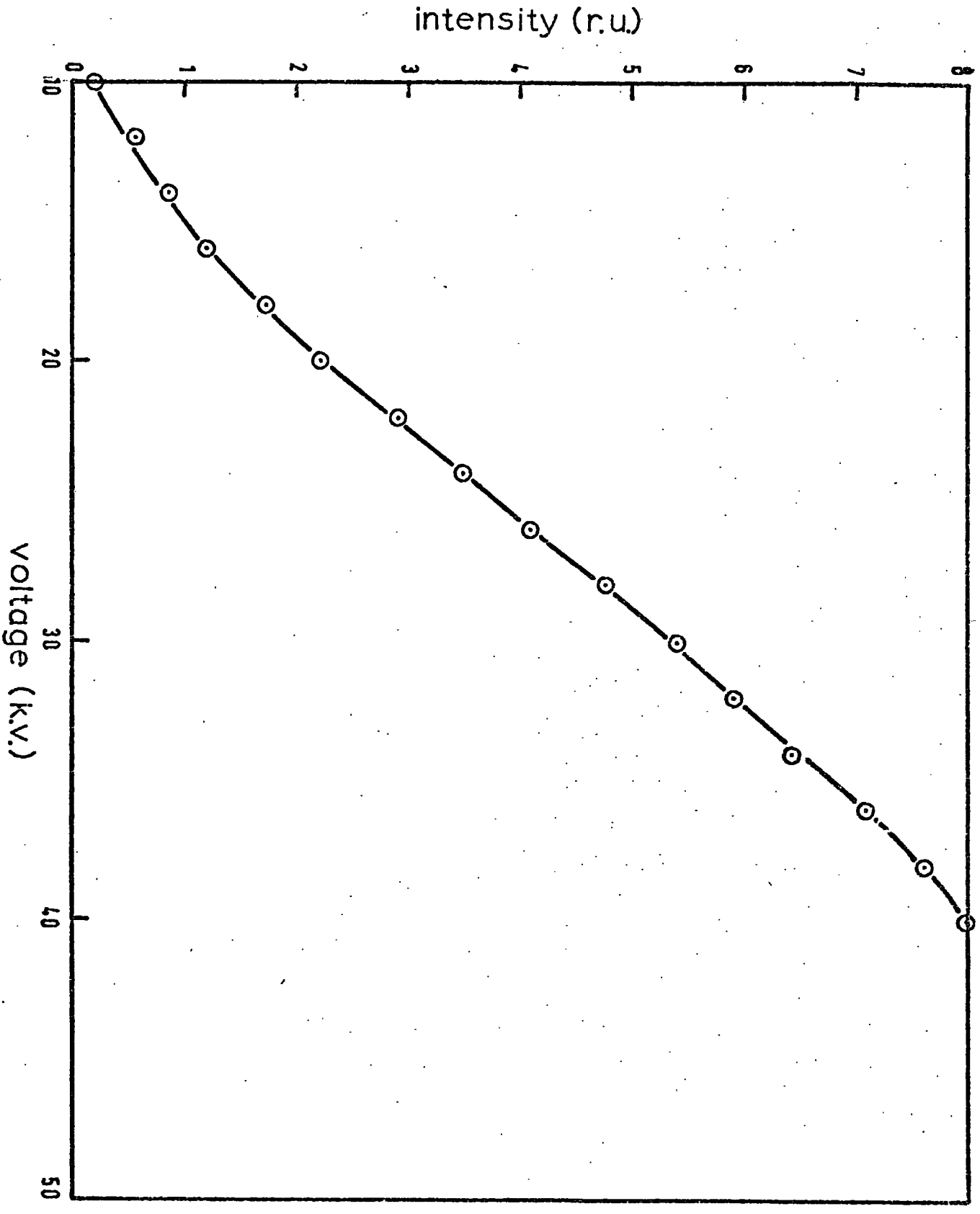

Fig 5.21

Luminescence intensity as a function of the X-ray tube operating voltage at constant power settings.

TABLE 5.13

Variation of Luminescence Emission of 2.88 Mole % Tb^{3+} in NS Glass as a Function of X-ray Tube Voltage and Current Settings

Voltage V ± 1kV	Current I ± 0.5 mA	Intensity of 546 nm Line I_1 (Relative Units)	Intensity of 498 nm Line I_2 (Relative Units)	$\frac{I_1}{I_2}$	I_1I	I_2I
10	30	1.6	1.2	1.3	48	36
15	20	4.1	2.6	1.6	82	52
20	15	5.3	3.7	1.4	80	55
25	12	6.2	4.3	1.4	74	52
30	10	7.7	5.3	1.5	77	53
			Mean	1.45	72	50

that the product of intensity and the tube current remained roughly constant for all settings. Also the relative intensities of the two peaks were not sensitive to the current-voltage setting and had a mean ratio of 1.45. Thus, the luminescence intensity is roughly constant with tube current and roughly proportional to tube voltage.

An increase of tube voltage will decrease the minimum wavelength of the X-ray continuum spectrum. Thus it would appear that the X-ray excited luminescence results largely from the continuum spectrum rather than from the line spectrum. This would imply that the maximum quantum efficiency for the X-ray excitation process lies above, say 40 keV, (which was the highest electron energy available with the equipment used).

5.2.4 Effects of Concentration on the Emission Intensities

The change in the intensity of the various observed emission bands was determined by direct comparison of specimens under conditions as near identical as could be practically achieved. Samples were cut to an equal thickness of 3 mm and irradiated by a circular beam of X-rays, 3 mm in diameter. Care was taken not to change the photomultiplier or X-Y recorder settings, nor to change the position of the monochromator or the location of the different specimens.

The relative intensities are given in Tables 5.14 and 5.15 for NS glass and LAS glass respectively. The intensities are all normalised to that of the 457 nm line for the NS glass specimen containing 0.031 mole % Tb^{3+} and are corrected for the photomultiplier tube sensitivity. The 383 nm line was not observed in the LAS glass with the highest

TABLE 5.14

Relative Intensity of the Emission Peaks of Tb^{3+} Ions in NS Glass at Various Concentrations

(Corrected for Photomultiplier Sensitivity)

Concentration mole %	Relative Intensity at :		
	546 nm	498 nm	457 nm
0.031	2.9	1.6	1.0
0.297	5.0	2.5	1.3
1.009	13.8	5.7	1.5
2.88	45.1	17.3	2.1
4.25	50.3	20.0	2.4

TABLE 5.15

Relative Intensity of the Emission Peaks of Tb^{3+} Ions in LAS Glass at Various Concentrations

(Corrected for Photomultiplier Sensitivity)

Concentration mole %	Relative Intensity at :				
	546 nm	498 nm	455 nm	417 nm	383 nm
0.364	13.4	7.7	5.1	2.2	0.3
0.728	36	19.4	8.2	3.3	0.4
1.81	38	17.5	3.6	7.0	< 0.1

terbium concentration, and hence an approximate upper limit for the intensity of this line is included. Figure 5.22 shows part of these data graphically. The relative intensities of all lines for NS glass and the three most intense lines in LAS glass are plotted as a function of molar concentration. Figure 5.23 is a graph of the concentration dependence of the intensity of all five lines in LAS glass normalised to unity at the lowest concentration.

The total intensity of luminescence (not allowing for the quantum efficiency of the photomultiplier tube) was determined at each concentration by integrating the intensity spectra by hand. The results are given in Figure 5.24 as a function of concentration. The shapes of these curves are dominated by the behaviour of the 546 and 498 nm lines, as these are the most intense.

All of these curves for NS glass follow the usual behaviour for such plots as was found with the photoluminescence of both NS and LAS glasses (see section 5.1.3 and reference 5.15); one slight difference is that the intensity does not rise so quickly with concentration for X-ray excitation. However, the curves for LAS glass do not follow this pattern. The lines corresponding to transitions from the $^5D_4$ level to the ^7F_J ground state levels do not greatly increase in intensity above about 0.7 mole %. Moreover, at higher concentrations, the intensities of lines arising from the $^5D_3$ state are significantly quenched by further additions of Tb^{3+} ions. Further, this effect occurs at a concentration intermediate to that at which the expected energy transfer processes become significant (viz ~0.5 mole % for multipolar transfer to the $^5D_4$ transitions and ~4 to 5 mole % for

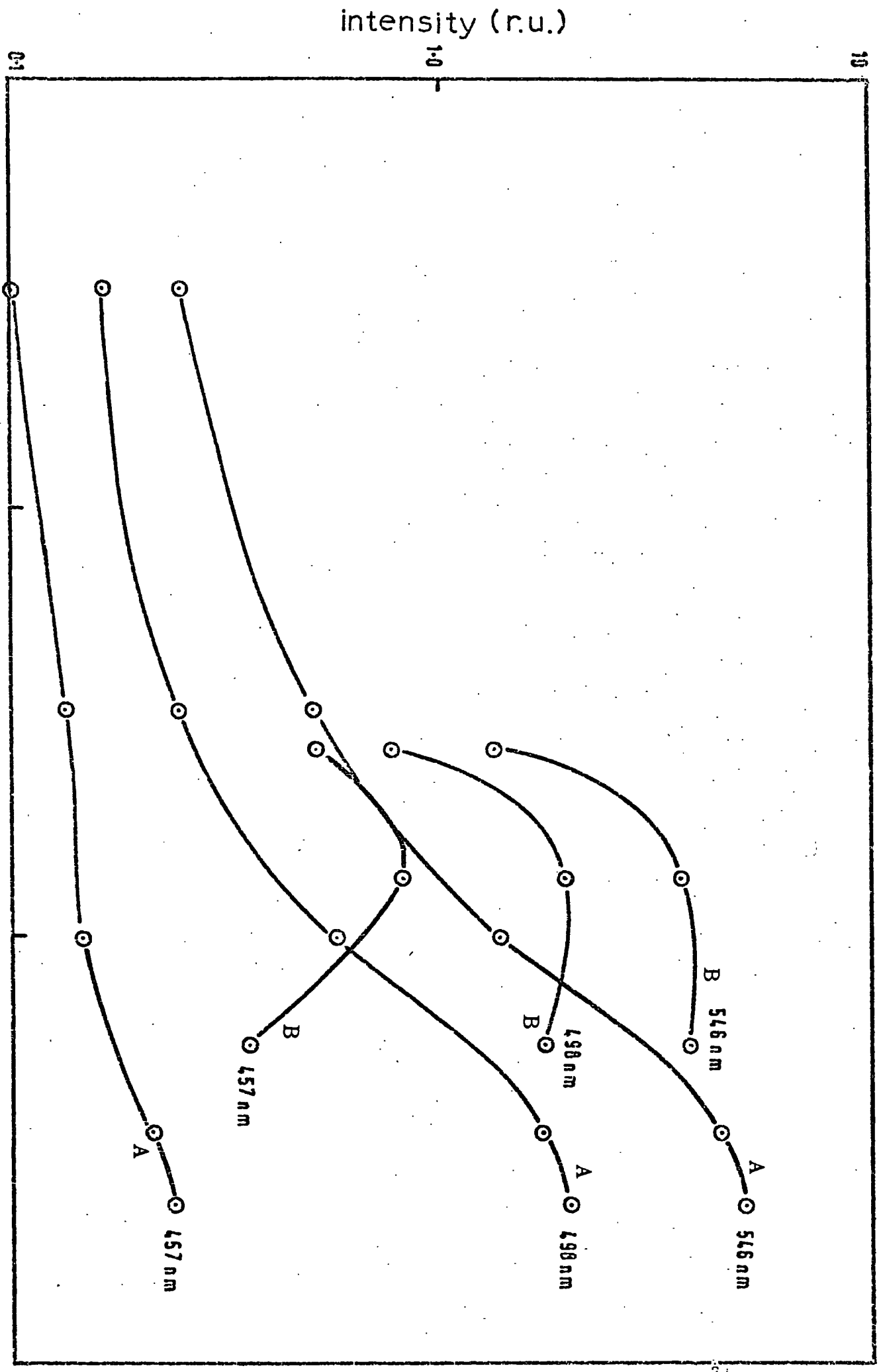

Fig 5.22 Luminescence intensity as a function of concentration of Tb^{3+} ions in NS glass (A) and LAS glass (B) with X-ray excitation

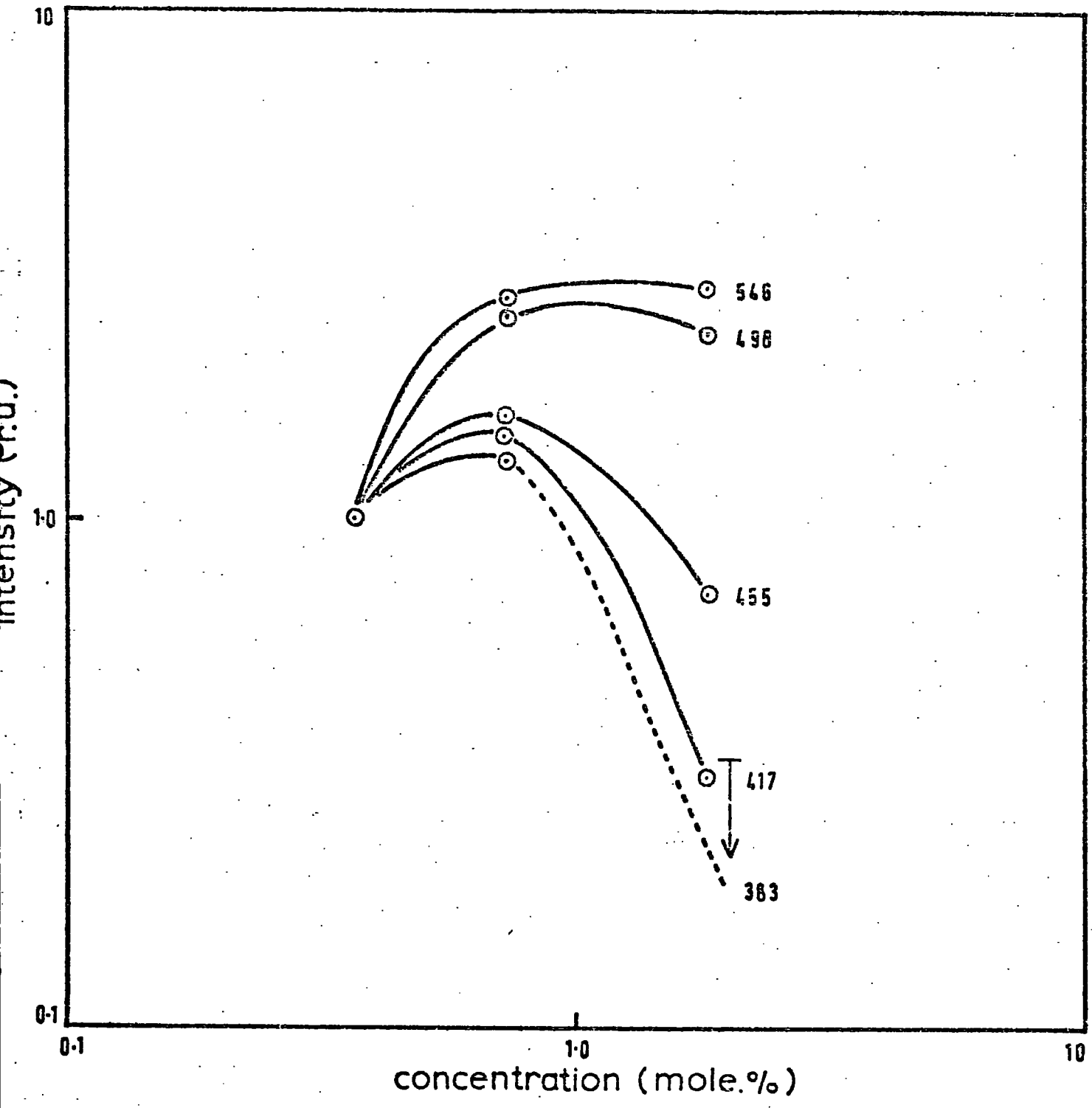

Fig 5.23

Luminescence intensity as a function of concentration of Tb^{3+} ions in LAS glass with X-ray excitation

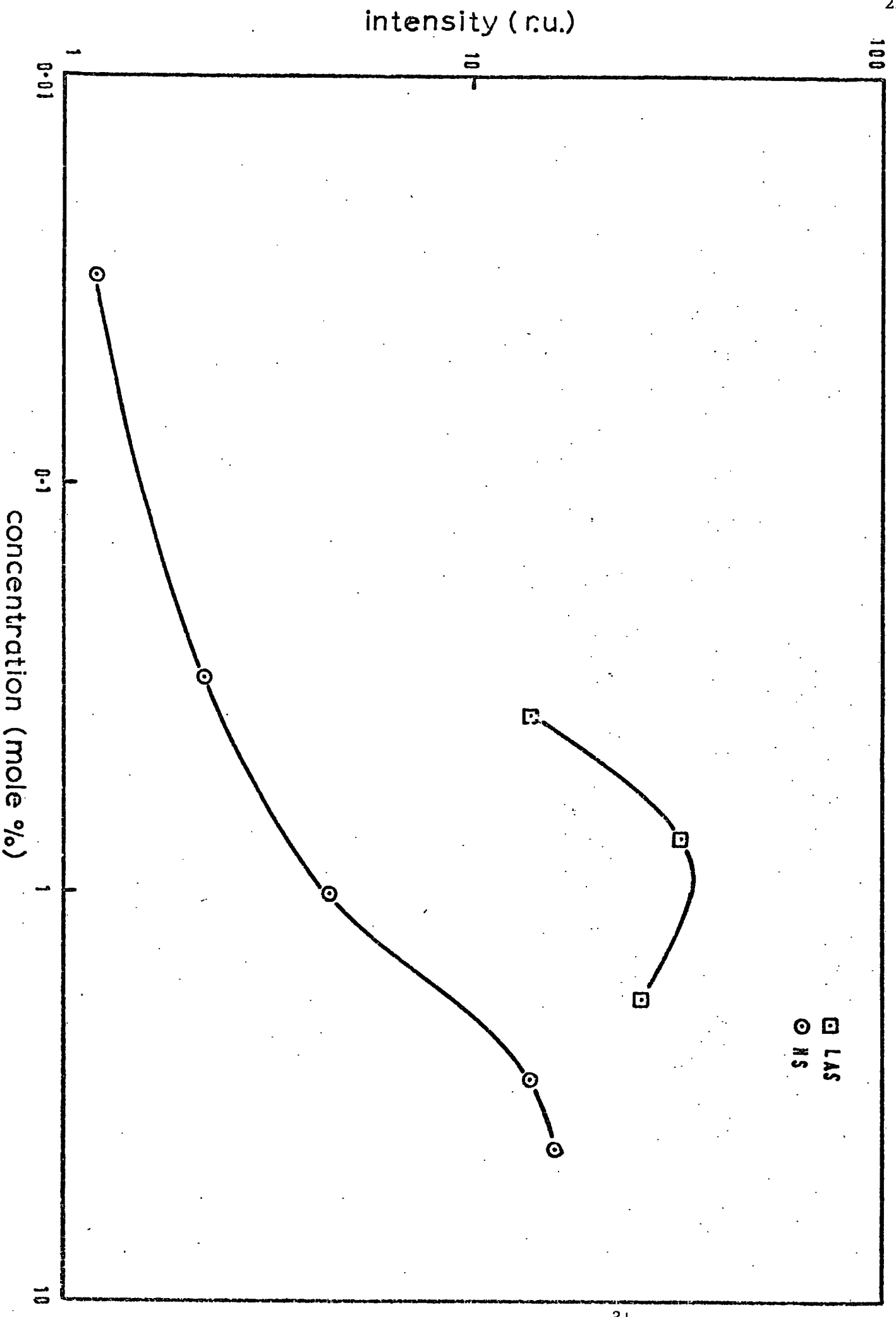

Fig 5.24 Total luminescence intensity as a function of Tb^{3+} ion concentration in NS and LAS glasses

dipole exchange to produce concentration quenching).

In order to examine the part played by energy transfer processes and the multipolar characteristics of the electronic transitions responsible for the emission, it is necessary to determine the behaviour of the ratios of line intensities as a function of concentration. Denote by I_1 the intensity of the 455 nm line, by I_2 the intensity of the 498 nm line, and by I_3 the intensity of the 546 nm line. Then the ratios $\frac{I_3}{I_1}$ and $\frac{I_2}{I_1}$ represent the ratio of intensities of emissi ons from the $^5D_4$ level to those from the $^5D_3$ level. Hence these ratios are related to the total efficiency of energy transfer for the process $^5D_3 \longrightarrow {}^5D_4$.

Consider the ratio

$$\frac{I_3}{I_2} = \frac{\text{Intensity of the transition } {}^5D_4 - {}^7F_5}{\text{Intensity of the transition } {}^5D_4 - {}^7F_6} \qquad (5.28)$$

In the numerator of this expression, the change in the total angular momentum quantum number is:-

$$\Delta J = +1$$

and in the denominator:-

$$\Delta J = +2$$

Hence, the latter transition is forbidden as a magnetic dipole transition, while both are allowable by a vibronically induced electric dipole transition via interactions with the glass matrix. Thus the ratio $\frac{I_3}{I_2}$ is approximately:-

$$\frac{I_3}{I_2} \sim \frac{\text{Magnetic dipole contribution + Electric dipole contribution}}{\text{Electric dipole contribution}}$$

$$= 1 + \frac{\text{Magnetic dipole contribution}}{\text{Electric dipole contribution}} \qquad (5.29)$$

Figures 5.25 and 5.26 are graphs of the ratios $\frac{I_3}{I_1}$, $\frac{I_3}{I_2}$ and $\frac{I_2}{I_1}$ for NS and LAS glass respectively. The curves for $\frac{I_3}{I_1}$ and $\frac{I_2}{I_1}$ for NS show that the energy transfer for the process $^5D_3 \longrightarrow {}^5D_4$ becomes increasingly more efficient with concentration up to about 3 to 4 mole %. This behaviour is similar for both glasses and also similar to ultra-violet excitation.

The ratio $\frac{I_3}{I_2}$, reflecting the relative contribution of magnetic dipole transitions, does not vary greatly with concentration. This implies that the vibronic interactions with the glassy environment do not depend strongly on the terbium ion concentration over the range studied. In this respect the ions may be regarded as isolated, since any vibronic coupling between Tb^{3+} ions would be expected to induce a larger electric dipole contribution. In fact, the opposite appears to be the case, and the magnetic dipole contribution increases with concentration.

The above argument tends to suggest that the energy transfer behaviour $^5D_3 \longrightarrow {}^5D_4$ in X-ray excited LAS:Tb glass is similar in all essentials to the behaviour of all other systems studied. Thus an explanation of the concentration quenching observed at around 0.7 mole % must be sought elsewhere. A detailed discussion of this phenomenon must be deferred until after a description of the thermoluminescence

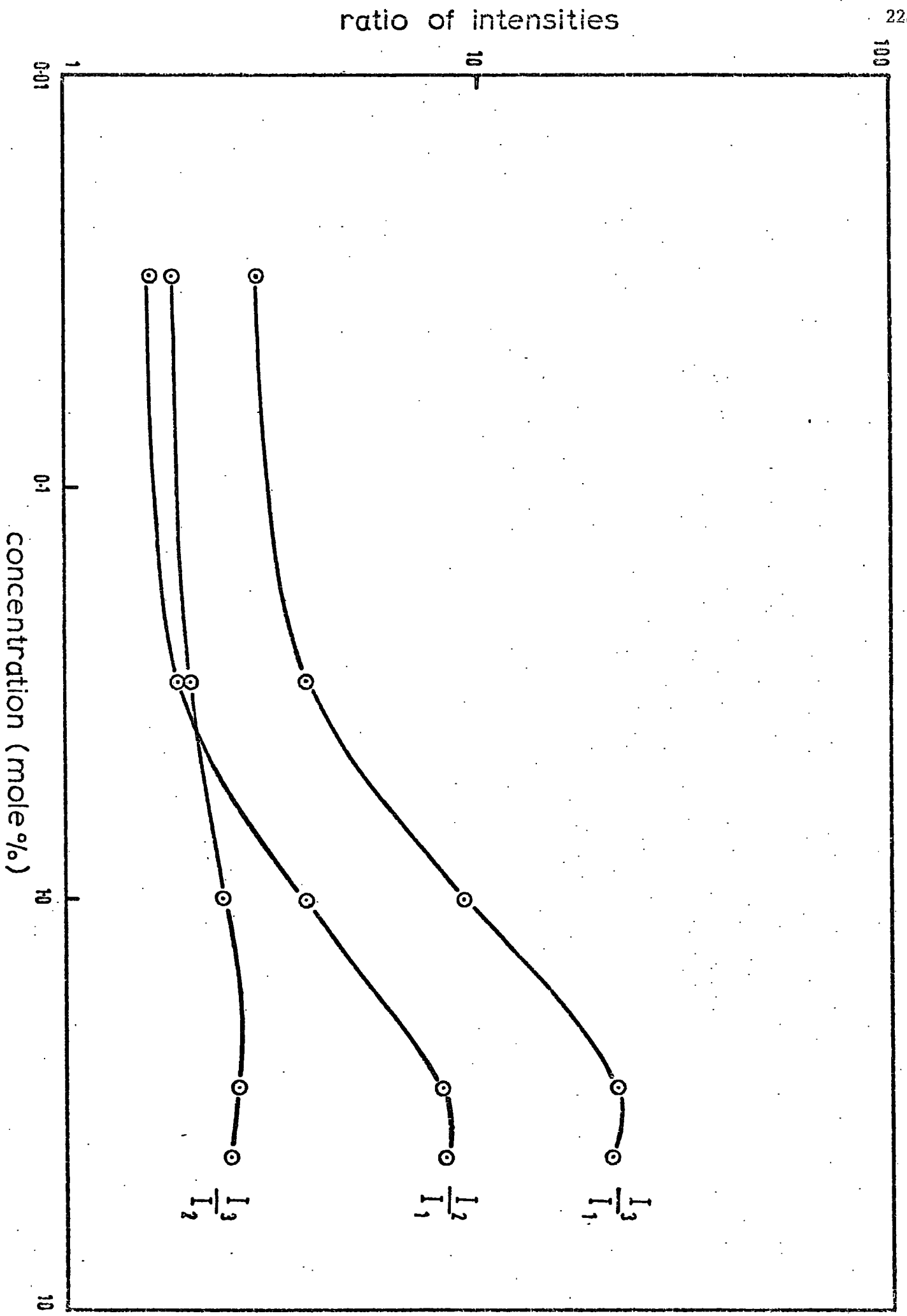

Fig 5.25
Intensity ratios $\frac{I_2}{I_1}$, $\frac{I_3}{I_1}$ and $\frac{I_3}{I_2}$ as a function of Tb^{3+} ion concentration showing energy transfer between Tb^{3+} ions in NS glass

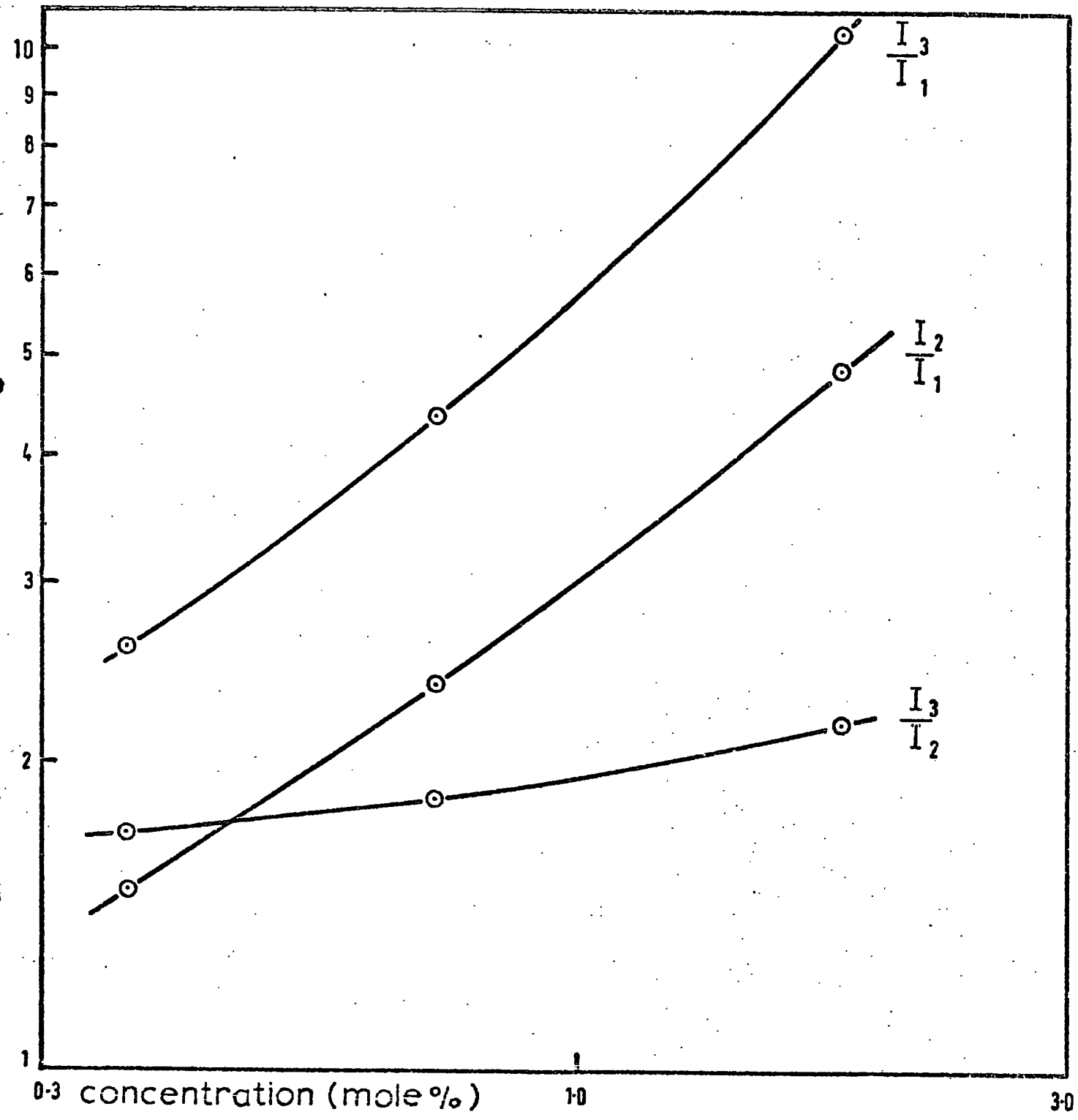

Fig 5.26

Intensity ratios $\frac{I_2}{I_1}$, $\frac{I_3}{I_1}$ and $\frac{I_3}{I_2}$ as a function of Tb^{3+} ion concentration showing energy transfer between Tb^{3+} ions in LAS glasses

behaviour of these glasses (see Chapter 6). At this stage, however, it is suggested that the effect is most likely caused by a change in the excitation mechanism of Tb^{3+} ions before the ions have relaxed to the lower ^5D_J states. Such interactions are ill-understood and this lack of information formed an extra reason for the comparison of thermoluminescence in binary and ternary glasses.

Further evidence of the similarity of the energy transfer characteristics of Tb^{3+} doped glasses under ultra-violet and X-ray excitation was discovered by examining the wavelength spread of the emission spectra. The resolution of the instrument was insufficient to resolve the individual bands completely, but the relative contribution of the $^5D_3$ and $^5D_4$ transitions could be discriminated. These relative emission intensities were estimated by plotting a "spread" function, S, defined by:-

$$S = \frac{\int I(\lambda)d\lambda}{I_{max}} \qquad (5.30)$$

as a function of concentration. Here the integral represents the area under a graph of intensity (I) plotted against wavelength (λ). The integral is normalised by I_{max}, the intensity of the most intense peak ($^5D_4 - {}^7F_5$). S represents the width the emission spectrum would be if $I(\lambda)$ were a constant between some wavelength λ and $\lambda + S$ and zero elsewhere. Hence, S has the dimension of wavelength. The spread, S, is thus a measure of the contribution of the $^5D_3$ emission bands to the total emission. A large value of S implies a more intense emission from the higher luminescent level relative to the total emission intensity

and a monochromatic emission has S→0. Consequently, the concentration dependence of S is expected to be opposite to that of the probability of energy transfer, as a higher transfer efficiency will increase the intensity of the green ($^5D_4$) emissions at the expense of the blue ($^5D_3$).

The concentration dependence of S is given in Figure 5.27, from which it may be seen that the change of energy transfer efficiency is similar to the results for ultra-violet excitation. Note, however, that the curve for LAS glass lies above that of NS glass, which is contrary to expectation if the plot of S against concentration is simply an inverse of the intensity/concentration curve. This indicates that, although the overall efficiency is higher for the ternary glass, the efficiency of energy transfer for the process $^5D_3 \longrightarrow {}^5D_4$ is lower. This behaviour was not evident from the simple intensity/concentration plots. Note that the higher S values were not a result of wider individual spectral bands, since the emission spectrum of LAS was sharper than that of the binary glass, and this would tend to produce lower values of S.

5.2.5 Decay Times and Luminescence Time Dependence

The decay curves of the X-ray excited luminescence were determined by displaying the output of a photomultiplier tube used in detecting the luminescence on a cathode ray oscilloscope. The resulting trace was then photographed for permanent recording. With NS glass, the measured times were not significantly different from those in photoluminescence and were similarly attributed to the transition times of the intra-4f transitions of Tb^{3+} ions. Since such studies led to no further understanding of the terbium glass systems, no additional discussion of these decay times is given here.

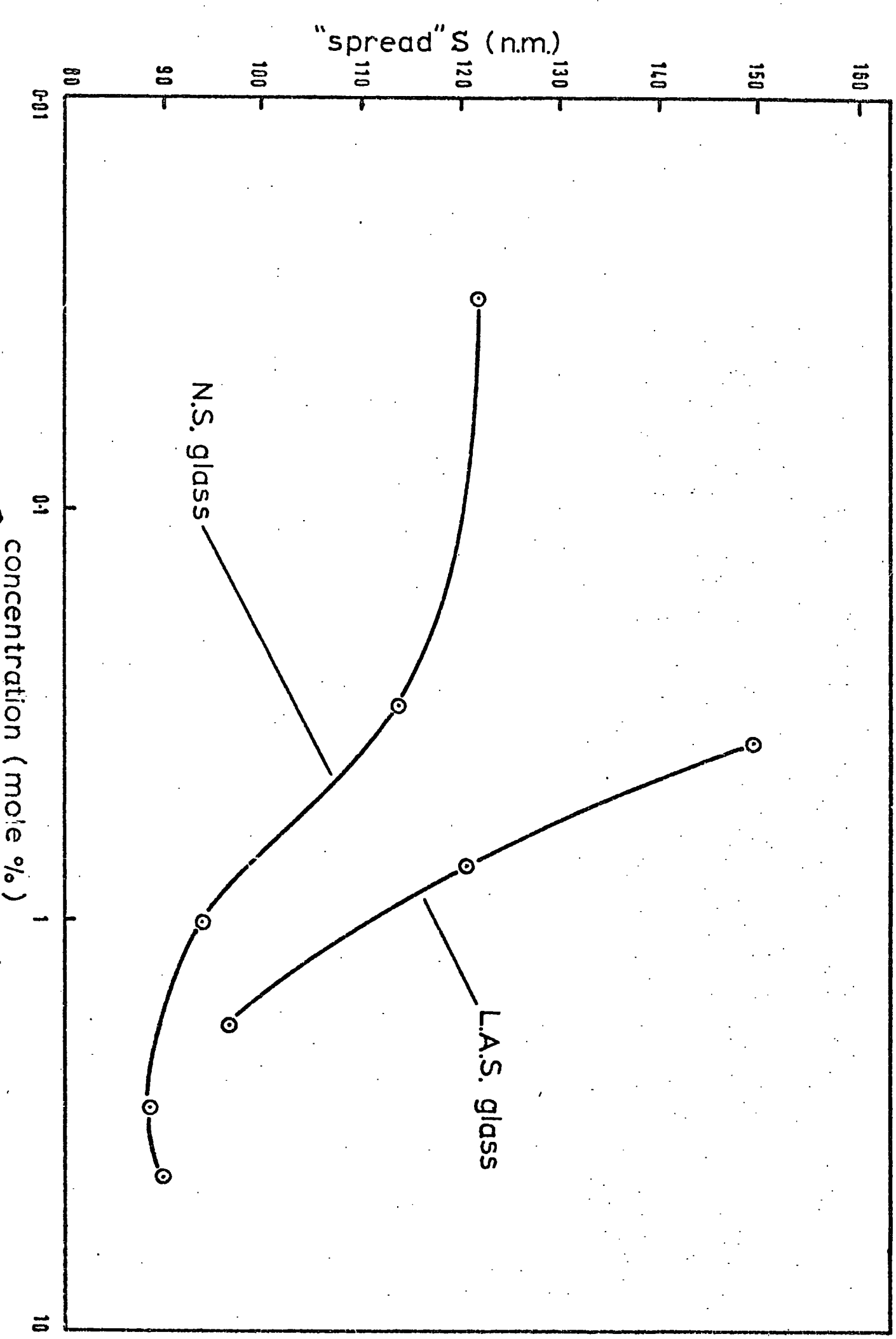

Fig 5.27 The "spread" S as a function of the concentration of Tb^{3+} ions in NS and LAS glasses

In the course of the above investigation it was discovered that LAS glasses have an additional long period component to the decay which was very striking. In a darkened room the blue-green luminescence could be easily discerned by the naked eye, often as much as five minutes after the excitation had ceased. A similar decay was not found for NS glasses even on examination of the specimens with a photomultiplier tube. For these reasons it was decided to concentrate work on time effects of $\sim$1 sec duration in the ternary glass.

A second feature of the X-ray excited luminescence of LAS glasses was that there was a small increase in the emission intensity with time under continuous irradiation. This increase took place over a period comparable to the long decay times described above, and was thus attributed to a similar process. Again such "saturation effects" were not noted with NS glasses.

The decay curves were examined in detail at different temperatures using the specially designed cryostat employed in the thermoluminescence measurements. Intensity–time curves were obtained by using the internal time-base of the X-Y recorder. A typical curve transferred to a log (Intensity) versus time plot is shown in Figure 5.28, for a specimen of 1.81 mole % Tb^{3+} in LAS glass. The data do not follow a simple exponential curve of the form:-

$$I = I_o \exp\left(\frac{-t}{\tau}\right) \qquad (5.31)$$

with τ a constant, as is typical for random decay processes. The curves in fact have a similar shape to those discovered in α-particle excited luminescence, which is discussed briefly in a later section on

Fig 5.28 Typical decay curve of the afterglow of LAS glass containing 1.81 mole % Tb ions showing method of analysis and decay constants

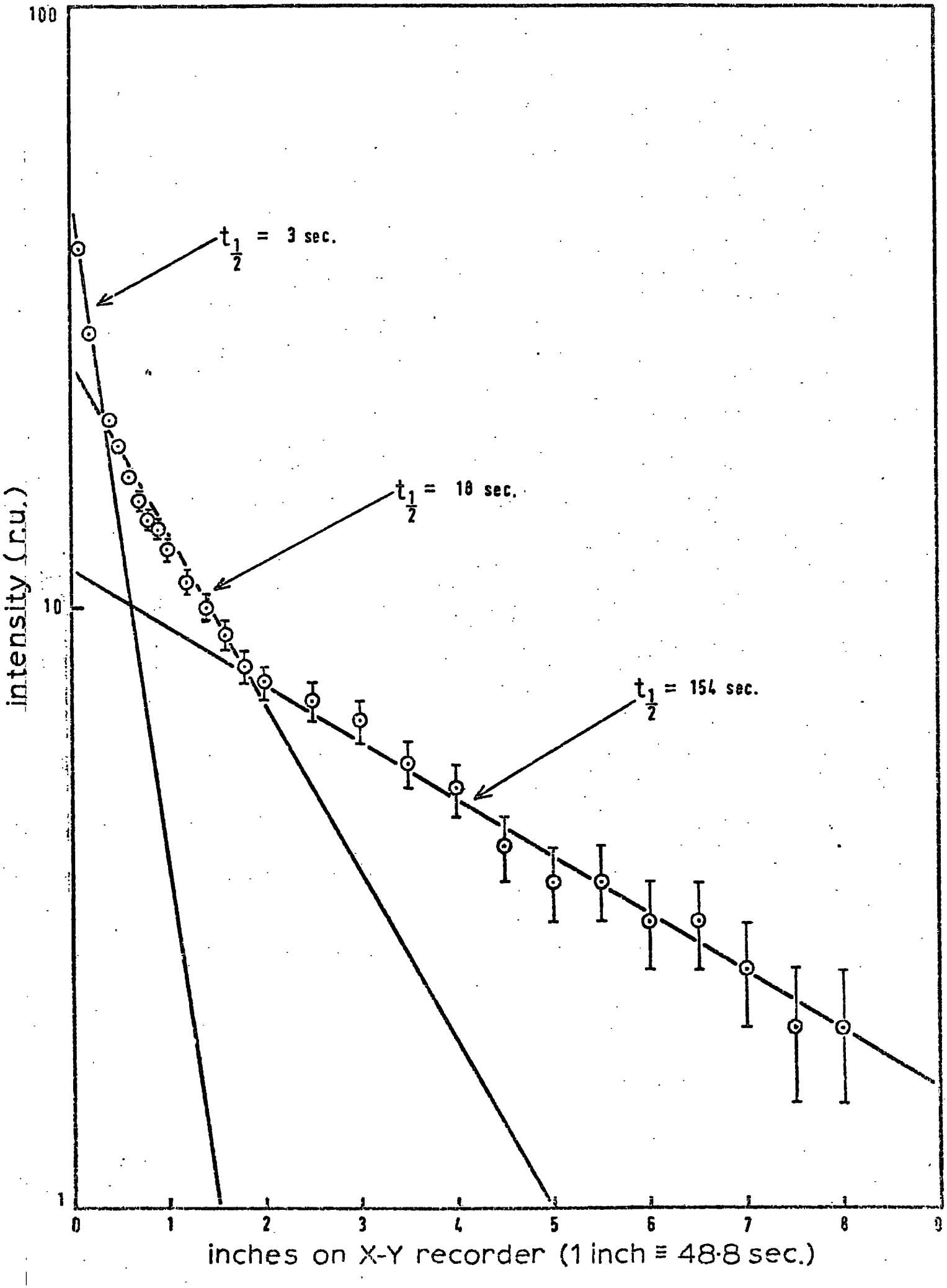

radioluminescence (section 7.1.5).

An attempt was made to fit these curves to a series of exponential decays, assuming an expression of the type:-

$$\ln\left(\frac{I}{I_o}\right) = -\frac{t}{\tau_1} - \frac{t}{\tau_2} - \frac{t}{\tau_3} \quad \ldots . \qquad (5.32)$$

with

$$\tau_1 \ll \tau_2 \ll \tau_3 \quad \ldots . \qquad (5.33)$$

Equation 5.32 was fitted "by hand" by obtaining a good straight-line fit to the long-time region of the curve. This line was then extrapolated to low times and the values obtained were then subtracted from the experimental data. These differences were subsequently plotted on the same scale, and a second straight line was constructed in a similar fashion to the first. If this did not fully describe the remaining (modified) data, the process was repeated to give a series of exponential decay components.

The "half lives" of these exponentials were then determined from the straight line fits. Figure 5.28 shows that three components with half lives of 3 sec, 18 sec and 154 sec were adequate to describe the experimental data shown there. (Note, the half life, $t_{\frac{1}{2}}$, and the decay constant, τ, are related by : $t_{\frac{1}{2}} = 0.6931\,\tau$.) A more rigorous regression analysis to obtain more accurate estimates of the half lives was not attempted for reasons which will become apparent in the following discussion.

The longer decay components were also measured by monitoring the

photomultiplier output with a digital voltmeter. Note that this, like the X-Y recorder, also has a very high input impedance.

Details of measured half lives for several different LAS glasses at 300°K and ~170°K are given in Table 5.16. A systematic feature in this table appears to be a doubling of the half lives at the lower temperature. The system may thus be described as having the following approximate half lives:-

At 300°K	2-3	15-20	60-70	~700-900 sec.
At 170°K	6-7	30-35	150-200	sec.

However, this crude description was eventually rejected for two important reasons. First, the "half life" values obtained by this method were very dependent on the range of time over which the first straight line was fitted. Thus, fitting a straight line to the decay "tail" to, say, 200 sec gave very different answers from a similar procedure beginning the fit by including data to, say, 400 sec. The decay curves thus appear to be described by a dissimilar function which may or may not have a single component. A series of exponential functions is not very satisfactory as the criterion

$$\tau_1 << \tau_2 << \tau_3 \ldots \qquad (5.34)$$

is not well satisfied.

The second reason for rejecting this type of analysis arose from the discovery that the resulting half lives were dependent on the duration of the irradiation. In order to demonstrate this quantitatively, the "fitting" procedure was done after the same elapsed time intervals along the decay curves. In fact, a time near four minutes was found convenient for the experiment. Typical results are given in Table 5.17

TABLE 5.16

Luminescence Half Lives of Tb^{3+} Doped LAS Glasses

Concentration of Tb^{3+} Ions in LAS Glass (mole %)	Method Used	Temperature °K	Half Lives Determined $t_{\frac{1}{2}}$ (secs)
1.81	DVM	300	21 180
			21 93 990
1.81	CR	300	3 15 72
			3 18 154
			7.2 67
0.728	CR	300	3 15 69
0.364	CR	300	2.5 13 63 680
1.81	CR	175	11 105
1.81	CR	152	6.3 34 175
0.728	CR	170	7.3 29 235

DVM = Digital voltometer; CR = Chart recorder.

TABLE 5.17

Half Lives of Long Period Decay Components of X-ray Excited Luminescence in LAS Glass Containing 0.364 mole % Tb^{3+} Ions as a Function of Period of Excitation

Period of Excitation	Half Lives Measured	
	Short Component	Long Component
5 sec	10 ± 3 sec	170 ± 70 sec
1 min	14 ± 1.5 sec	120 ± 20 sec
5 min	18 ± 1.5 sec	165 ± 20 sec
15 min	19 ± 1.5 sec	220 ± 20 sec

for LAS : 0.364 Tb^{3+} glass. These results are also shown graphically in Figures 5.29 and 5.30, from which it is clear that following increasing periods of irradiation the long decay component steadily increases in duration while the short decay component "saturates" at about 20 secs after about 15 minutes' irradiation. This is consistent with a "lengthening of the tail" of the decay curve, with increased irradiation periods.

The above behaviour is atypical of a monomolecular process which can be described by a simple exponential decay equation. Indeed the lengthening of the tail of the decay curves is indicative of an interactive process, the nature of which can only be inferred indirectly from measurements of the type described here. If this interaction is considered to be between the glass matrix and Tb^{3+} ions, the intervention of shallow trapping centres in the general decay scheme becomes a likely possibility. Further discussion will pre-suppose some of the experimental evidence of the following Chapter, but salient points are listed here:-

1) The rate of production of defects saturates after periods of irradiation which are typically several hours (c f the "saturation" time of the longer decay components must be >> 15 minutes).

2) At most of the temperatures available for study in thermoluminescence measurements, there are some traps which are roughly in thermal equilibrium. These could be interpreted as the metastable levels necessary to maintain prolonged luminescence decay.

3) No evidence of an energy transfer type of interaction between the trapping centres and the Tb^{3+} ions was apparent from glow curve

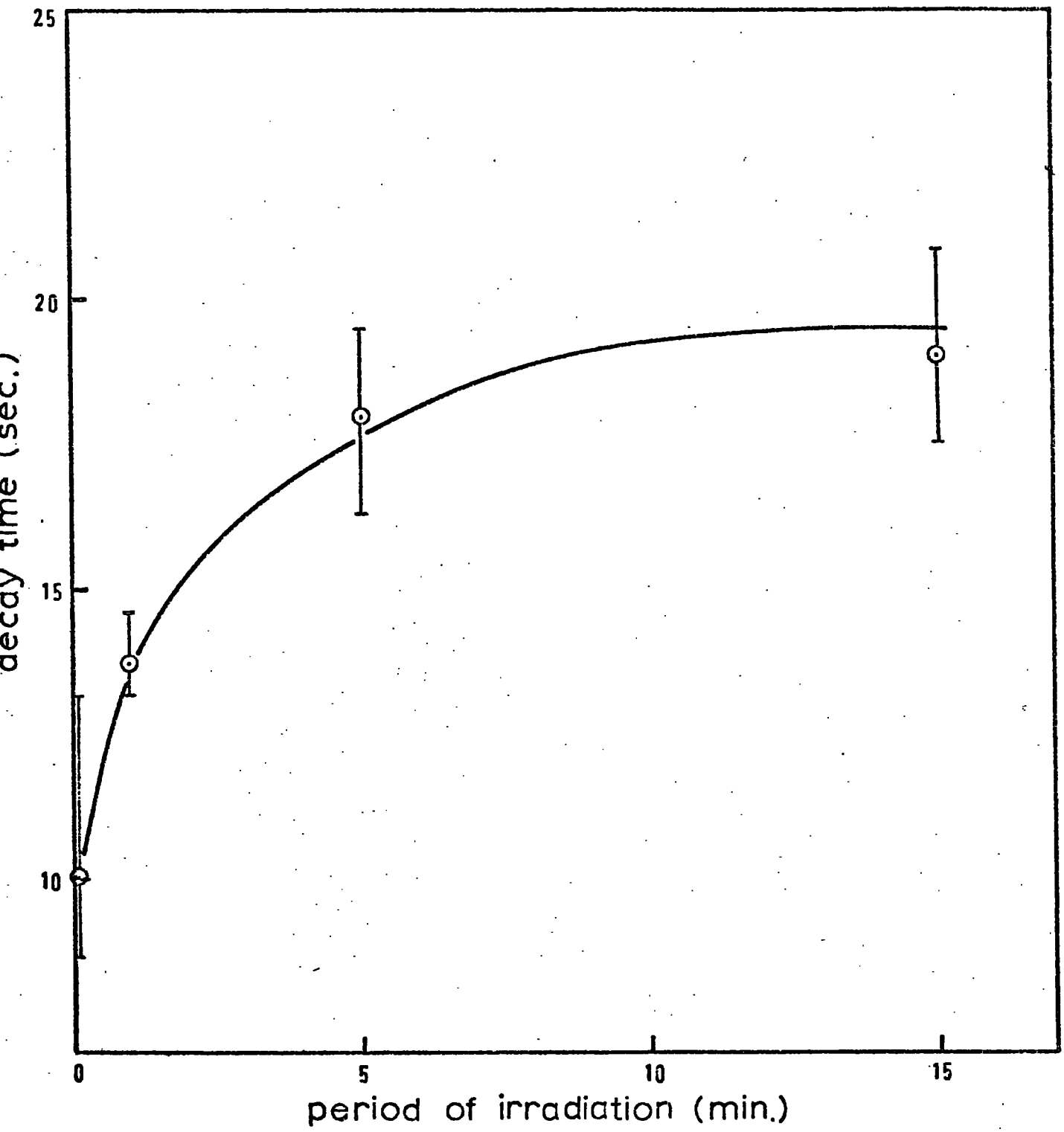

Fig 5.29

Variation of the shorter decay time with irradiation period, 0.364 mole % Tb^{3+} in LAS glass

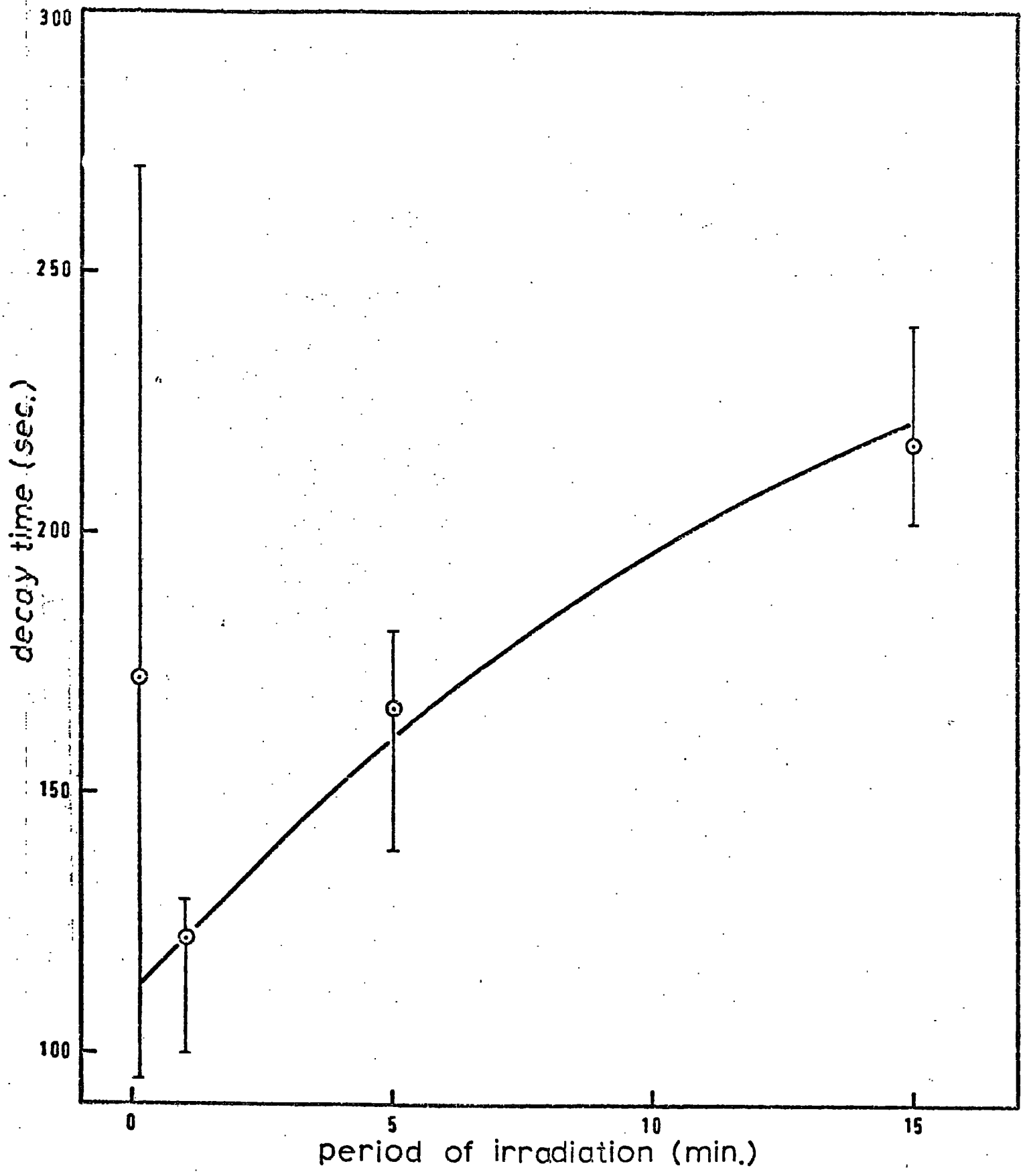

Fig 5.30

Variation of the longer decay time with irradiation period, 0.364 mole % Tb^{3+} in LAS glass

measurements. The thermoluminescence emission was not found in the characteristic terbium bands. This precludes any strong energy transfer processes between electrons in the glassy conduction band and the dopant ions.

4) Further to '3', there was no direct interaction between trapping centres, and the included lanthanide ion apparent in low temperature thermoluminescence.

These considerations indicate that there is a low probability for any energy transfer processes between either the conduction band of the glass or the trapping states within the glass and the ground state of the Tb^{3+} ions. However, the transfer of energy between these excited states of the glass and excited states of Tb^{3+} ions is not precluded.

Thus, if the excitation of the glassy conduction band is written:-

$$G + \gamma \longrightarrow G^*$$

where γ represents an X-ray photon, there will be little chance of the de-exciting transition

$$G^* \longrightarrow G$$

affecting transitions of the type

$$^7F_6 \longrightarrow {}^5D_J$$

in Tb^{3+} ions because of the extreme energy mismatch. Other excitations from the ground state of the lanthanide ion could be postulated, but in view of the experimental evidence they must also be regarded as having low transition probabilities.

However, in the course of the X-ray irradition the transitions

$$Tb + \gamma \longrightarrow Tb^*$$

become possible, but the exact nature of these transitions remains unknown until X-ray absorption data are available for trivalent terbium. Probably the state Tb^* includes higher ionisation states (for example, Tb^{4+}) (5.34) which may themselves be metastable, and perhaps are formed by losing an electron to one of the glassy state trapping centres. These excited states may also interact with other Tb^{3+} ions via different energy transfer processes, perhaps exciting several ions simultaneously. Further possible interactions include those between G* and Tb* involving a whole host of energy levels, many of which are yet to be determined.

Selection from among these possible mechanisms is not yet possible; however, the glass matrix must be involved in some manner. Hunt (5.42) and Kikuchi (5.43) have both described non-exponential decays in base glass. Here the luminescence must be attributed to "defect" centres in the glass. (It is interesting to note at this point that the description here of centres akin to defect centres in crystalline environments is indicative of the short-range ordering postulated for many glass types, as it is difficult to see how these could arise in a totally random network.)

The assumption of a square form of the distribution in occupied traps was shown by Kikuchi to predict a modified form of decay equation. The theory is reproduced in Chapter 2, but still leads to an exponential type of decay. It is conjectured in this work that, no matter what type of distribution is selected, the result will still be an essentially exponential decay. Thus the explanation of these decay curves must lie

elsewhere.

If the emission centre and the long-lived state which temporarily traps electrons are discrete and separate entities, rather than being the same site or associated sites, then it is reasonable to suppose that the mechanism of transfer of energy between these sites will be by means of multipolar or exchange forces. Thus, the decay rate may be more descriptive of the energy transfer process rather than the decay mode of the emission centre, particularly if the latter is a comparatively rapid process. Then, whether the emission centre is a point defect or an impurity ion may have little or no effect on the final decay rate.

The expression (equation 2.130) relating to the decay behaviour of a system coupled by multipolar interactions is:-

$$\frac{I}{I_o} = \exp\left[-\frac{t}{\tau} - \Gamma\left(1 - \frac{3}{S}\right)\gamma\left(\frac{t}{\tau}\right)^{3/S}\right] \qquad (5.35)$$

This can be simplified to

$$\frac{I}{I_o} = \exp\left[-\frac{t}{\tau} - Bt^{\alpha}\right] \qquad (5.36)$$

$$\text{with } B = \Gamma\left(1 - \frac{3}{S}\right)\gamma\left(\frac{1}{\tau}\right)^{3/S} \qquad (5.37)$$

$$\text{and } \alpha = \frac{3}{S}$$

$$= \frac{1}{2}, \frac{3}{8}, \frac{3}{10} \quad \text{for } S = 6, 8, 10 \text{ respectively} \qquad (5.38)$$

Taking natural logs of equation 5.36 gives:-

$$\ln\left(\frac{I}{I_o}\right) = -\frac{t}{\tau} - Bt^{\alpha} \qquad (5.39)$$

$$= \ln\left(\frac{I_1}{I_o}\right) + \ln\left(\frac{I_2}{I_o}\right) \qquad (5.40)$$

$$\text{with } \ln\left(\frac{I_1}{I_o}\right) = \frac{-t}{\tau} \qquad (5.41)$$

$$\text{and } \ln\left(\frac{I_2}{I_o}\right) = -Bt^{\alpha} \quad (\alpha \leq \tfrac{1}{2}) \qquad (5.42)$$

B has its maximum value for S = 6, so that

$$B \leq 1.8\,\gamma\sqrt{\frac{1}{\tau}} < \frac{1}{\tau} \qquad (5.43)$$

except at very high concentrations.

Hence, $\ln\left(\frac{I_1}{I_o}\right)$ dominates at low t and $\ln\left(\frac{I_2}{I_o}\right)$ dominates at high t. An expected transition region should occur where $B \simeq \frac{1}{\tau}$. Figure 5.31 shows a graph of $\frac{I}{I_o}$ against t for real data on a log - log plot, the graph apparently dividing into the two expected regions. A log - log plot was chosen to linearise equation 5.42.

Thus, analysis by this procedure appears justified, and the following regression procedure was then adopted. Since the form of equation 5.36 can not be linearised by means of a simple transformation, the strict method which should be adopted is one of non-linear regression. However, in view of the greater simplicity of linear regression, an approximate form of analysis along these lines was adopted.

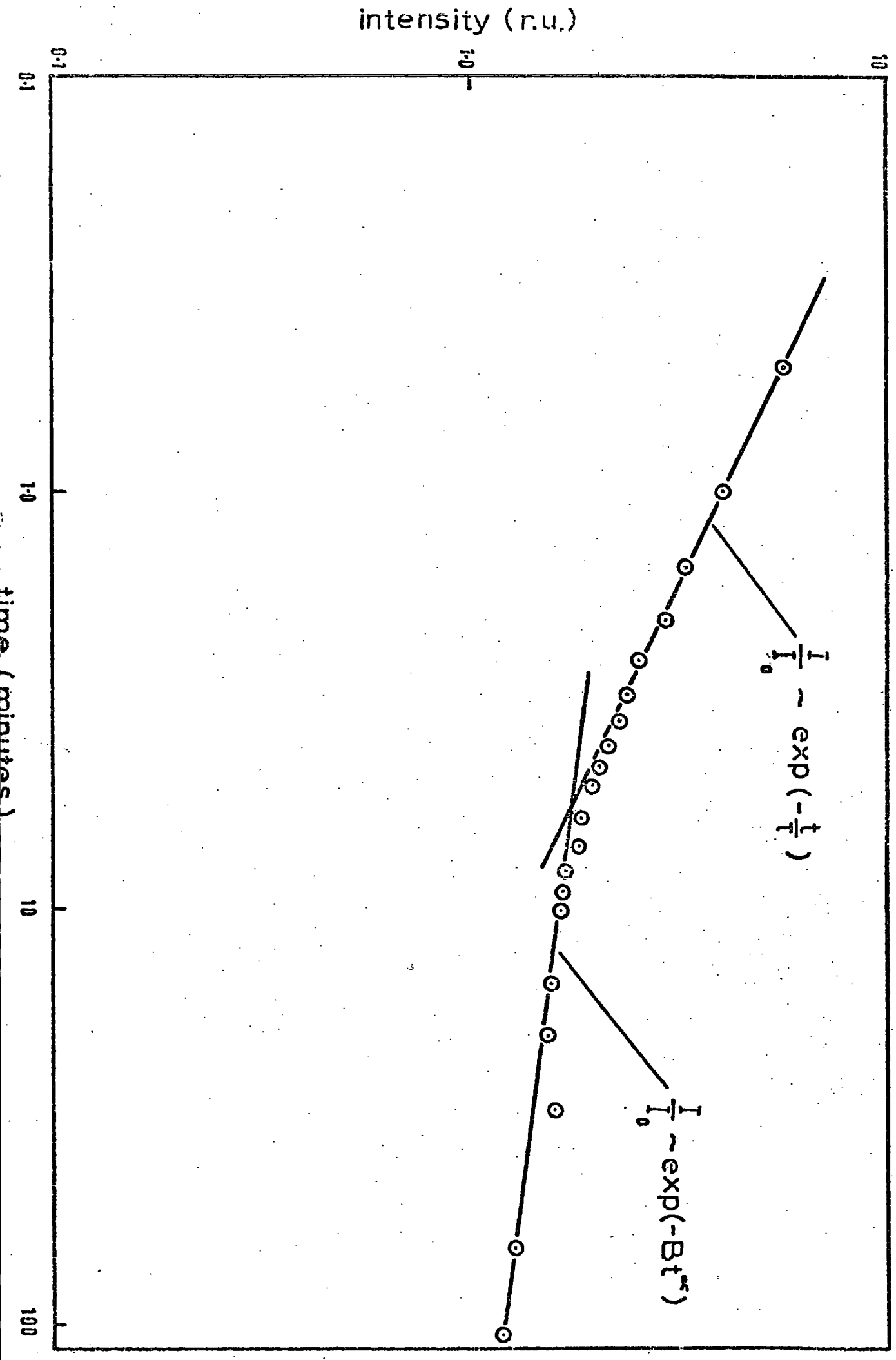

Fig 5.31 A luminescence decay curve replotted on a log-log scale to show evidence of two decay régimes due to an energy transfer mechanism.

Since the intensity scale had been chosen in arbitrary units, the ordinates are actually

$$C\frac{I}{I_o}$$

where C is a constant of proportionality.

Then, taking natural logs

$$\ln\left(C\frac{I}{I_o}\right) = \ln C + \ln\left(\frac{I}{I_o}\right)$$

$$= \ln C - \frac{t}{\tau} - Bt^{\alpha} \qquad (5.44)$$

This can be compared with the linear regression problem

$$Z = D + EX + FY \qquad (5.45)$$

where $Z = \ln\left(C\frac{I}{I_o}\right)$ (5.46)

and the regressors are $X = t$ (5.47)

and $Y = t^{\alpha}$ (5.48)

with the parameters $D = \ln C$ (5.49)

$E = -\frac{1}{\tau}$ (5.50)

and $F = -B$ (5.51)

The approximation in this technique results from the fact that the regressors t and t^{α} are not linearly independent, so that a high degree of correlation is expected to exist between them. Linear regression, however, assumes that there is essentially no correlation between any two of the regressors. The fitting procedure was facilitated by means of a standard computer programme prepared for general

statistical use. Details of this programme or of linear regression techniques are not given in this work, as these are readily available from standard texts (5.44).

Results were obtained from fitting the decay equation (5.44) to the four curves derived from the data of Table 5.17 for 0.364 mole % Tb^{3+} in LAS glass. A typical result is shown in Figure 5.32 where the energy transfer equation with S = 10 is compared with a best-fitting exponential curve. It may be seen that the former gives a more satisfactory fit, but there are some reservations about this method. Firstly, the value of τ when determined from the constant E was always found to be negative, contrary to expectation. Also the simple correlation coefficient between t and t^{α} was always >0.95, which results from the strong interdependence of these two parameters.

The fitted values for the four data sets are given in Table 5.18. The value for D was effectively constant, implying a roughly constant initial luminescence intensity. However, the values of E and F both decrease in absolute magnitude, implying τ increases for increased irradiation periods.

As an empirical approach, however, the energy transfer expression did provide a much improved fit. The regression analysis gave a multiple correlation coefficient, r, between intensity and time which was always > 0.98 irrespective of the value of S chosen, showing a strong functional relationship. Also, all the regression analyses performed gave large and thus significant values of t from the student's t-test (>6 for 17 degrees of freedom) for all parameters fitted. For

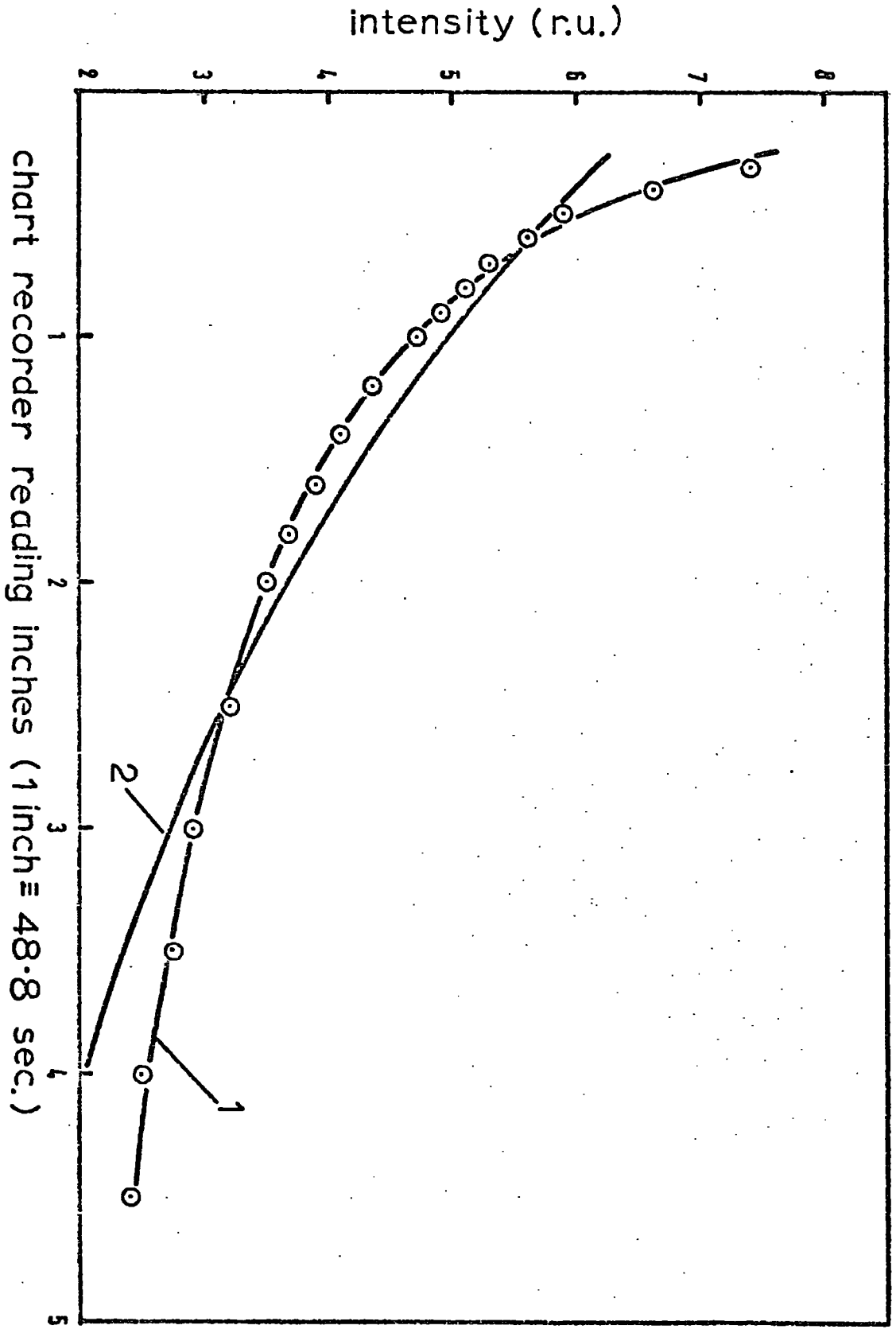

Fig 5.32

A luminescence decay curve fitted by (1) the energy transfer equation, and (2) a simple exponential, 0.364 mole % Tb^{3+} in LAS glass

TABLE 5.18

Regression Values Obtained from Fitting the Energy Transfer Decay Equation to Data from a Sample Irradiation for Differing Periods (S = 10)

Period of Irradiation	D	E ($\times 10^2$)	F
5 sec	2.6 ± 0.20	0.94 ± 0.10	-1.27 ± 0.07
1 min	3.2 ± 0.06	0.28 ± 0.04	-0.94 ± 0.03
5 min	3.4 ± 0.10	0.30 ± 0.08	-0.76 ± 0.05
15 min	3.0 ± 0.05	0.12 ± 0.03	-0.47 ± 0.02

only one data point in any of the regression analyses was a residual larger than two standard deviations.

In all four examples, the best fit was found for S = 10, corresponding to quadrupole - quadrupole type energy transfer. The better fit for S = 10 was indicated by:-

1) The smallest sum of squares of residuals.
2) The largest F-ratio - typically >70 for 17 degrees of freedom.
3) The smallest residual standard deviation.
4) The least evidence of serial correlation (serial correlation may in this case be taken to imply lack of fit) of residuals.

The changing values of the parameters E and F with irradiation period makes uncertain further analysis of the variation of the decay times with terbium concentration or with temperature. However, the results indicated little change with concentration and a lengthening of decay time with decreasing temperature. The longer decay periods at lower temperatures appear to indicate an interaction with the phonon spectrum of either the luminescing levels or, more likely, higher energy levels in the terbium glass system which relax to the luminescing levels. A detailed examination of these phonon interactions, however, was not possible with the existing data because of the variation of τ with irradiation period.

To summarise, it has been demonstrated that the observed long decay times have been well represented by an interactive energy transfer process which was probably quadrupole - quadrupole in nature.

The interaction can be regarded as a delayed route by which the luminescent levels become excited, and thus the same model may be used to describe the build-up of luminescence intensity or the "saturation" effect. Note that the model allows for direct excitation of Tb^{3+} ions which would produce a background level of luminescence with a comparatively fast decay mode and saturation rate.

The saturation only represented $\lesssim 5\%$ of the total luminescence intensity, so that inevitably the data were less accurate than the decay measurements. A typical decay characteristic (measured at 545 nm) result is shown in Figure 5.33 for 1.81 mole % Tb^{3+} in LAS glass. The graph is a plot of $I_{max} - I$ (where I_{max} is the saturation level of intensity) as a function of time and shows that the behaviour is well described by a simple exponential expression of the form:-

$$I_{max} - I = \exp\left(-\frac{t}{\tau}\right) \qquad (5.52)$$

and gives a half life $t_{\frac{1}{2}}$ of 210 ± 15 sec. The value of $t_{\frac{1}{2}}$ was not found to alter significantly with either Tb^{3+} concentration or with temperature. The resulting value of $\tau^{-1} = 3.3 \times 10^{-3}$ sec^{-1} is of the same order of magnitude as the values for E obtained in the regression analysis of the energy transfer equation in the study of luminescence decay. This further supports the conjecture that the same model describes the two phenomena.

5.2.6 The Emission Intensity as a Function of Temperature

The resolution of the monochromator used in determining X-ray excited spectra was insufficient to determine the actual line widths of

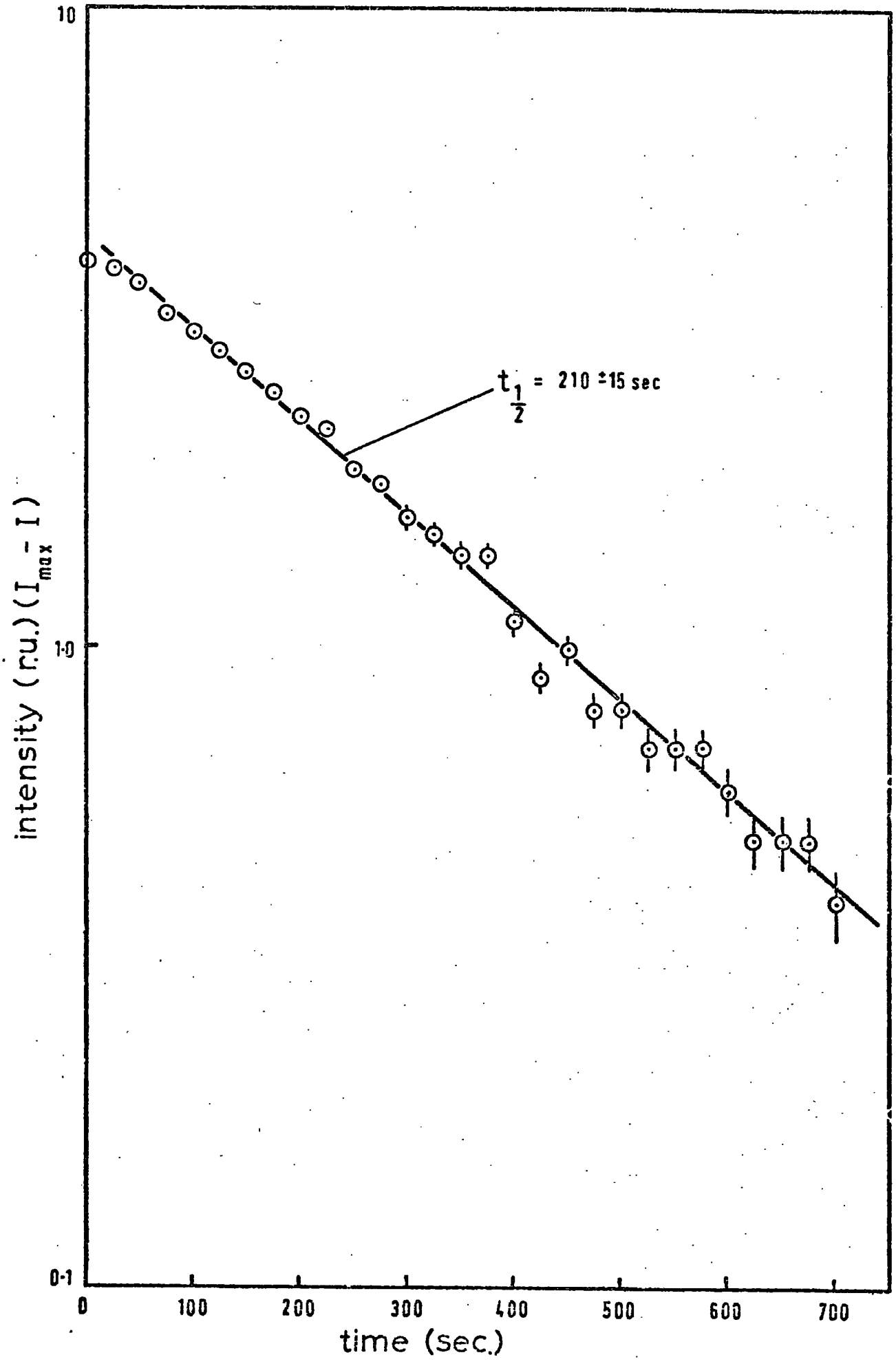

Fig 5.33

Saturation of X-ray excited luminescence of LAS glass activated by 1.81 mole % Tb^{3+}

the luminescence bands (see section 5.2.2). For this reason, no measurements could be made of the variation of line-widths with temperature which, for ultra-violet excited luminescence yielded information on the magnitude of the vibronic quanta of the luminescent levels. However, the luminescence intensity and decay properties of X-ray excited LAS:Tb glass have been investigated over a range of temperatures.

The temperature dependence of X-ray excited luminescence was studied using the cryostat designed for thermoluminescence measurements (described in Chapter 3). The sample was cooled by liquid nitrogen down to around 170°K and reheated to room temperature. The cooling was completed in about two minutes, while heating to room temperature took around 15 minutes. The photomultiplier output was displayed on the Y-axis of an X-Y recorder, while the thermocouple output was connected across the X terminals. A typical result is shown graphically in Figure 5.34 in which the thermocouple e m f has been converted directly to temperature. The two curves are for cooling and heating the specimen (2.88 mole % Tb in NS glass) and represent the total luminescence as measured by the photomultiplier tube. The graphs are uncorrected for the photodetector response since all luminescence bands were observed simultaneously.

The cooling curve is quite different from the heating curve. This dissimilarity can be ascribed to a superimposed intensity peak which lies at around 250°K and is in a similar position to one of the peaks in the glow curves (see Chapter 6). This phenomenon is thus attributed to thermoluminescence, and so the curve measured during heating must

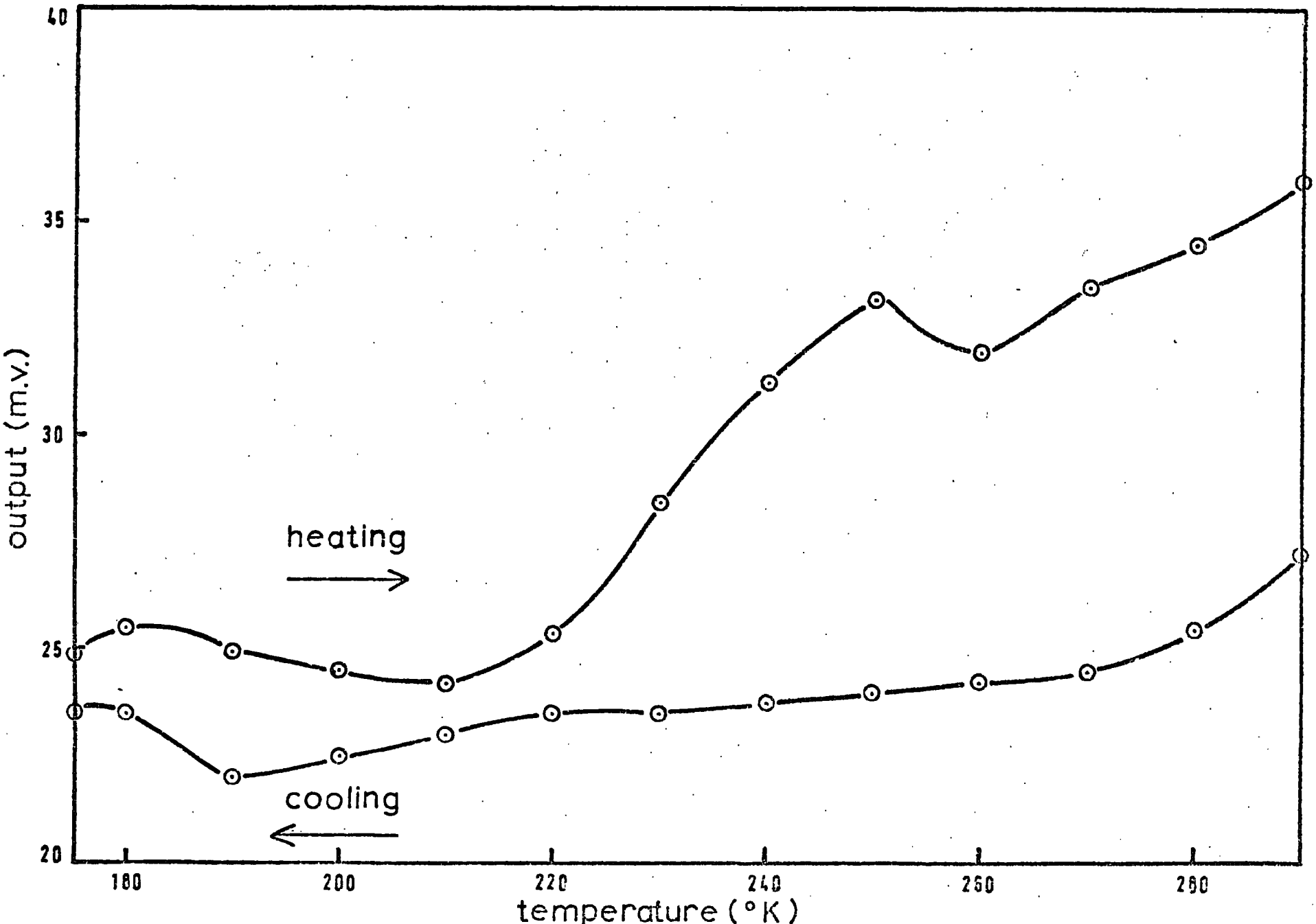

Fig 5.34
The temperature dependence of the intensity of X-ray excited luminescence of 2.88 mole % Tb^{3+} in NS glass showing differences when the sample is cooled and reheated

be disregarded as a valid description of the temperature dependence of the luminescence. With LAS glasses containing terbium there was an even larger peak superimposed on the heating curve commensurate with the larger thermoluminescence output of ternary glasses which was observed in direct glow curve measurements.

A second feature of Figure 5.34 is the disparity between the two curves at around 175°K, from which temperature the heating began. This is thought to be due to the fairly rapid cooling rate and the eventual saturation of luminescence at or near the lowest temperature attainable. As the system reaches equilibrium, the luminescence efficiency is thought to increase after the manner described in the previous section. Attempts to use slower rates of cooling resulted in erratic behaviour of the pen recorder with each addition of liquid nitrogen. This, it is believed, was due to thermo-mechanical shocks affecting the photodetector system. Such an effect was also observed on rapid cooling but was less difficult to allow for. The diagrams in this section do not display this feature.

From the preceding discussion it is possible to indicate an approximate relationship between the saturation effects, the glow curve intensity and the X-ray excited luminescence. Thus, saturation effects accounted only for around 5% of the total emission. Similarly, the thermoluminescence was approximately 25% as intense as the X-ray excited luminescence, but the actual value depended strongly upon the time elapsed between cooling and heating.

The fact that saturation effects do show themselves on these curves demonstrates that the diagram does not accurately represent

the luminescence of a system in equilibrium. However, it has been suggested above that saturation accounts for up to about 5% of the total emission. Also, the beginning of the curve represents saturated luminescence because of a five minute irradiation period before cooling. Hence, the 10 to 15% reduction in intensity with temperature must represent a real effect.

Similar cooling curves are shown in Figure 5.35 for both NS and LAS glasses containing a range of Tb^{3+} ion concentrations. In this diagram, the curves have all been drawn on the same intensity scale using the data from section 5.2.5 as calibration. The intensities have been normalised to that of 0.031 mole % Tb^{3+} in NS glass at 300°K.

In NS glass, the reduction in intensity at lower temperatures is noticeable only at higher concentrations. At $\lesssim$ 0.3 mole %, however, the intensity was actually found to increase as the temperature was lowered. In LAS glass, there was little change in intensity for the 0.728 mole % Tb^{3+} specimen, and perhaps an indication of a slight increase in the intensity of the 0.364 mole % Tb^{3+} sample.

These results are replotted in Figures 5.36 and 5.37 for NS and LAS glasses respectively. Here intensity is given as a function of concentration at four different temperatures. These graphs again show that at lower concentrations there is little change or perhaps a slight increase in intensity as the temperature is lowered, while at higher concentrations a reduction in the temperature produces a definite diminution of the luminescence efficiency as detected by the photomultiplier tube.

Variation of the total luminescence output with temperature for several silicate glasses doped with Tb^{3+} ions

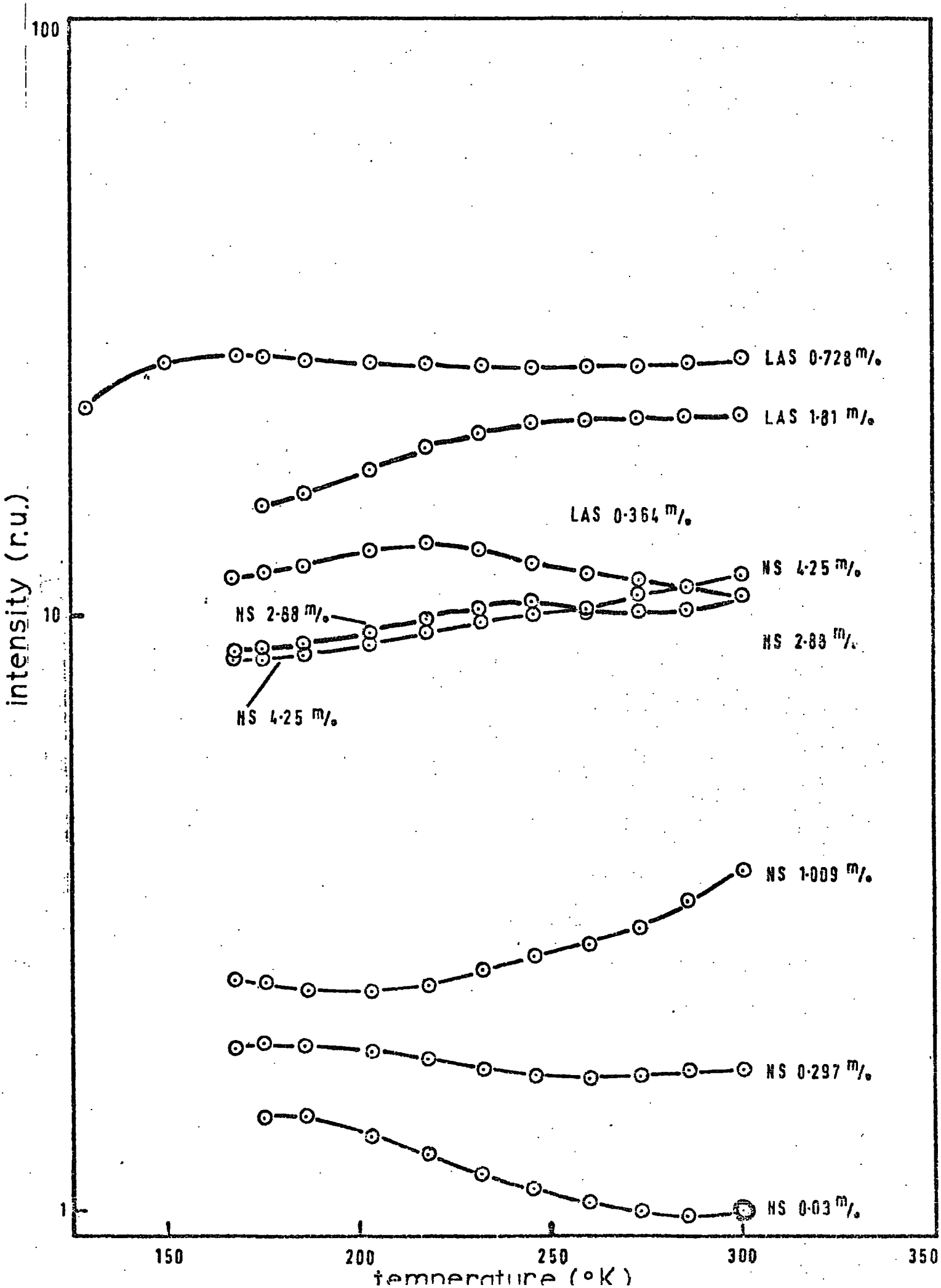

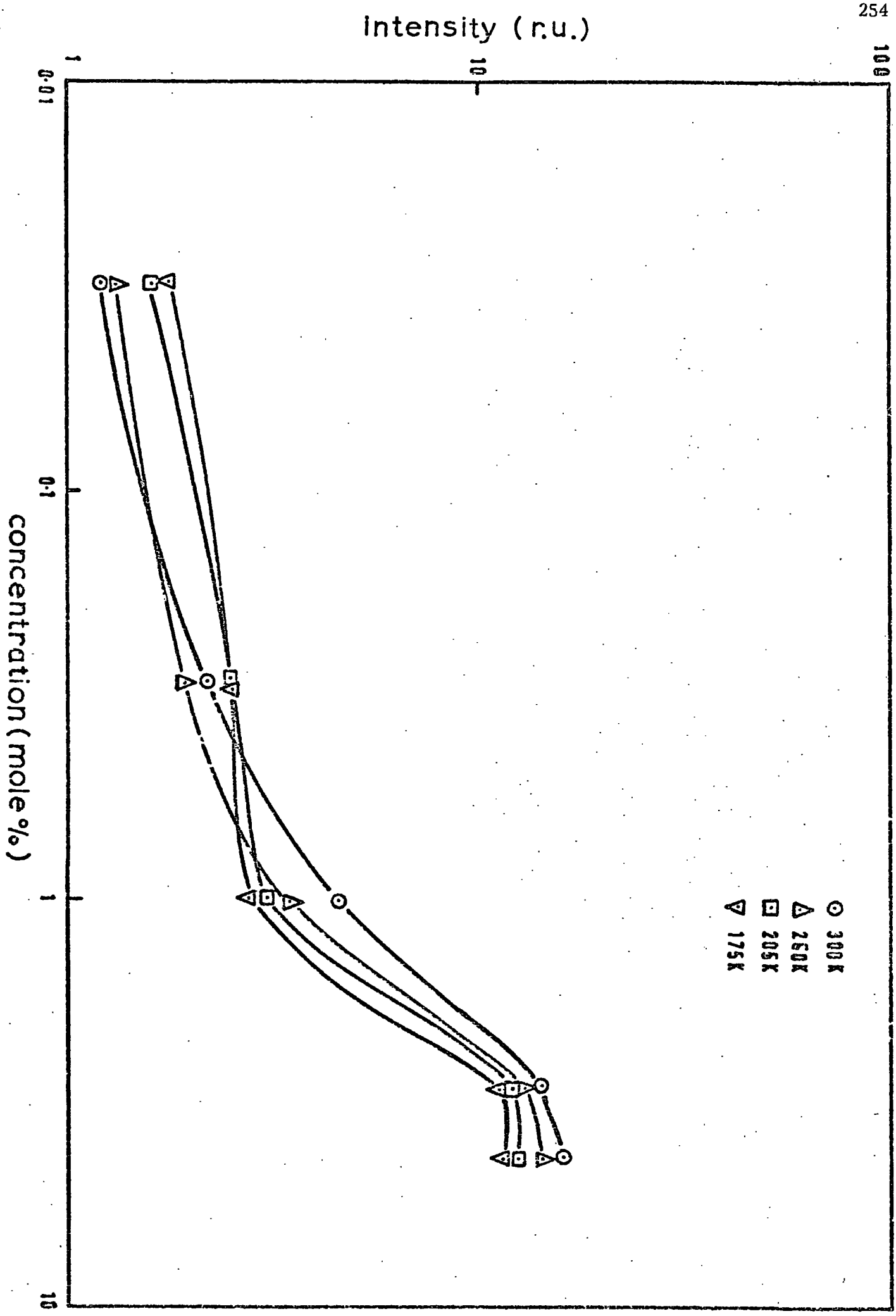

Fig 5.36

Total luminescence intensity as a function of Tb^{3+} ion concentration in NS glass at several temperatures

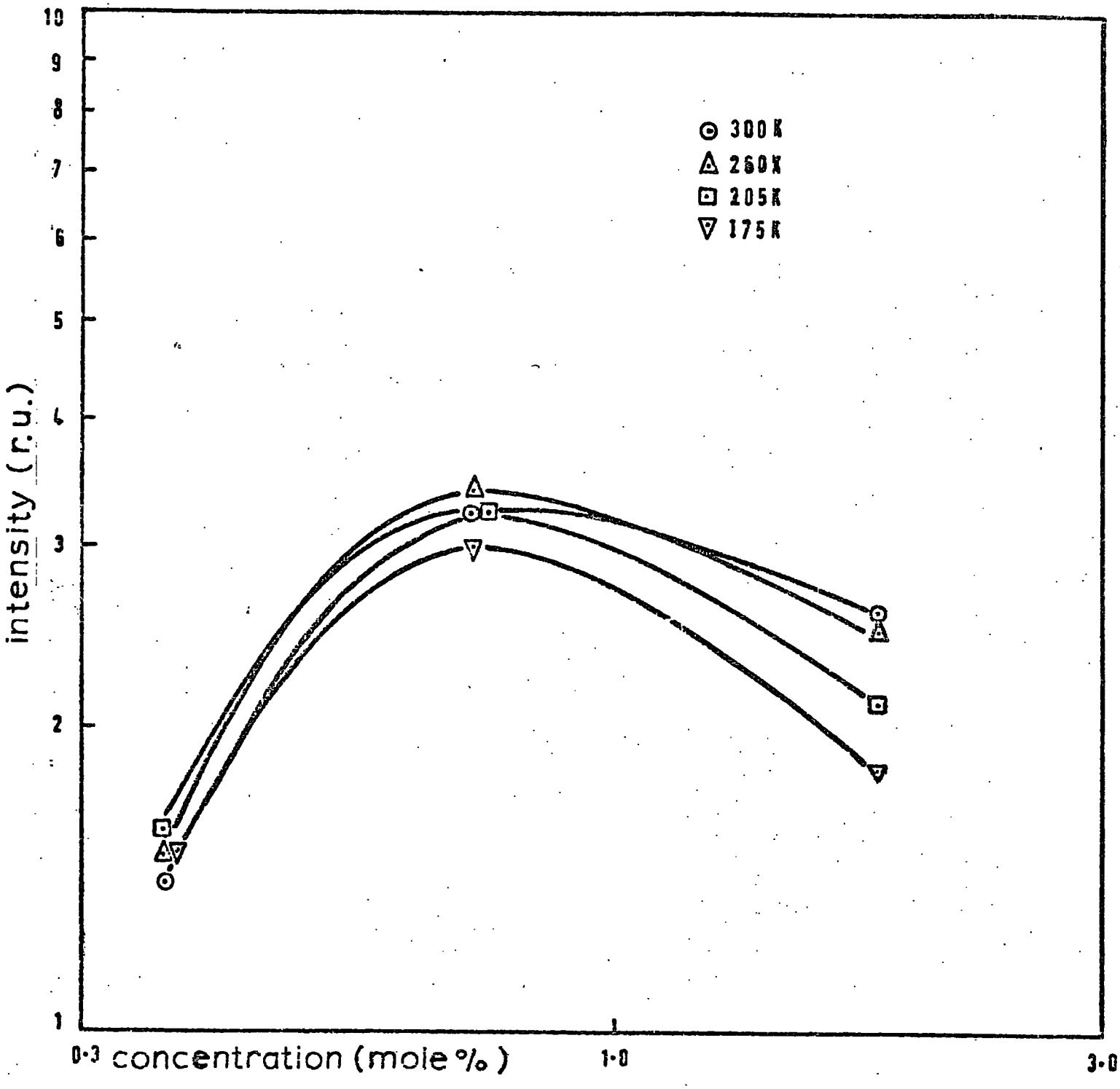

Fig 5.37

Total luminescence intensity as a function of Tb^{3+} ion concentration in LAS glass at several temperatures

A possible explanation of these results is that a change in temperature affects the energy transfer processes involved. As the temperature is reduced, so is the vibrational energy of the glass "lattice". As was shown in section 5.1.6, this leads to a narrowing of the emission bands and (it must be assumed) to a narrowing of the absorption bands of rare earth ions in glass, at least under conditions of ultra-violet excitation. However, if energy transfer processes may be described by the overlap integral (see Chapter 2), then narrower emission and absorption bands will have a smaller overlap region, and consequently the efficiency of the energy transfer process will be reduced. Thus the "green" $^5D_4$ - ^7F_J transitions will become less intense, while conversely the "blue" $^5D_3$ - ^7F_J transitions will increase in intensity.

With a glass phosphor the effect will not be enhanced by cooling much below, say, liquid nitrogen temperatures, as the reduction of the line-widths in emission and absorption is governed by the inhomogeneous broadening produced by the glassy environment where very narrow bandwidths are attainable at low temperatures (5.34, page 346 et seq). Note that this argument assumes that there is little change in the mean wavelengths of the emission and absorption bands with temperature, as with the ultra-violet excited luminescence.

Following the notation of Chapter 2, the overlap integral may be written as

$$\int \frac{f_e(E)F_a(E)dE}{E^4} \qquad (5.53)$$

where $f_e(E)$ is a function representing the shape of the emission spectrum

of the $^5D_3$ - ^7F_J transitions and $F_a(E)$ is a function representing the absorption spectrum of the ^7F_J - $^5D_4$ transitions.

On a much simplified picture, the energy transfer may be described as a four-level process. Also, the functions $f_e(E)$ and $F_a(E)$ may approximately be described as gaussian functions (see section 2.1.5), so that:-

$$F_a(E) = \frac{1}{L\sqrt{2\pi}} \exp\left(\frac{-(E - E_a)^2}{2L^2}\right) \qquad (5.54)$$

and

$$f_e(E) = \frac{1}{M\sqrt{2\pi}} \exp\left(\frac{-(E - E_e)^2}{2M^2}\right) \qquad (5.55)$$

where E_a and E_e are the mean energy of the photons involved in the appropriate absorption and emission transitions respectively, and L and M are the half widths of the emission and absorption bands. The functions $F_a(E)$ and $f_e(E)$ are temperature dependent:-

$$F_a(E) = F_a(E,T) \qquad (5.56)$$

$$f_e(E) = f_e(E,T) \qquad (5.57)$$

It is likely that the variation of these functions with temperature is chiefly determined by the variations of the widths of the emission and absorption bands. It has already been demonstrated experimentally that the variation in intensity with temperature is only $\sim$10%, and it is postulated that most of this is due to a change in the overlap integral due

to a change in the widths of the spectral lines. Thus, if the widths L and M, describe the principal temperature dependence:-

$$L = L(T) \tag{5.58}$$

$$M = M(T) \tag{5.59}$$

then the fractional decrease in intensity, Δ , of the transitions from the $^5D_4$ level on reducing the temperature from 300°K to 175°K is:-

$$\Delta \simeq \frac{L_2 M_2}{L_1 M_1} \frac{\int \exp\left(\frac{-(E-E_a)^2}{2L_1^2}\right) \exp\left(\frac{-(E-E_e)^2}{2M_1^2}\right) dE}{\int \exp\left(\frac{-(E-E_a)^2}{2L_2^2}\right) \exp\left(\frac{-(E-E_e)^2}{2M_2^2}\right) dE} \tag{5.61}$$

where the subscripts 1 and 2 refer to 185°K and 300°K respectively. If the fractional decrease in the width of the emission band with temperature is α, then:-

$$M_1 = \alpha M_2 \tag{5.62}$$

The fractional decrease in the width of the absorption band with temperature is likely to be very similar, so that:-

$$L_1 \simeq \alpha L_2 \tag{5.62}$$

Thus,

$$\Delta \simeq \frac{L_2 M_2}{L_1 M_1} \frac{\int \exp\left(\frac{-(E-E_a)^2}{2\alpha^2 L_2^2}\right) \exp\left(\frac{-(E-E_e)^2}{2\alpha^2 M_2^2}\right) dE}{\int \exp\left(\frac{-(E-E_a)^2}{2L_2^2}\right) \exp\left(\frac{-(E-E_e)^2}{2M_2^2}\right) dE} \tag{5.63}$$

or,

$$\Delta \simeq \frac{\int f_e(E)^{1/\alpha^2} \; F_a(E)^{1/\alpha^2} \; dE}{\int f_e(E) \; F_a(E) \; dE} \qquad (5.64)$$

Note that, if the absorption and emission levels involved in the energy transfer process are more complex, or if many such processes contribute to the resultant emission, then the form of equation 5.64 will be essentially unchanged, providing all band-widths decrease by the fraction α and f_e and F_a are treated as the summations:-

$$F_a(E) = \sum_i \frac{A_i}{L_i\sqrt{2\pi}} \exp\left(\frac{-(E - E_{ai})^2}{2L_i^2}\right) \qquad (5.65)$$

$$f_e(E) = \sum_i \frac{B_i}{M_i\sqrt{2\pi}} \exp\left(\frac{-(E - E_{ei})^2}{2M_i^2}\right) \qquad (5.66)$$

where the L_i and M_i are directly related to the bandwidths. However, the expressions for Δ will be a more approximate relationship, the accuracy of which will improve more as one transfer process dominates the complex interactions.

Experimentally determined values for Δ were - for LAS : 1.81 Tb^{3+}, $\Delta = 0.69 \pm 0.05$; and for NS : 2.88 Tb^{3+}, $\Delta = 0.81 \pm 0.05$.

The change in the relative luminescence intensities of the blue ($^5D_3$) and green ($^5D_4$) emission bands with temperature was successfully demonstrated experimentally by simply measuring the intensity/

temperature curves through coloured filters. The results are shown in Figure 5.38 for blue and green filters, together with the appropriate curve for unfiltered emission. Note that the three curves are not to the same scale. The LAS : 0.364 Tb^{3+} glass was chosen for presentation as it had both a reasonably high total emission intensity with a strong contribution from the $^5D_3$ bands, and consequently showed the largest divergence of blue and green intensities at low temperatures.

The curves demonstrate a decrease in both the total intensity and the green emission with decreasing temperature. Conversely, the blue emission intensity increases as the temperature is lowered. Similar effects, although not so pronounced, were observed for the other glass specimens investigated. These results simplify the complex temperature behaviour of the total emission which was described earlier, and allow an explanation in terms of the energy transfer model.

5.3 Excitation Spectra and Stokes Shifts

5.3.1 Excitation Spectra

Excitation spectra of terbium ions in NS glass were obtained by using the Optica spectrophotometer (in monochromator mode) in conjunction with a tungsten filament lamp or a deuterium discharge lamp, which gave continuum ultra-violet emissions. The more intense transition band ($^5D_4$ - ^7F_J) was monitored using a yellow or orange filter, the transmission properties of which were described in Chapter 3. Except for small changes in intensity, no differences were noted in the

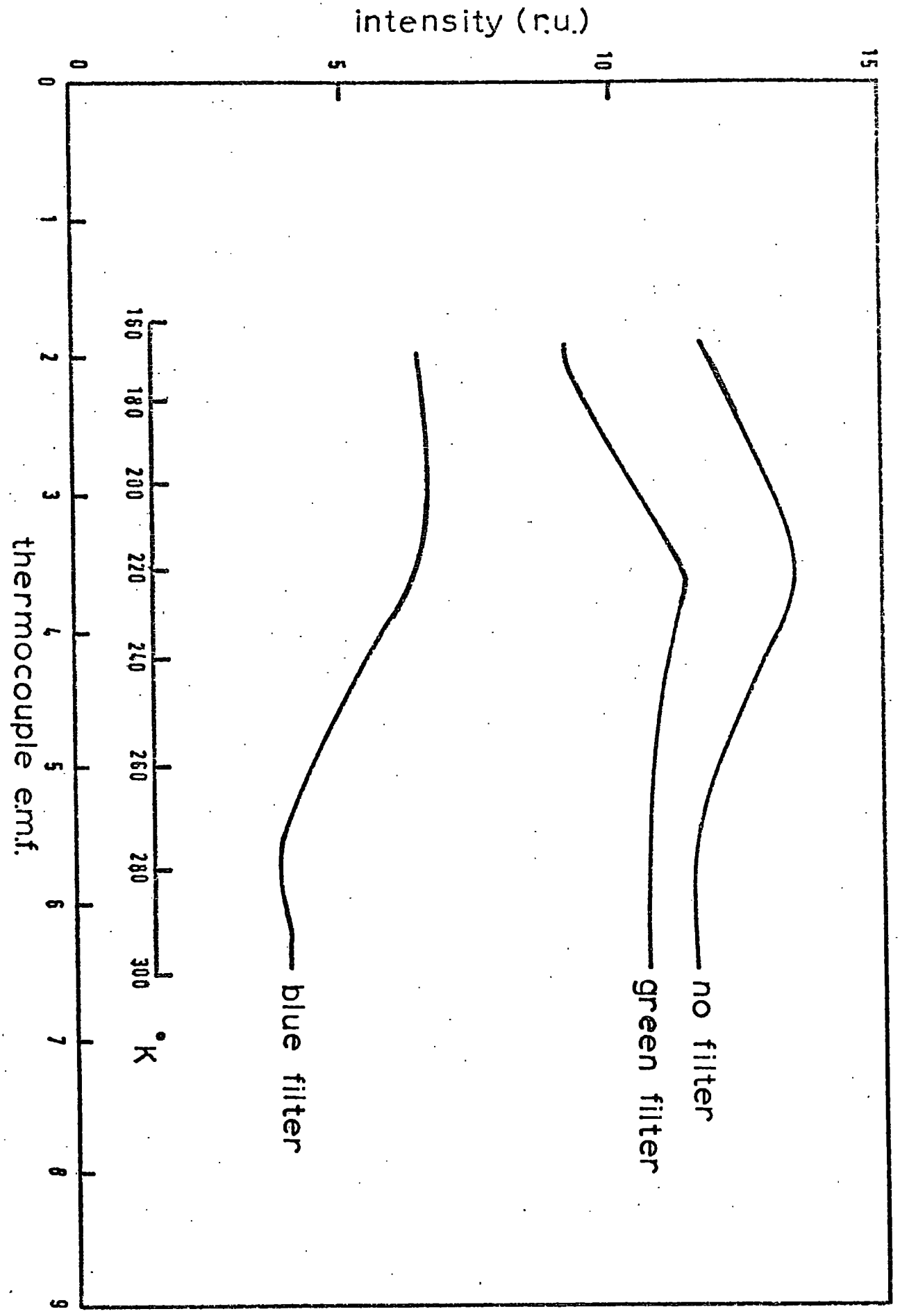

Fig 5.38

The effect of optical filters on the total intensity of the luminescence of 0.364 mole % Tb^{3+} in LAS glass when cooled from room temperature

excitation spectra determined with these filters.

A typical excitation spectrum is shown in Figure 5.39 for 2.88 mole % Tb^{3+} in NS glass. This curve has been corrected for both the response of the photodetector and the luminous efficiency of the lamp. The resulting spectrum is similar to that obtained by Herring et al (5.15) for terbium in a sodium calcium silicate glass.

The spectrum shows a series of definite peaks, the wavelengths of which are given in Table 5.19. Also given in this table is the relative quantum ouput associated with each peak. The wavelengths were found to correspond well with those of the peaks found in optical absorption (Chapter 4) and which were ascribed to various higher 4f levels of Tb^{3+}. A similar assignment of levels has been attempted in Table 5.19, comparing the results of these two experiments.

A further feature which was discovered in the excitation spectrum was a broad, strong band centred at 230 nm with a half-height full-width of 35 nm. The relative quantum output of this band was estimated to be comparable with the 377 nm excitation band. A similar excitation band has been reported by Blasse and Bril (5.2, 5.45) as occurring in many crystalline solids doped with terbium.

Reisfeld et al (5.23) have demonstrated that the optical excitation of luminescence in systems containing lanthanide ions is governed by three mechanisms:-

(a) excitation of the narrow 4f levels of the rare earth ion;

(b) excitation in the broad levels, due - for example - to 4f - 5d transitions or charge transfer processes;

(c) absorption due to the host lattice followed by energy

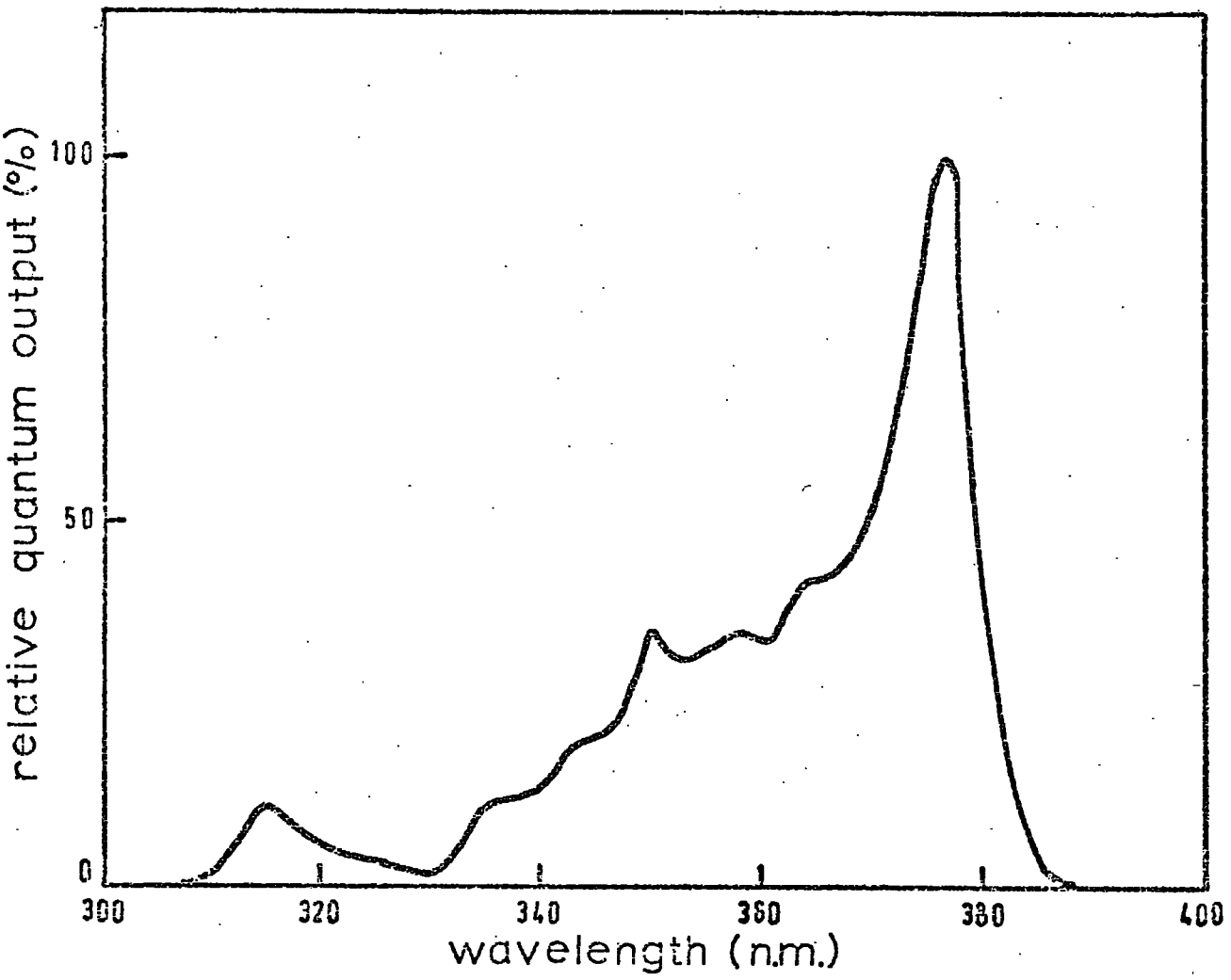

Fig 5.39

The excitation spectrum of 2.88 mole % Tb^{3+} in NS glass

TABLE 5.19

Wavelength and Relative Quantum Output of the Peaks in the Excitation Spectra

Wavelength (nm)	Relative Quantum Output (Relative units)	Level Assignment
377	100	$^5D_3$ ($^5G_6$) ($^5L_{10}$)
365	42	$^5G_5$
358	35	$^5L_9$
350	35	$^5L_8$
344	20	$^5L_7$
336	12	$^5H_7$ ($^5D_1$)
315	11	$^5H_6$

transfer from the host to the rare earth activator.

Mechanism (a) is evidently responsible for the excitation above 300 nm, while mechanism (b) is thought to be responsible for the broad band at 230 nm. The free Tb^{3+} ion is known to have the lowest $4f^n$ 5d configuration of all the trivalent lanthanides, except possibly Ce^{3+} (5.1, 5.34), while the charge transfer band lies at much higher energies (5.46). An assignment was first proposed by Ryan and Jørgensen (5.47) which is followed here. Two excitation bands were observed in terbium hexachloride at 42750 cm^{-1} (236 nm) and a weaker band at 36800 cm^{-1} (272 nm). The stronger band was assigned to absorptions by the ^7F term of the $4f^7$ 5d configuration. The weaker band was explained in terms of a spin foribdden transition ^7F - ^9D from the ground state, involving the same configuration.

Thus, the strong excitation peak at 230 nm in silicate glass is attributed to the spin allowed transition $^7F(4f^8)$ - $^7F(4f^7 5d)$. This transition may therefore be regarded as an additional feature of the absorption spectrum, the absence of which in optical absorption measurements is accounted for by the strong absorption of the base glass at these wavelengths.

There is probably a competitive process between the base glass and the dopant ion at these wavelengths whereby the efficiency of terbium luminescence is reduced. Increased efficiencies are expected for Tb^{3+} ions in media which are transparent at these excitation frequencies.

5.3.2 Stokes Shifts

A comparison between the optical absorption and the emission

spectra usually leads to a discrepancy between the energies determined for the luminescing levels. This is referred to as the Stokes shift and is most conveniently expressed in energy units. The shift is primarily caused by changes in energy due to the different radii of the ion in the ground and excited states.

The magnitudes of the Stokes shifts for the $^5D_4$ - ^7F_J transitions of Tb^{3+} in NS glass are listed in Table 5.20. They correspond to a mean value of $210\,cm^{-1}$. Note, therefore, that these shifts are only about 20% to 25% as large as the nephelauxetic shifts (Chapter 4) for which a mean value of $910\,cm^{-1}$ was determined. Thus the change in the coupling energy between the ion and the lattice on exciting the ion out of the ground state is smaller than the coupling energy of the ground state.

The situation for the $^5D_3$ level is less clear. In both the optical absorption and excitation spectra (section 5.3.1) the levels $^5D_3$, $^5L_{10}$ and $^5G_6$ are found to lie very close together. The identification of the $^5D_3$ level with the $26300\,cm^{-1}$ line leads to a negative average Stokes shift of $-120\,cm^{-1}$ (Table 5.21). However, if the $26600\,cm^{-1}$ line is chosen, the Stokes shift is positive and has a mean value of $170\,cm^{-1}$ which is similar to the shifts found for the $^5D_4$ level. This indicates that the $26600\,cm^{-1}$ line is associated with the $^5D_3$ level and that the weaker absorption found at $26300\,cm^{-1}$ corresponds to either the $^5G_6$ or the $^5L_{10}$ level, the former being more likely by comparison with the aquo ion (see Chapter 4).

The values $210\,cm^{-1}$ and $170\,cm^{-1}$ (equivalent to 47μ and 59μ) are much lower than the energies of the various absorption modes

TABLE 5.20

Stokes Shifts in the $^5D_4$ - ^7F_J Transitions

Transition	Energy of Transition		Stokes Shift (cm^{-1})
	Determined from Optical Absorption (cm^{-1})	Determined from Luminescence Spectrum (cm^{-1})	
$^5D_4$ - $^7F_6$	20900	20550	350
$^5D_4$ - $^7F_5$	18650	18450	200
$^5D_4$ - $^7F_4$	17350	17150	200
$^5D_4$ - $^7F_3$	16250	16150	100
$^5D_4$ - $^7F_2$	15500	-	-
$^5D_4$ - $^7F_1$	15120	-	-
$^5D_4$ - $^7F_0$	14900	-	-
			mean = 210 cm^{-1}

TABLE 5.21

Stokes Shifts in the $^5D_3$ - ^7F_J Transitions

Transition	Energy of Transition (cm^{-1})			Stokes Shift from 1) (cm^{-1})	Stokes Shift from 2) (cm^{-1})
	From Optical Absorption		From Luminescence Spectrum		
	1) Assuming $^5D_3$ = 26300cm	2) Assuming $^5D_3$ = 26600cm^{-1}			
$^5D_3$ - $^7F_6$	26300	26600	26200	100	400
$^5D_3$ - $^7F_5$	24050	24350	24050	0	200
$^5D_3$ - $^7F_4$	22750	23050	22950	-250	100
$^5D_3$ - $^7F_3$	21650	21950	21900	-250	50
$^5D_3$ - $^7F_2$	20900	21200	(21100)	(-200)	(100)
$^5D_3$ - $^7F_1$	20520	20820	-	-	-
$^5D_3$ - $^7F_0$	20300	20600	-	-	-
				Mean = -120cm^{-1}	Mean = 170cm^{-1}

associated with bond stretching (see Chapter 4), which are not found below $700\,cm^{-1}$. Thus it is assumed that the excess energy of the transitions ^5D_J - ^7F_J is disspiated by phonons due to bending modes in the glass. The existence of such phonon modes is also implied by the thermal broadening of spectral lines which is described in section 5.1.5. This effect suggests that the phonon energy is about $140\,cm^{-1}$, which is very similar to the value found here.

5.3.3 Configuration Co-ordinates

The configurational co-ordinate model was discussed in Chapter 2. One of the more important parameters is $h\upsilon_e$, the energy of vibrational quanta in the excited state. Measurements of thermal broadening and application of equation 2.62 leads to an experimental determination of this parameter. In section 5.1.6 a value of $h\upsilon_e = 140\,cm^{-1}$ was determined for the energy of the phonon interacting with the $^5D_4$ level of Tb^{3+} ions in silicate glass. It is reasonable to assume that a similar figure pertains to the $^5D_3$ level.

The Stokes shifts determined in the previous section were $210\,cm^{-1}$ and $170\,cm^{-1}$ for the $^5D_4$ and $^5D_3$ levels respectively. Thus it appears that the shift to longer wavelength corresponds to the creation of, say, a single photon in the excited state, leaving about $30\,cm^{-1}$ to $70\,cm^{-1}$ as the energy available for creation of phonons in the relaxation of the ground state. This is unusually low, as typical phonon numbers are about 50 (see Chapter 2 and reference 5.48). This implies an unusually weak coupling between the activator ion and the phonon flux, but there was no evidence of a zero-phonon line. In rare earth

ions, the optically active electrons (which are in the 4f orbital) are shielded from the matrix environment by outer electron shells. The extent of this shielding makes the calculation of interactions between the inner electrons and the ligand orbitals difficult. However, it is clear that the values of the Stokes shifts are due to this electronic shielding. A corollary of this is that there is only a small change in the expectation values of the radii of the orbitals upon exciting the ion out of the ground state.

A crude estimate of the change in the radial displacement of one of the optically active electrons can be made by using simple Bohr theory. The expectation value of an orbital radius is given by:-

$$\langle r \rangle = \frac{n^2 \hbar^2}{m Z e^2} \tag{5.67}$$

where Z is the effective charge at the radial displacement, r; thus, for the 4f electrons of terbium, $Z \simeq 11$.

The energy of an electron is:-

$$E = \frac{-m Z^2 e^4}{2n^2 \hbar^2} \tag{5.68}$$

$$= \frac{-n^2 \hbar^2}{2m} \cdot \frac{1}{r^2} \tag{5.69}$$

Then, if the expectation value of the electronic orbital changes from r_1 to r_2, the corresponding change in energy is:-

$$\Delta E = \frac{-n^2 \hbar^2}{2m} \left[\frac{1}{r_1^2} - \frac{1}{r_2^2} \right] \tag{5.70}$$

providing that the change in displacement

$$\Delta r = r_1 - r_2 \qquad (5.71)$$

is small. Then:-

$$\Delta E \quad \frac{-n^2 \hbar^2}{2m} \cdot \frac{\Delta r}{r^3} \qquad (5.72)$$

where r is the geometric mean of r, and r_2 :-

$$r = \sqrt{r_1 r_2} \qquad (5.73)$$

Thus, taking n = 4 for 4f electrons, the electronic mass $m = 9 \times 10^{-31}$ kg and the ionic radius as 1.0 Å = 10^{-10} m, and taking a typical values for ΔE as $200\,cm^{-1}$ gives:-

$$\Delta r = 2 \times 10^{-4} \text{ Å} \qquad (5.74)$$

This change in the orbital radius of the optically active electrons is much smaller than that determined for transition metal ions (5.48) and reflects the extreme stability of the shielded 4f electron configuration.

5.4 Quantum Efficiencies

The quantum efficiency of a phosphor is an important parameter to take into account when considering potential applications of the material. The visual appearance of the luminescence of terbium doped silicate glass was compared with that of copper activated zinc sulphide. To the naked eye, the highly doped terbium glasses appear almost as bright as the ZnS phosphor. The wavelength of the most intense peak in the spectrum of the ZnS sample was determined as 545 ± 5 nm,

which is very similar to the wavelength of the most intense emission line in the terbium spectrum ($^5D_4$ - $^7F_5$). However, the ZnS emission appeared more "whitish" due to a greater spectral width.

Samples of 2.88 mole % Tb^{3+} in NS glass and Zn S : Cu were ground and mixed with KBr and compressed into 1cm diameter discs using the method described in section 4.2.1. The samples were then irradiated by the 365 nm line from a mercury vapour lamp under similar conditions, and the spectra were examined by means of the Optica spectrophotometer. After correction for the photomultiplier detection efficiency, the total intensity of the spectra was determined by integrating the areas under the curves from the X-t recorder by "counting squares". This gave a ratio of the intensities ZnS : NS glass of approximately 50 : 1. However, because the terbium spectrum is much narrower, the ratio of maximum intensity at the peak of the two curves was approximately 5 : 1.

Values of the quantum efficiency of terbium doped glass were not determined experimentally because of the difficulty of obtaining a suitable standard phosphor, such as sodium salicylate, from commercial suppliers. However, Bourcet et al (5.49) have measured the quantum efficiencies of terbium doped lanthanum phosphate. They obtained a maximum apparent quantum efficiency of 0.5 for the excitation of the $^5D_3$ - ^7F_J and $^5D_4$ - ^7F_J transitions at 205 nm in samples of $La_{0.95}Tb_{0.05}PO_4$. The corresponding real efficiency was 0.8.

Blasse and Bril (5.45) report values of 0.7 and 0.3 for the real quantum efficiency of YBO_3 and $YAL_3B_4O_{12}$, both doped with 2 mole % of terbium oxide. In section 5.1.6 it was shown that both borate and

phosphate glasses doped with terbium have a lower fluorescence output. Thus the quantum efficiencies of the various excitation bands of terbium in silicate glasses are likely to be at least comparable with the values for the phosphors quoted above.

5.5 Energy Transfer in Terbium Co-doped Glasses

The subject of energy transfer has received considerable attention in the recent literature, so that only selected articles will be referred to in this work. Energy transfer has been found between trivalent terbium and most of the lanthanides, together with many other ions in a variety of host materials, both glass and crystalline. A selection of references are given in Table 5.22, categorised under the appropriate co-dopant together with the host material. A reader of any of these articles will find that a thorough study of a particular system constitutes a considerable amount of work. Thus, a totally comprehensive study is outside our scope here. The experimental data described below represent only a small fraction of work necessary. To complete the picture, consequently, it has been necessary to borrow heavily from the literature. All the work which is not original is credited to the appropriate author as it is discussed.

Research into energy transfer in systems containing Tb^{3+} ions is usually concerned with answering one of the following questions:-

1) Whether the total emitted intensity of either Tb^{3+} ions or the co-dopant is usefully increased by the addition of both ions to the host.

2) Whether the relative intensities of the various emission bands of

TABLE 5.22

Energy Transfer References - Transfer Between Terbium (Tb^{3+}) and Other Ions

Ion	Material Containing the Ions	Reference
Ln^{3+}	$NaYWO_4$	5.16, 5.65
La^{3+}	phosphate glass*	5.17
Ce^{3+}	phosphate glass	5.39
	$ScBO_3$	5.53
	various oxides	5.50, 5.45
Pr^{3+}	phosphate glass	5.17
	$NaYWO_4$	5.55
Nd^{3+}	phosphate glass	5.17
	borosilicate glass	5.54
	phosphate and silicate glasses	5.68
	$NaYWO_4$	5.51
Sm^{3+}	phosphate glass	5.17
	$NaYWO_4$	5.52
Eu^{3+}	fused silica	5.27
	phosphate glass	5.17
	phosphate and silicate glasses	5.68
	$NaYWO_4$	5.59
	CaF_2	5.61
Gd^{3+}	borate glass	5.56, 5.57, 5.58
	phosphate glass*	5.17
Dy^{3+}	borosilicate glass	5.54
	phosphate glass	5.17
	$NaYWO_4$	5.60

...../Continued

TABLE 5.22
(Continued)

Ion	Material Containing the Ions	Reference
Ho^{3+}	phosphate glass	5.17
	inorganic glasses	5.67
Er^{3+}	phosphate glass	5.17
	$NaYWO_4$	5.62
Tm^{3+}	phosphate glass	5.17
Yb^{3+}	phosphate glass*	5.17
	silicate glass	5.66
Cu^{+}	phosphate glass	5.39
	$(Sr,Mg)_3(PO_4)_2$	5.63, 5.64
Sn^{2+}	$(Sr,Mg)_3(PO_4)_2$	5.63
Bi^{3+}	various oxides	5.45
Eu^{2+}	phosphate and silicate glasses	5.68
	fused SiO_2	5.69
Tl^{+}	$(Sr,Mg)_3(PO_4)_2$	5.64

* Evidence of energy transfer was not found in these cases.

of one or other of the dopants is altered to give a more nearly monochromatic phosphor (or occasionally a phosphor with emission in a more useful spectral region).

3) Whether a co-dopant can affect the emission decay times.

4) What is the nature of the energy transfer process (multipolar or exchange).

5) Whether the extra absorptivity of a second ion can increase the population inversion of a given transition where materials are used in laser applications.

Only the first two topics will be discussed in this work. Other aspects which might be considered by other workers but to which no reference has been discovered in the literature are:-

1) Whether co-doping can increase the emissivity of rare-earth phosphors at high temperature for applications to hot environments.

2) Related to this, whether co-doping can produce a material with a more temperature-stable emissivity for application as a luminescence standard at differing temperatures.

3) Whether phosphors doped with several ions have better-defined excitation spectra, again for application as luminescence standards.

Details of the specimens prepared for this study are given in Chapter 3. Note that care was taken not to cross-contaminate specimens and that, in general, the purity of the chemicals used in their preparation was higher than those used to melt the NS glasses referred to in this Chapter. Also, only binary glasses were melted, and

equimolar quantities of all metal oxides added to the glass were used. These steps were taken in order to simplify the study as far as possible. The study of more complex systems must be left until a working understanding of interactions between two dopants is achieved.

The molar concentration of lanthanide ions included in the singly doped glasses was the same in each case. The concentration chosen was approximately 0.5 mole % as it was at about this concentration that energy transfer between pairs of Tb^{3+} ions was found to become significant. The doubly doped glasses were chosen to have this concentration for each ion.

Table 5.23 is a resumé (taken from the literature) of energy transfer processes between Tb^{3+} and various co-dopant lanthanide ions in several crystal lattices. Details are included of the ionic separation characteristic of each energy transfer process, the inferred nature of which is also given in this table. Note that these values for ionic separation may be very different in glasses, as the inhomogeneous broadening could radically alter the extent of the overlap between the emission spectrum of the sensitiser and the absorption spectrum of the activator. The data in the table show that the addition of a second ion usually quenches the emission from both the $^5D_3$ and $^5D_4$ band in crystalline phosphors.

The emission of the singly doped glasses was investigated first by using a mercury vapour lamp for excitation and the Optica spectrophotometer. Details are given in Table 5.24, where the distinction is made between cases where no emission was expected and where no emission could be detected in the range of measurement (400 nm to

TABLE 5.23

Quenching or Enhancement of Tb^{3+} (^5D_J) Luminescence

by Other Lanthanide Ions - After Van Uitert (1971)

and Nakazawa and Shionoya (1967)

Lanthanide Ion	Tb $^5D_3$			Tb $^5D_4$		
	r	Transfer	EorQ	r	Transfer	EorQ
Ce^{3+}(a)	6.0	exch	E	6.0	exch	E
Pr^{3+}	12.0	d-q	Q	8.3 (9.4)	d-q	Q
Nd^{3+}	13.6	d-q	Q	14.6 (12.3)	d-q	Q
Sm^{3+}	13.4	d-q	Q	10.7 (7.0)	d-q	Q
Eu^{3+}	9.1	d-q	Q	8.4 (6.9)	d-d	Q
Eu^{2+}(b)	?	exch	Q	?	exch	E
Gd^{3+}(c)	11.0	d-d	E	11.0	d-d	E
Tb^{3+}*	9.1	d-q	Q	(5.3)	exch	Q
Dy^{3+}	14.6	d-q	EorQ	6.6 (4.6)	d-d	EorQ
Ho^{3+}	13.4	d-q	Q	13.1 (11.3)	d-d	Q
Er^{3+}	14.0	d-d	EorQ	13.1 (10.8)	d-d	EorQ
Tm^{3+}	14.0	d-d	Q	8.4 (7.5)	d-d	Q

* Self quenching

E and Q are enhancement or quenching of the emission intensity from the appropriate Tb^{3+} level, respectively

r = interaction distance between sensitiser and activator

d-d = dipole - dipole interaction

d-q = dipole - quadrupole interaction

exch = exchange interaction

Data from ref 5.16, expect those in parentheses - ref 5.17; and (a) ref 5.45; (b) ref 5.61; (c) ref 5.58

TABLE 5.24

Emission Spectra of Singly Doped Lanthanide Glasses in the Range 400 - 690 nm

Lanthanide Ion	Wavelength of Luminescence Peaks (nm)	Relative Intensities	Transition Responsible for the Emission
Y^{3+}	none	-	-
La^{3+}	none	-	-
Pr^{3+}	none detected	-	-
Nd^{3+}	none detected	-	-
Sm^{3+}	542	0.041	$^4F_{3/2} - {}^6H_{5/2}$
	549	0.244	$^5G_{5/2} - {}^6H_{5/2}$
	601	1.000	$^4G_{5/2} - {}^6H_{7/2}$
Dy^{3+}	436	0.010	$^4G_{11/2} - {}^6H_{13/2}$?
	483	0.377	$^4G_{9/2} - {}^6H_{15/2}$
	575	1.000	$^4F_{9/2} - {}^6H_{13/2}$
Er^{3+}	none detected	-	-

690 nm). Level assignments have been made by comparison with details given in the literature (see Table 5.22).

Table 5.25 is a summary of the emission properties of the doubly doped glasses with those of singly doped terbium glass. This table compares the emission intensity of the most intense Tb^{3+} emission band (at 542 nm) for each of the glasses studied. Thus, for example, the glass doped with twice the standard Tb^{3+} ion concentration (i.e., 0.974 mole %) has an emission intensity 4.11 times that for the standard terbium glass (i.e., 0.487 mole %). The table also gives values for the ratio of intensities at 542 nm ($^5D_4$ - $^7F_5$) and 436 nm ($^5D_3$ - $^7F_4$). This ratio for glasses doped with terbium alone was shown earlier to reflect the energy transfer efficiency for the process $^5D_3 \longrightarrow {}^5D_4$. For doubly doped glasses this may also be the case, but the ratio may also be increased by energy transfer from the $^5D_3$ level to the co-dopant ion, or by energy transfer from the co-dopant ion to the $^5D_4$ level.

Further discussion will be related to the individual systems, the energy levels for which have been represented diagrammatically in Figure 1.3. Some further detail from the literature on Gd co-doped glasses is included; these were not studied here.

The Systems Tb,Y and Tb,La

The emission spectra of terbium glasses co-doped with either yttrium or lanthanum were not found to differ significantly from the singly doped terbium glass, either in terms of total luminescence output or relative output from the two metastable levels $^5D_3$ and $^5D_4$.

TABLE 5.25

Comparative Emission Intensities of

Various Co-Doped Lanthanide Glasses

Dopant Ions	Relative Emission at 542 nm (Relative units)	Ratio of Intensities $\frac{^5D_4 \text{ (542 nm)}}{^5D_3 \text{ (436 nm)}}$
Tb^{3+}, Y^{3+}	0.98	2.36
Tb^{3+}, La^{3+}	0.90	2.27
Tb^{3+}, Pr^{3+}	4.63	10.64
Tb^{3+}, Nd^{3+}	0.35	1.08
Tb^{3+}, Sm^{3+}	0.55	1.56
Tb^{3+}	1.00	2.42
Tb^{3+}, Tb^{3+}	4.11	6.23
Tb^{3+}, Dy^{3+}	0.55	1.58
Tb^{3+}, Er^{3+}	0.86	1.81

Thus, it is concluded that there is no significant energy transfer in these systems. This is not unexpected, as the first excited states of La^{3+} and Y^{3+} are f - d transitions which are at much higher energies than those being studied here (5.34).

The System Tb, Pr

Although no emission spectrum could be detected for NS glass containing Pr^{3+} alone, the addition of praeseodymium to terbium containing glass had a pronounced effect on the luminescence. Reference to Table 5.25 indicates that both the absolute intensity of the green emission bands and the intensity of these bands relative to the blue emission peaks was increased. The effect was to produce an emission spectrum similar to that of NS glass containing about 1.3 mole % of Tb^{3+} ions while the glass actually contained about 0.95 mole % of Ln^{3+} ions. This then is a definite case of energy transfer enhancing the emission of Tb^{3+} ions and was the only case discovered in this work. Further, the total emission on addition of Pr^{3+} ions was greater than that produced by addition of a similar amount of terbium. This is important in terms of cost efficiency, as praeseodymium is considerably cheaper than terbium oxide at similar purity levels.

The behaviour outlined above may be contrasted with that of Tb^{3+} and Pr^{3+} doped scheelites, which has been reported by Van Uitert et al (5.55). In these systems the addition of praeseodymium reduces the emission intensity of Tb^{3+} ions. The following energy transfer processes governing the interactions between Tb^{3+} and Pr^{3+} were proposed:-

Transfer Tb⟶Pr

1) $Tb\ {}^5D_3 \longrightarrow Tb\ {}^7F_{0-4}$: $Pr\ {}^3P_{2-0} \longleftarrow Pr\ {}^3H_4$

2) $Tb\ {}^5D_3 \longrightarrow Tb\ {}^5D_4$: $Pr\ {}^3F_3 \longleftarrow Pr\ {}^3H_4$

3) $Tb\ {}^5D_3 \longrightarrow Tb\ {}^5D_4$: $Pr\ {}^3F_2 \longleftarrow Pr\ {}^3H_4$

4) $Tb\ {}^5D_4 \longrightarrow Tb\ {}^7F_4$: $Pr\ {}^1D_0 \longleftarrow Pr\ {}^3H_4$

5) $Tb\ {}^5D_4 \longrightarrow Tb\ {}^7F_6$: $Pr\ {}^3P_0 \longleftarrow Pr\ {}^3H_4$

Transfer Pr⟶Tb

6) $Pr\ {}^3P_0 \longrightarrow Pr\ {}^1D_2$: $Tb\ {}^7F_4 \longleftarrow Tb\ {}^7F_6$

7) $Pr\ {}^1D_2 \longrightarrow Pr\ {}^1G_4$: $Tb\ {}^7F_0 \longleftarrow Tb\ {}^7F_6$

8) $Pr\ {}^1G_4 \longrightarrow Pr\ {}^3F_{4-2}$: $Tb\ {}^7F_5 \longleftarrow Tb\ {}^7F_6$

Evidently, to enhance the terbium emission a further process must exist. Possibly such processes are:-

$Pr\ {}^3P_2 \longrightarrow Pr\ {}^3H_5$: $Tb\ {}^5D_4 \longleftarrow Tb\ {}^7F_6$

$Pr\ {}^1I_6 \longrightarrow Pr\ {}^3H_4$: $Tb\ {}^5D_4 \longleftarrow Tb\ {}^7F_6$

$Pr\ {}^3P_1 \longrightarrow Pr\ {}^3H_4$: $Tb\ {}^5D_4 \longleftarrow Tb\ {}^7F_6$

Evidently this is an example of inhomogeneous broadening producing very different energy transfer properties in glassy materials.

The System Tb, Nd

This system behaves conversely to that just described, in that the green emission bands of Tb^{3+} ions are significantly quenched by the addition of Nd^{3+} ions. Also, the ratio of the intensities of the green emission ($^5D_4$) to the blue emission ($^5D_3$) was much lower

than any previously observed, so that the luminescence was distinctly bluish. Again, emission bands due to 4f transitions of the co-dopant ion (Nd^{3+}) were not detected.

Van Uitert et al have also described the energy transfer properties of Tb^{3+} and Nd^{3+} in tungstates (5.51). These workers also found quenching of the Tb^{3+} ion emission on addition of neodymium. The proposed energy transfer scheme was:-

Transfer Tb ⟶ Nd

1) $Tb\ {}^5D_3 \longrightarrow Tb\ {}^7F_{2-3}$: $Nd\ {}^4G_{11/2-9/2} \longleftarrow Nd\ {}^4I_{9/2}$

2) $Tb\ {}^5D_3 \longrightarrow Tb\ {}^5D_4$: $Nd\ {}^4I_{15/2} \longleftarrow Nd\ {}^4I_{9/2}$

3) $Tb\ {}^5D_4 \longrightarrow Tb\ {}^7F_4$: $Nd\ {}^2G_{7/2}$ (or ${}^4G_{5/2}$) $\longleftarrow Nd\ {}^4I_{9/2}$

4) $Tb\ {}^5D_4 \longrightarrow Tb\ {}^7F_6$: $Nd\ {}^4G_{9/2} \longleftarrow Nd\ {}^4I_{9/2}$

Transfer Nd ⟶ Tb

5) $Nd\ {}^4F_{3/2} \longrightarrow Nd\ {}^4I_{15/2}$: $Tb\ {}^7F_2 \longleftarrow Tb\ {}^7F_6$

The evidence of this work is that processes '3' and '4' are the most important in determining the energy transfer properties in NS glass. Note particularly that process '4' involves a small energy mismatch in crystals. This mismatch is likely to be much less important in glasses because of the greater widths of the 4f eigenstates caused by inhomogeneities in the glass.

The System Tb, Sm

Sm^{3+} ions were found to produce a yellow luminescence in NS glass. Co-doping with Tb^{3+} ions increased the intensity of this

characteristic emission of samarium by a factor of 5.3, thus producing an intense yellow phosphor. The intensity of the terbium green bands were decreased by a factor of approximately two in the doubly doped glass, while a smaller reduction was also noted for the blue series of emissions.

The luminescence of tungstates doped with terbium and samarium also has been investigated by Van Uitert et al (5.52). A similar net transfer of energy from Tb^{3+} ions to Sm^{3+} ions was found by these workers and attributed to the following multipolar energy transfer processes:-

Transfer Tb ⟶ Sm

1) $Tb\ {}^5D_4 \longrightarrow Tb\ {}^7F_6 \quad : \quad Sm\ {}^4G_{7/2}\ ({}^4I_{9/2},\ {}^4M_{15/2}) \longleftarrow Sm\ {}^6H_{5/2}$

2) $Tb\ {}^5D_4 \longrightarrow Tb\ {}^7F_5 \quad : \quad Sm\ {}^4G_{5/2}\ ({}^4F_{3/2}) \longleftarrow Sm\ {}^6H_{5/2}$

No interactions were proposed for quenching of the $^5D_3$ level of Tb^{3+}. However, one possible interaction is:-

$$Tb\ {}^5D_3 \longrightarrow Tb\ {}^5F_6 \quad : \quad Sm\ {}^4G_{11/2}\ ({}^4K_{11/2},\ {}^4M_{21/2},\ {}^4L_{15/2}) \longleftarrow Sm\ {}^6H_{5/2}$$

The System Tb, Dy

Dy^{3+} ions in NS glass produce a greenish-blue luminescence and addition of dysprosium to terbium containing glass reduces the emission of both parts of the Tb^{3+} spectrum. Again this pair of rare earth ions has been studied by Van Uitert et al (5.60) in tungstates, but the only energy transfer which was found was from Dy^{3+} to Tb^{3+} via the interaction:-

$$Dy\ {}^4F_{9/2} \longrightarrow Dy\ {}^6H_{15/2} \quad : \quad Tb\ {}^5D_4 \longleftarrow Tb\ {}^7F_6$$

The following interaction may be the one responsible for the quenching of the Tb^{3+} ion luminescence in NS glass:-

$$Tb\ {}^5D_3 \longrightarrow Tb\ {}^7F_4 \quad : \quad Dy\ {}^4G_{11/2} \longleftarrow Dy\ {}^6H_{15/2}$$

The System Tb, Er

A small amount of energy transfer was found from Tb^{3+} to Er^{3+} in NS glasses containing these ions. However, only quenching effects were observed, as no emission from the Er^{3+} ions was found in either of the glasses studied. Van Uitert et al (5.62) have determined the following energy transfer scheme for this pair of ions:-

Transfer Tb⟶Er

1) $Tb\ {}^5D_3 \longrightarrow Tb\ {}^7F_6 \quad : \quad Er\ {}^4G_{11/2} \longleftarrow Er\ {}^4I_{15/2}$

2) $Tb\ {}^5D_3 \longrightarrow Tb\ {}^7F_0 \quad : \quad Er\ {}^4F_{5/2} \longleftarrow Er\ {}^4I_{15/2}$

3) $Tb\ {}^5D_4 \longrightarrow Tb\ {}^7F_5 \quad : \quad Er\ {}^4F_{5/2} \longleftarrow Er\ {}^4I_{15/2}$

4) $Tb\ {}^5D_4 \longrightarrow Tb\ {}^7F_5 \quad : \quad Er\ {}^4S_{3/2} \longleftarrow Er\ {}^4I_{15/2}$

5) $Tb\ {}^5D_4 \longrightarrow Tb\ {}^7F_2 \quad : \quad Er\ {}^4F_{9/2} \longleftarrow Er\ {}^4I_{15/2}$

Transfer Er⟶Tb

6) $Er\ {}^4S_{3/2} \longrightarrow Er\ {}^4I_{9/2} \quad : \quad Tb\ {}^7F_0 \longleftarrow Tb\ {}^7F_6$

7) $Er\ {}^4I_{9/2} \longrightarrow Er\ {}^4I_{13/2} \quad : \quad Tb\ {}^7F_0 \longleftarrow Tb\ {}^7F_6$

8) $Er\ {}^4I_{11/2} \longrightarrow Er\ {}^4I_{13/2} \quad : \quad Tb\ {}^7F_4 \longleftarrow Tb\ {}^7F_6$

9) $Er\ {}^4I_{13/2} \longrightarrow Er\ {}^4I_{15/2} \quad : \quad Tb\ {}^7F_0 \longleftarrow Tb\ {}^7F_6$

Evidently the schemes '1' to '5' are more important in NS glass as there is an overall reduction in the terbium luminescence.

The System Tb, Gd

This system was not studied in the present work. However, extensive work has been published by Reisfeld et al (5.58) and by Pearson et al (5.56, 5.57) on energy transfer between Gd^{3+} and Tb^{3+} in borate glass. The addition of 3 mole % of Gd^{3+} ions to borate glass containing 3 mole % of terbium was found by Reisfeld et al to increase the intensity of the Tb^{3+} ion emission bands uniformly by about 60%. The energy transfer mechanism is uncertain but may involve such processes as:-

$$Gd\ {}^6P_{7/2} \longrightarrow Gd\ {}^8S_{7/2} \quad : \quad Tb\ {}^5H_6 \longleftarrow Tb\ {}^7F_6$$

Other Systems Containing Tb

No measurements were made on terbium doped glasses doped with the remaining lanthanide ions and no reports of any such measurements in glass have been found in the literature. The data in Table 5.23 indicate that enhancement of terbium luminescence is unlikely from the other ion pairs. However, no definite conclusions can be drawn as the energy transfer characteristics of doubly doped glasses may be very different from their crystal counterparts (for example, Tb, Pr).

CHAPTER 6

THERMOLUMINESCENCE

6.1 Introduction

Thermoluminescence (hereafter abbreviated as TL) in silicate glasses has found considerable application in dosimetry (6.1). So far, results have mostly been explained empirically, and little work has been done on amorphous materials containing an ion which acts as an activator in photoluminescence. However, a terbium doped glass has been developed as a γ-ray dosimeter (6.2).

X-ray irradiation of many glasses (6.3) and crystalline materials (6.4) generally produces defects with visible absorption. Such solarisation was found to impart an orange-brown coloration to both NS and LAS glasses.

The X-ray induced TL of silicate glasses, doped with terbium and other rare earths, was studied in order to understand the effectiveness of such materials in dosimetry. Energy transfer processes between rare earth ions can be a very efficient process in photoluminescence. Thus there was no a priori reason to suppose that such effects would not be important in TL.

In other words, if on heating, the energy stored in the material at certain defect centres is transferred to the Tb^{3+} ions, emission may occur in the bands characteristic of the lanthanide. In general the emission would then be in much narrower bands, and, in the case of terbium, in the green region of the spectrum ($^5D_4$ to $^7F_{6,5,4}$ transitions). This spectral region is very convenient for photomultiplier detection in

glow curve measurements.

The overall efficiency of TL, η, may be loosely defined as:-

$$\eta = \frac{\text{the integrated area under the glow curve}}{\text{the total energy input of the X-rays}}$$

Increased efficiencies mean that lower dose rates can be determined, and higher dose rates can be estimated more easily.

The efficiency of TL is usually low, as most of the X-ray input is not converted into TL. The glasses were found to be quite transparent to X-rays at the thicknesses studied (a few mm). The overall efficiency will also be decreased by competitive processes such as X-ray excited luminescence and the non-radiative de-excitation of damage centres.

Thus, TL measurements were also made to gain some information on these defects, and to try to ascertain if they are affected by the inclusion of rare earths into the matrix.

A further possible application of work of this nature is in the field of laser physics, where the solarisation of laser end windows is undesirable. If the discolouring processes can be fully understood, this would mean improvements on present-day performances of high-powered lasers (6.5).

6.2 Optical Absorption by X-ray Irradiation of Silicate Glasses

The optical absorption of various silicate glasses after X-ray irradiation was measured on a Unicam SP 800 spectrophotometer. The samples used were typically 0.3 cm thick and were irradiated for a period of 24 hours at room temperature with X-rays from a cobalt target,

the tube operating at 15 mA, 20kV.

Little difference was found in the absorption due to solarisation in NS or LAS glasses, either undoped or doped with terbium (both glasses) or gadolinium (LAS glass only). The resulting absorption spectrum for a typical glass is shown in Figure 6.1.

The principal feature is a large absorption band in the blue region of the spectrum. The effect is to bring the absorption cut-off of the un-irradiated glass to longer wavelengths. The cut-off begins at about 450nm instead of 380nm or less. (The latter value depends upon the type of glass.)

Little difference was found between samples due to variations of their thickness, as the solarisation is essentially a 'surface' phenomenon. The brown colour was only visible, to the naked eye, to a depth of perhaps $\frac{1}{2}$mm.

Similar results have been reported by Stroud (6.5) for X-ray induced optical absorption in sodium silicate glasses containing cerium. Stroud attributed the strong absorption band (the f_1 band) and a "tail" of weak absorption extending to about 600nm (the f_2 band) to trapped electron centres. Their production was shown to be little affected by the concentration of trivalent cerium (Ce^{3+}) which would preferentially capture holes, and reduce the absorptivity.

The second feature of the absorption spectra is the enhancement of the peaks A and B, which were referred to in Chapter 4.2.3. They are about ten times more intensely absorbing than those observed in un-irradiated samples. These absorptions are at about 660nm and 440nm respectively, and are superimposed upon the absorption of the trapped

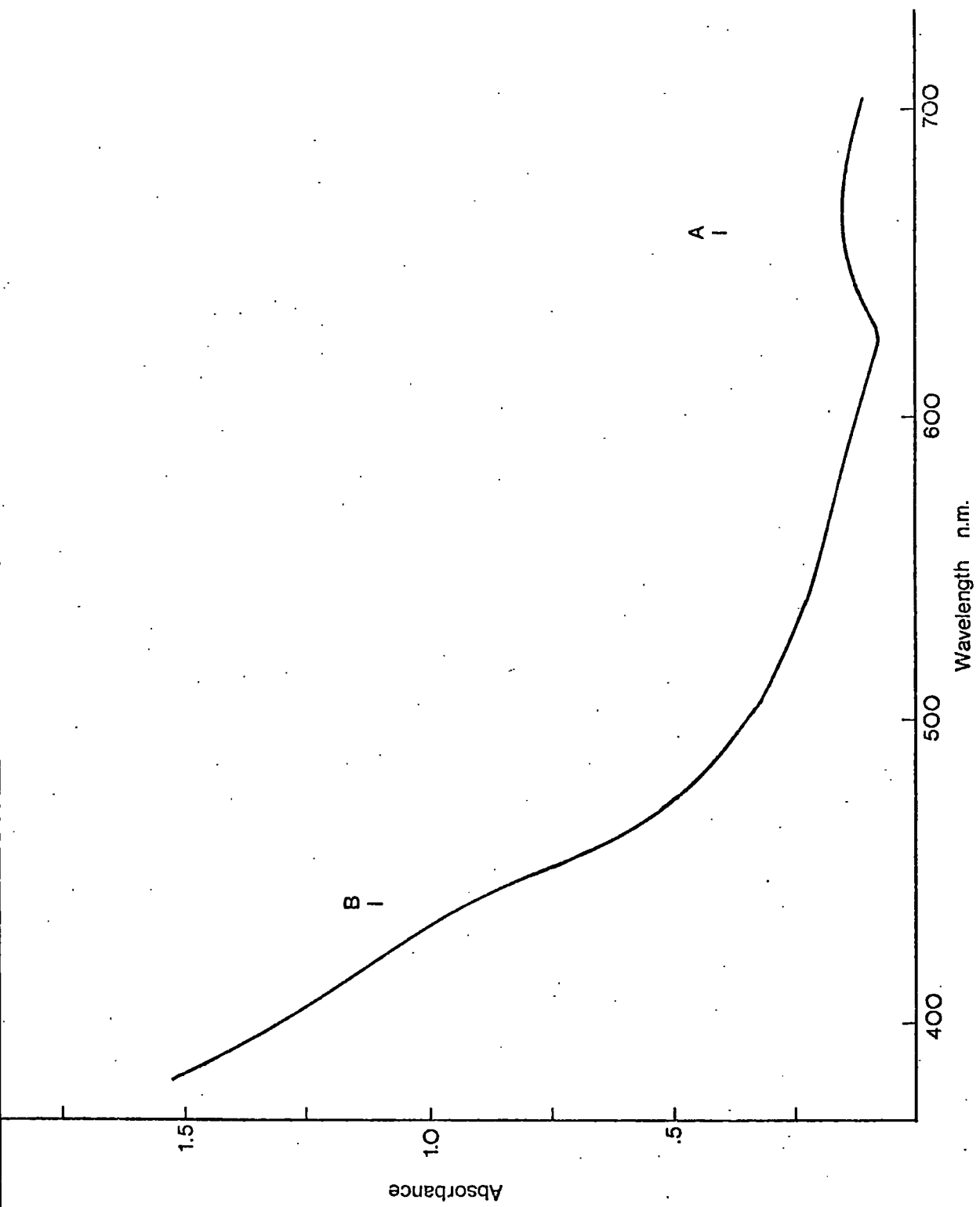

Fig 6.1 Optical absorption spectrum characteristic of silicate glasses after a 24-hour period of X-ray irradiation

holes.

These absorption bands were also reported by Stroud and were attributed to trapped hole centres (6.7). The absorption bands are inhibited by increased cerium concentration. This was shown by Stroud to be due to Ce^{3+} ions capturing holes to form Ce^{3++} centres, which are similar to, but not identical with, Ce^{4+} ions (6.8). Such effects are not observed in terbium glasses, probably because the charge transfer band of terbium ions lies at much higher energies (above at least $50,000\,cm^{-1}$).

The solarisation in all silicate glasses may be attributed to the production of similar trapped electrons and holes, but the position of these centres with respect to the valence and conduction bands of glass is uncertain.

The optical absorption bands observed as a result of X-ray irradiation of silicate glasses are summarised in Table 6.1.

The absorption was completely bleached after heating the samples to above 600°C and was reproducible if the specimen was re-irradiated.

6.3 Glow Curve Characteristics

TL glow curves were measured using the techniques outlined in Section 3.3. Although, in principle, irradiation could be carried out at any temperature within the working range of the equipment (100°K to 600°K), all measurements were made after irradiation at about 100°K (the minimum temperature obtainable by cooling with liquid nitrogen) and at room temperature (~300°K).

On occasion "false" peaks appeared slightly above the tempera-

TABLE 6.1

X-ray Induced Absorption in Silicate Glasses

Absorption Band dentification due to Stroud, References 6.6, 6.7)	Absorption Wavelengths
Trapped holes A	peaks at 660nm
Trapped holes B	peaks at 440nm
Trapped electrons f_1	450nm to 600nm
Trapped electrons f_2	< 450nm
Conduction band-edge of glass	< 380nm *

* This depends very much on the glass type

ture of irradiation, due to the thermal annealing of trapping states in near thermal equilibrium. This was overcome for peaks at just above room temperature simply by referring to the low temperature TL.

Since this work is principally concerned with the applications of rare earth doped glasses, the work was concentrated on TL after irradiation at room temperature. Also, because of the more general application of silicate glasses in dosimetry (6.1), only these glasses were studied. In particular, the characteristics of binary silicate glasses (NS) are compared with those of LAS glasses.

Typical glow curves are shown in Figure 6.2 and were found to have similar peaks for both NS and LAS glasses. However, it was noted that the LAS glasses had slightly narrower peaks, and the base glass had a luminescence output more than 100 times greater than the NS glass. These points are considered further in the discussion section (section 6.9).

The positions of the peaks of the glow curves varied but slightly for Gd^{3+}, Nd^{3+} and Tb^{3+} in LAS glass, and also for Sm^{3+}, Dy^{3+} and Tb^{3+} in NS glass. The results are not entirely consistent : variations in glow peak intensities were about 5% in similar experiments on the same sample. The differing results for the several lanthanides (except Nd^{3+}) were within this level of fluctuation.

The position of the glow peaks for NS and LAS glasses are given in Table 6.2. They are very similar to the results reported in the literature for quartz and fused silica (Halperin et al, reference 6.9, Medlin, reference 6.10, Kikuchi, reference 6.11). In particular, there is an approximate agreement for the large glow peak at about

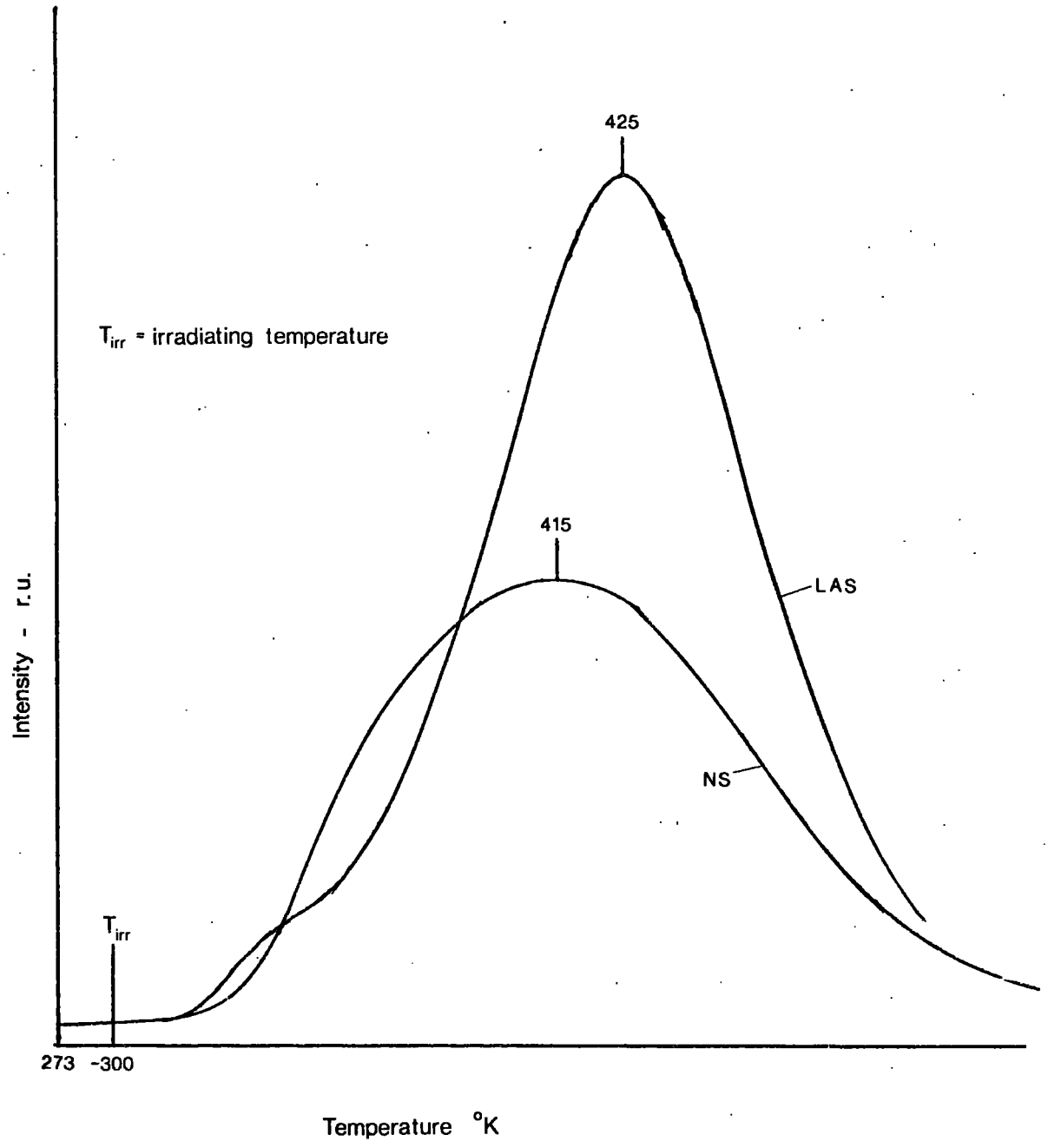

Fig 6.2 Typical room temperature thermoluminescence glow curves for NS and LAS glasses

TABLE 6.2

Details of Glow Peaks Observed in Silicate Glasses and Comparison with Results in Other Silicate Materials from the Literature

Silicate Material	Position of Thermoluminescence Peaks °K (± 3°K) and Estimate of Trap Depths in eV (in brackets)						
LAS Glass	----	185 (0.41)	250 (0.56)	345 (0.77)	425 (0.94)	----	----
NS Glass	175 (0.39)	205 (0.46)	----	----	415 (0.92)	----	----
Data from various forms of SiO_2 (after Medlin, 1963, Ref 6.10)	165 (0.37)	----	260 (0.58)	350 (0.78)	----	----	----
	165 (0.37)	----	260 (0.58)	350 (0.78)	----	500 (1.11)	600 (1.33)
	190 (0.42)	210 (0.47)	260 (0.58)	350 (0.78)	----	500 (1.11)	600 (1.33)

170°K.

The depths of the traps associated with the various peaks were estimated from the equation (see equation 2.118):-

$$E = k T_m \ln \left[\frac{b T_m}{\beta} \right] \qquad (6.1)$$

and are also given in Table 6.2.

The frequency factor, b, is taken as $\sim 10^9$ sec^{-1} (6.12), so that a very approximate form of equation 6.1 may be written:-

$$E(eV) \approx \frac{T_m (°K)}{450} \qquad (6.2)$$

No attempt has been made to determine the value of the activation energy more accurately as, in any case, it is probable that there is a distribution of trap depths in glass.

For the low temperature irraditation of the glasses, the most intense peak was found at 165°K to 185°K, and the intensity of peaks above 300°K was very small. However, if the samples were irradiated at room temperature, the intensity of the peaks above 300°K was increased.

This implies that, at low temperatures:-

(a) the filling of traps is a competitive process, and the shallower traps are preferentially filled.

(b) there is little interaction between the populations of these two types of trapping centre. If there were, the deeper traps would be filled at the expense of the shallower traps on thermal annealing.

6.4 Saturation of Trapping Centres

In general, the intensity of the glow curve maximum increases with the length of the irradiation period. However, after a suitable period, the TL intensity will not increase greatly with higher dose levels because there is a limit to the number of trapping centres which can be filled. Eventually the density of traps will saturate, so that the TL output will be insensitive to further irradiation. The saturation level is a function of both the maximum number of traps which can be filled and the extent to which the defects are in thermal equilibrium at the temperature of formation.

The variation of TL intensity of the main peak above room temperature (~420°K) with the irradiation period was determined for several silicate glasses. This peak was chosen as it is the one most likely to find application in dosimetry.

The results are shown graphically in Figure 6.3 for the 2.88 mole % Tb^{3+} in NS sample, and in Figure 6.4 for the 0.364 mole % Tb^{3+} in LAS glass. The curves are very similar, and saturate after an irradiation period of approximately four hours. As before, irradiation was with X-rays from a cobalt target, the tube operating at 15 mA, 20kV.

Little difference was observed between NS and LAS glasses, but the TL did saturate more quickly for samples with higher terbium concentration. Similar saturation curves were reported by Palma and Gagosz (6.3) in fused silica.

The density of filled traps can be estimated from the absorption spectrum from the relationship (see ref 6.13):-

$$N \sim 10^{16} . \Sigma_o \Delta E \qquad (6.3)$$

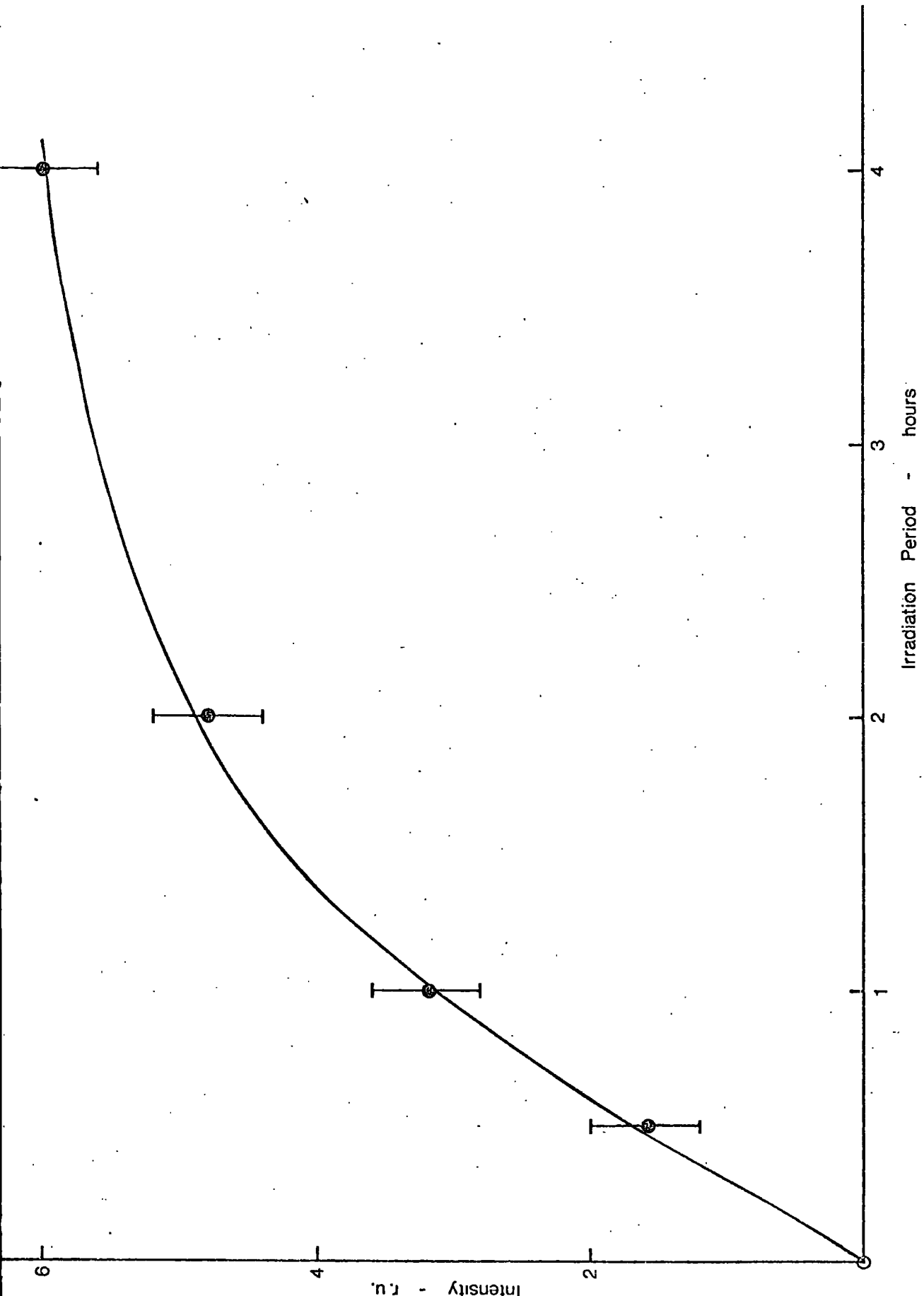

Fig 6.3 Glow peak intensity as a function of irradiation period, 2.88 mole % terbium in NS glass

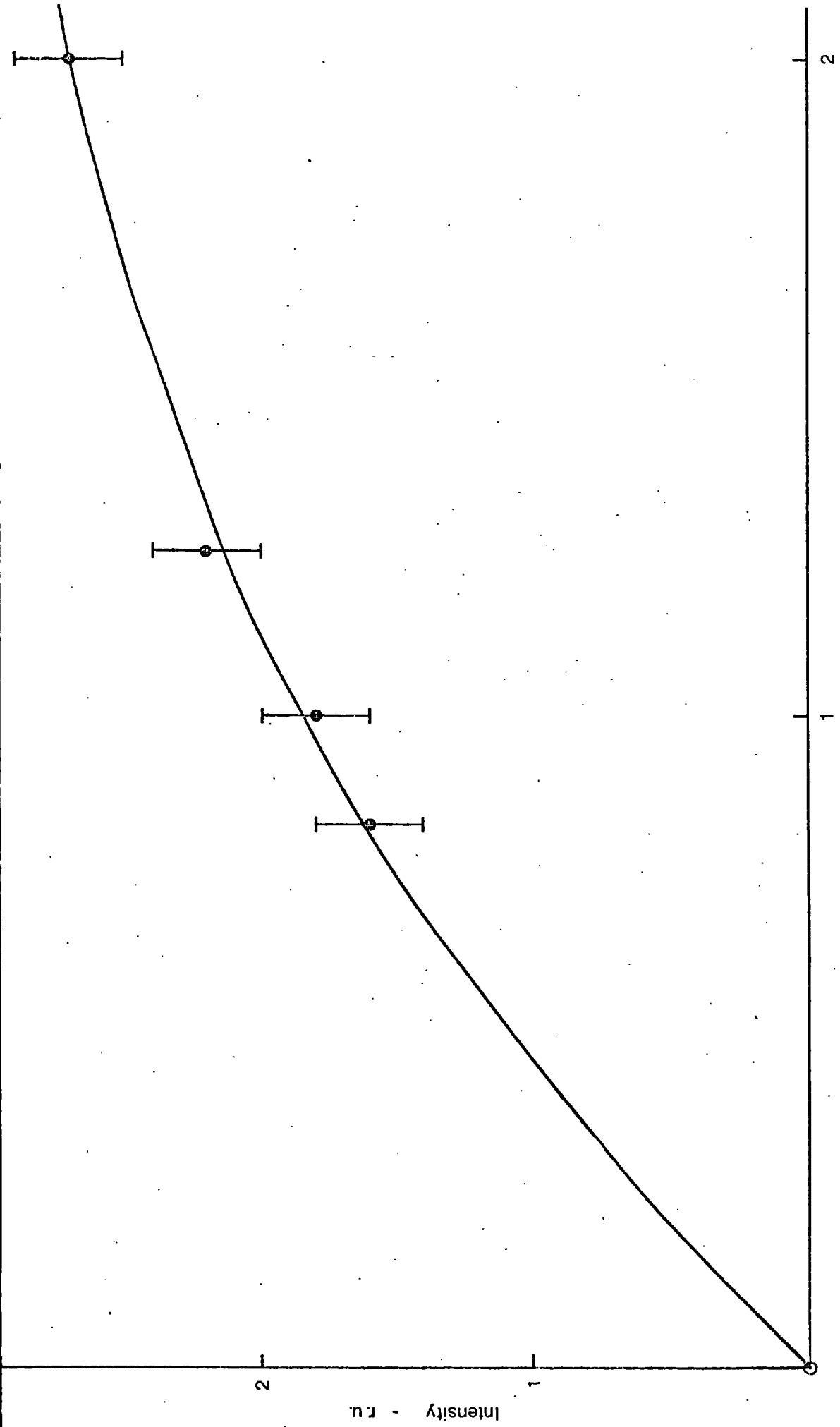

Fig 6.4 Glow peak intensity as a function of irradiation period, 0.364 mole % terbium in L A S glass

where N (cm^{-3}) is the density of a single type of electron trap, ΔE(eV) is the width of the absorption band, and Σ_o (cm^{-1}) is the maximum absorbance per unit thickness.

ΔE is of order a few eV (say 1 eV) and the absorbance is of order, say, 1 cm^{-1}, so that

$$N \sim 10^{16} \text{ cm}^{-3} \qquad (6.4)$$

Thus there is a large average separation between traps (~300Å), and this justifies the assumption of isolated defect centres, with little interaction between them.

6.5 Effect of Rare Earth Doping on Glow Curves

As was outlined in section 6.3, the position of the peaks in the glow curves varied little between samples containing different rare earth oxides and undoped samples. However, there was a marked reduction in the intensity of the room temperature TL with increasing lanthanide ion concentration.

Figure 6.5 shows the dependence of the intensity of the glow peak at 415°K in NS glass on terbium concentration. The TL efficiency was found to decrease logarithmically with the concentration of Tb^{3+} ions if the irradiation period was half an hour. Similar results were found for longer exposures to X-radiation.

Figure 6.6 shows the dependence of the TL intensity at 425°K in LAS glasses doped with terbium. Here the Y-axis of the graph (intensity) is also plotted logarithmically so that the reduction in TL efficiency is even more pronounced. A slightly more pronounced effect

Fig 6.5 Glow peak intensity as a function of terbium concentration in NS glass, half-hour irradiation period

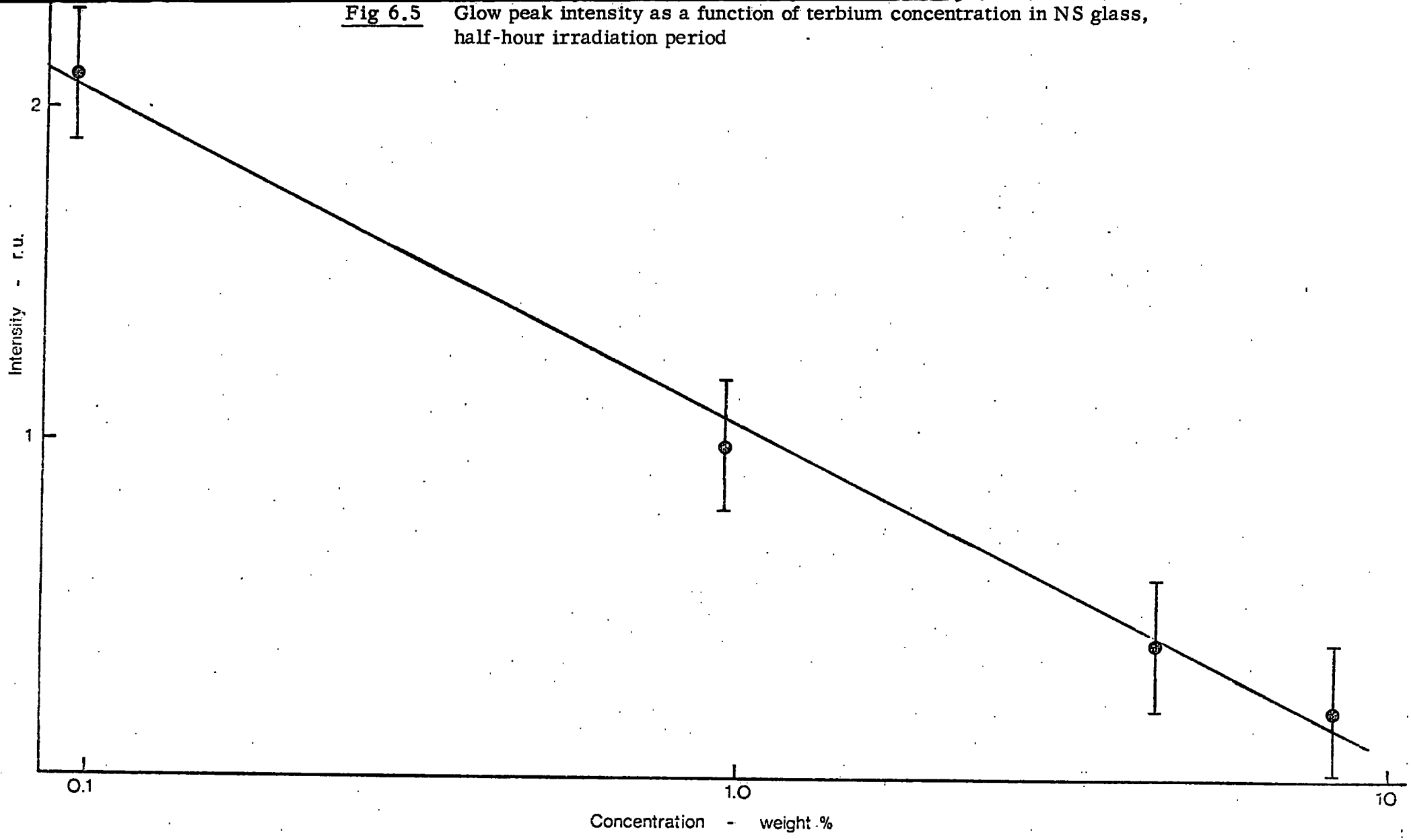

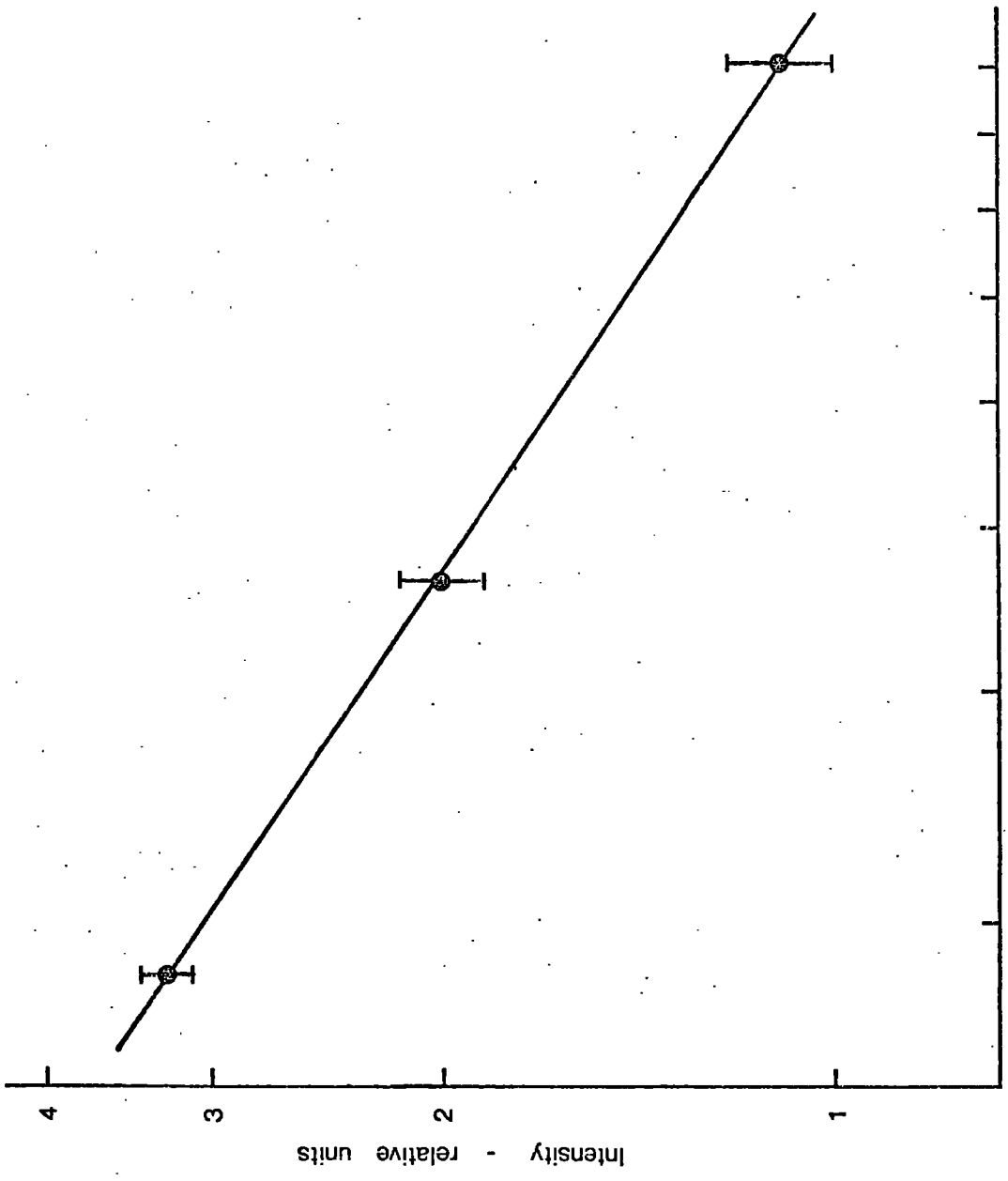

Fig 6.6 Glow peak intensity as a function of terbium concentration in L A S glass, half-hour irradiation period

on glow peak intensity was observed for Nd^{3+} ions in LAS glass.

Similar reductions of glow curve intensity are also reported for the room temperature TL of gadolinium and titanium oxides in LAS glass by Hunt (6.14), who also found that the inclusion of titanium changed the position of the peaks.

Hunt investigated the effect of the base glass composition on TL intensities. In general, an increase of the concentration of alkali metals in the glass reduced the size of the glow peak. This latter result is consistent with the present work, since both rare earth oxides and alkali metal oxides act as network modifiers in a glass matrix.

No direct comparison between the TL efficiency of NS and LAS glasses can be made in terms of network modifier concentrations because of the inclusion in the latter of the intermediate oxide, Al_2O_3. The increased efficiency of the ternary glasses was, in fact, shown by Hunt to be largely due to the aluminium concentration.

6.6 Spectral Distribution of Room Temperature Thermoluminescence

Terbium oxide was added to silicate glasses in the hope that the Tb^{3+} ions would act as TL activators. From the quenching effects described in the previous paragraph, it appears that this is not the case, and that the effect of lanthanide oxides on the emission characteristics is less direct.

To decide whether or not the luminescence is emitted in the typical bands of terbium, the spectral distribution of the TL output was measured. This was achieved by measuring glow curves with various filters in front of the photodetector, as described in Chapter 3.4.

The resulting intensities were corrected for both the percentage transmission of the filters and the spectral response of the photomultiplier tube.

The results for a sample of 0.297 mole % Tb^{3+} in NS glass are shown in Figure 6.7. The wavelength region studied extends from 370nm to 550nm.

A continuous distribution is indicated in the figure, which is all that can be inferred from these results, as the pass bands of the filters used are quite large. Similar results were obtained from LAS glasses containing terbium.

A maximum in the plot shown in Figure 6.7 could be taken to be present at about 550nm, and this would be in approximately the correct position for the most intense transition observed in the photoluminescence of this sample ($^5D_4$ to $^7F_5$). However, in photoluminescence, the peaks at about 415nm and 440nm are almost as intense. Unless, therefore, the efficiency of transfer mechanism between the $^5D_3$ and $^5D_4$ levels of the terbium ions is increased by a factor of about ten (which seems unlikely), it must be concluded that the emission centre is not the lanthanide ion.

This conclusion is borne out, since the same spectral distribution was observed in undoped NS glass. In addition, Hunt (6.14) reports similar results in LAS doped with Gd^{3+} ions. Detailed TL emission spectra are reported by Bettinali and Ferraresso (6.15) in undoped NS glass. These spectra peak at about 520nm and correspond closely with the ultra-violet excited luminescence spectrum of the undoped glass.

Thus, the emission spectrum of the TL is interpreted as the

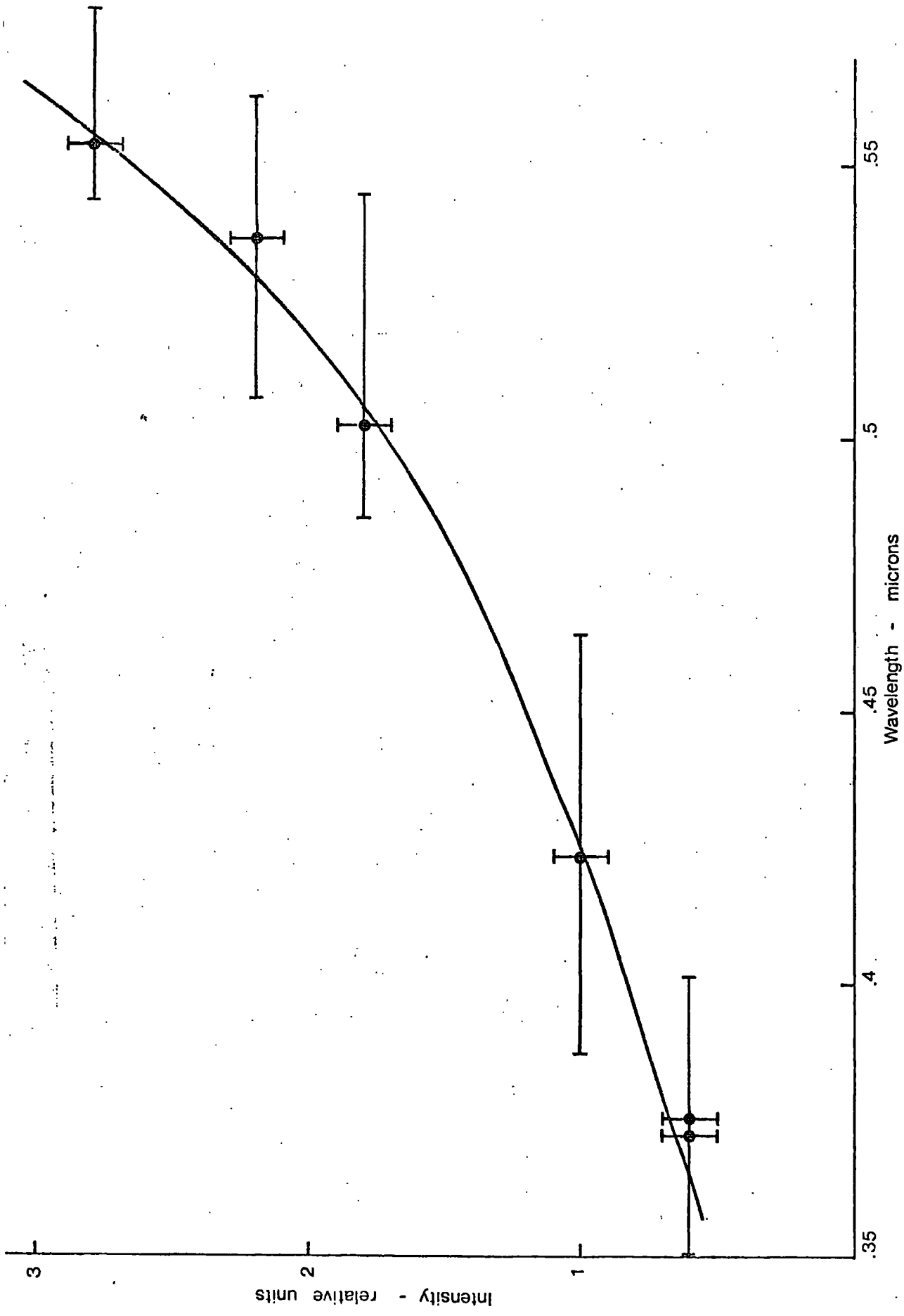

Fig 6.7 Glow peak intensity of thermoluminescence from room temperature as a function of wavelength (through filters) 0.297 mole % terbium in NS glass.

base glass emission spectrum, and not that characteristic of terbium.

A second feature of the observation of glow curves through filters is that the position of the peak shifts to lower temperatures when the blue or ultra-violet components are monitored. The position of the peak of TL glow curves excited at room temperature as a function of wavelength is shown in Figure 6.8. Similar results were obtained in both NS and LAS glasses.

The effect can be explained by, firstly, assuming that NS glass, as well as LAS glass, has a second peak at around 350°K. The generally slightly wider glow curve, typical of NS glasses, may then obscure this peak.

This would mean that the TL emission spectrum of silicate glasses is divided into two bands : a blue band from the 350°K peak, and a yellow-orange band from the 420°K peak. This means that the deeper traps have a lower recombination energy.

6.7 Discussion of Results

The choice of rare earth probes as luminescence indicators was made because the photoluminescence emission of these probes persists to quite high temperatures (see Chapter 5). Secondly, when studying the relationship of glass composition with TL efficiency, the effect of rare earth ions on the matrix of the glass is very localised, so that the inclusion of such probes will not greatly affect the overall structure. Also, the rare earths, in general, show a pronounced tendency to become acceptors in energy transfer processes because of their well defined energy levels.

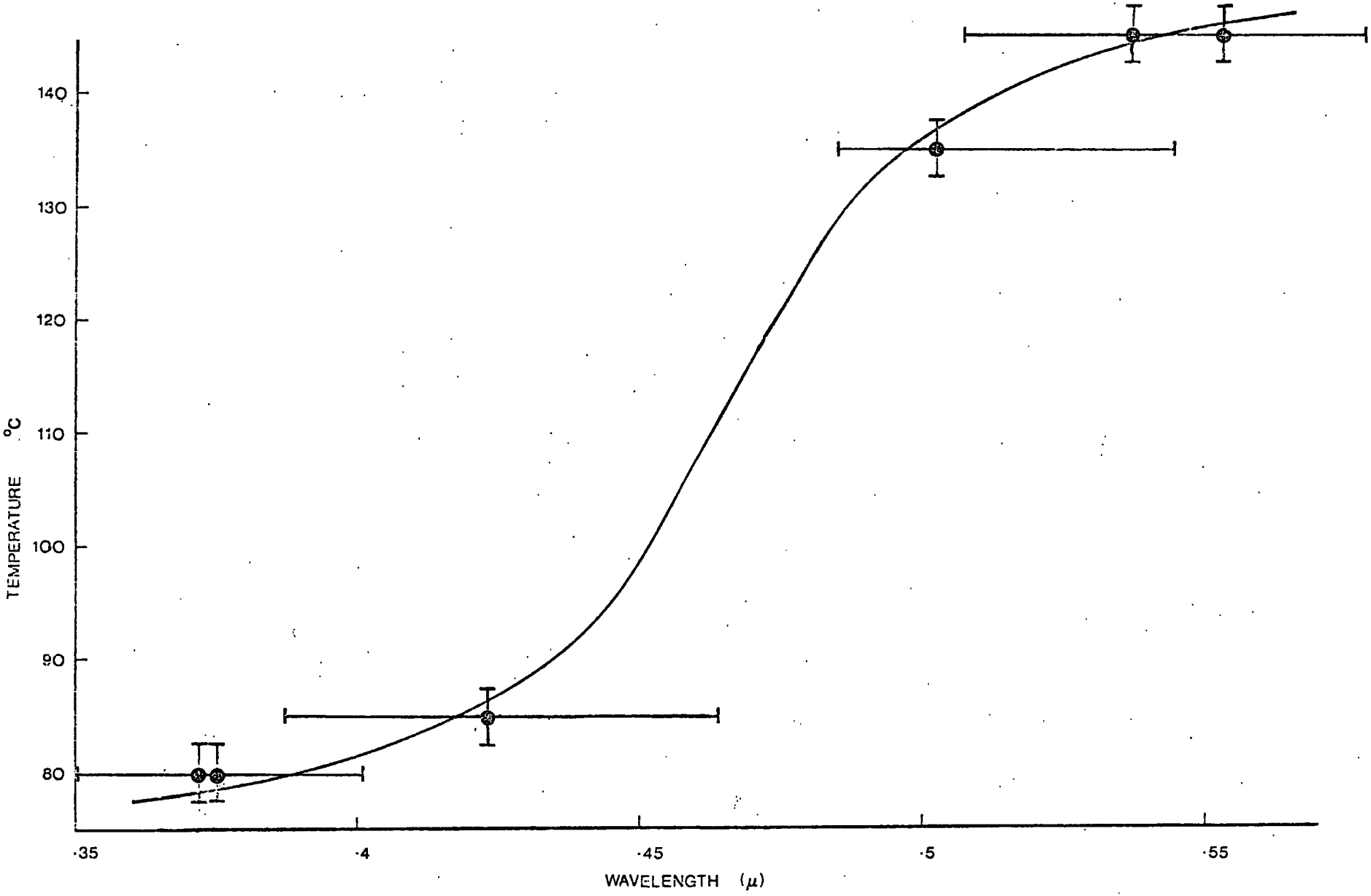

Fig 6.8 Variation of the temperature of the glow peak maximum for themoluminescence from room temperature with wavelength (through filters)

For these reasons, Tb^{3+} ions were included in glass in the hope that transfer processes would enhance the effective TL efficiency by concentrating the emission into narrow bands. However, as was demonstrated earlier in this chapter, this does not happen in practice. Not only does the emission remain in the broad bands characteristic of the glass, but terbium oxide actually quenches the TL output. The reasons for this are now discussed.

The lack of energy transfer to Tb^{3+} activators is evidently due, in part, to the large separation of electron trapping centres even at saturation. A rough calculation, given earlier, shows the average distance between occupied traps to be about 300Å.

Thus, each damage centre is essentially isolated. The concentration of these traps is much lower than the concentration of Tb^{3+} ions, so that, even if there were 100% efficient transfer of energy to the rare earth ions, only a small proportion of the dopant centres would ultimately luminesce.

In addition, perhaps the main reason is that the most intense TL emission is at about 550nm. This is at a lower energy than the lowest luminescent level of Tb^{3+} (the $^5D_4$ level), so that energy transfer can only take place as a phonon assisted process, the cross sections of which are generally very low.

The reason for the reduction of glow curve intensity with terbium concentration is thought to be connected with the fact that terbium oxide acts as a network modifier in inorganic glasses. This is in parallel with the behaviour of oxides such as Na_2O which also quench TL emission.

Before discussing the effect of strongly electropositive ions, such as

Na^+ and Ln^{3+}, on the TL characteristics of a glass, some general indications of the nature of the defects must be deduced. It must be made clear at this stage that only the TL above room temperature will be dealt with in detail here. It has been suggested the low temperature TL is due to the randomness of the O-Si-O bond angle (6.15).

The TL of all silicate glasses above 300°K is thought to consist of two peaks, even though these can not be resolved in the glow curves for NS glass. The peaks are assigned to two electron traps, labelled f_1 and f_2 following the notation of Stroud (6.6).

The TL due to the hole trapping centres (centres A and B) is thought to give rise to the very high temperature glow peaks at around 500°K and 600°K, as seen in quartz (6.10), although this is not observed in silicate glasses.

The f_1 and f_2 centres are defined by Stroud as those absorbing at 450nm to 600nm and <450nm respectively. The absorption due to f_1 centres disappeared between 50°C and 100°C, while the f_2 centres were annealed at temperatures between 100°C and 300°C. Thus the 345°K peak can be identified as due to f_1 centres and the 420°K peak as due to f_2 centres.

The observation of TL through filters showed that in the yellow-orange region of the spectrum the glow peak maximum was at 420°K. Hence it is assumed that the f_2 centres recombine to give emission of wavelength, say, 550nm. Similarly, the blue TL at 345°K implies that the f_1 electrons recombine with the emission of photons at, say, 440nm.

It should also be noted that the more intense of the two glow

curve peaks is the f_2 peak. As expected, the f_2 centres also give rise to the more intense optical absorption. The population, n, of traps at room temperature is thus much larger for the f_2 centres:-

$$n(f_2) > n(f_1)$$

If the TL results from the transition of electrons from the trapping centre to the valence band, a total band scheme can be drawn as in Figure 6.9. In this diagram the transitions labelled E are those resulting in TL emission, while the label T refers to the thermal activation energy (taken from the glow curves). The transitions observed in optical absorption are labelled A and terminate at either an excited state of the defect or the conduction band. The latter is more likely as both absorptions terminate at similar energies above the valence band. Also, the value of 5.5 eV (230nm) corresponds closely with the centre of the conduction band in many silicate materials. Sharma and Riekhoff (6.16) report a strong optical absorption band in glasses at this energy and attribute this to the transition of an electron from a non-bridging oxgyen ion to the conduction band.

By correlating the rate of change of absorption with the thermal glow curves, Bieringer and Montgomery (6.17) were able to demonstrate that, in the case of vitreous silica, the excited level of trapping centres responsible for room temperature TL is, in fact, the conduction band. Measurements of the optical absorption, both as a function of temperature, while heating the samples at a constant rate, and as a function of time at a given elevated temperature, were inconsistent with a model involving bound-bound optical transitions.

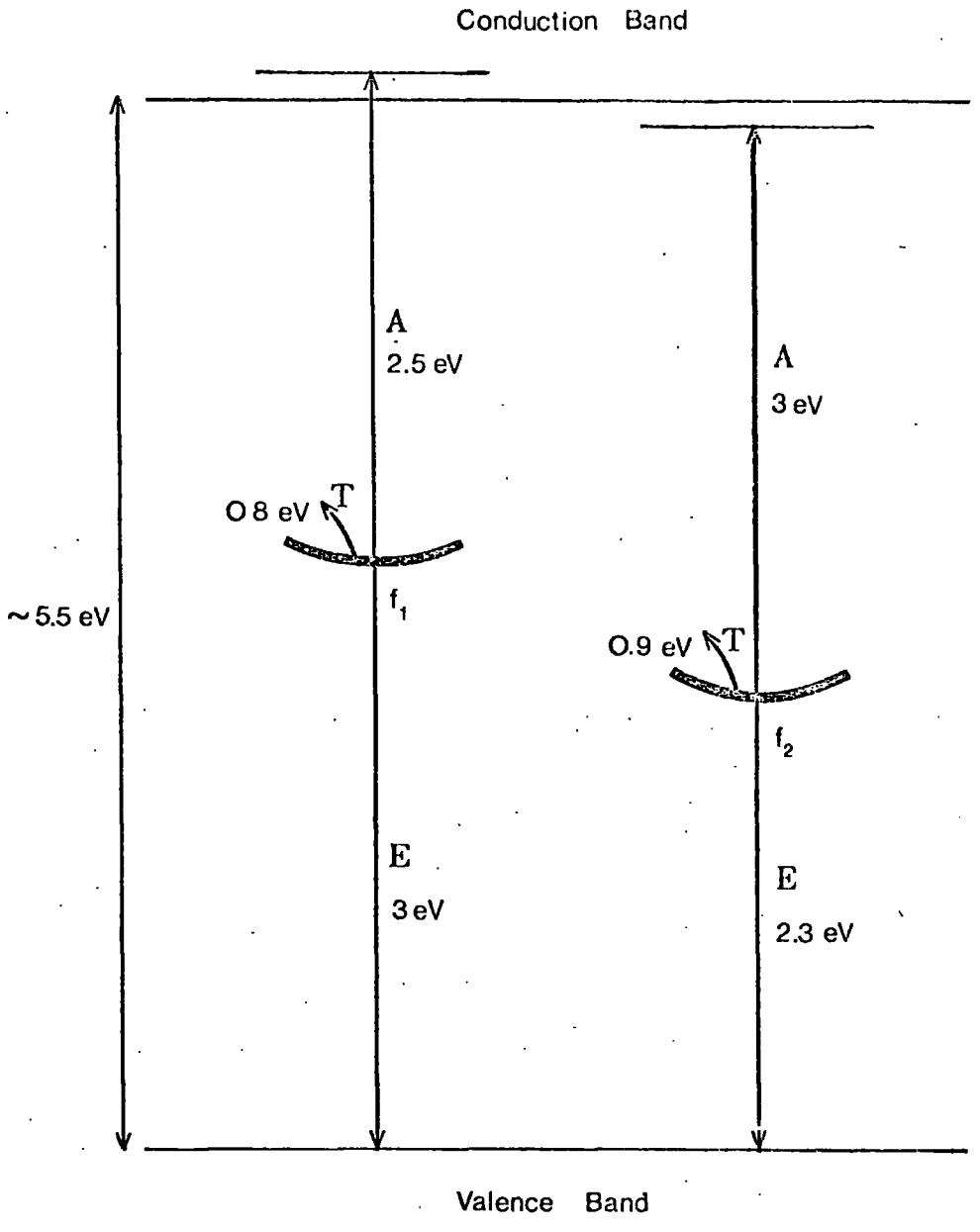

A – absorption processes

T – thermal activation

E – emission

Fig 6.9 Energy level diagram of the f_1 and f_2 centres responsible for thermoluminescence above room temperature in silicate glasses

Thus, it appears that rare earth ions are not directly involved in the TL, so that the inclusion of strongly electropositive ions must in some way, either inhibit the formation of trapping centres, or permit their non-radiative de-excitation.

It is well-known that transition metal ions can give rise to TL quenching because of the existence, within these ions, of energy levels which allow non-radiative decay processes to occur. However, in the case of terbium, such decay processes should be at least partly radiative. Also, the quenching efficiency of terbium is quite large, particularly in LAS glasses.

Further, the addition of a lanthanide oxide to the glass does not greatly affect the optical absorption due to the production of trapping states, if at all. Thus it is unlikely that the cross section for the production of traps is dependent on the terbium concentration.

In order to try to remove this apparent dilemma, recourse must first be made to possible models for the damage centre and the mechanisms of radiative recombination.

The overall similarity of the position of the glow peaks of many materials with a high silicate composition led Barry et al (6.18) to associate the defects with Si-O bonds with non-bridging oxygen ions, which are known to be present even in pure vitreous silica.

There seems to be some confusion in the literature between truly non-bridging oxygen ions, which are interstitial to the network of silica tetrahedra, and metal-ion-associated non-bridging oxygen ions, which link included cations into the glass matrix. Evidently, in both binary and ternary glasses, the latter will be far more prevalent.

It should be noted that the energy of these two types of oxygen ion, relative to the lattice, will in general be quite different.

No estimates have been discovered for the concentration of non-bridging oxygens in pure vitreous silica, but the level is likely to be quite low. The inclusion of M^+ ions (M = Li, Na, K) will reduce the number of true non-bridging oxygens by tending to attract these as ligands. Because of the high viscosity of the silicate melts, however, it is not believed that all of this type of non-bridging oxygens will be removed.

The trivalent lanthanide ions are likely to be more efficient at removing such structures because, being triply charged, they have a higher affinity for these negatively charged ions, to achieve a local charge compensation.

Sidorov et al (6.19, 6.20, 6.21), by a combination of electron paramagnetic resonance techniques and TL measurements, propose a model for the damage site which involves the formation of a trapped hole at a non-bridging oxygen:-

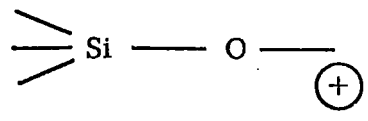

while Schreurs (6.22) proposes models of the type:-

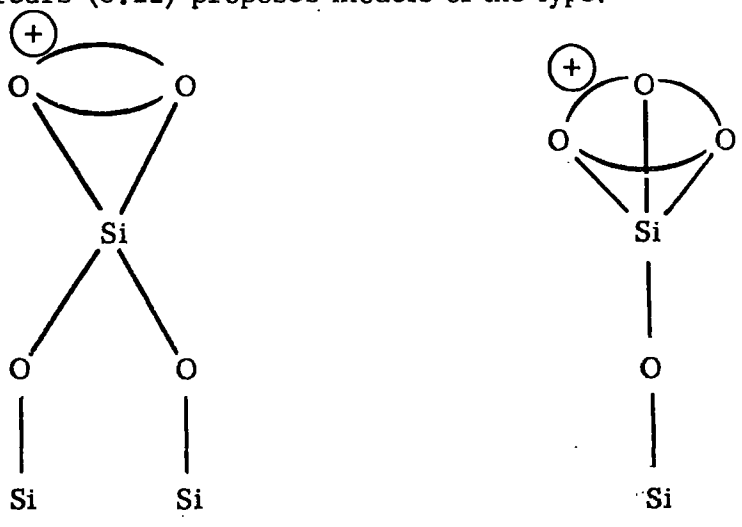

It is likely from evidence of optical absorption that the hole trapping centre, whichever model is applicable, has an associated electron trapping centre, which is relatively shallow and produces the room temperature TL. It is also considered possible that the electron trap may be similar to the F-centres in alkali halides.

The hole traps are likely to be more stable, since they preserve local charge compensation, and could be produced in the melt. Thus, as has been observed, hole traps (A and B) do produce some optical absorption, even in unirradiated samples, and are responsible for high termperature TL ($\sim$500°K and 600°K).

The rate of recombination of electrons and holes will depend on their relative separation and will be a function of temperature.

The site of the electron trap is unknown, but may depend more on the nature of the glass than the hole site. It is proposed that, in glasses with a low proportion of the network modifier, the electrons will remain either at impurity centres or distribute themselves generally at random in the glass. Thus, there is a low probability of electron-hole recombination.

Conversely, in glasses with large concentrations of the network modifier, electrons may be trapped at the positive cation sites. In general the average separation of electrons and holes will be much smaller, so that the probability of their recombination is high.

The evidence of optical absorption is that TL results from the separate de-excitation of the trapping centres. It is likely that simple recombination of electrons and holes does not produce TL. The energy released from the annihilation of an electron-hole pair may be converted

into phonons or produce photons which are subsequently absorbed by the glass.

Thus the effect produced by network modifiers, predicted by this model, is to 'pin' electrons in a site near the production site (that is near the associated trapped hole) so increasing the probability of the de-excitation, which is effectively non-radiative.

Two further points about this theory may be made. Firstly, the proportion of defect centres which will ultimately produce TL will not be completely eliminated, since not all non-bridging oxygen ions will be cation associated. However, the proportion of such sites will be reduced by increasing the metal ion concentration.

Also, the effect of a given ion on the TL will increase with its charge and oxygen co-ordination number. This explains the increased effect of a triply charged ion such as Tb^{3+} over that produced by a singly charged alkali metal ion. The effect of a given lanthanide ion is also expected to decrease with increasing atomic number, as the lanthanide contraction (of ionic radii - see Chapter 1) will tend to reduce the average number of co-ordinated oxygens in this order. The increased quenching of Nd^{3+} ions over that of Tb^{3+} ions may be due to the larger ionic radius of trivalent neodymium.

6.8 Applications in Laser End Windows

The possible applications of rare earth doped glasses to laser technology are twofold. Firstly, the lanthanide glasses (particularly Nd^{3+} doped glasses) find large-scale use as actual lasing materials. This topic is returned to in more detail in Chapter 7. Secondly, the solar-

isation of glasses, which is undesirable in both the lasing rod and the end windows (6.23, 6.24), may be reduced by the inclusion of rare earth ions.

The difference must be emphasised between damage processes associated with undissolved inclusions in the glass and intrinsic damage associated with solarisation. The former is dependent on sample purity and the thermal history of the glass, while the latter is related to the production of electronic trapping centres.

Ginther and Claffy (6.25) reported the existence of TL in glasses subjected to pulses from a neodymium glass laser (at 1.06 microns), but they were unable to correlate the TL with the laser induced damage. However, as has been demonstrated in this work, (see sections 6.2 and 6.5), the glow curve intensity is not directly related to the number of defect centres in the glass, as the optical absorption differs little in glasses with very different TL efficiencies.

If the solarisation damage produced by laser exposure is similar to that observed in this work, then rare earth glasses would be expected to have similar properties to the base glass. Although rare earth ions are seen to reduce the TL intensity of silicate glasses, these ions do not appreciably reduce the optical absorption after irradiation. Thus there is no indication that any of the rare earth glasses would find application here.

6.9 Discussion on the Difference between NS and LAS Glasses

The results from photoluminescence and thermoluminescence experiments - in this chapter and Chapter 5 - showed that there are

several differences between NS and LAS glasses doped with terbium. These are listed below:-

(1) The photoluminescence and TL glow curves are distinctly narrower in LAS glass. This implies that the inhomogeneity of the rare earth ion site is less in the ternary glass.

(2) The X-ray excited luminescence of LAS glasses doped with Tb^{3+} has a long decay period of order 15 minutes. This is not seen in NS glass.

(3) The intensity of X-ray excited luminescence as a function of Tb^{3+} concentration reaches a maximum at much lower concentrations for LAS glass than for NS glass.

(4) The TL glow curve intensity is much higher in undoped LAS glass than in undoped NS glass.

(5) The TL intensity falls off much more rapidly with terbium concentration in LAS glasses than in NS glasses.

These diverse results may be explained by taking a slightly different model for the rare earth ion site in the ternary glass.

In glasses containing only network forming and network modifying oxides, the results of optical experiments are consistent with the site model outlined in Chapter 1. The terbium ions are thought to be co-ordinated by eight oxygens, each of which is part of the network forming polyhedra. Because of the deformation of the bond angles in these polyhedra, all terbium sites are not equivalent, and the resulting spectra (both in photoluminescence and TL) are inhomogeneously broadened.

The effect of introducing the intermediate oxide Al_2O_3 into the glass matrix evidently introduces a higher degree of ordering to the

microstructure. Thus, the terbium environment is affected by the inclusion of Al_2O_3. However, it is not clear whether some of the ligand oxygens of the terbium ions are bonded to Al^{3+} ions rather than Si^{4+} ions, or whether the effect of Al_2O_3 is to introduce a higher ordering into the silicate polyhedra by partially polarising the molecular structure.

The evidence of optical absorption spectra (which are similar in both glass types) is that the co-ordination number of ligand oxygens is unchanged by the inclusion of Al^{3+} ions. Consistent with this is the fact that the line shape of photoluminescent spectra is similar in both binary and ternary glasses.

Larger amounts of Al_2O_3 in the glass would promote crystallisation with consequent higher degrees of ordering. The ternary glasses may thus be considered to approach crystalline ordering with increasing alumina content.

The photoluminescent behaviour of terbium doped LAS glasses again indicates an association of the Tb^{3+} ions with the aluminium content. The long luminescent decay times of terbium in LAS glass are consistent with energy transfer processes occurring between long-lived excited states in Al^{3+} ions and the excited states of Tb^{3+} ions.

Thus, the X-ray luminescence of Tb^{3+} in LAS is thought to be a four-stage process. Absorption, principally at aluminium ion sites, is followed by energy transfer to the terbium ions. The time scale for these energy transfer processes is of the order of several minutes. The Tb^{3+} ions then relax to lower levels ($^5D_3$ and $^5D_4$) which emit the characteristic luminescence in a time scale appropriate to the for-

bidden transitions involved (of order a few milliseconds).

The energy transfer processes are thought to involve energy levels much higher than those which produce the luminescence. The subsequent concentration quenching observed in LAS glasses may then involve the non-radiative de-excitation of these upper levels in a similar manner to the self quenching observed in neodymium glasses (6.26).

The effect of Al^{3+} ions on the TL characteristics of a silicate glass is thought to be somewhat different. If the model of TL kinetics outlined in section 6.7 is correct, then Al^{3+} ions may act as stable trapping centres for electrons. The recombination of electrons and holes, which would reduce the glow curve intensity, is thus inhibited, and the ternary glasses have a much higher TL output.

The inclusion of Tb^{3+} ions in the glass would provide competitive centres for electron capture. As the terbium ions are thought to permit the recombination of electrons and holes, the glow curve intensity will be reduced. Evidently, if this model is correct, the Tb^{3+} ions must have a higher electron affinity and/or be much closer (spatially) to the hole trapping centre (non-bridging Si-O bonds).

The fact that Al_2O_3 is an intermediate oxide implies that it can function, at least partially, as a network former. A corollary of this is that the Si-O-Al bond is not dissimilar to the Si-O-Si bond. This means that Al^{3+} ions will be surrounded by ions which may effectively be regarded as bridging oxygens. Hence, aluminium trapping sites will not be as close as the terbium sites to the hole trapping sites.

The more rapid reduction of TL intensity with terbium

concentration in LAS glasses is thus thought to be caused by the terbium ions providing a recombination process which is more efficient than the separate de-excitation of trapped electrons and holes produced by Al^{3+} ions.

CHAPTER 7

LITERATURE SURVEY AND CONCLUSIONS

7.1 Literature Survey

7.1.1 Faraday Rotation in Terbium Doped Glasses

Of the various magneto-optic effects, perhaps the most widely studied in glasses to date is the Faraday effect. In terms of device potential, glasses have a twofold advantage. The preparation of sizable samples which are optically homogeneous is much easier than for crystals. Also the specimens may be cut without regard to an optic axis, as all axes are equivalent.

The magnetic rotation produced by a material is usually expressed in terms of the Verdet constant, V, which is defined by:-

$$\theta = V H d \qquad (7.1)$$

where θ is the angular rotation of the plane of polarisation of linearly polarised light produced by a longitudinal magnetic field, H, in a sample with an optical path length, d.

Except for small variations near intra 4f transitions of rare earth ions, the Verdet constant varies with the wavelength of light in the visible region of the spectrum and takes the form:-

$$V = K (\lambda^2 - \lambda_t^2)^{-1} \qquad (7.2)$$

The constant, K, is independent of the wavelength, λ, of the incident light, and in general is a function of the effective wavelength, λ_t, of an electric dipole transition. K is also a function of the matrix element, C_t, of the transition, temperature and the concentration of active

ions (7.1). The exact nature of the electronic transition responsible for the magnetic rotation must be determined by experiment.

The wavelength dependence (equation 7.2) corresponds to paramagnetic type rotation (7.2). The expression assumes a single transition is responsible for the rotation. In general, several levels will be involved, but the model still provides a reasonable description if we interpret λ_t as a weighted mean value of all transition wavelengths.

Berger et al (7.3) have investigated the Faraday rotation of all the trivalent lanthanide ions (except Pm^{3+}) in phosphate glasses at room temperature. Metaphosphate glass types of the approximate composition $Ln(PO_3)_3$ were investigated. The results showed no simple relationship for the relative magnitudes of the Faraday effect for differing rare earth ions.

For the terbium glass they found λ_t = 215 nm, which on comparison with absorption data is seen to correspond to the 4f-5d transitions of Tb^{3+}. This is the expected result, because these transitions are the least energetic of the allowed electric dipole transitions of this ion.

Table 7.1 gives values of the Verdet constant measured at various wavelengths. The value for Tb^{3+} is larger than that for most of the other lanthanides, only Ce^{3+}, Pr^{3+}, Dy^{3+} being comparable. With these ions the sign of the Verdet constant is negative, while some other ions give small positive values (for example Gd^{3+}).

If two or more ions are included in the glass, the resultant Verdet constant can be shown to be a linear function of the concentration of the separate ions. The effective Verdet constant is thus:-

$$V = a V_1 + (1 - a) V_2 \qquad (7.3)$$

where a is the mole fraction of the ion with Verdet constant V_1, and the second ion has a Verdet constant V_2.

This linear relationship has been demonstrated for cerium neodymium phosphate glasses. The linearity is a result of the large interionic distances (actually 5.6 Å) and also of the shielding of the 4f electrons in the lanthanide ion by electrons in outer orbitals.

Systems with higher Verdet constants are feasible by increasing the number of Ln^{3+} ions per unit volume, but this would only produce a factor of three or four for the pure oxides (Ln_2O_3).

Since the glass matrix contains no unpaired electrons in the ground state, magnetic rotation associated with the base glass is diamagnetic and hence is small with a positive Verdet constant. Also, since the concentration of the base glass component is essentially the same, any differences in the Verdet constant of various glasses may be attributed to the lanthanide ions.

The increase of the Verdet constant with the number of Ln^{3+} ions per unit volume suggests that larger rotations will be obtained from glasses with smaller glass forming groups. Rubinstein et al (7.4) investigated borate glasses, because the borate group is smaller than the phosphate group. The glasses had the approximate composition $Ln_2O_3.(0.85La_2O_3).4.73B_2O_3$, which is within 5% of the molecular density of the phosphate glasses described above. In the borate system they found $\lambda_t = 225$ nm, which is much the same as in phosphate glass. This, it is inferred, implies that the two glass formers produce similar environments for rare earth ions.

The values of the Verdet constant at various optical wavelengths

are given in Table 7.1, together with the results for a mixed terbium/praseodymium oxide in borate glasses. It will be seen that these values are larger than those for phosphate glasses as expected.

The mixed oxide glass was chosen since Tb^{3+} and Pr^{3+} both have large, negative Verdet constants, while La^{3+} has a (small) positive rotation. This glass has a larger Verdet constant than any of the other glasses investigated.

Borrelli (7.5) examined rare earth-sodium silicate glasses in the region of 700 to 1,100nm. A glass of composition $25Na_2O.75SiO_2$ containing 32 weight % of Tb_2O_3 was found to have a Verdet constant of -0.072 at 700nm. This was the largest of all the rare earths investigated in this system, only Pr^{3+} being comparable. The concentration of this glass is lower than the phosphate and borate glasses cited earlier, but, even on correction for this, the rotation is still smaller for the silicate glass.

By way of comparison, the Corning company manufacture a glass (Code 8363) with a large positive Verdet constant (0.1 at 600nm). This has been taken as a reference material for Faraday rotation (7.6). The rotation produced by the Tb-Pr glass outlined above is nearly an order of magnitude larger.

A terbium ammonium phosphate glass of compostion $30Tb_2O_3.70(NH_4)_2HPO_4$ has been patented (7.7) by the Western Electric Co for use in various devices because of its high Verdet constant.

Rubinstein et al (7.8) measured the Verdet constant of terbium aluminium garnet, and found it to be approximately 1.4 times that in phosphate and borate glasses. The Verdet constant was also increased

TABLE 7.1

The Verdet Constant of Terbium Glasses as a Function of Wavelength, after Berger et al (1964)

Wavelength nm	Verdet Constant Min of arc/cm.Oe		
	Tb^{3+} in Phosphate Glass	Tb-La in Borate Glass	Tb-Pr in Borate Glass
405	-0.560	-0.512	-0.940
420	-0.501	-0.458	-0.836
436	-0.458	-0.419	-0.786
450	-0.419	-0.382	--
465	-0.385	-0.347	--
480	-0.357	-0.319	-0.560
500	-0.323	-0.288	-0.536
520	-0.295	-0.262	-0.489
546	-0.261	-0.234	-0.436
578	-0.226	-0.205	-0.380
600	-0.206	-0.186	-0.348
635	-0.190	-0.167	-0.306
670	-0.164	-0.142	-0.265
700	-0.150	--	--

by a factor of 3.3 on cooling to liquid nitrogen temperatures.

7.1.2 Other Glasses Containing Terbium - Nitrate Glasses

Only glasses based on the oxides of silicon, phosphorous and boron have been studied in this work. This is because these network formers account for almost all commercially produced glasses, and also since they are easiest to manufacture. Little work is reported in the literature on other glass systems.

However, Belyaeva et al (7.9) have recently succeeded in doping nitrate glasses of the composition $40Ca(NO_3)_2.60KNO_3$ with 0.05 to 5 mole % of Tb^{3+}. The base glasses are transparent from 0.35 to 3 microns. The excitation and luminescence spectra were measured. On excitation by the 365 nm line from a mercury lamp, an intense luminescence was found, which showed the characteristic inhomogeneous broadening typical of glasses. The luminescence intensity remained roughly constant from 77°K to 380°K.

7.1.3 Electroluminescence

Cylindrical samples of 1.81 mole % Tb^{3+} in L A S glass were prepared with dimensions of 2mm diameter by 2mm thick. Indium contacts were evaporated on to the ends of the specimen, and various voltages up to 100V were applied. No electroluminescence was detected; which is thought to be due to the very high resistivity of silicate glasses. The current passed by the sample was of the order of a few microamps.

Electroluminescence of various rare earths has been reported in solutions of sodium aluminate ($NaAlO_2$) (7.10). In addition, Heller et al (7.11) give details of the electroluminescence of Tb^{3+} in phosphorous

oxychloride ($POCl_3$) solutions. The emission becomes visible at voltages above 6V dc.

Emission from trivalent terbium in various II-VI compounds was observed by Kahng (7.12) on the application of field strenghts of the order of 10^6 V/cm. The luminescence proceeds via the electron impact excitation of molecular centres. These phenomena are called LUMOCEN (luminescence from molecular centres) effects. The external power conversion efficiency is $\sim 10^{-4}$ at several optical frequencies, including the 548 nm emission line of Tb^{3+}.

Single crystals of ZnS doped with Tb^{3+} ions were prepared by Razi and Anderson (&.13) by vapour transport techniques. The crystals showed the sharp line emission spectrum of the rare earth ion on application of dc voltages. Voltage-current measurements gave evidence of a space charge limited current. Details of decay time measurements were also given.

Dubovik et al (7.14) succeeded in producing electroluminescence from calcium fluoride crystals doped with 0.2 to 2 at % of Tb^{3+}. The intensity of emission was a linear function of current density up to 1,000 mA/cm^2. Kazakov et al (7.15) measured the effect of temperature on the electroluminescent emission of CaF_2:Tb. They found practically no thermal quenching of the luminescence at temperatures of 400°C to 500°C, at which temperatures there is a significant increase in the electrical conductivity without any essential loss in the photoluminescent intensity.

In oxide crystals, very efficient electroluminophors have been reported (7.16) for rare earth doped yttria (Y_2O_3). The efficiency of

crystals doped with 1.5 mole % of Tb_4O_7 was 0.41 and was higher than with the other lanthanide dopants tried (Eu, Gd, Dy). Terbium in gadolinium oxide had an efficiency of 0.15. Rise times and decay times were typically of the order of milliseconds. Nakano (7.17) also reported emission from Y_2O_3:Tb when a small dc voltage was applied together with an ac voltage.

The success of work on semiconductor materials suggests that semiconducting glasses containing terbium may produce efficient electroluminescent phosphors, but no reference to experimentation with such materials could be found in the literature.

7.1.4 Cathodoluminescence

The samples of NS glass containing 2.88 mole % of Tb^{3+} ions were shown, in the present work, to exhibit a strong green luminescence when bombarded with cathode rays. The visual appearance of the emission was very similar to that for photon excitation. The emission was shown to be in the bands characteristic of trivalent terbium by photographing the spectrum produced by a diffraction grating, but quantitative measurements were not made.

Considerable work is reported in the literature on the cathodoluminescence properties of terbium in various media – such as zinc sulphide (7.18, 7.19), alkaline-earth fluorides (7.20), oxychlorides (7.21) and several other crystal matrices (7.22, 7.23, 7.24).

Avella et al (7.25) compare the cathodoluminescence properties of various orthoborate crystals doped with terbium. They investigated systems of the type MBO_3:Tb (with M = In, Y, Sc, Lu, La) and found the highest intensities for indium borate.

On excitation with 15kV electrons, terbium in $InBO_3$ shows little emission from the $^5D_4$ to $^7F_{6,4,3}$ transitions, while the $^5D_4$ to $^7F_5$ transition is very intense. Avella (7.26) presents additional data for $InBO_3$:Tb and compares the properties of this phosphor with a widely used phosphor : Zn_2SiO_4:Mn. Both these materials produce an intense green emission, and they are comparable in efficiency and luminous output.

Similar results were obtained by Peters (7.27) in the investigation of various terbium doped silicate materials. The highest efficiencies were found for Tb^{3+} in lanthanum and gadolinium diorthosilicate ($La_2Si_2O_7$ and $Gd_2Si_2O_7$) and in yttrium oxyorthosilicate (Y_2SiO_5). These phosphors were found to be comparable in luminosity and conversion efficiency to borates and phosphate containing terbium, and were superior to (Zn, Cd)S:Ag in their performance at high current densities.

The data given by Avella and Peters are summarised in Table 7.2 and are compared with the values for some commercially available phosphors. The CIE colour co-ordinates (7.28) are also listed; for terbium phosphors they are typically x = 0.33, y = 0.60.

Cathodoluminescence spectra of Tb^{3+} in strontium phosphate ($Sr_3(PO_4)_2$) are reported by Bril et al (7.29). The emission was bluish-white because of a significant contribution to the luminescence from the $^5D_3$ to ^7F_J transitions. Decay times of the order of 6ms were measured for these materials.

Gavrilenko et al (7.30) measured the cathodoluminescence spectra of silicate and borate glasses doped with from 0.1 to 10 weight % of Tb_2O_3. In silicate glasses, the shortwave ($^5D_3$) bands disappeared

TABLE 7.2

Comparison of the Cathodoluminescent Properties of some Terbium Doped Phosphors with some Commercially Produced Phosphors, after Avella (1966) and Peters (1969)

Phosphor	Relative Luminosity	Decay to $I_o/10$ (m sec)	CIE colour co-ordinates		Lumen equivalent (Lumen/rad watt)
			x	y	
$Zn_{0.72}Cd_{0.28}S$:Ag	100	0.05	0.27	0.62	500
Zn_2SiO_4:Mn	60	15.00	0.22	0.71	540
Y_2O_3:Tb	15	--	--	--	--
$InBO_3$:Tb	65	15.00	0.31	0.66	610
$3CaO.B_2O_3$:Tb	25	4.00	0.32	0.63	550
YBO_3:Tb	20	5.00	0.31	0.64	570
MBO_3:Tb (M = Sc, Lu, Gd, La)	15	--	--	--	--
$La_2Si_2O_7$:Tb	45	7.00	0.32	0.61	530
$Gd_2Si_2O_7$:Tb	40	7.00	0.33	0.59	519
Y_2SiO_5:Tb	65	5.00	0.33	0.59	516
YPO_4:Tb	65	5.00	0.35	0.57	504

at temperatures below 100°K in the 0.1 weight % sample and were not found in samples with more than 3 weight % of terbium. Also, the shortwave bands were not found in any of the borate glasses studied. In borate glasses segregation of the activator was observed and, in consequence, the effect of concentration quenching was strong.

7.1.5 Radioluminescence

The time decay properties of the radioluminescence of the 1.48 mole % Tb^{3+} in NS glass sample were investigated by Bateman (7.31). The sample was irradiated with α-particles from a ^{241}Am source, and the emission was detected by a single photon counting technique with an efficiency of ~10%. The photomultiplier tube used was a D224B, the amplified response of which was digitised and displayed on a scaler. The resulting decay curve is shown in Figure 7.1 and is very similar to the decay curves found in LAS glasses excited with X-ray irradiation. It is thought that a similar mechanism may be involved in the two excitation processes.

Vakhidov et al (7.32) report the γ-ray excited luminescence of sodium calcium silicate glass ($Na_2O.1.5CaO.5SiO_2$) doped with various rare earths, added as the oxide. The spectra of Tb^{3+} ions excited by γ-rays from a ^{60}Co source were measured at 77°K and 300°K. The solarisation produced by the γ-rays was also studied. Decreasing the temperature of the glass led to an attenuation of the luminescence and an enhancement of the solarisation.

7.1.6 Triboluminescence in Glass

Because of the limited application of triboluminescence and the

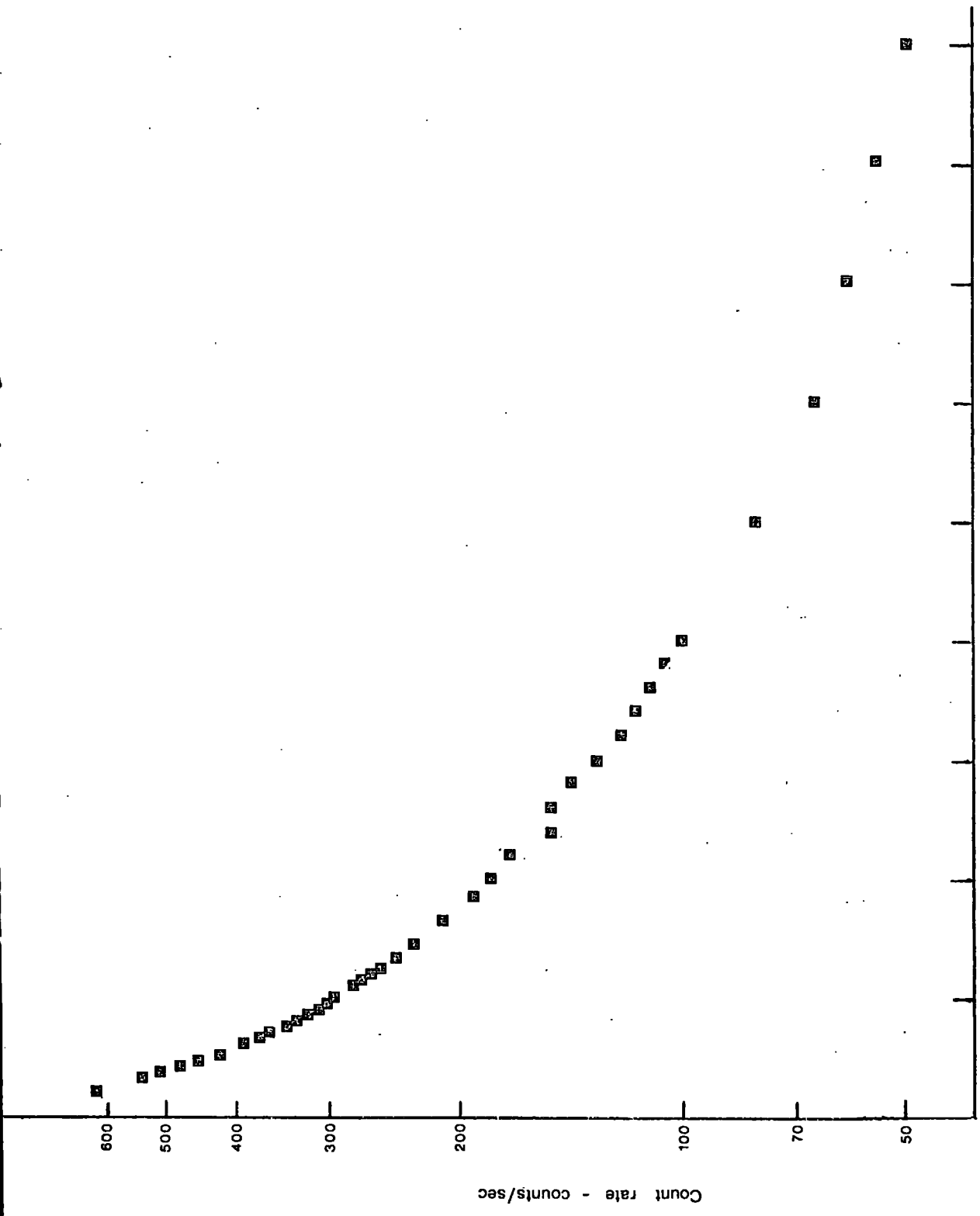

Fig 7.1 Luminescence decay of 1.48 mole % Tb^{3+} in NS glass, irradiated with α-particles from a ^{241}Am source at room temperature. (After Bateman 1971)

difficulty of obtaining reproducible results, little work of this nature has been done on glasses.

Outwater and Gerry (7.33) report the observation of triboluminescence in Pyrex glass fracturing under compressive loads in the range 3×10^5 to 5×10^5 psi. Such stresses are among the highest ever recorded in any material.

No reference can be found in the literature to the occurrence of triboluminescence in rare earth doped glasses.

7.1.7 Effects of the Thermal History of a Glass on its Luminescence Properties

A second batch of the 1.81 mole % Tb^{3+} in L A S glass was melted under the same conditions as the other L A S glasses, except that the glass was maintained in the molten state for a period of 23 hours. The annealing conditions were as before (see Chapter 3). The resulting luminescence spectra produced by ultra-violet excitation were essentially similar to those obtained for the glasses melted for a much shorter period. No differences were found in either the width or intensity of the emission bands.

Labutina et al (7.34) measured the effect of the thermal history on silicate glasses doped with neodymium. On heating the glass at temperatures of 675°C for periods of up to 72 hours, the half width of the neodymium luminescence was observed to decrease by about 10%. Variations in the intensities of the peaks of several of the emission bands were not systematic, but the tendency was towards higher intensities for more prolonged periods of heat treatment. Again the change was of the order of 10% for the emission line at 1.06 microns.

Komiyama et al (7.35) studied the relation between changes in the emission spectra of Eu^{3+} and Tb^{3+} ions and the structure of a lithium silicate glass ($67SiO_2.30Li_2O.2P_2O_5.Ln_2O_3$). This glass could be easily crystallised to form a phase of $Li_2O.2SiO_2$ on heat treatment. The addition of the rare earths in small amounts suppressed the formation of the crystalline phase.

The emission spectrum of Eu^{3+} showed a splitting of the $^5D_0$ to $^7F_1$ and $^5D_0$ to $^7F_2$ transitions due to the Stark effect of the crystalline field having become more distinct with increasing degrees of crystallisation. Prolonged heat treatment also reduced the half widths of the emission bands and also increased the intensity of the $^5D_0$ to $^7F_1$ (magnetic dipole) transition.

Essentially similar results were obtained for the terbium doped glass. The conclusion was that the uniformity and symmetry of the crystal field around the lanthanide ion was increased by the increasing degree of local ordering in the glass.

7.1.8 Glass Lasers

Transparent materials containing various rare earth ions have recently found considerable application in the field of laser physics. Trivalent neodymium has been the most important because it can be operated at room temperature with high efficiency. In crystals, Nd^{3+} was the first lanthanide ion to produce an optical maser action (7.36).

The first glass laser was reported by Snitzer (7.37) in a barium crown (silicate) glass activated with Nd^{3+}. Several other of the rare earths have since been found to lase in silicate glass hosts : Yb^{3+} (7.38), Ho^{3+} (7.39), Er^{3+} (7.40), Tm^{3+} (7.41). However, no report can be

found in the literature of the successful lasing of Tb^{3+} in any material.

The principal advantages of a glass laser host are the variability of size and shape possible and the excellent optical homogeneity. Glasses also are capable of a large range of refractive indices, and the composition may be adjusted to give a very low temperature coefficient of refractivity, which enables thermally stable devices to be produced.

The inhomogeneous broadening of emission bands in glasses makes it more difficult to obtain the population inversion necessary for the threshold condition to be achieved. However, this is in part compensated for by the broader absorption bands in glasses. Also, the wider emission line provides an advantage in Q-switched and amplifier applications (7.42, 7.43, 7.44).

Most materials which have been usefully employed as lasers have a four-level system of possible energy states. Trivalent terbium has a four-level system which is apparently well suited to this purpose. Absorption at the $^5D_3$ and higher levels is followed by an efficient energy transfer process to the $^5D_4$ level which emits most strongly by a transition to the $^7F_5$ level. The latter may then relax to the ground state ($^7F_6$).

The required pump lamp would have to have a high output in the blue and ultra-violet regions of the spectrum. Also, the lamp should preferably have emission in the region of the 4f to 5d transitions of Tb^{3+}, as these produce more efficient excitation.

The lack of success in producing a Tb^{3+} laser may be explained by comparing the optical properties of terbium compounds with those of neodymium. The Schawlow-Townes (7.45) condition requires that a population inversion must exist before stimulated emission can occur.

A population inversion is more easily obtained in materials with a high absorptivity in the pump bands. In other words, a high transition probability is required for the absorbing transition.

Neodymium has a strong absorption in several pump bands at around 600nm to 800nm. There are many bands in this region with oscillator strengths of the order of 10^{-7} and higher. Comparison with the figures obtained for Tb^{3+} in glass (Chapter 4) shows that a much higher threshold would be expected in the case of terbium.

Energy transfer processes have been usefully employed in increasing the effective absorption of lasing ions. Absorption by coactivator ions, followed by energy transfer to the lasing ions, has considerably reduced the threshold power for lasing in silicate glasses (7.46).

Terbium ions have been used as a sensitiser in borosilicate glasses to promote the efficiency of the lasing action of Nd^{3+} ions (7.47).

Further work may produce a viable terbium laser, but it is doubtful if these will be as efficient as the existing lanthanide lasers. Some investigations have already been made (7.48) into the possibilities of terbium lasers, but threshold powers were not achieved (7.49).

7.1.9 Infra-red Excited Visible Luminescence

The concept of an infra-red quantum counter (IRQC) is originally due to Bloembergen (7.50). In this process a rare eath ion is excited by the absorption of an infra-red photon and a second pump photon and then produces a (usually visible) luminescent emission which is distinct from the pump light.

Auzel (7.51) first discovered the sensitisation of Er^{3+} and Tm^{3+}

by Yb^{3+} in $Na_{0.5}Yb_{0.5}WO_4$ where the pump photons are also the infra-red radiation. The processes involved require two and three successive transfers respectively from the excited state of Yb^{3+} (at around 1 micron).

Successful IRQC effects have since been reported in many crystal systems coactivated with Yb^{3+} and Er^{3+}, Ho^{3+} or Tm^{3+} (references 7.52 to 7.57). Such systems may be of considerable importance in converting the infra-red emission from light emitting diodes of the GaAs type. It should be emphasised, however, that the conversion efficiency is strongly dependent on the intensity of infra-red illumination.

The glasses listed in Table 3.5 were prepared in the hope of producing IRQC effects in lanthanide glasses. Because of the wider absorption bands in glasses, increased energy transfer was anticipated in these materials due to an increase in the overlap integral (see equation 2.122).

All the samples were found to have a strong absorption band due to Yb^{3+} from approximately 900nm to 1,000nm. The glasses were irradiated with infra-red radiation of approximately 950nm from a hot filament source. However, no visible emission could be detected in any of the samples.

Antipenko et al (7.58 recently reported the transformation of neodymium laser radiation to the luminescence of Tb^{3+} in borosilicate glasses coactivated with Tb^{3+} and Yb^{3+} ions. This, however, is unlikely to find commercial application, as high conversion efficiencies are already available from frequency doubling devices of the lithium niobate type.

7.2 Conclusions and Possible Applications

Terbium phosphors in general produce an intense visible lumin-

escence under many forms of excitation. The emission is mainly from a narrow band in the green region of the spectrum (~ 550nm) for mole fractions of Tb^{3+} ions above 0.01.

The luminescence increases very rapidly with concentration above 1 mole % due to multipolar energy transfer processes. An optimum efficiency is found at concentrations of about 5 mole %, since at higher doping levels concentration quenching, thought to be due to exchange dipole interactions, occurs.

The colour of the luminescence is not appreciably altered by changes in the glass matrix produced by the inclusion of Al^{3+} ions. The site of the Tb^{3+} ions is thought to be very similar in all oxide glasses. However, much higher efficiencies were found in alkali aluminosilicate glasses than in alkali silicates.

The glasses all had quite fast decay rates (of the order of a few milliseconds) when irradiated with ultra-violet radiation, but very long decay times (of the order of five to 15 minutes) were found in some glasses for X-ray and α-particle excitation.

The practical aspects of luminescent glass lie in the ease of manufacture and the high transparency to its own emission. The detection of shortwave radiation or ionising radiation in inaccessible places is possible by fabricating light guides of these glasses. Luminescence at the end of a filament of glass may be transmitted along its length by 'cladding' the fibre with glass of higher refractive index. Such a system would alleviate the necessity of optically matching a phosphor to the end of a light guide.

X-ray screens for viewing objects under irradiation in situ could

readily be made from terbium doped glasses. The X-ray transmission (harmful to an observer) may be reduced by the incorporation of other ions of heavy metals. However, because of the high material cost of the large amounts of terbium oxide which would be required, such applications are likely to be prohibitively expensive.

The low intensity of the blue component of the luminescence of Tb^{3+} ions in borate glasses may result in phosphors with a high monochromaticity and a reasonable efficiency being produced from mixed oxide (borosilicate) glasses.

High efficiencies were observed for glasses at temperatures up to 500°C, so that these materials would find application where high temperature phosphors are required.

Radioluminescence efficiencies have not been determined but are thought to be reasonably high. This, coupled with the fact – already mentioned – that the glasses are transparent to their own luminescence, may mean that these glasses could find application in high energy particle detection. The glass could be coupled with usual types of photomultiplier tubes, as most of the luminescence is within the region of high photocathode sensitivity (blue-green). Limitations may be encountered, however, because of the long decay times of these glasses under such forms of excitation. Output pulse widths of such a system would be quite large, so that high pulse repetition rates could not be discriminated.

Cathodoluminescence efficiencies have not been determined, but it is thought that they are comparable in glasses and terbium doped crystals. Although the latter have already found some commercial application (see section 7.1.4), glass phosphors are likely to have few additional

advantages.

Any energy transfer processes between the glass matrix and the included lanthanide ions was found to be slight. It is thought that for this reason terbium does not act as an emission centre in thermoluminescence. The inclusion of highly charged ions was found to signficantly reduce the intensity of the glow curve peak, particularly in aluminosilicate glasses. Dosimeters relying on the thermoluminescence properties of glasses are likely to be more efficient for lower concentrations of any network-forming oxide.

Terbium doped glasses may, however, find application in a different form of dosimetry. If the glass is positioned in a light-tight container, the luminescence produced by incident ionising radiation can be recorded photographically on high sensitivity film. The resulting detection efficiency may be comparable with devices using more conventional scintillation materials.

The peak positions of the luminescence of terbium doped glasses are fairly insensitive to composition, temperature, the inclusion of impurity ions and the method of excitation. This, coupled with the ease of manufacture, may mean that terbium doped inorganic glasses could be used as simple and convenient emission wavelength standards in a somewhat similar manner to the use of holmium glasses as the standard for the calibration of absorption spectra.

REFERENCES

Chapter 1

1. 1 Overview No 32 (1972) Molybdenum Corporation of America

1. 2 Overview No 28 (1971) Molybdenum Corporation of America

1. 3 Herring, A P, Dean, R W, Drobnick, J L, Report from the American Ceramic Society 70th Annual Meeting, Glass Division, Chicago, Illinois (1968)

1. 4 Warren, B E, Z Krist, 86 (1933) 349-358

1. 5 Randall, J T, Rooksby, H P, Cooper, B S, J Soc Glass Tech, 14 (1930) 219-229

1. 6 Moriya, T, J Japan Cer, A55 (1957) 60-62

1. 7 Prod'homme, L, Kreidl, N T, Glass Industry, 39 (11) (1958) 587-589 (plus two pages)

1. 8 Angell, C A, J Amer Cer Soc, 51 (3) (1968) 117-124

1. 9 Mackenzie, J D, "Modern Aspects of the Vitreous State", Volume 1 (1960) pub Butterworths, London

1.10 Debye, P, Ann Physik, 46 (1915) 809

1.11 Weyl, W A, Marboe, E C, "The Constitution of Glasses : A Dynamic Interpretation", Vol II, part 1 (1964), especially pages 429-627, pub John Wiley and Sons, New York

1.12 Zachariasen, W H, J Amer Chem Soc, 54 (1932) 3841-3851

1.13 Valenkov, N, Porai-Koshitz, E, Nature, 137 (1936) 273-274

1.14 Prebus, A F, Michener, J W, Ind Eng Chem, 46 (1954) 147-153

1.15 Oberlies, F, Glastech Ber, 22 (1948) 41

1.16 Stookey, S D, U S Pat 2, 920, 971 (1960)

1.17 Stroud, J S, J Chem Phys, 35 (3) (1961) 844-850

1.18 Ioffe, A F, Regel, A R, Progr Semiconductors, 4 (1960) 239-291

1.19 Inglis, G B, Williams, F, J Non-crystalline Solids, 5 (1971) 313-327

1.20 Katsin, L I, Barnett, M L, J Phys Chem, 68 (1964)3779-3785

1.21 Spedding, F H, Daane, A H, "The Rare Earths" (1961) pub John Wiley and Sons, New York

1.22 Felsche, J, Structure and Bonding, 13 (1972) 99-198

1.23 Resifeld, R, Eckstein, Y, J Solid State Chem, 5, (2) (1972) 174-185

1.24 Toropov, N A, Galakhov, F Y, Bondar, I A, Izvest Akad Nauk S S S R Otdel Khim Nauk (1956) 641-648

1.25 Kan Fu-Hsi, Jeung Chung-Hung and Chai Ying-Shih, Scientia Sinica, 14, (8) (1965) 1159-1170

1.26 Ziman, J M, J Phys C (Proc Phys Soc), 1 (1968) 1532-1538

1.27 Rice, D K, De Schazer, L G, Phys Rev, 186 (1969) 387-392

1.28 Mann, M M, PhD thesis (1969) University of Southern California

1.29 Hunt, R P, PhD thesis (1973) University of Durham

1.30 Mann, M M, De Schazer, L G, J Appl Phys, 41, (7) (1970) 2951-2957

1.31 Snitzer, E, Bull Am Phys Soc, 9 (1964) 447

1.32 Goldschmidt, V M, Olrich, F, Barth, J, Skrifter utgit ov det Norske Videnskap-Akademi i Oslo, Matem Natur viol Klasse 5 (1925) 5

1.33 Wilbert, Y, Duquesnoy, A, Marion, F, Compt Rend Acad Sci Ser C, 271, (17) (1970) 1080-1083

1.34 Guth, E D, Eyring, L, J Am Chem Soc, 76 (1954) 5242-5244

1.35 Hubbert-Paletta, Von E, Müller-Buschbaum, H, Z Anorg Allg Chem, 363 (1968) 145-150

1.36 Salamang, H, "Ceramics; Physical and Chemical Fundamentals" (trans M Francis) (1961) pub Butterworths

1.37 Kan Fu-Hsi, Jeung Chung-Hung and Chai Ying-Shih, Scientia Sinica, 14 (7) (1965) 1079-1082

1.38 Wybourne, B G, "Spectroscopic Properties of Rare Earths" (1965) pub Interscience, New York

1.39 Reisfeld, R, Velapoldi, R A, Bohem, L, Ish-Shalmom, M, J Phys Chem, 75 (1971) 3980-3983

1.40 Reisfeld, R, Velapoldi, R A, Bohem, L, J Phys Chem, 76 (1972) 1293-1297

1.41 Reisfeld, R, Lieblich, N, Phys Chem of Solids, 34 (1973) 1467-1476

1.42 Velapoldi, R A, Reisfeld, R, Bohem, L, unpublished results (1972)

1.43 Rajnak, K, J Chem Phys, 43 (1965) 847-855

1.44 Dieke, G H, Crosswhite, H M, Dunn, B, J Opt Soc Am, 51, (8) (1961) 820-827

1.45 Dieke, G H, "Spectra and Energy Levels of Rare Earth Ions in Crystals" (1968) pub John Wiley and Sons, New York

1.46 Racah, G, Phys Rev, 76 (1949) 1352-1365

1.47 Judd, B R, Phys Rev, 127 (1962) 750-761

1.48 Judd, B R, Proc Phys Soc (London), A69 (1956) 157-164

1.49 Ofelt, G S, J Chem Phys, 38 (1963) 2171-2180

1.50 Reisfeld, R, Honigbaum, A, Michaeli, G, Harel, L, Ish-Shalom, M, Isr J Chem, 7 (1969) 613-625

1.51 Wickersheim, K A, Buchanan, R A, Appl Phys Lett, 17, (5) (1970) 184-187

1.52 Hosina, T, J Chem Phys, 50, (12) (1969) 5158-5162

1.53 Blasse, G, Bril, A, Philips Res Repts, 22 (1967) 481-504

1.54 Blasse, G, Bril, A, J Chem Phys, 47, (6) (1967) 1920-1926

1.55 Shionoya, S, Nakazawa, E, Appl Phys Lett, 6, (6) (1965) 118-120

1.56 Weyl, W A, Marboe, E C, "The Constitution of Glass : A Dynamic Interpretation", Volume I (1963) pub John Wiley (Interscience), New York

1.57 Karapetyan, G O, Izv Akad Nauk C C C P Ser Fiz, 25, (4) (1961) 539-541

1.58 Linwood, S H, Weyl, W A, J Opt Soc Am, 32 (1942) 443-453

1.59 Rindone, G E, "Luminescence in the Glassy State" in Lumin Inorg Solids (1966) 419-464

Chapter 2

2. 1 Curie, D, "Luminescence in Crystals" (1960) trans Garlick, G F J, (1963) pub Methuen, London

2. 2 Perrin, F, Ann Phys, 12 (1929) 169-275

2. 3 Williams, F E, Johnson, P D, Phys Rev, 113 (1959) 97

2. 4 Williams, F E, J Phys Chem, 57 (1953) 780-784

2. 5 Kristoffel, N N, Opt i Spektr, 7,(1) (1959) 78-82

2. 6 Maeda, K, Phys and Chem Solids, 9 (1959) 335-336

2. 7 Mann, M M, Ph D thesis (1969) University of Southern California

2. 8 Smakula, A, Z Physik, 59 (1929) 603-614; and 63 (1930) 762-770

2. 9 Dexter, D L, Phys Rev, 101, (1) (1956) 48-55

2.10 Hoogshagen, J, Physica, 11 (1946) 513-517

2.11 Carnall, W T, Fields, P R, Rajnak, K, J Chem Phys, 49,(10) (1968) 4412-4423

2.12 Bril, A, Klasens, H A, Philips Res Repts, 7 (1952) 401-420

2.13 Janin, J, Bourcet, J C, Jorus, J P, J Phys C sup, 14 (1966) 2-81

2.14 Moeller, T, Birnbaum, E R, Forsberg, J H, Gayhart, R B, Progr Sci Technol Rare Earths, 3 (1968) 61-128

2.15 Ephraim, F, Bloch, R, Ber (Deutsch Chem Ges), 59 (1926) 2692-2705; and 61 (1928) 65-72

2.16 Jørgensen, C K, Proceedings 5th Rare Earth Research Conference Ames Iowa (1965)

2.17 Jørgensen, C K, Pappalardo, R, Rittershaus, E, Z Naturforsch A, 19, (4) (1964) 424-433

2.18 Ellis, M M, Newman, D J, Phys Lett, 21, (5) (1966) 508-510

2.19 Jørgensen, C K, Rittershaus, E, Mat Fys Medd Dan Vid Selskab, 35 (1967) No 15

2.20 Sinha, S P, "Complexes of the Rare Earths" (1966) pub Pergamon, Oxford

2.21 Reisfeld, R, Structure and Bonding, 13 (1973) 53-98

2.22 Duffy, J A, Ingram, M D, J Chem Phys, 52, (7) (1970) 3752-3754

2.23 Jørgensen, C K, "Absorption Spectra and Chemical Bonding in Complexes" (1962) pub Pergamon, New York

2.24 Carrington, A, Jørgensen, C K, Molecular Physics, 4 (1961) 395-400

2.25 Edmonds, A R, "Angular Momentum in Quantum Mechanics" (1957) Princetown University Press, Princetown, New Jersey

2.26 Lomont, J S, "Applications of Finite Groups" (1959) pub Academic Press, New York

2.27 Slater, J C, Phys Rev, 34 (1929) 1293-1322

2.28 Condon, E U, Shortly, G H, "The Theory of Atomic Spectra" (1963) pub University Press, Cambridge

2.29 Judd, B R, Proc Roy Soc, A228 (1955) 120-128

2.30 Racah, G, Phys Rev, 63 (1943) 367-382; and 76 (1949) 1352-1365

2.31 Ofelt, G S, J Chem Phys, 38,(9) (1963) 2171-2180

2.32 Wybourne, B G, J Chem Phys, 36, (9) (1962) 2295-2300

2.33 Thomas, K S, Singh, S, Dieke, G H, J Chem Phys, 38, (9) (1963) 2180-2190

2.34 Judd, B R, Lindgren, I, Phys Rev, 122, (6) (1961) 1802-1812

2.35 Blasse, G, Bril, A, Philips Res Repts, 22 (1967) 481-504

2.36 Elliot, R J, Stevens, K W H, Proc Roy Soc, A215 (1952) 437-453

2.37 Stevens, K W H, Proc Phys Soc, A65 (1952) 209-215

2.38 Rotenberg, M, Bivins, R, Metropolis, N, Wooten, J K, "The 3-j and 6-j Symbols" (1959), pub Technology Press, MIT, Cambridge, Mass

2.39 Dieke, G H, "Spectra and Energy Levels of Rare Earth Ions in Crystals" (1968) pub John Wiley, New York

2.40 Fritzsche, H, J Non-Crystalline Solids, 6, (1971) 49-71

2.41 Sidorov, T A, Tyulkin, V A, Aksenov, V S, Zh Prikl Spectrosk, 7 (1967) 778-780

2.42 Swallow, A J, "Radiation Chemistry of Organic Compounds" (1960) pub Oxford

2.43 Urbach, F, Sitzb Akad Wiss Wien Ber Abt II A, 139 (1930) 349-352 and 473-481

2.44 Randall, J T, Wilkins, M H F, Proc Roy Soc, A184 (1945) 366-380 and 390-407

2.45 Bonfiglioli, G, "Thermoluminescence of Geological Materials" (1968) pub Academic Press, London, 15-25

2.46 Yokota, R, Phys Rev, 91 (1953) 1013-1014

2.47 Kikuchi, T, J Phys Soc Japan, 13, (5) (1963) 1132-1145

2.48 Spurny, Z, Novotny, J, J Phys Chem Solids, 26 (1965) 1107-1110

2.49 Brcser, I, Broser-Warminsky, R, Brit J Appl Phys Suppl No 4 (Luminescence) (1955) S90-S94

2.50 Shalgaonkar, C S, Narlikar, A V, J Mat Sci, 7 (1972) 1465-1471

2.51 Buhl, O, Z Phys, 109 (1938) 180-203

2.52 Franck, J, Z Phys, 9 (1922) 259-266

2.53 Klassens, H A, Nature, 158 (1946) 306-307

2.54 Frenkel, J, Phys Rev, 37 (1931) 17-44

2.55 Botden, T P J, Philips Res Repts, 6, (6) (1951) 425-473

2.56 Botden, T P J, Philips Res Repts, 7, (3) (1952) 197-235

2.57 Schön, M, Z Phys, 119 (1942) 463-471

2.58 Butler, K H, J Electrochem Soc, 95 (1949) 267-281

2.59 Murata, K J, Smith, R L, Am Mineral, 31 (1946) 527-538

2.60 Botden, T P J, Kröger, F A, Physica, s-Grav, 14 (1948) 553-566

2.61 Schulman, J H, Ginther, R J, Klick, C C, J Electrochem Soc, 97 (1950) 123-132

2.62 Van Uitert, L G, Johnson, L F, J Chem Phys, 44, (9) (1966) 3514-3522

2.63 Perrin, F, J Phys et Radium, 7 (1936) 1-11

2.64 Förster, T, Ann Physik Lpz (Folge 6), 2, (1-2) (1948) 55-75; and Z Electrochem, 53 (1949) 93

2.65 Dexter, D L, J Chem Phys, 21,(5) (1953) 836-850

2.66 Blasse, G, Philips Res Repts, 24 (1969) 131-144

2.67 Inokuti, M, Hirayama, F, J Chem Phys, 43, (6) (1965) 1978-1989

2.68 Nakazawa, E, Shionoya, S, J Chem Phys, 47, (9) (1967) 3211-3219

2.69 Van Uitert, L G, J Luminescence, 4 (1971) 1-7

2.70 Van Uitert, L G, Dearborn, E F, Rubin, J J, J Chem Phys, 47, (2) (1967) 547-553

2.71 Van Uitert, L G, J Electrochem Soc : Solid State, 114, (10) (1967) 1048-1053

2.72 Cabezas, A Y, De Schazer, L G, Appl Phys Lett, 4, (2) (1964) 37-39

2.73 Reisfeld, R, Greenberg, E, Velapoldi, R A, Barnett, B, J Chem Phys, 56, (4) (1971) 1698-1705

Chapter 3

3. 1 See, for instance, Ealing Science Teaching Catalog (1969) Ealing Scientific Limited

3. 2 Becke, F, Sitzber Akad Wiss Wien, C11, Abt 1 (1893) 358-378

3. 3 Hotchkiss, W O, Am Geol, 36 (1905) 305-308

Chapter 4

4.1 Kan Fu-Hsi, Jeung Chung-Hung, Chai Ying-Shih, Scientia Sinica, 14, (8) (1965) 1159-1170

4.2 Miller, F A, Wilkins, C H, Anal Chem, 24, (8) (1952) 1253-1294

4.3 Hunt, J M, Wisherd, M P, Bonham, L C, Anal Chem, 22, (12) (1950) 1478-1497

4.4 Borrelli, N F, Su, G J, Mater Res Bull, 3, (2) (1968) 181-192

4.5 Borrelli, N F, Phys Chem Glasses, 10, (2) (1969) 43-45

4.6 Lippincott, E R, Van Valkenburg, A, Wier, C E, Bunting, E N, J Res Nat Bur Stand, 61 (1958) 61-70

4.7 Sweet, J R, White, W B, Phys Chem Glasses, 10, (6) (1969) 246-251

4.8 Ferraro, J R, Manghnani, M H, Phys Chem Glasses, 13, (4) (1972) 116-121

4.9 Ferraro, J R, Manghnani, M H, J Appl Phys, 43, (11) (1972) 4595-4599

4.10 Ferraro, J R, Hazdra, J J, Boether, W, J Chem Phys, 57, (11) (1972) 4540-4542

4.11 Scholze, H, Dietzel, A, Naturwiss, 42 (1955) 342-353

4.12 Sadagopan, V, Gatos, H C, Mater Sci Eng, 2 (1967/68) 273-275

4.13 Bradbury, B T, Maddocks, W R, J Soc Glass Technol, 43 (1959) 325T-336T

4.14 Thomas, K S, Singh, S, Dieke, G H, J Chem Phys, 38 (1963) 2180-2190

4.15 Karapetyan, G O, Lunter, S G, Zh Prikl Spektroskopii, 5, (3) (1966) 310-315

4.16 Ofelt, G S, J Chem Phys, 38 (1963) 2171-2180

4.17 Carnall, W T, Fields, P R, Rajnak, K, J Chem Phys, 49, (10) (1965) 4447-4449

4.18 Nelson, W F, King, F T, Barber, S W, in "Proceedings of the Third Conference on Rare Earth Research" (1963). Published in "Rare Earth Research II", ed K S Vorres

4.19 Feofliov, P P, Opt i Spektrosk, 10,(1) (1961) 142-144

4.20 Herring, A P, Dean, R W, Drobnick, J L, Report from the American Cermaic Society 70th Annual Meeting, Glass Division, Chicago, Illinois (1968)

4.21 Carnall, W T, Fields, P R, Rajnak, K, J Chem Phys, 49, (10) (1968) 4412-4423

4.22 Weber, M J, Sharp, E J, Miller, J E, J Phys Chem Solids, 32 (1971) 2275-2284

4.23 Reisfeld, R, Lieblich, N, J Phys Chem Solids, 34 (1973) 1467-1476

4.24 Karapetyan, G O, Izv Akad Nauk SSSR Ser Fiz, 27, (6) (1963) 779-802

4.25 Reisfeld, R, Gur-Arieh, Z, Greenberg, E, Anal Chim Acta, 50 (1970) 249-254

4.26 Phillips, C S G, Williams, R J P, "Inorganic Chemistry", Vol 2, (1966) pub Clarendon Press, Oxford

4.27 Reisfeld, R, Structure and Bonding, 13 (1973) 53-98 (see page 79)

4.28 McClure, D S, Kiss, Z, J Chem Phys, 39 (1963) 3251-3257

4.29 Blasse, G, Bril, A, Philips Res Repts, 22 (1967) 481-504

4.30 Hutton, D R, Milne, R J, Proc Phys Soc London (Solid State Physics), 2 (12) (1969) 2297-2300

4.31 Hunt, R P, Private Communication

Chapter 5

5. 1 Hoshina, T, J Chem Phys, 50 (12) (1969) 5158-5162

5. 2 Blasse, G, Bril, A, Philips Res Repts, 22 (1967) 481-504

5. 3 Wickersheim, K A, Buchanan, R A, Appl Phys Lett, 17 (5) (1970) 184-187

5. 4 Levshin, V L, Maksimova, N D, Optics and Spectrosc (USA), 27 (1969) 342-343

5. 5 Barsanov, S S, Koberts, L I, Kazakov, V P, Izv Sib Otd Akad Nauk SSSR Ser Khim Nauk, 4 (1967) 14-16

5. 6 Mizuno, H, Masuda, M Proc Internationai Conf Luminescence 1966 (Pub 1968) 2, 1703-1708

5. 7 Loh, E, Phys Rev, 147 (1) (1966) 332-335

5. 8 Barasch, G E, Dieke, G H, J Chem Phys, 43 (3) (1965) 988-994

5. 9 E I Du Pont de Nemours and Co, German Pat No 1, 178, 965

5.10 Dolgopolova, A V, Kovaleva, L V, Sazanova, S A, Skorobogatov, B S, Opt i Spektrosk, 17 (1) (1964) 141-143

5.11 Harrigan, R W, Crosby, G A, J Chem Phys, 52 (9) (1970) 4912-4914

5.12 Karraker, D G, J Chem Phys, 49 (2) (1968) 957-958

5.13 Janowski, A, Sadlej, N, J Luminescence, 3 (1970) 198-202

5.14 Van Uitert, L G, Soden, R R, J Chem Phys, 36 (7) (1962) 1767-1800

5.15 Herring, A P, Dean, R W, Drobnick, J L, American Ceramic Society 70th Annual Meeting, Glass Division, Chicago, Illinois (1968)

5.16 Van Uitert, L G, J Luminescence, 4 (1971) 1-7

5.17 Nakazawa, E, Shionoya, S, J Chem Phys, 47 (9) (1967) 3211-3219

5.18 Karapetyan, G O, Lunter, S G, Zh Prikl Spektrosk, 5 (1966) 310-315

5.19 Reisfeld, R, Velapoldi, R A, Bohem, L, J Phys Chem, 76 (1972) 1293-1297

5.20 Reisfeld, R, Structure and Bonding, 13 (1973) 53-98

5.21 Shulgin, B V, Taylor, K N R, Hoaksey, A, Hunt, R P, J Phys Chem : Solid State Physics, 5 (1972) 1716-1726

5.22 Avella, F J, Sovers, O J, Wiggins, C S, J Electrochem Soc, 114 (6) (1967) 613-616

5.23 Reisfeld, R, Honigbaum, A, Michaeli, G, Harel, L, Ish-Shalom M, Isr. J Chem, 7 (1969) 613-625

5.24 Overview No 28 (1971) Molybdenum Corporation of America

5.25 Dike, G H, Hall, L A, J Chem Phys, 27 (2) (1957) 465-467

5.26 Dieke, G H, Crosswhite, H M, Dunn, B, J Opt Soc Am, 51 (8) (1961) 820-827

5.27 Nelson, W F, King, F T, Barber, S W, in "Proceedings of the 3rd Donference on Rare Earth Research" (1963) published in "Rare Earth Research II", 573-582, ed K S Vorres, pub Gordon and Breach, New York

5.28 Gurney, R W, Mott, N F, Trans Farad Soc, 35 (1939) 69-73

5.29 Komura, H, J Phys Soc Japan, 21 (1966) 207

5.30 Parke, S, J Phys Chem Solids, 32 (1971) 669-675

5.31 Parke, S, Webb, R S, J Phys Chem Solids, 34 (1973) 85-95

5.32 Miller, F A, Wilkins, C H, Analyt Chem, 24 (8) (1952) 1253-1294

5.33 Grayson, M, Griffith, E J (eds), 1969, "Topics in Phosphorous Chemistry", vol 6, p 270, pub Interscience (Wiley and Sons) New York

5.34 Dieke, G H, "Spectra and Energy Levels of Rare Earth Ions in Crystals" (1968) pub Interscience (Wiley and Sons) New York

5.35 Dieke, G H, Leopold, L, J Opt Soc Am, 47 (1957) 944-954

5.36 Kurkjian, C R, Gallagher, P K, Sinclair, W R, Sigety, E A, Phys Chem Glasses, 4 (6) (1963) 239-246

5.37 Rabbiner, N, J Opt Soc Am, 57 (1967) 217-231

5.38 Mann, M M, PhD thesis (1969) University of Southern California

5.39 Shionoya, S, Nakazawa, E, Appl Phys Lett, 6 (6) (1965) 118-120

5.40 Reisfeld, R, Gur-Arieh, Z, Greeburg, E, Anal Chim Acta, 50 (1970) 249-254

5.41 Thomas, K S, Singh, S, Dieke, G H, J Chem Phys 38 (9) (1963) 2180-2190

5.42 Hunt, R P, PhD thesis (1973) University of Durham

5.43 Kikuchi, T, J Phys Soc Japan, 13 (5) (1963) 1132-1145

5.44 Draper, N, Smith, H, "Applied Regression Analysis" (1966) pub John Wiley, New York

5.45 Blasse, G, Bril, A, J Chem Phys, 47 (6) (1967) 1920-1926

5.46 Jørgensen, C K, Pappalardo, R, Rittershaus, E, Z Naturforschung 20a (1) (1965) 54-64

5.47 Ryan, J L, Jørgensen, C K, J Phys Chem 70 (9) (1966) 2845-2857

5.48 Curie, D, "Luminescence in Crystals" (1960) trans Garlick, G F J (1963) pub Methuen, London

5.49 Bourcet, J-C, Grafmeyer, J, Janin, J, 9th Rare Earth Research Conference, Blacksburg, Va. USA, 10th-14th October 1971, pub Virginia Polytechnic Inst and State University, 1971, 441-451

5.50 Blasse, G, Bril, A, J Chem Phys, 51 (8) (1969) 3252-3254

5.51 Van Uitert, L G, Dearborn, E F, Rubin, J J, J Chem Phys, 47 (2) (1967) 547-553

5.52 Van Uitert, L G, Dearborn, E F, Rubin, J J, J Chem Phys, 45 (5) (1966) 1578

5.53 Blasse, G, Bril, A, J Luminescence, 3 (1970) 18-20

5.54 Cabezas, A Y, De Shazer, L G, Appl Phys Lett, 4 (2) (1964) 37-39

5.55 Van Uitert, L G, Dearborn, E F, Rubin, J J, J Chem Phys, 47 (5) (1967) 1595-1599

5.56 Pearson, A D, Peterson, G E, Northover, W R, J Appl Phys, 37 (2) (1966) 729-734

5.57 Pearson, A D, Peterson, G E, Appl Phys Lett, 5 (11) (1964) 222-223

5.58 Reisfeld, R, Greenberg, E, Velapoldi, R, Barnett, B, J Chem Phys, 56 (4) (1972) 1698-1705

5.59 Van Uitert, L G, Dearborn, E F, Marcos, H M, Appl Phys Lett, 9 (7) (1966)

5.60 Van Uitert, L G, Dearborn, E F, Rubin, J J, J Chem Phys, 46 (9) (1967) 3551-3555

5.61 Amster, R L, J Electrochem Soc, 117 (6) (1970) 791-794

5.62 Van Uitert, L G, Dearborn, E F, Rubin, J J, J Chem Phys, 47 (9) (1967) 3653-3661

5.63 Wanmaker, W L, Bril, A, ter Vrugt, J W, Appl Phys Lett, 8 (10) (1965) 260-261

5.64 Mizuno, H, Masuda, M, Bull Chem Soc Japan, 37 (8) (1964) 1239-1240

5.65 Van Uitert, L G, J Electrochem Soc, 114 (10) (1967) 1048-1053

5.66 Antipenko, B M, Dmitryuk, A V, Karapetyan, G O, Zubkova, V S, Kosyakov, V I, Mak, A A, Mikhailova, N V, Opt Specktrosk, 35 (3) (1973) 540-545

5.67 Zhmyreva, I A, Kolobkov, V P, Veinberg, T I, Spetrosk Tverd Tela, (1969) 150-158

5.68 Kovaleva, I V, Kolobkov, V P, Reishakhrit, A L, Bondarenko, E G, Zh Prikl Spectrosk, 11 (6) (1969) 1090-1096

5.69 Weaver, E A, Heckman, R W, Williams, E L, J Chem Phys, 47 (12) (1967) 4891-4895

Chapter 6

6. 1 Fischer, R, (1969) German Pat No 1,298,205; and Schiekel, M (1969) German Pat No 1,287,703

6. 2 Ginther, R J, in "Luminescence Dosimetry", ed Attix, F H (1967) US Dept of Commerce, Sprinfield, Va, 118-131

6. 3 Palma, G E, Gagosz, R M, J Phys Chem Solids, 33 (1972) 177-189

6. 4 Schlesinger, M, Whippey, P W, Phys Rev, 162 (2) (1967) 286-290

6. 5 Miller, R A, Borrelli, N F, Appl Optics, 6 (1) (1967) 164-165

6. 6 Stroud, J S, Phys Chem Glasses, 5 (3) (1964) 71-75

6.7 Stroud, J S, J Chem Phys, 37 (4) (1962) 836-841

6. 8 Stroud, J S, J Chem Phys, 35 (3) (1961) 844-850

6. 9 Halperin, A P, Braner, A A, Shapira, J, J Luminescence, 2 (1970) 385-397

6.10 Medlin, W L, J Chem.Phys, 38 (1963) 1133-1143

6.11 Kikuchi, T, J Phys Soc Jap, 13 (1958) 526-531

6.12 Shalgaonkar, C S, Narlikar, A V, J Mater Sci, 7 (1972) 1465-1471

6.13 Carbury, M, "Optical Physics" (1965) pub Academic Press, New York. See page 101

6.14 Hunt, R P, PhD thesis (1973) University of Durham

6.15 Bettinali, C, Perraresso, G, J Chem Phys, 44 (6) (1966) 2262-2265

6.16 Sharma, B S, Rieckhoff, K E, Canadian J Phys, 45 (12) (1967) 3781-3792

6.17 Bieringer, R J, Montgomery, C G, Phys Rev B, 2 (12) (1970) 4988-4994

6.18 Barry, T I, Clinton, D, Lay, L A, Mercer, R A, Miller, R P, J Mater Sci, 5 (1970) 117-126

6.19 Sidorov, T A, Tyul'kin, V A, Izv Akad Nauk SSSR Neorg Mater, 2 (11) (1966) 2033-2038

6.20 Sidorov, T A, Tyul'kin, V A, Aksenov, V S, Dokl Akad Nauk SSSR, 175 (5) (1967) 1094-1096

6.21 Sidorov, T A, Tyul'kin, V A, Aksenov, V S, Zh Prikl Specktrosk, 7 (5) (1967) 778-780

6.22 Schreurs, J W H, J Chem Phys, 42 (2) (1967) 818-830

6.23 Young, C G, Proc I E E E, 57 (7) (1969) 1267-1289

6.24 American Society for Testing and Materials Special Technical Publication 469 (1969) Philadelphia, Pa

6.25 Ginther, R J, Claffy, E W, J Appl Phys, 42 (11) (1971) 4519-4521

6.26 Peterson, G E, Brindenbaugh, P M, J Opt Soc Am, 54 (1964) 644-650

Chapter 7

7. 1 Becquerel, J, Communications Kamerlingh Onnes Laboratory, Leiden University - during period 1925-1936

7. 2 Van Vleck, J H, "Electric and Magnetic Susceptibilities" (1932) p 368 pub Oxford University Press, London

7. 3 Berger, S B, Rubinstein, C B, Kurkjian, C R, Treptow, A W, Phys Rev A, 133 (3) (1964) 723-727

7. 4 Rubinstein, C B, Berger, S B, Van Uitert, L G, Bonner, W A, J Appl Phys, 35 (8) (1964) 2338-2340

7. 5 Borrelli, N J, J Chem Phys, 41 (11) (1964) 3289-3293

7. 6 Robinson, C C, Appl Opt, 3 (10) (1964) 1163-1166

7. 7 Western Electric Co Inc, French Pat No 1,395,984

7. 8 Rubinstein, C B, Van Uitert, L G, Grodkiewicz, W H, J Appl Phys, 35 (10) (1964) 3069-3070

7. 9 Belyaeva, N A, Garber, P R, Kamarzin, A A, Kann, K B, Kravchenko, L K, Sokolova, T E, Stonoga, Y A, Zh Prikl Spektrosk, 18 (2) (1973) 275-278

7.10 Gruss, L, Marcus, T, J Electrochem Soc, 120 (3) (1973) 337-340

7.11 Heller, A, French, K W, Haugsjaa, P O. J Chem Phys, 56 (5) (1972) 2368-2377

7.12 Kahng, D. Appl Phys Lett, 13 (6) (1968) 210-212

7.13 Razi, S, Anderson, W W, Trans Met Soc, AIME, 239 (3) (1967) 350-354

7.14 Dubovik, M F, Petrenko, Y B, Skorobogatov, B S, Spektrosk Krist Mater Simp 2nd 1967 (pub 1970) 232-236

7.15 Kazakov, V P, Korobeinikova, V N, Koberts, L I, Opt i Spektrosk, 26 (2) (1969) 319-321

7.16 Hansen, W W, Myers, R E, Appl Phys Lett, 6 (3) (1965) 58-59

7.17 Nanko, R, Jap J Appl Phys, 9 (8) (1970) 1003

7.18 Levshin, V L, Fridman, S A, Chikhacheva, V A, Schaenko, V V, Izv Akad Nauk SSSR Ser Fiz, 29 (3) (1965) 500-502

7.19 Brown, M R, Cox, A F J, Shand, W A, Williams, J M, Solid State Commun, 9 (1) (1971) 37-40

7.20 Iwase, E, Nishiyama, S, Bull Chem Soc Japan, 36 (9) (1963) 1179-1183

7.21 Yocom, P N, Shrader, R E, Proc 7th Rare Earth Conf 1968 (pub 1969) 2, 601-608

7.22 Hansen, W W, Myers, R E, Appl Phys Lett, 6 (3) (1965) 58-59

7.23 Buchanan, R A, Wickersheim, K A, Weaver, J L, Anderson, E E, J Appl Phys, 39 (9) (1968) 4342-4347

7.24 Ludwig, G W, Kingsley, J D, J Electrochem Soc, 117 (3) (1970) 348-353

7.25 Avella, F J, Sovers, O J, Wiggins, C S, J Electrochem Soc, 114 (6) (1967) 613-616

7.26 Avella, F A, J Electrochem Soc, 113 (11) (1966) 1225-1226

7.27 Peters, T E, J Electrochem Soc, 116 (7) (1969) 985-989

7.28 "The Science of Colour", Chapter 8 (1963) pub Optical Society of America, Washington DC

7.29 Bril, A, Wanmaker, W L, ter Vrugt, J W, J Electrochem Soc, 115 (7) (1968) 776-777

7.30 Gavrilenko, T B, Karapetyan, G O, Kachibaya, V N, Zh Prikl Spektrosk, 15 (4) (1971) 663-666

7.31 Bateman, E, unpublished results

7.32 Vakhidov, S A, Karapetyan, G O, Sanaev, B, Izv Akad Nauk Uzb SSR Ser Fiz - Mat Nauk, 14 (3) (1970) 48-51

7.33 Outwater, J O, Gerry, D J, J Appl Phys, 38 (2) (1967) 893-894

7.34 Labutina, L V, Pavlushkin, N M, Artamonova, M V, Likvatzionnye Yavleniya Steklakh, Tr Vses Simp 1st 1968 (pub 1969) 137-140

7.35 Komiyama, T, Sakurai, T, Shionoya, S, Kogyo Kagaku Zasshi, 72 (4) (1969) 839-843

7.36 Johnson, L F, Nassau, K, Proc I R E, 49 (1961) 1704

7.37 Snitzer, E, Phys Rev Lett, 7 (12) (1961) 444-446

7.38 Etzel, H W, Gandy, H W, Ginther, R J, Appl Opt, 1 (1962) 535

7.39 Gandy, H W, Ginther, R J, Proc I R E, 50 (1962) 2113-2114

7.40 Snitzer, E, Woodcock, R, Appl Phys Lett, 6 (1965) 45-46

7.41 Gandy, H W, Ginther, R J, Weller, J F, J Appl Phys, 38 (7) (1967) 3030-3031

7.42 Mann, M M, De Shazer, L G, J Appl Phys, 41 (7) (1970) 2951-2957

7.43 Borrelli, N F, Charters, M L, J Appl Phys, 36 (7) (1965) 2172-2174

7.44 Vance, M E, Appl Opt, 6 (1967) 775

7.45 Schawlow, A L, Townes, C H, Phys Rev, 112 (6) (1958) 1940-1949

7.46 Gandy, H W, Ginther, R J, Weller, J F, Appl Phys Lett, 6 (1965) 46-49

7.47 Cabezas, A Y, De Schazer, L G, Appl Phys Lett, 4 (1964) 37-39

7.48 Heindl, R, Damay, F, Der Agobian, R, Loriers, J, Compt Rend, 261 (17) (1967) 3335-3338

7.49 Mizuno, H, Masuda, M, Bull Chem Soc Japan, 37 (8) (1964) 1239-1240

7.50 Bloembergen, N, Phys Rev Lett, 2 (3) (1959) 84-85

7.51 Auzel, F, Compt Rend, 262B (1966) 1016-1019; and 263B (1966) 819-821

7.52 Hewes, R A, Sarver, JF, Phys Rev, 182 (2) (1969) 427-436

7.53 Geusic, J E, Ostermayer, F W, Marcos, H M, Van Uitert, L G, van der Ziel, J P, J Apply Phys, 42 (5) (1971) 1958-1960

7.54 Sommerdijk, J L, Wanmaker, W L, Verriet, J G, J Luminescence, 4 (1971) 404-416; and 5, (1972) 297-307

7.55 Rich, T C, Pinnow, D A, J Appl Phys, 43 (5) (1972) 2357-2365

7.56 Kuroda, H, Shionoya, S, Kushida, T, J Phys Soc Japan, 33 (1) (1972) 125-141

7.57 Sommerdijk, J L, J Luminescence, 6 (1973) 61-67; and 8 (1973) 126-130

7.58 Antipenko, B M, Dmitryuk, A V, Karapetyan, G O Zubkova, V C, Kosyakov, V E, Mak, A A, Michaelova, E V, Opt i Spektrosk, 35 (3) (1973) 540-543